The Mangrove Tale

Mechanistic Modelling of Mangrove-Eco-Geomorphic Interactions

Beselly, S.M.

DOI
10.4233/uuid:17a9d384-5416-40d0-a714-306b1e284976

Publication date
2024

Document Version
Final published version

Citation (APA)
Beselly, S. M. (2024). *The Mangrove Tale: Mechanistic Modelling of Mangrove-Eco-Geomorphic Interactions*. [Dissertation (TU Delft), Delft University of Technology]. IHE Delft Institute for Water Education. https://doi.org/10.4233/uuid:17a9d384-5416-40d0-a714-306b1e284976

The Mangrove Tale: Mechanistic Modelling of Mangrove-Eco-Geomorphic Interactions

Sebrian Mirdeklis Beselly Putra

THE MANGROVE TALE:
MECHANISTIC MODELLING OF MANGROVE-ECO-GEOMORPHIC INTERACTIONS

Sebrian Mirdeklis Beselly Putra

THE MANGROVE TALE: MECHANISTIC MODELLING OF MANGROVE-ECO-GEOMORPHIC INTERACTIONS

DISSERTATION

for the purpose of obtaining the degree of doctor
at Delft University of Technology
by the authority of the Rector Magnificus Prof.dr.ir. T.H.J.J. van der Hagen,
chair of the Board for Doctorates
and
in fulfilment of the requirement of the Rector of IHE Delft
Institute for Water Education, Prof.dr. E.J. Moors,
to be defended in public on
Friday, 12 July 2024 at 10:00 hours

by

Sebrian Mirdeklis BESELLY PUTRA
Master in Civil Engineering, Brawijaya University, Indonesia
Master in Civil and Environmental Engineering, University of Miyazaki, Japan
born in Malang, Indonesia

This dissertation has been approved by the (co)promotor.

Composition of the doctoral committee:

Rector Magnificus TU Delft	chairperson
Rector IHE Delft	vice-chairperson
Prof.dr.ir. J.A. Roelvink	IHE Delft / TU Delft, promotor
Dr.ir. M. van der Wegen	IHE Delft, copromotor
Independent members:	
Prof.dr.ir. A.J.H.M. Reniers	TU Delft
Prof.dr. F. Dahdouh-Guebas	Vrije Universiteit Brussel, Belgium
Prof.dr. K.R. Bryan	University of Waikato, New Zealand
Dr.ir. B.C. van Prooijen	TU Delft
Prof.dr. M.E. Mc Clain	IHE Delft/ TU Delft, reserve member

Dr.rer.nat. Uwe Grüters of the Institute for Plant Ecology in Justus-Liebig University Giessen, Germany has been a key contributor to the preparation of this dissertation.

This research was conducted under the auspices of the Graduate School for Socio-Economic and Natural Sciences of the Environment (SENSE)

Cover design by Siska Adinata Rahman

Published by IHE Delft Institute for Water Education
www.un-ihe.org
ISBN 978-90-73445-63-5

To my mother Lily, my wife Siska, and my son Khalifi

Thank you for all of your unconditional love

In memory of my late father Bambang Endrosubono

ACKNOWLEDGEMENTS

After years of wrestling with mangroves, mud, and codes, it is time to resurface and honour the hard work. It is still unbelievable to have mangroves as my study interest. Living in a gorgeous mountainous town region in the eastern part of Java, I never had any thought that in the future to have a deep connection with the sea, let alone mangroves. It was started in mid-2016, being “under pressure” to write a PhD application proposal, by coincidence, I came across a documentary on television. It covered the story of the 2004 Indian Ocean Tsunami. In one section, the documentary showed villagers in a small fishing village in the south of Thailand survived the waves, with few casualties – thanks to the protection provided by the wide and dense mangrove forest. It suddenly triggered my curiosity, and the ideas swiftly flowed. I believe it is not just coincidence, but it is part of God’s way of showing me the path where should I go and pursue. In this particular, I feel blessed and grateful, that Allah the Almighty has revealed the way and rewarded me much more than I deserved. It reminded me of a hadith mentioned: "Allah makes the way to Heaven easy for him who treads the path in search of knowledge.". There are also countless people, to whom I owe the deepest gratitude for their unconditional support and love. Without them, this journey would have been impossible to go through.

I think the one who deserves the first place is my wife, Siska, your love, your kindness, your patience, your encouragement, your creativity, and your talent in cooking, are the boosters that propelled me from my lowest. With you, we have a wonderful son, Khalifi, that makes our life in Delft filled with marvellous colours. Khalifi with his giggle has always been a continuous inspiration. We started our life in Delft, 12,000km away from home, as a young family. It was not an easy beginning, sometimes as a father and husband becoming absent-minded, and drawn into my models and lines of codes. We would not be this persistent without the encouragement and prayers set by our family. My mother, Lily, you remain faithful through all the reservations and sufferings and keep me in your prayers. She always radiates positivity and remains faithful, even after the passing of my father. Somewhere, in heaven Papa is smiling down at us, I miss you, Papa. My sister, Xandra, you have grown into a mature and wise lady, I apologize for missing the important times. However, thank you for becoming a great sister, positive vibe, and for your support to us. My parents-in-law (Surahman and Astinah), thank you for your trust and also for keeping us in your prayers, apologize for missing out the precious moments. My brother and sister-in-law (Agung and Happy), thank you for sharing your stories and good wishes. I can proudly say to all of you that the PhD journey has Ph*inise*D.

I am indebted to the trust and guidance of my supervisors, to whom I express my sincere gratitude. They have irreplaceable roles in my intellectual journey. My promotor, Professor Dano Roelvink, his name might be a synonym for coastal hydromorphological modelling. I am always amazed by your way of interpreting physical processes into codes

and impressive results. Your supervision style is a combination of giving me the freedom to explore my research but also not hesitating to pull me back on the right track when I am drifting too far. My co-promotor, Associate Professor Mick van der Wegen, you are always available for questions and doubts. I always like our discussion sessions, you are open to any 'possible' solutions but also criticize them. It allowed me to develop and elaborate new ideas. I learned a lot, especially in interpreting the reviewers' comments. My mentor, Johan Reyns, your skill in (almost any major) programming language is intimidating. I remember when I first started my PhD, with zero skill in programming and was inexperienced at modelling, following your modules is helpful. You are always a go-to person for any advice in Delft3D-FM, thank you. I also thank Dr. Jasper Dijkstra, I enjoyed your provoking questions during our discussion in Deltares. Your experience in vegetation hydrodynamics has contributed to shaping this research. My sincere thanks to Dr.rer.nat. Uwe Grüters – you have been an important mentor in vegetation dynamics. I value your passion for mangroves and deeply appreciate your willingness to have hours of discussion and debugging the mangrove model. You have contributed greatly to the completion of the thesis. I thank you the supervisory team for the advice and support throughout the research period. Lastly, I am grateful to the independent doctoral committee members who took the time to read and assess the dissertation and their willingness to be part of the PhD defense.

I witnessed the evolution of our department, from the Water Science and Engineering Department to the formation of Coastal and Urban Risk & Resilience. Despite the changes, the group remains the same, filled with highly intellectual, warm, and lovely people. I learned not only in coastal science and engineering by following their classes, but also in networking and other soft skills. I would convey my gratitude to Associate Professor Ali Dastgheib for our nice cooperation between IHE Delft and Indonesia. I enjoyed our work together, you are good at executing and organizing academic activities. It seems you always have solutions for bureaucratic hurdles. I appreciated the opportunity to work together with Dr. Alvaro Semedo, with him I firstly had a chance to open the door for nice cooperation that we are nurturing with Indonesian stakeholders. I thank you Professor Rosh Ranasinghe and Dr. Trang Duong for your kindness in sharing about what is being a PhD candidate and some tips to survive the first year. We haven't had a chance to work together during my PhD period, but I believe more collaborations to come in the future.

I thank and acknowledge the current and graduated IHE friends, both MSc students and PhD candidates. I have a great memory of all of you, either in the modules or just a small chat at the IHE restaurant. Thanks to Liqin, Abdi, Vo, Duoc, Janaka, Jeewa, Taha, Musaed, Aftab, Üwe, Hesham, Saidee, Ahmed, Ha, Milk, Adele, Haris, and Khin. I thank to the Muslim Student Association (MSA) IHE Delft and PhD Association Board (PAB) for the wonderful activities together.

I am very lucky to be surrounded by awesome Indonesian community and friends in Delft. I highly appreciate Keluarga Muslim Delft (KMD) which has become our big family here.

Thank you to Mas Agung, Pak Aries, Kang Mamin, Mas Nasikun, Mas Ando, and Mas Gilang for your good deed in leading KMD for all of us. Many thanks to fellow Indonesian PhD and family in Delft, Pak Dikman and family for the warm welcome at your house, I mean a real warm with tea when we first arrived, Pak Aries and family for your kindness and SIMPUL, and Mas Ifan, good luck for the rest of your PhD. Current and graduated PhD friends at TU Delft, Mas Bramka and family, Mas Mikhta and family, Mas Aga and family, Pak Luthfi and family, Mas Arry and family, Mas Gilang and family, and Mbak Reni. Thanks also to Mas Tofan and family, Mas Marwan and family, Albert Stroop and family, Pak Sigit and family, and Mas Wicak and family.

Finally, my PhD was possible due to the unwavering support from LPDP Indonesia, for financing my PhD. I acknowledge Rijkwaterstaat-IHE Nature-based Solutions for their support in PhD fellowship which resulted in Chapter 3. Chapters 2 and 4 would become possible due to the fieldwork with partial financial support provided by Het Lammingafond.

SUMMARY

The over-exploitation of mangrove forests since the 1980s has led to biodiversity loss and coastal erosion in several parts of the world. Still, about 80-90% of mangrove restoration projects have been reported to fail. The main reasons are related to a poor understanding of the eco-geomorphological dynamics and mangrove species-specific ecological requirements. Although several guidelines are available, they are mostly site-specific, with a management focus on coastal protection schemes. A better system understanding of the feedback processes between mangrove forests and mudflat dynamics is required.

The thesis objective is to gain a better insight into complex eco-geomorphic interactions and feedback processes in coastal mangrove environments to the benefit of developing trustworthy tools for predicting their dynamics. To achieve the objective, the thesis describes the development of hybrid modelling by coupling the landscape-scale process-based hydro-morphodynamic model Delft3D-Flexible Mesh (DFM) and the individual-based MesoFON mangrove model (MFON). This coupled model (DFMFON) resolves the feedback process between seasonal and decadal environmental changes (waves, tides, river flow, sediment supply, salinity, and morphodynamics) and mangrove life-stages ranging from (dispersal of) propagules to development of seedlings and sapling into mature trees.

Since it covers a unique, rapidly progressing delta setting with concomitant mangrove expansion, Porong Estuary in Indonesia is used as a case study to validate the newly developed modeling tool (DFMFON). Imagery from off-the-shelf unoccupied aerial vehicles (UAV's) and satellites was used and groundthruthed to retrieve accurate mangrove structural attributes and mangrove belt dynamics. The DFMFON model successfully reproduced observed spatiotemporal (seasonal-decadal) mangrove development, like the age-height relationship, as well as morphodynamic delta features.

DFMFON was then used to explore optimizing mangrove restoration strategies and carbon sequestration capacity in coastal systems. Best results were obtained for higher level (above mean sea level) and patchy mangrove restoration schemes.

The observations and tool presented in this thesis open up possibilities to assess and gain a better system understanding of the interactions between mangroves and environmental drivers. DFMFON will be a helping hand in directing mangrove management schemes for climate change mitigation and adaptation

SAMENVATTING

De overexploitatie van mangrovebossen sinds de jaren tachtig heeft in verschillende delen van de wereld geleid tot verlies van biodiversiteit en kusterosie. Toch wordt gerapporteerd dat ongeveer 80-90% van de mangroveherstelprojecten mislukt. De belangrijkste redenen houden verband met een slecht begrip van de eco-geomorfologische dynamiek en ecologische, mangrovesoortspecifieke vereisten. Hoewel er verschillende richtlijnen beschikbaar zijn, zijn deze meestal locatiespecifiek en gericht op het beheer in kustbeschermingsprogramma's. Een beter systeembegrip van de feedbackprocessen tussen mangrovebossen en de dynamiek van de slibkusten is daarom belangrijk.

Het doel van dit proefschrift is om beter inzicht te krijgen in complexe eco-geomorfologische feedbackprocessen van mangrovebossen aan de kust, ten behoeve van de ontwikkeling van betrouwbare instrumenten voor het voorspellen van de hun dynamiek. Om dit doel te bereiken beschrijft het proefschrift de ontwikkeling van hybride modellering door het procesgebaseerde, hydro-morfodynamische model Delft3D-Flexible Mesh (DFM) op landschapsschaal te koppelen aan het individueel gebaseerde MesoFON-mangrovemodel (MFON). Dit gekoppelde model (DFMFON) beschrijft het feedbackproces tussen seizoensgebonden (en langere tijdschaal) veranderingen van omgevingsfactoren (golven, getijden, rivierstroming, sedimentaanvoer, zoutgehalte en morfodynamiek) en levensfasen van mangroves, variërend van (verspreiding van) propagulen en ontwikkeling van zaailingen tot jonge en volwassen bomen.

Aangezien het een unieke en zich snel ontwikkelende delta beschrijft inclusief de daarmee gepaard gaande mangrove-uitbreiding, wordt het Porong-estuarium in Indonesië gebruikt als casestudy om het nieuw ontwikkelde modelleringsinstrument (DFMFON) te valideren. Beelden van Unoccupied Aerial Vehicles (UAV's or Drones) en satellieten werden gebruikt om kenmerken van de mangroven en hun dynamiek te beschrijven. Het DFMFON-model reproduceerde met succes de waargenomen spatiotemporele (seizoensgebonden) ontwikkeling van mangroven, zoals de relatie tussen leeftijd en lengte en de morfodynamische delta ontwikkeling.

DFMFON werd vervolgens gebruikt ter optimalisatie van strategieën voor mangroveherstel en koolstofopslag ('carbon sequestration') in kust systemen. De beste resultaten werden verkregen voor mangroveherstel schema's op een hoger niveau (boven gemiddeld zeeniveau) en in kleinere blokken in plaats van grotere gebieden.

De observaties en het ontwikkelde modeleringsinstrument gepresenteerd in dit proefschrift bieden de mogelijkheid om een beter inzicht te krijgen in de interacties tussen mangroven en hun omgeving. DFMFON zal een helpende hand kunnen bieden bij het aansturen van mangroveherstelprogramma's voor de mitigatie van en aanpassing aan de klimaatverandering

IKHTISAR

Eksploitasi hutan mangrove secara berlebihan yang terjadi sejak tahun 1980-an telah mengakibatkan kehilangan biodiversitas dan erosi pantai pada beberapa bagian dunia. Apalagi dengan 80-90% pekerjaan restorasi mangrove telah dilaporkan mengalami kegagalan. Alasan utamanya adalah pemahaman yang kurang mendalam tentang dinamika ekogeomorfologis dan kebutuhan ekologis yang spesifik pada tiap spesies. Walaupun pedoman telah tersedia, pedoman tersebut kebanyakan dibuat berdasarkan pengalaman pada lokasi tertentu yang berfokus pada manajemen/ skema perlindungan pantai. Dengan demikian, pengetahuan akan sistem yang lebih baik pada proses timbal balik antara hutan mangrove dan dinamika dataran lumpur sangatlah dibutuhkan.

Tesis ini bertujuan untuk mendapatkan wawasan yang lebih baik pada interaksi ekogeomorfis yang kompleks dan proses timbal balik pada lingkungan pantai bermangrove yang bertujuan untuk mengembangkan alat bantu yang terpercaya untuk memrediksi dinamika tersebut. Untuk mencapai tujuan tersebut, tesis ini mendeskripsikan pengembangan dari pemodelan hibrid yang menggabungkan model hidromorfodinamik berlandaskan pada proses dan berskala-lansekap Delft3D-Flexible Mesh (DFM) dengan model mangrove berbasis individu MesoFON (MFON). Model gabungan ini (DFMFON) menyelesaikan proses timbal balik daripada perubahan secara musiman hingga dekade (gelombang, pasang surut, debit sungai, suplai sedimen, salinitas, dan morfodinamika) dan daur hidup mangrove dari (penyebaran) propagul hingga perkembangannya menjadi bibit dan anakan hingga pohon dewasa.

Muara Porong di Indonesia dipilih sebagai lokasi studi untuk validasi model (DFMFON) karena memiliki karakteristik unik berupa delta yang bertumbuh dengan cepat dengan ekspansi hutan mangrove yang mengikutinya. Citra dari pesawat nirawak dan satelit digunakan dan dikoreksi dengan data lapangan untuk mendapatkan atribut struktur mangrove yang akurat dan dinamika sabuk mangrove yang terjadi. Model DFMFON berhasil mereproduksi pengamatan perkembangan spasial dan temporal dari mangrove (musiman-dekade) berupa hubungan umur-tinggi, begitu pula fitur morfodinamis delta.

DFMFON kemudian digunakan untuk mengeksplorasi optimalisasi strategi restorasi mangrove dan kapasitas penguncian karbon pada sistem pantai. Hasil restorasi yang terbaik didapatkan ketika mangrove diletakkan pada elevasi yang cukup tinggi (di atas muka air laut rerata) dan skema restorasi dengan petak-petak dan berjarak.

Pengamatan dan alat yang disajikan pada tesis ini bisa membuka beragam kesempatan untuk menilai dan mendapatkan pemahaman akan sistem yang lebih baik pada interaksi antara mangrove dan faktor-faktor lingkungannya. DFMFON akan menjadi alat bantu yang cocok untuk mengarahkan skema manajemen mangrove untuk tujuan mitigasi dan adaptasi perubahan iklim

CONTENTS

1

INTRODUCTION

This chapter provides research questions and context of the PhD thesis.

1.1 CONTEXT

Values and functions of mangrove forests

Mangrove forests, in the past, were often misunderstood to be associated with a wasteland (Dahdouh-Guebas et al., 2020) with a smelly, rotten-egg-like environment and a swarm of mosquito-borne diseases (Yeo et al., 2021). That undervalued perspective is somewhat of a justification for clearing mangrove swamps, primarily in favour of aquaculture and agriculture (Hagger et al., 2022) or other developments. Between 2000 and 2016, a satellite remote sensing analysis study revealed that 62% of global losses of mangrove area were human-driven through land conversion (Goldberg et al., 2020). This decline mostly happened in developing countries, where the mangrove forests were cleared for other high-economic-value activities. Mangroves have been declining at an alarming rate, about 1-2% annually, even faster than coral reefs or tropical rainforests (Alongi, 2002; Duke et al., 2007). These factors make mangroves one of the threatened ecosystems.

In contrast to the previous justifications for mangrove forest deforestation, the loss of mangrove forests, in reality, deprives the population of the high intrinsic value of mangrove forests. The intrinsic values are derived from the high capacity of primary productivity, terrestrial ecosystem supports, and marine food webs (Dahdouh-Guebas et al., 2022). The presence of mangrove forests has proven to be an effective buffer for storm surges (De Dominicis et al., 2023). The effectivity of the wave attenuation function is non-linear, dependent on the width, density, and fragmentation of the forest (De Dominicis et al., 2023; van Zelst et al., 2021; Zhang et al., 2012) where scientists have acknowledged wave height reduction between 13 to 66% over 100m mangrove forest width (McIvor et al., 2012). Another benefit can be correlated with how communities perceive their relation with mangrove ecosystems in cultural non-materialistic interrelationships. Here, mangrove forests serve as places for recreational and intangible spiritual purposes for people (Das et al., 2022). These benefits have been recognised as the mangrove ecosystem services (Barbier et al., 2011; Mehvar et al., 2018), which can be divided into habitat, regulating services (e.g., regulating climate and disaster risk reduction), provisioning services (e.g., source of food), and cultural services (Das et al., 2022).

Mangrove forests under threat

Over-exploitation and loss of mangroves significantly impact biodiversity and the surrounding ecosystems (Carugati et al., 2018). A dramatic impact of mangrove forest loss to biodiversity can be seen, for example, in Indonesia – home of the largest mangrove forest, about 20% of the global mangrove area. The United Nations Environment Programme (UNEP) (2023) reports that large-scale mangrove land conversion to oil palm plantations, rice fields, and aquaculture is directly linked to habitat destruction and has endangered 41 bird species unique to mangrove forests. Winterwerp et al. (2020) report

a direct relationship between mangrove loss and the severe erosion of the muddy coast on Java's north coast, comprising about 44% of all coastlines. This is an alarming situation for the community, whose lives to a major extent depend on the mangrove ecosystem. In Demak, Central Java, aquaculture establishment close to the waterline and mangrove loss has resulted in self-accelerated coastal erosion (World Bank Group, 2018). Land subsidence and mismatch of infrastructure development aggravated the coastline retreat up to 1.5 km, where 70,000 people have been affected (Damastuti et al., 2022). That caused significant income loss for almost 80% of the village inhabitants (Winterwerp et al., 2016).

Impacts of climate change

The recent sixth assessment of the IPCC reports that human activities have caused 1°C global warming with already widespread and intensifying impacts (IPCC, 2022). The primary evidence of climate change impacts in coastal areas, among others, are sea level rise (SLR) and more frequent and stronger storms. The current estimate shows that 23% of the world population has been exposed to flood inundation of over 0.15 m in a 100-year return period (Rentschler et al., 2022). This figure may increase following the SLR scenario, where the frequency and intensity will become higher. When compounded with the changing patterns of precipitation in the hinterland, it increases the depth and duration of flooding in urbanised coastal cities, where more than 600 million people live in these low lying regions (Magnan et al., 2022; Merkens et al., 2016). The exposure to coastal flooding will increase with the growing population and social-economic activities, where the destruction effect will be multiplied.

Mangroves for climate mitigation

Sustainable approaches to mitigation and adaption measures are critical to address the impacts posed by climate change. The goal of mitigation is to reduce the amount of greenhouse gases in the atmosphere by reducing the sources or enhancing the carbon sink. As climate change is inevitable, followed by the global target of achieving net zero emissions by 2050 (Saintilan et al., 2023), the high potential of ocean and coastal ecosystems referred to as Blue Carbon Ecosystems (BCE) have been proposed as the natural climate solution (Macreadie et al., 2021). The BCE consists of tidal marshes, seagrass meadows, and including mangroves.

Owing to its co-benefit of carbon sequestration and climate adaptation, the potential of BCE for climate mitigation has been subject of extensive research (Kusumaningtyas et al., 2022). BCE has a disproportionally large carbon storage, storing half of carbon sequestration in the ocean while only occupying 0.5% of the sea floor (Macreadie et al., 2021). Even though the sequestering capacity highly varies among sites (Sidik et al., 2023), among the other ecosystems, mangrove forests have the highest rate of carbon sequestration (Kusumaningtyas et al., 2022; Zhu et al., 2022). The mangrove area,

nevertheless, can shift the role from carbon sink to carbon source when deforested. It is estimated, with global annual deforestation of 0.4% (Hamilton and Casey, 2016), that the carbon emitted due to the loss of mangroves will contribute to 3-19% of total carbon emission (Donato et al., 2011; Pendleton et al., 2012). Between 1996 and 2020, the global carbon stocks net reduction associated with mangrove loss was estimated to equal 139 megatonnes (Mt) (United Nations Environment Programme, 2023). This net reduction equals four times the carbon produced globally in 2018, originating from fossil fuels burning and cement manufacture. On the other hand, when rehabilitation attempts to increase mangrove extent can be achieved, the potential climate benefit can reach more than 424 Mt carbon by 2030 (Sasmito et al., 2023).

Mangroves for climate adaptation

Climate adaptation involves measures to reduce the risk and vulnerability to climate change already in the pipeline. Adaptation measures include building coastal defences, early warning systems, or setting the setback area. Traditionally, coastal defences are approached from an engineering perspective and comprise man-made or 'grey' structures. The grey structures are designed to interact and mitigate a specific part of the physical processes, e.g., waves, sediment transport, and water level (*Coastal engineering manual*, 2002; *Shore Protection Manual*, 1973). Given the continuous physical environment actions, grey structures require careful operations and likely costly maintenance to fulfil their design function and reach the expected service life (Cheong et al., 2013; Duarte et al., 2013). In mangrove-muddy coastal systems, the solutions using conventional permanent structures could lead to fragmentation and disruption of ecological connectivity of the mangrove ecosystem services (Borsje et al., 2011) or in the muddy coasts can induce scour due to the reflective surface (Winterwerp et al., 2020). Several studies mentioned the benefits of incorporating vegetation or ecosystem-based approach have been approved to be more sustainable and cost-effective compared to hard structure measures (Tiggeloven et al., 2022; van Zelst et al., 2021). The approaches utilising natural elements for coastal hazard mitigation, such as mangroves in this work are commonly termed Nature-based Solutions (NbS) (Narayan et al., 2016). Mangroves can aid climate adaptation with their coastal protection function (Temmerman et al., 2023), with the highest economic value per hectare (Macreadie et al., 2019). The role of mangroves as coastal defence is well appreciated. Many studies have shown mangrove functionality, such as a buffer from tsunamis (Dahdouh-Guebas et al., 2005) or attenuating wind waves and storm surges (Marois and Mitsch, 2015; Montgomery et al., 2018).

Coordinated actions

Acknowledging the wide range of ecosystem services, mangroves have been considered one of the high priorities with coordinated global communities for mangrove conservation (Friess et al., 2020). Countries have committed to their National Determination Contribution to conserve mangrove forests as a derivation of the Paris Agreement. Up to

the present time, countries and international organisations have been advocating green belt policies (Su et al., 2021). For example, the UN Framework Convention on Climate Change (UNFCCC. Secretariat, 2021), Australia (Kelleway et al., 2017; Morris et al., 2021), China (Fu et al., 2021), Engineering With Nature in the USA (Bridges et al., 2018; *Nature-Based Solutions Resource Guide*, 2022) or the US National Academy of Sciences agenda (Board and National Academies of Sciences, 2019), and Indonesia (Sasmito et al., 2023). Globally, mangrove restoration and conservation are in urgent need as targeted by UN Decades of Ecosystem Restoration 2021-2030, Sustainable Development Goals, and Aichi Biodiversity Targets. The global conservation community has committed to increasing mangrove cover by 20% in 2030 (Global Mangrove Alliance, 2021; Sasmito et al., 2023). Given the close deadline of both targets in climate change mitigation-adaptation and mangrove conservation, prompt actions in this recent year are critical. When it is successful, conserving the remaining and restoring degrading mangroves not only could mitigate climate change but also reduce the impacts to 296 million vulnerable population in tropical coastal region (Sasmito et al., 2023).

Altogether, recognising mangroves as nature-based solutions will include conservation, restoration, or ecosystem creation (Temmerman et al., 2023). Despite global commitment and optimism, conserving and rehabilitating mangroves should be ecologically sound. As an illustration, of the reported mangrove restoration projects, 80-90% experienced failures (Lewis and Brown, 2014). The reasons for failures are mainly a mismatch of mangrove species and lack of understanding of the eco-geomorphological characteristics and the mangrove species-specific ecological requirements (Ellison et al., 2020; Kodikara et al., 2017; Lewis and Brown, 2014; Primavera and Esteban, 2008). Additionally, it requires more than a decade for mangrove forests to reach their optimal forest capacity for mitigation-adaptation purposes. In order to achieve that objective, mid-course adjustment is often required, emphasising the need for operation and maintenance.

Mangrove restoration

Global targets have mandated mangrove restoration and conservation as one of the high priorities and are in urgent need (Friess et al., 2020) —recognising their multi-functionalities for climate mitigation and adaptation. Those ambitious targets have promoted a push for slowing down mangrove deforestation from annual average loss of 0.21% during 1996-2010 to 0.04% during 2010-2020 (*The State of the World's Mangroves 2022*, 2022). Nevertheless, many past restoration attempts have failed due to the misunderstanding of the mangrove wetlands' ecological-physical processes (Lee et al., 2019) and, or land (social) conflicts (Sasmito et al., 2023). At first, ensuring mangrove restoration success requires a mechanistic understanding of the ecological-physical processes, where current knowledge is segregated.

Several guidelines exist, either in mangrove restoration (Lewis, 2005; SER (Society for Ecological Restoration Science and Policy Working Group), 2002; Zimmer et al., 2022)

or focusing on the practical design (engineering) and management (procedures to achieve) on the mangroves' integration in the coastal protection (Bridges et al., 2021; Van Wesenbeeck et al., 2021; World Bank, 2016). Those guidelines have resulted from ongoing learning-by-doing processes (Aerts et al., 2014; Wilms et al., 2021; Winterwerp et al., 2020). Some guidelines remain quite site-specific, so that duplication of such approaches should be conducted carefully. However, given the dynamic nature of mangroves, it requires a system understanding from the tree, forest, and ecosystem levels. The system understanding requires field observation, periodic monitoring and assessment, and quantification approaches with modelling.

Need for prediction tools

Understanding the urgent needs mandated by global targets coupled with complexities and the state of the current knowledge mentioned above reassures us that advancing new knowledge in mechanistic understanding of mangrove-intertidal flat interactions is critical. Field observation and monitoring techniques have been experiencing rapid growth, for instance, the Global Mangrove Alliance initiative (www.mangrovealliance.org) with their mangrove restoration tracker and global mangrove watch. However, tools that can mechanistically assess and predict the process components and interactions of mangrove forest evolution are yet underdeveloped. Examples of these modelling tools resolving eco-geomorphological interactions are spatial and statistical models, followed by process-based and conceptual models (Rivera-Monroy et al., 2022). All of these approaches express mangrove dynamics as a top-down hierarchy. In this hierarchy, the response of the mangroves is averaged or pre-defined based on specific environmental conditions.

In light of climate change uncertainty, the pre-defined response of mangroves, as in a top-down approach, may not be valid under the changing physical-environmental stressors. Pretzsch (2009) suggests the system's understanding may be built upon integrating all known processes, components, and their interactions from the bottom up. As in our work, we could mechanistically model forest expansion, retreat, and colonisation influenced by physical-environmental drivers. In this regard, this research will contribute to obtaining more realistic projections of forest structure and eco-geomorphological change that account for the dynamic environmental conditions, for example driven by climate change.

1.2 INTERACTIONS BETWEEN MANGROVES AND ENVIRONMENT

1.2.1 Understanding mangrove dynamics

By definition, mangroves are plants thriving in the wedge of the intertidal zone (Spalding et al., 2010). Mangrove presence globally is limited within the (sub)tropics and warm temperate, between 30°N to 37°S (Mukherjee et al., 2014), and specifically located in a

sheltered waterlogged environment (Krauss et al., 2014; Sharma et al., 2022). Mangroves can only thrive in specific eco-geomorphological characteristics determined by their species-specific tolerance. For instance, the latitudinal range of mangroves is limited by the tolerance of mangroves to cold temperatures due to the efficient temperature range of photosynthesis (Ball and Sobrado, 1999) and limited capability to assimilate CO_2 in cold temperatures (Ward et al., 2016). Regional climate variability, such as precipitation and evapotranspiration, can affect mangrove zonation. In the condition of high net evaporation, dieback within the interior of a mangrove forest can occur due to an increase in salinity (Cortés, 2019). In contrast, during events of high precipitation, mangrove productivity increases (Gilman et al., 2007), and subsequent increase of mangrove area due to landward migration into the salt marsh zone because of the decrease in porewater salinity and sulfate concentration (Ward et al., 2016). More locally, hydrological forcings, e.g., river discharge, tides, and waves, determine the lateral expansion of mangrove forest, whereas soil biogeochemistry determine the structure, e.g., basal area and tree height (Jennerjahn et al., 2017). The regional scale geophysical description of coastal environments guided the ecological classification of mangroves into fringe, basin, scrub, or riverine mangroves (Twilley et al., 2017).

Utilising mangroves as a measure in the face of climate change uncertainty requires well-defined predictability of their functional capacity (Morris et al., 2018) and the potential to persistently restore after disturbance (Temmerman et al., 2023). However, mangrove capacity in attenuating waves, for example, varies over locations. It depends on the mangroves' biophysical characteristics (frontal area, density, and composition) and wave conditions (wave height and wave period), where the latter may benefit from highly detailed local observation or global hindcast. However, predicting the wave attenuation capacity, for instance, leads to a logistical challenge for forest inventory to carry out on the ground (Bispo et al., 2019) as it is labour intensive. Studies have used different proxies to characterise the forest, e.g., forest age (Maza et al., 2021a), characterisation of mangrove root structure (Mori et al., 2022), and remote sensing (Beselly et al., 2021). Attempts to approximate short-period wave propagation through vegetation fields have been formulated in the earliest original work by Dalrymple et al. (1984) and adapted in several recent works, e.g. Maza et al. (2019) and Mendez and Losada, (2004). The formulation requires an estimation of vegetation bulk drag coefficient (C_D) where it is typically obtained through field measurement (Horstman et al., 2021) or flume experiments (van Hespen et al., 2021). Another approach is to estimate C_D as a function of mangrove projected area and volume (van Maanen et al., 2015).

Mangroves have species-specific critical thresholds on the physical-environmental forcings that control their establishment or collapse. As an effect, these species-specific thresholds influence how we can predict the mangrove forest evolution and, therefore, measure persistence capacity. To add complexity, the critical thresholds are also varied

over the life-stages (propagule, seedling, sapling, mature). The natural successful establishment would require propagule availability (Lewis, 2005), where the parental trees could be from the vicinity or adjacent as the propagules could float up to several months and be transported by hydrodynamic processes within short/long distances (Shih et al., 2022). Successful seedling recruitment requires propagules to survive the Window of Opportunity (WoO), where external disturbances remain within their critical threshold. This WoO concept (Balke et al., 2011) determines the set of species-specific thresholds on 1) the inundation-free phase, where a propagule can germinate and anchor the root within the low tide period, 2) a calm wave period, where waves remain low enough to prevent the seedling dislodgment, and 3) limited accretion-erosion, where the accretion will lead to burial and suffocate the seedling while erosion can lead to toppling and dislodgement (Balke et al., 2014, 2013). Seedling establishment is an important factor in the forest's lateral (horizontal) expansion (Shih et al., 2022; van Hespen et al., 2022a). The species-specific optimum mangrove (vertical) growth is reduced by their local environmental conditions, i.e., salinity, pH, and hydrogen sulphide (Berger et al., 2008; Chen and Twilley, 1998; Grueters et al., 2014) in addition to the competition with the neighbouring trees. The inter-specific competition to sources (space, nutrients, light, and reduced by environmental forcings) limits the growth and, hence, leads to mortality.

1.2.2 Mangrove-mudflat interactions

Mangroves interact with the environment and provide feedback (Figure 1.1) dependent on the three factors in the physical processes, i.e., nutrients as the resources, salinity as the regulators, and sea level/hydroperiod (Grueters et al., 2014; Krauss et al., 2014; Wimmler et al., 2021). These factors are intertwined and affect the growth and productivity of mangroves by regulating the zonation of the mangrove forest as an influence on the porewater salinity distribution (Lovelock et al., 2006; Piou et al., 2006), limiting the growing capacity due to the availability of the chemical/ biochemical nutrient (Lovelock et al., 2006; Reef et al., 2010), and defining the spatial expansion dependent on the tidal flooding and duration (Balke et al., 2015; Lovelock et al., 2015). These factors determine the mangroves' growth, dieback, and seaward expansion (through tree recruitment).

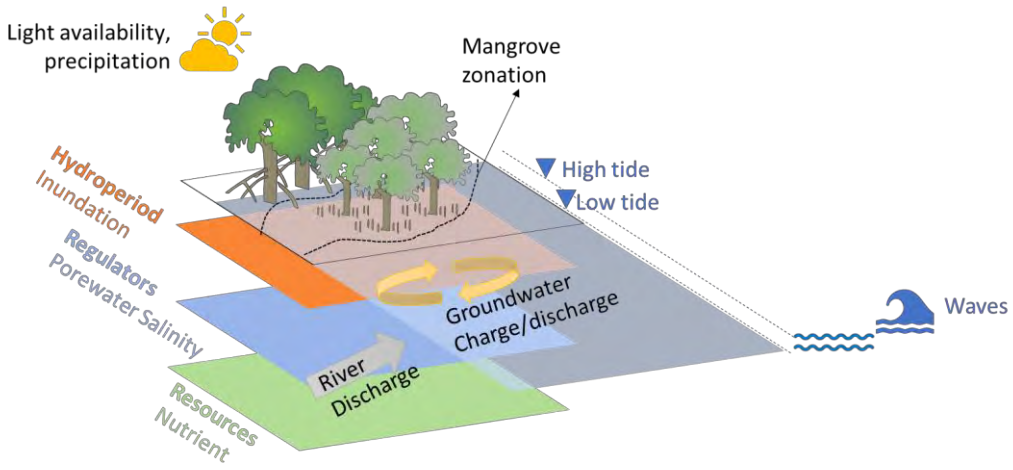

Figure 1.1. Schematic of hydrological factors (tides, waves, groundwater, and river discharge) and the regulating-resources factors along with the hydrological connectivity between mangrove forest and coastal waters (adapted from Rivera-Monroy et al., (2022))

Spatially explicit processes and feedback between mangroves and soil can be explained in three vertical soil layers, as in Figure1.2. The relatively stable layer that comprises bedrock is located at the very bottom of the soil. In this layer, the movement is merely related to the geologic processes. Thus, it is assumed to remain stable along the life of the mangrove stands (Krauss et al., 2014). Above the deep layer, sub-surface layer processes are mainly related to the mangroves' rooting system (Cahoon et al., 2003; McIvor et al., 2013; McKee, 2011). The root production contributes to the increase in soil volume and the sub-surface elevation gain.

On the other hand, following the decomposition and compression of the roots after dieback, shallow subsidence may occur as root remnants take less space, decrease soil porosity, and promote soil collapse. Moreover, the shrink-swell of soil can be referred to as the increasing and decreasing soil water content due to the water absorption of the roots. In short, the subsurface processes comprise biological factors due to root production-decomposition and the physical factor in soil compaction and shrink/swell (Roskoden et al., 2020). The top and the most active layer is related to the surface processes that dynamically interact with the seawater. Here, the active processes are governed by hydrodynamics due to waves, tides, storm surges, and interactions with the mangrove's roots, stem, and canopy. This layer represents the transport and fate of materials in the form of sediment transport, nutrient exchange, salinity mixing, and mangroves' seedlings dispersal. The materials can be derived from outside of the mangrove forest (allochthonous) and inside the mangrove forest (autochthonous) (McIvor et al., 2013).

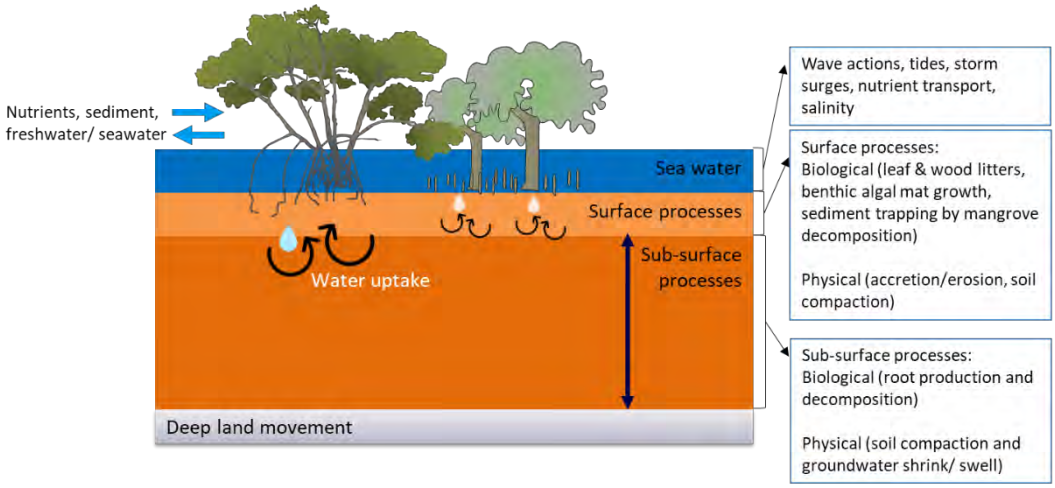

Figure 1.2. Illustration of the conceptual model mangroves-soil interactions adapted from (Krauss et al., 2014). The interactions in soils are presented in three layers: the static and stable deep land movement layer, the sub-surface layer related with root growth and decay processes, and the active layer associated with the hydromorphodynamic processes. Mangrove trees responded with growth, dieback, and tree recruitment, providing new environmental feedback (adapted from Krauss et al., (2014)).

1.2.3 Modelling the interactions

1.2.3.1. Eco-geomorphic hierarchical approach

Due to the high variety of mangrove ecosystems, hierarchical approaches based on the biophysical characteristics describing their abiotic controls (hydroperiod, resources, and regulators, see section 1.2.2) have been adopted and recommended (Krauss et al., 2008; Rivera-Monroy et al., 2004). This approach can be adopted, for example, at geomorphological level, such as assessing mangrove vulnerability due to sea-level rise (Lovelock and Ellison, 2007), at forest levels such as in the ecological mangrove restoration technique (Lewis and Brown, 2014) that provide structured restoration attempts by considering wetland's geomorphology and hydrology, and a detailed tree-level investigation on nutrition competition and hydroperiod effect on growth and change in community structure (Rivera-Monroy et al., 2004). It shows how mangrove ecosystems interact and operate on different spatiotemporal and life-stage scales. Any disturbance on each hierarchy would alter the ecosystem processes and may cascade into the higher hierarchical level and, in turn, affect the interactions and traits of the abiotic-biotic component at the lower levels. For example, if the change in sea level exceeds the sediment build-up, it may lead to the collapse and reorganisation of mangrove zonation. To this end, no single model is capable of representing and simulating the processes

encompassing all levels; they were designed to explain processes occurring at their own level (Rivera-Monroy et al., 2022).

1.2.3.2. Model classifications

A mangrove ecosystem model is essential to assess and predict forest structure development. Still, ecological models need to parametrise interactions and processes in mangrove wetlands because it is impossible to cover the entire spectrum of spatial scales and time scales involved in mangrove biocomplexity. In other words, a model should be complex enough to pay tribute to the complexity it aims to describe but simple enough to understand what is going on. Mangrove ecosystem models can be classified into conceptual, statistical, spatial, and process-based (Rivera-Monroy et al., 2022).

Conceptual models

Conceptual models draw the intercorrelation causal effect of bio-complex responses with the change of stressors and the related attributes varying from the habitat unit to the global scale (Davis et al., 2005; Day et al., 2008). An example of the conceptual model is the windows of opportunity during calm periods on the variability of tides and winds to determine the recovery of salt marsh, mangrove, and floodplain vegetation (Balke et al., 2014). The authors used a time-series analysis of the water level and calculated how long the low water level lasted with respect to bed level, defined as an undisturbed period. The undisturbed period is then compared with the threshold of the inundation-free period required for each ecosystem to determine whether such an ecosystem is capable of establishing. The same holds for windspeed, where the threshold of low wind velocity period should prevail to estimate the establishment of the vegetation.

Statistical and spatial models

Statistical and spatial models are the most widely used, accounting for 60% of the papers reviewed (Rivera-Monroy et al., 2022). It is partly because of the increasing (open) data availability, such as satellite constellation Sentinel (European Space Agency, 2015) by the European Space Agency and Landsat (USGS, 2013) by the NASA/USGS mission and the improvement in satellite sensor resolution and monitoring frequency. The development of open tools and processing methods, especially attributed to the cloud computing analysis, for instance, Google Earth Engine (Gorelick et al., 2017), allows for global and near-daily to weekly analysis of satellite imagery. The dominant usage of those big spatial datasets is to update mangrove inventory maps (United Nations Environment Programme, 2023). When complemented with field-based observation and statistical models, these maps can be used, for example, to evaluate mangrove spatial distribution (Bunting et al., 2022) and assess carbon stocks (Murdiyarso et al., 2015). The statistical models utilise the curated information of either remotely sensed or field-based datasets to infer the relationship between environmental variables and mangrove biophysical

characteristics. For instance, an estimate of global mangrove above-ground biomass based on the climate, assuming mangrove biomass corresponds to temperature and precipitation (Hutchison et al., 2014). Although the application of statistical and spatial models has played an important role in explicitly explaining, e.g., the drivers of mangrove loss and gain (Hagger et al., 2022) or impacts of climate change on mangrove carbon stocks and fluxes (Alongi, 2022), what empowers this approach is also the major limiting factor, which is the datasets. The available dataset is rarely long enough or lacks consistency (Macreadie et al., 2019; Sharma et al., 2022; Zimmer et al., 2022). The information gap may add complication in validating the prediction of the fate of the mangrove ecosystem on the climate uncertainty scenarios.

Process-based models

Process-based, sometimes known as mechanistic models (Cox et al., 2006), are numerical representations based on explicit causal mechanisms or processes on how the systems work, grounded in proven scientific knowledge (Cuddington et al., 2013; Roelvink and Reniers, 2012). The explicit nature of process-based in representing reality and its transparency on the assumptions of the processes provide more confidence in understanding phenomena either in hindcast or forecast simulations, see the works by van der Wegen et al. (2011) in hindcasting and van der Wegen and Roelvink, (2008) for forecasting. In this thesis, we define process-based for two subclasses, i.e., hydro-morphodynamic and vegetation dynamic model. Process-based hydro-morphodynamic models have long been used in wetland analysis, e.g., modelling estuarine hydrodynamics (Thanh et al., 2017), wave attenuation (Yoshikai et al., 2023), tidal circulation (Horstman et al. 2015), and sediment dynamics (Willemsen et al., 2016). Another sub-class, the vegetation dynamic model, aims to simulate the mangrove forest trajectory.

Process-based: hydro-morphodynamics

Process-based hydro-morphodynamic model, in this context is identical to abiotic processes, e.g., hydro-morphodynamics (Roelvink and Reniers, 2012). We can find examples of hydro-morphodynamic models in the application of mangrove wetlands, such as the investigation of tidal circulation within the wetland (Horstman et al., 2015), wave attenuation function of mangrove forests (De Dominicis et al., 2023; Pelckmans et al., 2023), and effect on hydrodynamic and sediment exchange (Bryan et al., 2017; Nardin et al., 2016). Simulation exercises above assumed that physical processes occur in a static vegetation state, ignoring forest structure changes. Those studies commonly include detailed spatially-varying hydro-morphodynamic-ecology interactions in a relatively limited vegetation time scale (seconds to weeks) where vegetation development within that period can be assumed does not significantly affect hydrodynamics (Bryan et al., 2017; Friess et al., 2012; Nardin et al., 2016). Therefore, the model structure does not allow the inclusion of the feedback loop mechanisms of environmental (abiotic) changes to vegetation growth (biotic).

Process-based: vegetation dynamics

The detailed physical processes involved in the hydro-morphodynamic model have proven to be capable of elucidating mangroves' functional capacity on the physical drivers (van Hespen et al., 2022a). However, the persistence or capacity to recover in mangrove forests is reflected in their ecological processes, which occur on a longer time scale, and encompass life stages from seedling to mature trees (Wang et al., 2014). Over time, mangrove forest structure and composition will change in response to environmental conditions. Evidence can be obtained from past studies observing the vegetation dynamics based on satellite imagery or aerial photographs, which take years to decades of observation. For example, a study by Kleinhans et al., (2019) shows the migration and succession of riparian vegetation due to the river meandering process and the impacts of mangrove extent variation to estuarine hydro-morphodynamics in Waikaraka Estuary, New Zealand (Glover et al., 2022). With this in mind, introducing the co-evolution of morphology and vegetation has an important role in providing a process understanding of the interactions of vegetation and physical drivers. We describe vegetation dynamic models in two types: population dynamic and Individual-based Model (IBM).

a. *Vegetation dynamics – population dynamic*

   One approach to simulate vegetation dynamics is the population dynamic model, assuming the composition of individuals who share similar traits (e.g., species and biophysical properties) are grouped on a grid/ plot and behave under a set of rules (Cappuccino, 1995). This grid-based population model can change simultaneously depending on the endogenous (e.g., density, above-belowground biomass) and exogenous factors (e.g., inundation frequency, wave energy). To our knowledge, many studies focused more on the dynamics of mangrove primary productivity, e.g., the phenology of *Rhizophora apiculata* on seasonal climate variation (Christensen and Wium-Andersen, 1977), the effect of nutrient availability on *Rhizophora mangle* (Onuf et al., 1977), biomass production of *Rhizophora apiculata* (Christensen, 1978), and effect of nutrient and irradiance to seedling growth of *Ceriops australis* and *Ceriops decandra* (Ball, 2002). Exception is in Thi Ha et al., (2003), where they investigate the seasonality of seedling growth and production rates of *Kandelia candel*. The main issue in population dynamic models, specifically in mangrove, is not able to treat propagule dispersal. Instead, consider individuals within populations following homogenous behaviour without individual variation (Jørgensen and Fath, 2011).

b. *Vegetation dynamics – individual-based*

   Another approach is the IBM, where populations and communities are composed of discrete individuals and emerge by following the feedback loop of individual

interactions with their environment (DeAngelis and Grimm, 2014). Individual organisms (biotic) are considered explicitly with their variability, local interactions, and specific adaptive behaviour in their physical environment (Grimm and Railsback, 2005), where they distinguish themselves from each other. Individuals can have different growth, survival probability, or reproduction capacities due to their relative position with other individuals (competition/endogenous factor) and with regards to the environmental conditions (exogenous factor). In this approach, individuals have self-directed motivation and adapt or modify their environment through their actions (Jørgensen and Fath, 2011). The main challenges in IBM modelling are their extensive computational requirement to run in large spatial scales (>1 km^2) and the need for long-term species-specific biophysical characteristics datasets. With the growing number of field datasets available and advances in IBM architecture, there is a possibility to improve IBMs performance.

Integration of vegetation dynamics and hydro-morphodynamics

In recent years, few attempts have been made to integrate two-way couplings of biotic-abiotic processes. In wetland modelling, several studies have attempted to include complex interactions on ecology, hydrodynamic, and morphological changes. This eco-morphodynamic modelling: ranges from riparian (Oorschot et al., 2016), salt marshes (Best et al., 2018; Brückner et al., 2019), and mangroves (van Maanen et al., 2015; Xie et al., 2020). Those models were based on well-appreciated knowledge of hydro-morphodynamic processes. They assumed an abundant supply of seedlings to fill the numerical grid when the inundation threshold allowed, indicating colonisation. Meanwhile, the numerical grid area is a proxy to explicitly define above-ground competition for resources (maximum density or biomass capacity), which drives growth and mortality. Eventually, the models do not consider the dispersal mechanism in a smaller time scale (Friess et al., 2012; Piercy et al., 2023) that is closely correlated with hydrodynamic processes (Duke et al., 1998; Shih et al., 2022), which determines vegetation establishment and lateral expansion. On the other hand, the development of IBM has incorporated abiotic interactions in a somewhat limited way. One example is MANGA (Bathmann et al., 2020), which includes mangrove's effect on groundwater salinity by coupling IBM with OpenGeoSys. Integrating IBMs with abiotic processes is still mainly occurring in plot scale and short period. Despite already including the complex abiotic-biotic interactions, all integrated models discussed still lack representation of feedback loop processes at each life stage. Thus, it can be a challenge when we want to assess the wetland responses on non-stationary drivers such as variation in wave climate, sediment supply and multispecies vegetation dynamics.

1.3 RESEARCH GAPS IN MODELLING MANGROVE-ECO-HYDRO-MORPHODYNAMIC

Detailed mangrove dynamics

Despite the increasing number of numerical models evaluating the physical-ecological processes, those models still focus on the detailed abiotic interactions and use 'prescribed' ecological interactions, and thus may not reflect the actual mangrove dynamics, losing the important interactions at the lower level. Examples are models that consider interactions of the wave, tidal, and sediment trapping efficiency in mangrove forests but do not include dynamic ecological processes (Willemsen et al., 2016), simulation of morphological evolution in sandy tidal embayments with aggregated mangrove feedback (van Maanen et al., 2015), and mangrove response to sea-level rise with pre-defined species composition concerning inundation depth (Buffington et al., 2021; Rodríguez et al., 2017; Xie et al., 2022). Mechanistic interactions should consider the full life stages of the mangrove from propagule, seedling, sapling, and to mature tree. An important note is given in (Zainol et al., 2022) on the role of propagule dispersion in determining colonisation and regeneration of mangrove forests, which is affected by hydrodynamic processes (Shih et al., 2022).

Optimising restoration strategies

There have been explicit approaches in mangrove restoration attempts; examples are ecological restoration (Lewis and Brown, 2014) and assisted rehabilitation/ planting (Primavera et al., 2011). Even though these approaches have considered the hydro-morphology and ecological system in the planning, they lack mechanistic understanding as time progresses. Therefore, restoration practice is still site-specific and results from long trial-and-error processes (Primavera and Esteban, 2008; Tom Wilms et al., 2021). While the (long-term) prediction of the abiotic system has been well understood, e.g., in Roelvink et al. (2020) and van der Wegen et al. (2011), when the biotic system is involved, either the spatiotemporal scale may be reduced to include details (Bryan et al., 2017) or such simplification in vegetation dynamics should be required (Brückner et al., 2020). The lack of spatial-explicit understanding of the biotic-abiotic system encompassing local to ecosystem scales may hinder successful restoration attempts. When looking at the global targets, the approaching deadline to cut carbon emissions and climate actions require prompt solutions in developing restoration strategies. Therefore, a full life stage process-based model may be a helping hand to understand the interactions and the important factors determining a successful restoration.

1.4 RESEARCH OBJECTIVE

This study aims to assess the importance of complex eco-geomorphic interactions and feedback processes of physical-environmental drivers in coastal mangrove environments to the benefit of developing trustworthy tools for predicting mangrove forest dynamics, to be used, for example, in the design of mangrove restoration strategies.

1.5 RESEARCH QUESTIONS, APPROACH, AND OUTLINE

1.5.1 Research questions and approach

To achieve the research objective, several research questions have been formulated:

1. What are the various timescales of mangrove dynamics on a prograding delta?

   Using the Porong Delta in Indonesia as a case study, we investigate the mangrove dynamics on a prograding delta by means of integrating Unoccupied Aerial Vehicle (UAV) and satellite imagery. We explore how to use very high-resolution photogrammetry techniques to derive field-scale mangrove biophysical properties (canopy height and individual position of the mangroves) as well as to discover seasonal patterns of mangrove dynamics by combining optical and synthetic aperture radar satellite datasets from different constellations (Landsat and Sentinel). Data obtained will be used to validate the process-based mangrove-eco-hydromorphodynamic model.

2. What is the skill of a mangrove-morphodynamic model that explicitly represents biocomplex interactions of individual mangroves and physical-environmental stressors?

   To consider the complex eco-geomorphic interactions of mangroves and physical environmental stressors, we develop a hybrid modelling approach that couples the landscape-scale process-based hydro-morphodynamic model Delft3D-Flexible Mesh and the individual-based MesoFON mangrove model. The coupling of these different model paradigms covers the temporal resolution of tides, seasonal, and decadal environmental changes (water level, flow, sediment availability, and salinity) with full mangrove life-stages from propagule, seedling, sapling into mature including short/long distance propagule dispersal.

3. Can we optimise the design of mangrove restoration strategies in support of carbon sequestration optimization?

   Applying the validated eco-geomorphodynamic model, we predict the mangrove forest trajectory under mangrove restoration strategies with the inclusion of detailed physical-environmental scenarios to optimise carbon sequestration

potential in an open coastal setting. The landscape and intertidal flat development are simulated and assessed for a period of 20 years, with multispecies of mangroves.

1.5.2 Outline of the thesis

The thesis is outlined with research questions and context of the research introduced in Chapter 1. Chapter 2 explains the influence of seasonal hydrological variation and sediment load on delta formation and mangrove ecosystem dynamics through UAV and satellite imagery analysis. Chapter 3 provides a detailed description of the new coupled process-based and individual-based models. Chapter 4 describes the configuration of strategic mangrove restoration to increase carbon sequestration potential. Finally, Chapter 5 summarises the findings and discusses the recommendations for future research.

2

MONITORING MANGROVE-MUDFLAT DYNAMICS: INTEGRATION OF UNOCCUPIED AERIAL VEHICLE AND SATELLITE IMAGERY

This chapter is based on the following publication:

Beselly, S.M., van der Wegen, M., Grueters, U., Reyns, J., Dijkstra, J., Roelvink, D., 2021. Eleven Years of Mangrove–Mudflat Dynamics on the Mud Volcano-Induced Prograding Delta in East Java, Indonesia: Integrating UAV and Satellite Imagery. Remote Sensing 13, 1084. https://doi.org/10.3390/rs13061084

Abstract: This chapter presents a novel approach to explore mangrove dynamics on a prograding delta by integrating unoccupied aerial vehicle (UAV) and satellite imagery. The Porong Delta in Indonesia has a unique geographical setting with rapid delta development and expansion of the mangrove belt. This is due to an unprecedented mud load from the LUSI mud volcanic eruption. The mangrove dynamics analysis combines UAV-based Structure from Motion (SfM) photo-grammetry and 11 years (2009–2019) satellite imagery cloud computing analysis by Google Earth Engine (GEE). Our analysis shows unique, high-spatiotemporal-resolution mangrove ex-tent maps. The SfM photogrammetry analysis leads to a 3D representation of the mangrove canopy and an estimate of mangrove biophysical properties with accurate height and individual position of the mangroves stand. GEE derived vegetation indices resulted in high (three-monthly) resolution mangrove coverage dynamics over 11 years (2009–2019), yielding a value of more than 98% for the overall, producer and consumer accuracy. Combining the satel-lite-derived age maps and the UAV-derived spatial tree structure allowed us to monitor the mangrove dynamics on a rapidly prograding delta along with its structural attributes. This analysis is of essential value to ecologists, coastal managers, and policymakers.

Keywords: Mangroves; Remote Sensing; Google Earth Engine; SfM Photogrammetry; UAV

2.1 INTRODUCTION

Mangroves are trees or large shrubs that grow in or adjacent to the intertidal zone and are distributed along (sub-)tropical coasts and estuaries (Spalding et al., 2010; Van Bochove et al., 2014). Mangroves are well-known for providing a range of ecosystem services such as timber production, carbon sequestration, soil formation, nutrient cycling, habitat creation for marine and terrestrial species, and protecting coastlines by attenuating waves and limiting erosion (Hill et al., 2020; Murdiyarso et al., 2015; Van Bochove et al., 2014). However, land use conversion has caused mangrove forests to decline at a rate three to five times larger than the average forest loss. Hence, mangroves' important ecosystem services will be diminished (Van Bochove et al., 2014).

In order to gain a better understanding of the value of important ecological services provided by mangroves, further efficient collection of data, e.g., mangrove extent, height, individual position, and species membership are necessary. Earth observation offers a method for the large-scale monitoring and assessment of the environment, especially when it comes to the mangrove forest inventory and spatial extent monitoring that are generally difficult to carry out on the ground (Bispo et al., 2019). Mapping mangrove forests is one of the most challenging tasks in remote sensing since the forests are mostly quite large, located in a remote area, and persistent cloud cover in the tropical areas (Gillis et al., 2014; Van Bochove et al., 2014; Walters et al., 2008). Several efforts have been made to monitor the spatial extent of mangrove forests from local to the global scales. Two global-scale mangrove extent maps were released for 2000, i.e., the World Atlas of Mangrove (WAM) (Spalding et al., 2010) and the Global Mangrove Forest Distribution v1 (GMFD) (Giri et al., 2011). Other current global products are the Continuous Global Mangrove Forest Cover for the 21st Century (GCMFC-21) that showing annual global mangrove forest cover from 2000 to 2012 (Hamilton and Casey, 2016) and Global Mangrove Watch (GMW) v2.0 (Bunting et al., 2018).

Information on important structural attributes of mangroves such as tree height, age, and diameter at breast height at 130cm above the ground (D_{130}) is required to characterise the mangrove forest stands. Accurate information of tree height is essential, since there is a high correlation of the height and the D_{130}, basal area (BA), and above ground biomass (AGB) (Bispo et al., 2019; Feldpausch et al., 2012). Mangrove forests with their harsh physical conditions hinder surveyors from carrying out direct measurements in the field. In principle, a number of remote sensing approaches have been developed as supplement or substitute for ground-based inventory (Lucas et al., 2020; Navarro et al., 2020, 2019, p. 1; Otero et al., 2018). A Canopy Height Model (CHM)—that is, a three-dimensional representation of the forest—can be derived by using airborne or terrestrial LiDAR, Synthetic Aperture Radar (SAR), and high-resolution optical imagery (Lagomasino et al., 2016).

Global satellite datasets such as Shuttle Radar Topography Mission (SRTM) and ICESat/GLAS [16,17], and ICESat-2/ATLAS launched in 2018 (Narine et al., 2020) have proven to be useful in deriving canopy height, but they were released in a medium resolution of 30 m × 30 m. TanDEM-X InSAR, a DEM product developed by the German Space Agency (2011–2015) with a ground resolution of 12.5 × 12.5 m, has also been used to estimate canopy height (Lucas et al., 2020). Recently, Very High Resolution (VHR) CHM derived from Unoccupied Aerial Vehicle (UAV)-based Structure from Motion (SfM) Photogrammetry has been deployed (Lagomasino et al., 2016; Otero et al., 2018) often at a local scale. The SRTM, ICESat, and TanDEM are the most commonly utilised methods to estimate CHM since they have global coverage, and the data are easily accessible (T. Hu et al., 2020). However, the passive/optical sensors solely obtain surface canopy information, and radar has at least limited penetration capability (T. Hu et al., 2020).. LiDAR, on the other hand, is able to penetrate the canopy cover to some extent depending on the acquisition design and lidar system (Wulder et al., 2012). However, this technique can be associated with high cost which limits the use of this system (T. Hu et al., 2020; Lagomasino et al., 2016).

This study takes the Porong Estuary, Indonesia, as a case study. Porong Estuary provided a unique setting as this area is characterised by a rapidly prograding delta and concomitant mangrove expansion (Karyadi et al., 2012; Mazzini et al., 2007; Sidik et al., 2016). It is because of the mud volcanic eruption in 2006 and subsequent mudflow diversion known as LUSI (acronym of lumpur (mud) and sidoarjo (the regency name)) (Karyadi et al., 2012). Several studies have been conducted to investigate the effects of LUSI's high sediment load on the Porong River, the Porong Estuary, and surrounding coastal waters (Jennerjahn et al., 2013; Kure et al., 2014; Sidik et al., 2016) and the development of mangrove on the created wetland in general (Hamzah et al., 2015; Setiawan et al., 2019; Sidik et al., 2013). However, none of them explored the mangrove dynamics and investigated the structural characterisation of the mangroves in the rapidly prograding delta.

This study aims to analyse mangrove dynamics on a rapidly prograding delta by a novel integration of UAV SfM Photogrammetry and multiple sources of satellite imagery in cloud computing Google Earth Engine (GEE). The first objective of this study is to retrieve mangrove biophysical properties (height and individual location of trees) employing the off-the-shelf UAV SfM photogrammetry, in combination with ground-truthing based on field data. The second objective is to generate a three-monthly classification of mangrove areas using Landsat 7, Landsat 8, Sentinel 1, and Sentinel 2 in GEE. These mangrove extent maps represent the dry season and wet season, where two maps were created during each of these seasons every three months. The third objective is to estimate the mangrove age and age-height relationship based on the combination of UAV and GEE analysis.

2.2 MATERIAL AND METHODS

2.2.1 Study area

The Porong Delta, as presented in Figure 2.1 is located in East Java Province, Indonesia (7.569 S, 112.872 E). It is approximately 37 km southeast of Surabaya, the second-largest city in Indonesia. It has a monsoon climate with a dry (April-September) and wet (October-March) season (Badan Meteorologi dan Geofisika, 2020), in which the high precipitation contributes up to 80% of the mean annual precipitation (Aldrian et al., 2008). The Porong River is one of the two major branches of the Brantas watershed. The watershed is regulated with several large dams, barrages, and flood gates. During the dry season, the flow is diverted to Surabaya, and therefore the flow in the Porong River is often reduced to almost zero (Hoekstra, 1989a). During the wet season flood discharge is diverted from the upstream barrage and high precipitation contributes to high river flow that discharges into the Madura Strait (Jennerjahn et al., 2013; Kure et al., 2014). Madura Strait has a micro to the meso-tidal range and is categorised by a mixed diurnal-semidiurnal tide (Hoekstra, 1989b).

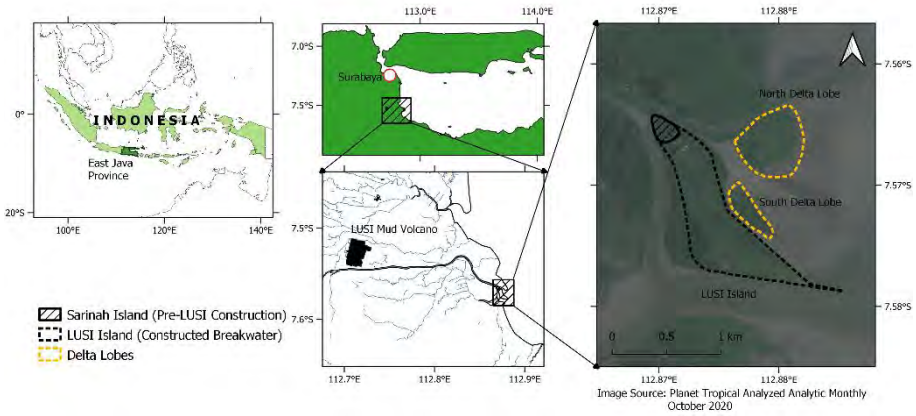

Figure 2.1. The study area is described in a sequence: (A) Indonesian border (light green) with East Java Province depicted in dark green, (B) East Java Province and the capital city Surabaya (represented as a red circle), (C) LUSI (lumpur (mud) and sidoarjo (the regency name)) mud volcano represented as a black polygon, and the Porong River as the black line flowing from the west to the east part of the map, and (D) Porong Estuary with LUSI island and the delta lobes.

The Brantas river originates from the volcanic complex of the Semeru and Arjuno Mountains (Hoekstra, 1989a). Erosion rates on the slopes of Mount Semeru are among the highest recorded in the world (105–106 m3 km−2 a−1) (Lavigne, 2004). Sediment yield in several drainage basins of Mount Semeru is dominated by rain-triggered events during the wet season (Aldrian et al., 2008; Lavigne, 2004). The Brantas watershed is

densely populated and affected by anthropogenic activities such as deforestation, intensive agriculture (mainly rice cultivation), and industries (Jennerjahn et al., 2004). Due to the geological conditions consisting of the presence of easily erodible soils and high anthropogenic activities, surface erosion is high (Hoekstra, 1989a). The Porong River drains off high sediment loads, causing a prograding delta (Jennerjahn et al., 2004; Milliman and Syvitski, 1992) with a progradation rates of approximately 0.4 × 106 m2 y−1 over the 1935–1981 period (Hoekstra, 1989a; Sidik et al., 2016).

In addition to the sediment load due to runoff from the hinterland, the Porong River has been experiencing an extreme sediment load due to the mud volcanic eruption in Sidoarjo, Indonesia. The LUSI mudflow is reported to be the 'largest mud eruption in the world' (Mazzini, 2018), about 18 km west of Porong Delta (Figure 2.1). On 29 May 2006, the boiling mud erupted at a peak flow rate of up to 180,000 m3 day−1 (Mazzini et al., 2007) which declined to 50,000 m3 d−1 in September 2011 (Karyadi et al., 2012). Sixty thousand residents were forced to evacuate, and 7 km2 of residential area was submerged with mud (Mazzini, 2018) (Figure 2.2a). The excessive LUSI is still actively erupting material, gas, water, clasts, and oil, albeit at a considerably reduced rate (Mazzini, 2018). The continuous discharge of mud has been diverted to the Porong River since 2007 (Karyadi et al., 2012). To reduce damage to the nearby community and environment, the mud in LUSI is first stored in a reservoir contained by 10-m-tall dyke and then diluted and disposed of by pumping to the river (Mazzini, 2018; Sidik et al., 2016). This operation has increased sediment concentration and loads of the Porong River by a factor of 3–4 compared to pre-LUSI conditions (Jennerjahn et al., 2004; Karyadi et al., 2012; Sidik et al., 2016). As shown in Figure 2.2b, due to the mudflow, the delta is rapidly prograding along with the development of mangrove belts. To date, the LUSI mud volcano is still erupting with no end in sight (Mazzini, 2018).

The delta lobes (Figure 2.1) have naturally developed, while LUSI Island was created as a spoil bank to contain sediment dredged from Porong River, after severe siltation due to the mud diversion operations. It was constructed between February and November 2009 by building a 4 km series of geotube breakwaters which were attached to the natural existing Sarinah Island (Karyadi et al., 2012). In 2009, 5000 *Avicennia* spp. seedlings were planted at this newly created wetland (Karyadi et al., 2012; The Jakarta Post, 2009), and the Ministry of Marine Affairs and Fisheries continued planting thousands of Rhizophora spp. seedlings between 2010 and 2011 (Hamzah et al., 2015; Sidik et al., 2013).

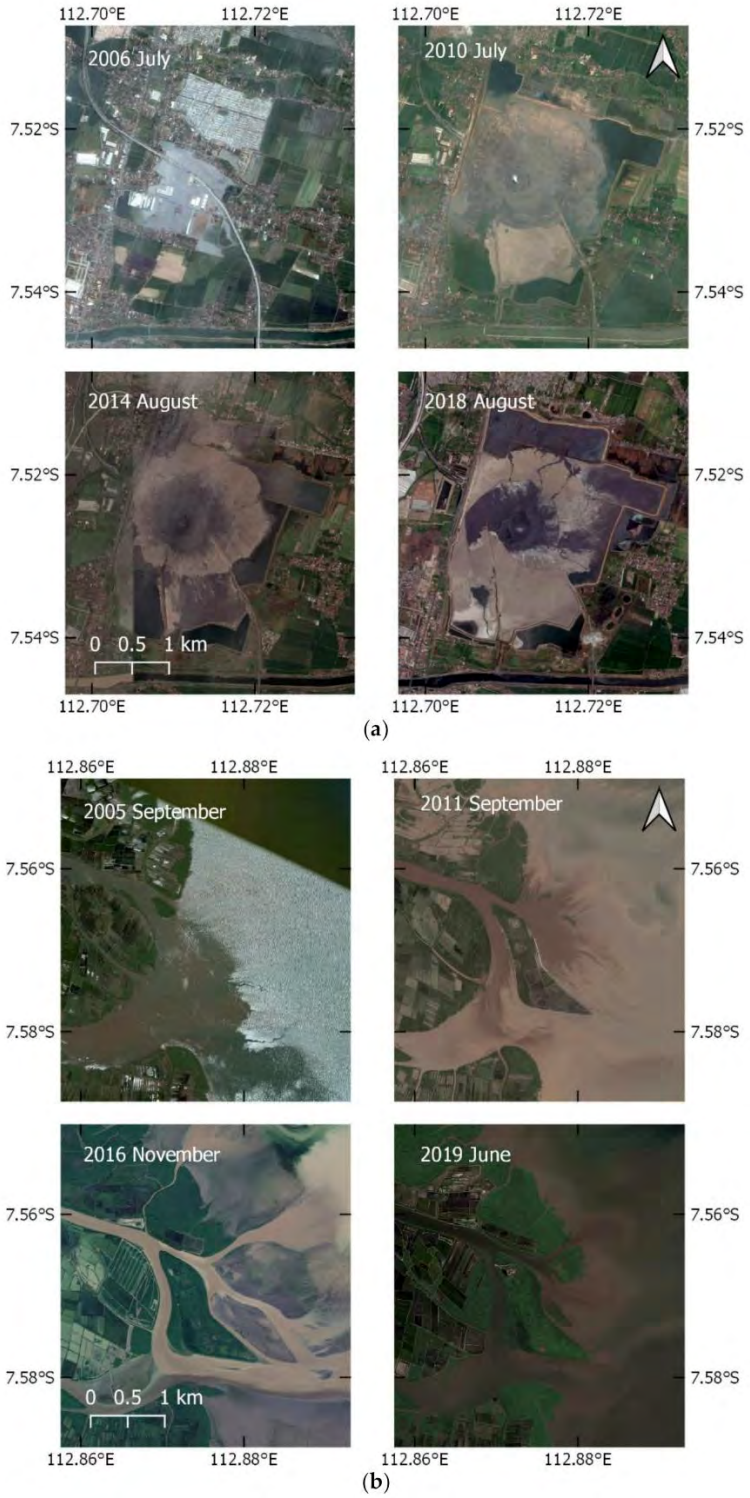

Figure 2.2. (a) Series of images of LUSI mud volcano eruption that show the expansion of the inundated area due to the mud volcanic eruption and the ring dyke to contain the mud and (b) Porong Delta development after diversion operation which shows rapid delta and mangrove belt expansion. Source: Google Earth Pro.

2.2.2 UAV Data Collection and Processing

The fieldwork was conducted at the end of the dry season (October–November) in 2019, focusing on two delta lobes (northern and southern deltas) with a total area of approximately 0.3 km^2. This timeframe was expected to have a higher probability of clear satellite images with limited cloud cover, and more sunlight as well as less shadows to reach an optimum condition for Unoccupied aerial vehicle (UAV) image acquisition. UAV/ drones are widely accepted as standard survey tools in many environment settings (Moloney et al., 2018), generating high-resolution data in a safe, straightforward, and cost-effective way (Casella et al., 2020). Coastal environments are challenging for the UAV-based surveying method because of the low texture and contrast of the bed surface (Casella et al., 2020).. Careful planning of the GCPs placement and flight path can lead to reach centimetres of vertical accuracy (Casella et al., 2020; Otero et al., 2018).

2.2.2.1. Data acquisition

Several studies demonstrated that consumer-grade UAV could achieve vertical accuracies in the order of a few centimetres to a few decimetres in coastal topographical surveying (Casella et al., 2020; Mazzoleni et al., 2020; Moloney et al., 2018). In comparison with other low-cost platforms (e.g., kite, pole, and fixed-wing), a consumer (rotary) drone system with its integrated positioning system, inertial measurement unit, and stabilised camera offers flexibility and efficiency while attaining the accuracy in coastal area application (Casella et al., 2020; Conlin et al., 2018; Joyce et al., 2019).

In this study, we used consumer-grade UAV DJI Mavic Pro (DJI, Shenzen, China) during the field campaign. The drone has four propellers and a built-in true colour camera. The camera is equipped with 1/2.3″ CMOS sensor with total effective pixels of 12.35 M, which produces a 4000 × 3000 image resolution and equipped with an electronic shutter. Information on shutter type is important since it will affect the setting on the camera calibration to compensate the rolling shutter issues as in the electronic shutter-type cameras. The overall flight time in optimal condition is 21 min with 15% remaining battery level (DJI Mavic Pro & Mavic Pro Platinum Documentation).

The DroneDeploy web app (DroneDeploy, San Fransisco, CA, USA) was used to define the flight path (Mazzoleni et al., 2020). It was planned with a flight altitude of 60 m, an overlay of 80% front overlap and 75% side overlap. Each flight was designed to cover 0.02 km^2 area with 15 min flight time to limit one battery per flight. An enhanced 3D mode was activated to improve 3D structures quality which will capture an oblique image of the objects, facing toward the inner centre of the target by carefully not to include horizon in the shots (DroneDeploy Documentation). We added a buffer zone approximately 20 m apart from the edge of the low tide limit that was cropped during the processing later on to prevent interference with the SfM Photogrammetry processing

(Otero et al., 2018). With these settings, we were able to build 15 grids covering around 0.3 km^2. All the grids created in the web app then can be synced into the mobile app to manage the flight and photo acquisition on-field automatically. The flights were conducted between 09:00 and 12:00 to get optimum natural sunlight, primarily limit the appearance of shadows on the photos. Additionally, this short time window was chosen to avoid high variation in sun intensity (Zhu et al., 2019) and it covered the low-tide period. Before the flight, we placed the custom made printed red cross-shape tarpaulin as a ground control point (GCP). The GCP size is 1 m × 1 m rectangle in the inner side and 1 m diagonal cross in the outer side to make it identifiable from the 60 m altitude. We placed GCPs over the mudflat and in the middle of the delta, which has low vegetation density and registered them with DGPS in RTK mode.

In total, the properties and location of 69 mangrove trees were measured concurrently with the mudflat topography. We recorded diameter at breast height at 130cm above the ground (D_{130}), height, and location for each tree. The D_{130} was recorded using a measuring tape at 130 cm above the ground. Tree height was recorded with laser rangefinder by measuring horizontal distance and hypotenuse from surveyor location to the tree stem and treetop, respectively. For the trees that were located in the proximity of the mangrove edge we recorded the position with DGPS. Trees that were located more in the centre of the forest were recorded with GPS (horizontal accuracy ± 3.5 m) because it is difficult to walk inside the forest with heavy equipment. Mudflat topography was measured with DGPS in RTK mode. The mangrove trees dataset was used as control points and groundtruthing for the created Digital Surface Model (DSM).

2.2.2.2. Data processing

We estimated the tree's location and height based on point clouds created by the Structure from Motion (SfM) photogrammetry method. Three-dimensional point clouds derived from SfM photogrammetry produced conservative and realistic measures of tree heights (Navarro et al., 2019). Alongside with point clouds, a DSM, Digital Terrain Model (DTM), and an orthomosaic were also generated from these processes (Navarro et al., 2020).

The workflow comprises of three phases, namely pre-processing, processing, and post-processing. The workflow in point clouds generation and processing is illustrated in Figure 2.3. Pre-processing is mainly related to data acquisition including flight route planning, GCP placement and processing of overlapped images with SfM Photogrammetry. After the data is acquired, we process the images in commercial SfM photogrammetry software Agisoft Metashape Professional 1.6.1 (Agisoft LLC, St. Petersburg, Russia). The workflow is in general as follows: (1) photo alignment, (2) photo marking, (3) dense point clouds generation, (4) exporting dense point clouds, and (5)

DSM and orthomosaic generation. A detailed description of this workflow can be read in the Appendix 2-A, Table 2-A.1.

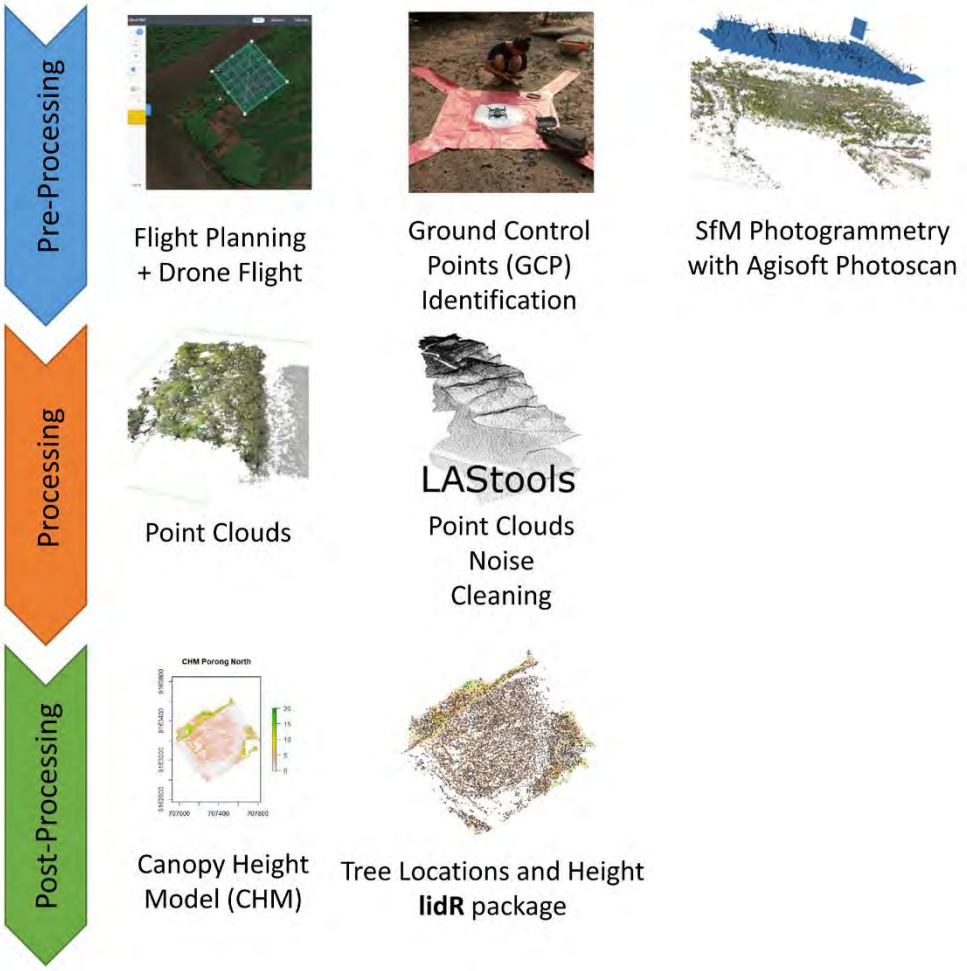

Figure 2.3. The workflow of the Unoccupied aerial vehicle (UAV)-based point clouds generation and processing.

Since the UAV camera cannot penetrate the mangrove canopy, the DSM includes vegetation and any above ground covers. Therefore, on the next workflow, we processed the point clouds to estimate the DTM. Orthomosaic was created by using surface information provided by the DSM and orthorectifying of the overlapping images.

The processing phase consists of nine steps, which are quality checking, clipping, indexing, tiling, sorting, noise removal, ground classification, height normalisation, and generating the Canopy Height Model (CHM). Details in this phase are described in Figure 2.4. We used LASTools (rapidlasso GmbH, Gilching, Germany) to clean the artefacts. The Cloth Simulation Filter (CSF) algorithm (W. Zhang et al., 2016), which is efficient to extract the bare earth in lidR package (Roussel et al., 2020), was employed for ground

classification. As the first step, we assess the quality and information, e.g., number of points, projection, and point density with lasinfo module. Dense point clouds derived from SfM photogrammetry still contain noise and uncertainties (Du et al., 2016; Widyaningrum and Gorte, 2017). Therefore, to get an optimal application in the mangroves' environment, a cleaning procedure should be considered. The waterbody is the main noise contributor of the SfM photogrammetry point clouds. We visually inspected the orthomosaic and draw a polygon which excludes water and selected the area of interest. The raw point clouds were then clipped based on the polygon with lasclip module. Next, we tiled and indexed the clipped point clouds into a smaller tile of 40 × 40 m and added a buffer that was 20% of the tile size. The tiling procedure is useful to decrease the computational time by taking advantage of parallel computation. Another consideration is that, the free licensed LASTools has a point limitation about 1~15 million points (Martin Isenburg, LASTools). Therefore, tiles should be adjusted with the allowable number of points as attached to the license. The tiled points were then sorted to rearrange the points into a space-filling curve order. Afterward, we reclassified the highest points, find the highly isolated points in the dense forest, to create a temporary ground classification. Next, we mapped all the points located 0.2 m below the temporary ground as noise. These high and low noise were removed with the lasthin and lasnoise module. The cleaned photogrammetry point clouds then were processed with the CSF algorithm in the lidR package to define the ground points. An exhaustive manual revision of the ground-no ground classification was done in the dense forest to avoid ground misclassification. The point clouds were created only from what is visible to the camera within the path not penetrating the canopies, because of that only vegetation tops/canopies were included. Therefore, careful manual revision had to be made. Finally, points were height-normalised by replacing the height of each point to the relative height of the ground-classified points. Subsequently, we converted the height-normalised points into CHM and the ground-classified points into DTM.

In the post-processing phase, we used a CHM which is a gridded canopy model with 5.3 cm resolution. To locate individual trees in this very high-resolution CHM, the lidR 'tree_detection' provides two algorithms—Layer Stacking (Ayrey et al., 2017) and Local Maximum Filter (LMF) (Popescu et al., 2002). We set the LMF algorithm parameters window size to 5 m (Otero et al., 2018), a minimum height of 1.37 m, and a circular moving window shape which represent the crown of a mangrove tree. The resulting data CHM were tree location (x,y) and tree height (z). The detected trees were manually checked to avoid errors (Navarro et al., 2019).

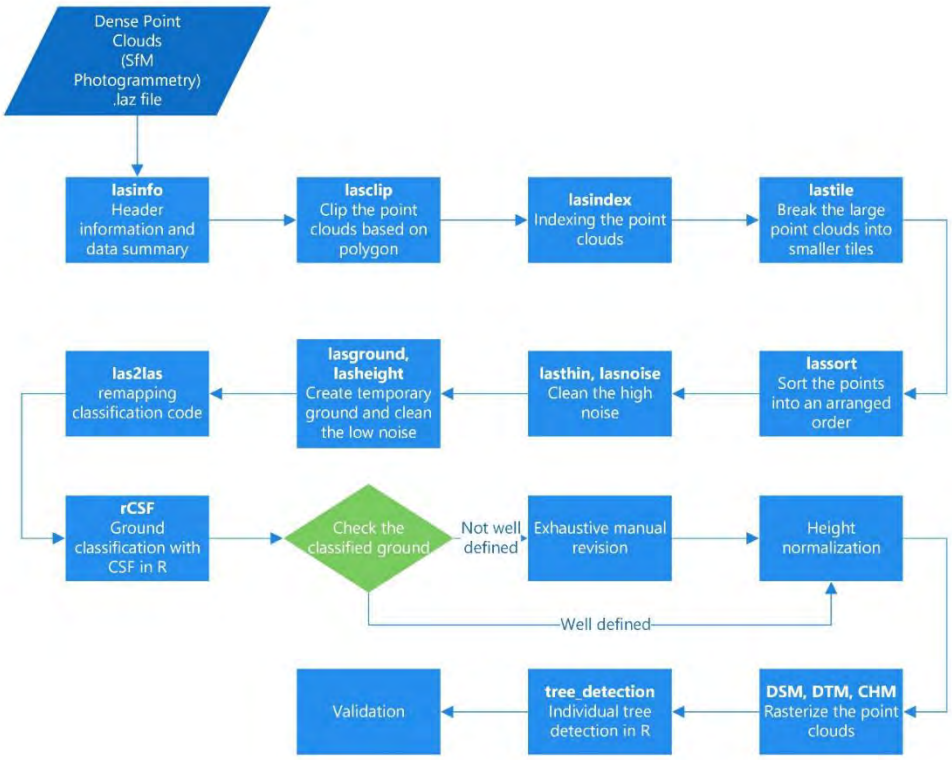

Figure 2.4. Working steps of the processing and post-processing phase of the point clouds.

2.2.2.3. Tree detection validation

The latest forest inventory was conducted by the Ministry of Marine Affairs and Fisheries (MMAF) in 2010 (Ministry of Marine Affairs and Fisheries, 2010, 2009). Therefore, we could not directly validate presence of individual trees detected in CHM. Most of the tree inventory collected during the fieldwork was located around the edge of mangrove forests. Therefore, we performed visual interpretation undertaken by the three researchers (Otero et al., 2018). We pre-selected 30 × 30 m plots reflecting the plot size as in traditional forest inventories. For each of the two delta lobes three plots were chosen, one being located at the centre, another at the northern and still another at the southern edge of the forest. The background of the researchers is (1) a groundwater engineer with no experience in ecology and remote sensing, (2) a hydraulic engineer with basic experience in remote sensing and no knowledge in ecology, and (3) a coastal engineer with basic knowledge in ecology and advanced knowledge in remote sensing. The horizontal accuracy of the detected trees and validation data can be quantified with widely used guidelines by the National Standard for Spatial Data Accuracy (NSSDA) (Federal Geographic Data Committee, 1998) to measure the positional accuracy of the spatial datasets (Pulighe et al., 2016).

2.2.3 Satellite Data and Processing

Google Earth Engine (GEE) has been used as a tool to perform climate and hydrology and natural disaster analysis, and image processing, land use/land cover classification (LU/ LC), and urban planning (Amani et al., 2020; Tamiminia et al., 2020). GEE consists of petabytes of science-ready datasets and is equipped with high performance computing that can be accessed through an application programming interface (API) that is available in JavaScript and Python (Gorelick et al., 2017). Some notable applications of GEE are, for instance, the Global Mangrove Watch (Bunting et al., 2018), global forest cover change (Hansen et al., 2013), global surface water changes (Donchyts et al., 2016; Pekel et al., 2016), global shoreline changes (Luijendijk et al., 2018), and continent level agricultural mapping (Xiong et al., 2017). To understand the mangrove extent development, we processed satellite imagery, such as Landsat 7/8 and Sentinel 1/2, in GEE with Python package geemap (Wu, 2020).

2.2.3.1. Available dataset

We used combinations of satellite imagery from four satellites constellations available and science-ready in the GEE platform, i.e., Landsat 7 (L7), Landsat 8 (L8), Sentinel 1 (S1), and Sentinel 2 (S2). S1 and S2 are satellite constellations developed by ESA (European Space Agency) along with other constellations such as Sentinel 3 and 5. S1 and S2 satellites hold the sensors that are suitable for the mangrove classification study. S1 satellite carries a dual-polarisation C-band Synthetic Aperture Radar (SAR) instrument (European Space Agency, 2012; “User Guides - Sentinel-1 SAR - Overview - Sentinel Online”). Each S1 scene in GEE has been pre-processed with the Sentinel-1 Toolbox and is science ready (“Sentinel-1 SAR GRD”). We employed Sentinel-1 SAR Ground Range Detected (GRD) products with 10 m spatial resolution with available dataset in GEE (‘COPERNICUS/S1_GRD’) from October 2014. The S2 satellite carries a Multispectral Instrument (MSI) with 13 spectral bands: 10 m resolution RGB and NIR, 20 m red edge and SWIR, and 60 m atmospheric band (European Space Agency, 2015; “User Guides - Sentinel-2 MSI - Overview - Sentinel Online”). The S2 MultiSpectral Instrument (MSI) Level-1C products were used with available dataset in GEE (‘COPERNICUS/S2’) from June 2015. L7 and L8 are satellite constellations developed by a joint program of the USGS and the NASA. Within the GEE platform, L7 scenes have been atmospherically corrected using LEDAPS (Masek et al., 2006; “USGS Landsat 7 Surface Reflectance Tier 1 | Earth Engine Data Catalog”) and L8 using LasRC (“USGS Landsat 8 Surface Reflectance Tier 1 | Earth Engine Data Catalog,”, p. 8; Vermote et al., 2016) (USGS Landsat Surface Reflectance Tier 1). Clouds, shadow, water, and snow were masked with the CFMASK algorithm (Fassnacht et al., 2019; “USGS Landsat 7 Surface Reflectance Tier 1 | Earth Engine Data Catalog,”; “USGS Landsat 8 Surface Reflectance Tier 1 | Earth Engine Data Catalog”). The L8 Surface Reflectance Tier 1

('LANDSAT/LC08/C01/T1_SR') which is available from April 2013 onwards and Landsat 7 Surface Reflectance Tier 1 ('LANDSAT/LE07/C01/T1_SR') dataset available from January 1999 onward were employed in this study.

Seasonal varying precipitation, flood control measures, and diversion operations are likely to influence the sediment yield. Mangrove flowering and seedling dispersal periods are also influenced by the season. By considering those conditions and dynamics on the delta, we proposed to map mangrove extent on a seasonal time scale. We mapped the mangrove extent that represents dry season (May and August) and wet season (November and February). A composite from one-month scenes of the particular month was created with the median value of the selected bands and indices for mangrove classification for optical sensor (S2, L7, L8). A mean function was applied for the satellite with SAR instrument (S1) (Anchang et al., 2020; Ghorbanian et al., 2020). The median value was chosen because it is less affected by outlier values that arise, for instance, from pixels affected by clouds or snow during the masking procedures (Fassnacht et al., 2019). To optimise the dataset availability and account for mangrove–mudflat dynamics, we employed the combination of S1 and S2 during the period of November 2015 to November 2019. The combination of optical S1 and S2 SAR was reported to improve the classification accuracy (Carrasco et al., 2019; Fassnacht et al., 2019; Navarro et al., 2019; Yuan et al., 2020). L8-based classification was for the period of August 2013 to August 2015, and L7-based classification was from dry season 2009 to dry season 2012. An exception has been made for L7-based classification. The L7 series of scenes has gaps due to Scan-Line Connector (SLC) failure or stripping problem (USGS, 2013). Therefore, instead of using the one-month scenes we applied median values of full seasons (six months for each) during 2009–2012. Since in that period the diversion operation had just begun and the LUSI Island reclamation project had been conducted, we observed less mangrove succession in the delta. A presentation of the seasonal classification with a single map for the period of 2009–2012 is considered sufficient. All available datasets in a particular classification period were used to generate a cloud-free composite and improve the classification accuracy (Carrasco et al., 2019; Ghorbanian et al., 2020).

2.2.3.2. Vegetation indices

We assessed the mangrove vegetation cover by way of four optical-related vegetation indices that are widely used in land cover characterisation (Carrasco et al., 2019; Lucas et al., 2020; Mercier et al., 2019; Otero et al., 2019), i.e., NDVI (Normalised Difference Vegetation Index) (Tucker, 1979), NDMI (Normalised Difference Moisture Index) (Otero et al., 2018), EVI (Enhanced Vegetation Index) (Huete et al., 2002), and SAVI (Soil-Adjusted Vegetation Index) (Huete, 1988). The S1 images were first pre-processed with a speckle filter (Lee refined) at a window size of 7 × 7 pixels (Lee et al., 1994; Mercier et al., 2019). A ratio channel (VV/VH) from the backscattering was

generated. Lastly, the mean value of all S1 images was employed. This mean function makes the S1 composite less susceptible to variation in image acquisition (Anchang et al., 2020; Ghorbanian et al., 2020). With this additional dataset, each S1 mosaic had two bands and one index, while S2, L7, and L8 had 10, 6, and 7 spectral bands, respectively, and each was composed of four vegetation indices (Table 2. 1). Table 2.2 specifies the vegetation indices formulas used in the analysis. Figure 2.5 describes the flowchart of the image processing procedure.

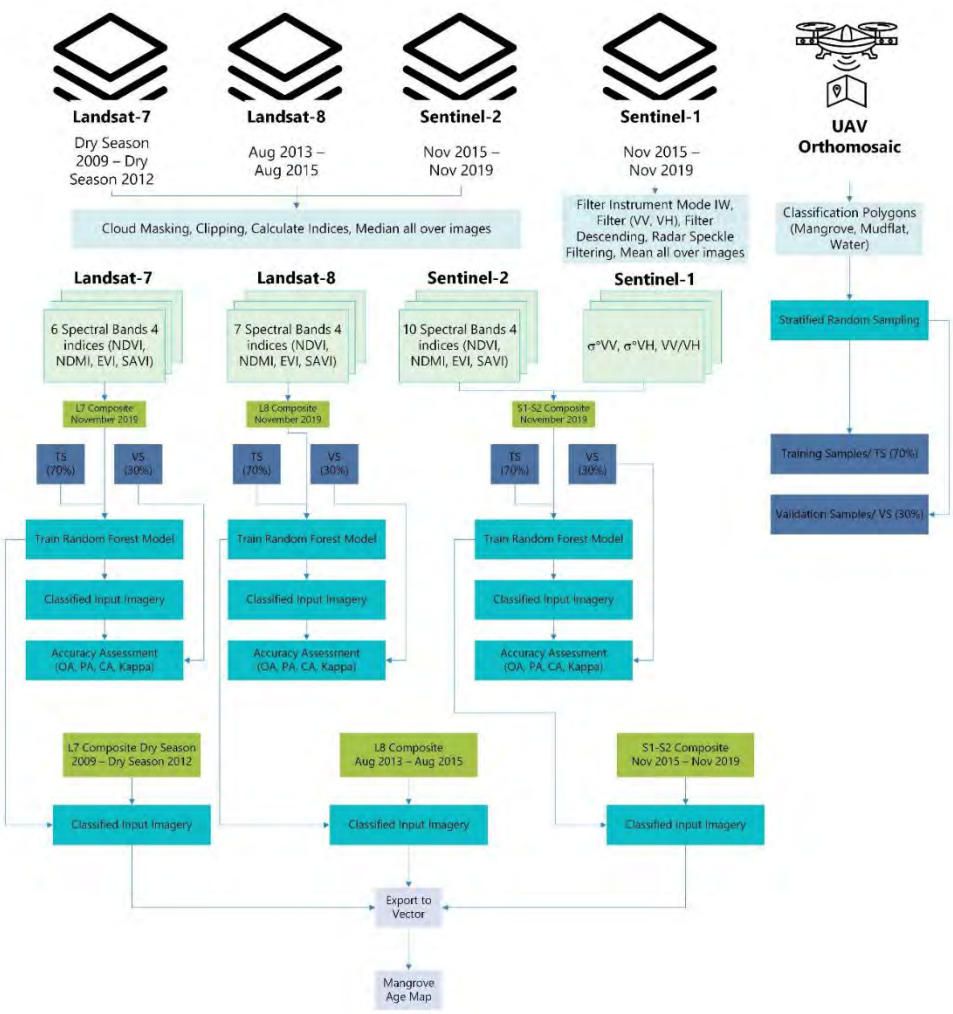

Figure 2.5. Flowchart of the satellite imagery processing in Google Earth Engine (GEE) with Landsat 7, Landsat 8, Sentinel 1, and Sentinel-2. The UAV orthomosaic is used as the training and validation dataset.

Table 2. 1. Datasets used as input for each satellite constellation product.

Mission	Bands/ Indices	Metric
Sentinel-1	VV, VH, VV/VH	mean
Sentinel-2	B2-B8, B8A, B11-12, NDVI, NDMI, EVI, SAVI	median
Landsat-7	B1-5, B7, NDVI, NDMI, EVI, SAVI	median
Landsat-8	B2-8, NDVI, NDMI, EVI, SAVI	median

Table 2.2. Vegetation indices formulas used for the optical sensor.

Indices	Formulas	S-2	L-7	L-8
NDVI	(NIR – R) / (NIR + R)	(B8 – B4) / (B8 + B4)	(B4 – B3) / (B4 + B3)	(B5 – B4) / (B5 + B4)
NDMI	(NIR - SWIR) / (NIR + SWIR)	(B8 – B11) / (B8 + B11)	(B4 – B5) / (B4 + B5)	(B5 – B6) / (B5 + B6)
EVI	2.5*((NIR - R)/ (NIR + 6*R – 7.5*B + 1)	2.5*((B8 – B4)/ (B8 + 6*B4 – 7.5*B2 + 1)	2.5*((B4 – B3)/ (B4 + 6*B3 – 7.5*B1 + 1)	2.5*((B5 – B4)/ (B5 + 6*B4 - 7.5*B2 + 1)
SAVI	(NIR - R)*1.5 / (NIR + R + 0.5)	(B8- B4)*1.5 / (B8 + B4 + 0.5)	(B4- B3)*1.5 / (B4 + B3 + 0.5)	(B5- B4)*1.5 / (B5 + B4 + 0.5)

2.2.3.3. Land cover classification

A supervised land cover classification with machine learning algorithm was employed in GEE. Several of those algorithms have been embedded in GEE. These classifiers are Classification and Regression Tree (CART), Random Forest (RF), NaiveBayes, and Support Vector Machine (SVM) (Gorelick et al., 2017). Wetland mapping, as in mangrove swamps, is one of the most challenging areas for remote sensing. RF supervised classification is reported to have the highest accuracy among widely used machine learning algorithms, e.g., K-Nearest Neighbour (KNN), SVM, Maximum Likelihood (ML), and CART (Amani et al., 2017; Ghorbanian et al., 2020). RF comprises a collection of tree-structured classifiers to make prediction (Breiman, 2001). RF is more robust to noise and size reduction of the training set than CART (Rodriguez-Galiano et al., 2012), easier to implement than SVM (Mahdianpari et al., 2019), and is particularly suitable to handle high dimensional remote sensing data (Belgiu and Drăguţ, 2016).

The land cover classification was conducted using the following workflow: (1) training data collection, (2) initiating classifier and adjusting parameters, (3) train the classifier with training dataset, (4) classify the image based on the trained dataset, and (5) accuracy checking. In the first step, the training dataset is provided from the very high-resolution

orthomosaic created on the UAV data processing. We created three classifications (water, mangroves, and mudflat area) by plotting region of interests (ROIs) which represent these classifications. As the intertidal mudflat varies over time by tidal variation, proper consideration should be made by not only referencing the mudflat's ROI based on the orthomosaic but also considering the median composite in November 2019. The ROIs polygons were made in QGIS as a shapefile and uploaded to GEE as assets. Next, sample points were created based on supervised ROIs. Accuracy of RF classification is sensitive to the sample size and spatial distribution (Jin et al., 2014). Within each stratum, which is based on supervised ROIs, the stratums are randomly sampled (Congalton and Green, 2008). Stratified random sampling function in GEE was used to sample the training data. Cochran's formula (Eq. 2.1) was employed to determine sample size by assuming an unknown proportion for each class (Cochran, 1977).

$$n_0 = Z^2 \frac{pq}{e^2} \qquad (2.1)$$

Here, n_0 is the sample size per class, p is the proportion of the population which has the class in question, $q = 1 - p$, Z is the z-value for the given confidence, e is the margin of error. The samples were subdivided into a 70% training set and 30% of validation (Breiman, 2001). In the next step, to optimise the computational performance, RF classifier with 200 decision trees (Carrasco et al., 2019) was initiated and trained as several studies suggested 100–500 as the optimal number (Belgiu and Drăguţ, 2016; Du et al., 2015; Guan et al., 2013; Rodriguez-Galiano et al., 2012; Topouzelis and Psyllos, 2012). The trained dataset then is used to classify the composite.

2.2.3.4. Accuracy assessment and validation

We used accuracy assessment functions embedded in GEE for those parameters. The final ground-truthing is based on the VHR orthomosaic derived from UAV image acquisitions in November 2019. We used the confusion error matrix with these parameters: Overall Accuracy (OA), Kappa Coefficient, Producer Accuracy (PA), and Consumer Accuracy (CA) (Amani et al., 2017; Mahdianpari et al., 2019). The OA is calculated by summing the number of correctly classified values and divided by the total number of values. PA is determined by comparing the number of correctly classified values of a particular class and number of reference pixels of the same class, while CA can be calculated by dividing the number of correctly classified values of a particular class and number of classified pixels in the class (Patel and Kaushal, 2010). The OA, PA, and CA are expressed as percentage, with 100% accuracy representing a perfect classification. Kappa measures the difference between the actual agreement in the error matrix and the chance agreement that is indicated by the row and column total (Congalton and Green, 2008). A kappa value of 0 represents no agreement, and a value of 1 indicates perfect agreement.

2.3. RESULTS

This section outlines the result of drone-based point clouds, tree detection and validation, and satellite-based mangrove extent change over time.

2.3.1. Point clouds

In total, we processed 2860 UAV images (2020 images for north delta lobe and 840 images for the southern delta lobe), which is equal to an average of 200 images per grid. SfM Photogrammetry provided point clouds, DSM, and orthomosaic for each delta lobe. The generated raw point clouds had 400.5 million and 136.6 million points, which correspond to average point densities of 951.25 m^{-2} and 736 m^{-2} for the northern and southern delta lobes, respectively. The derived DSM has a resolution of 5.33 cm/pixel and an orthomosaic with 2.66 cm/pixel resolution. The products in total covered an area of 0.44 km^2 and were corrected based on GCPs with a total error of 0.06 m. The discrepancy between the planned flight area and the product is generated from other areas captured during the UAV image acquisition.

A small subset of the point clouds is shown in Figure 2.6. The set of figures illustrates the step-by-step point clouds processing. Figure 2.6a shows subtle noise yielded on the SfM-based point clouds. The raw point clouds were refined by classifying the high and low noise, resulting in cleaned points as depicted in Figure 2.6d. The ground-classified points with the CSF method were then evaluated, especially those situated below the dense vegetation since SfM-based point clouds provide no information below the canopy cover. Hence, an exhaustive manual revision was conducted by checking and correcting the classified ground points. The final point classification categories chosen for the analysis were non-ground (1), ground (2), high vegetation (5), and noise (7). The final result of the point cloud processing is a height-normalised point clouds that can be described with all elevations were normalised with respect to the ground, i.e., an elevation of 0 m. Figure 2.7 shows DTM and DSM derived from the final classification of the point clouds.

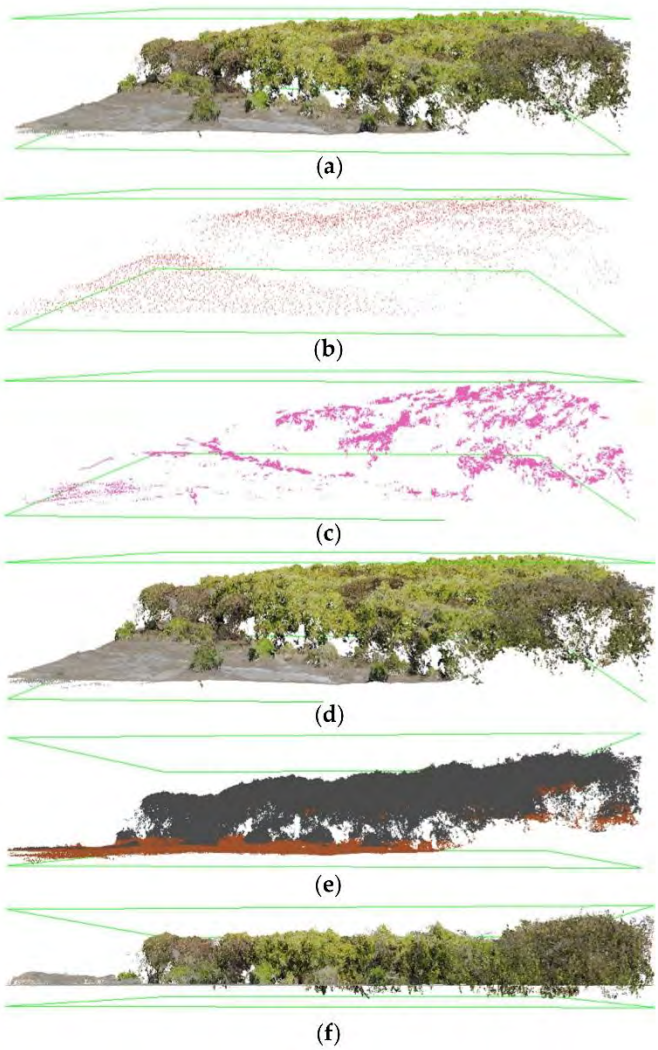

Figure 2.6. Point clouds processing: (a) raw point clouds, (b) the thinned 20% elevation percentile points, (c) high noise-classified points, (d) cleaned photogrammetry point clouds, (e) ground points classification (brown colour represents ground points and grey represents non-ground), (f) height normalisation.

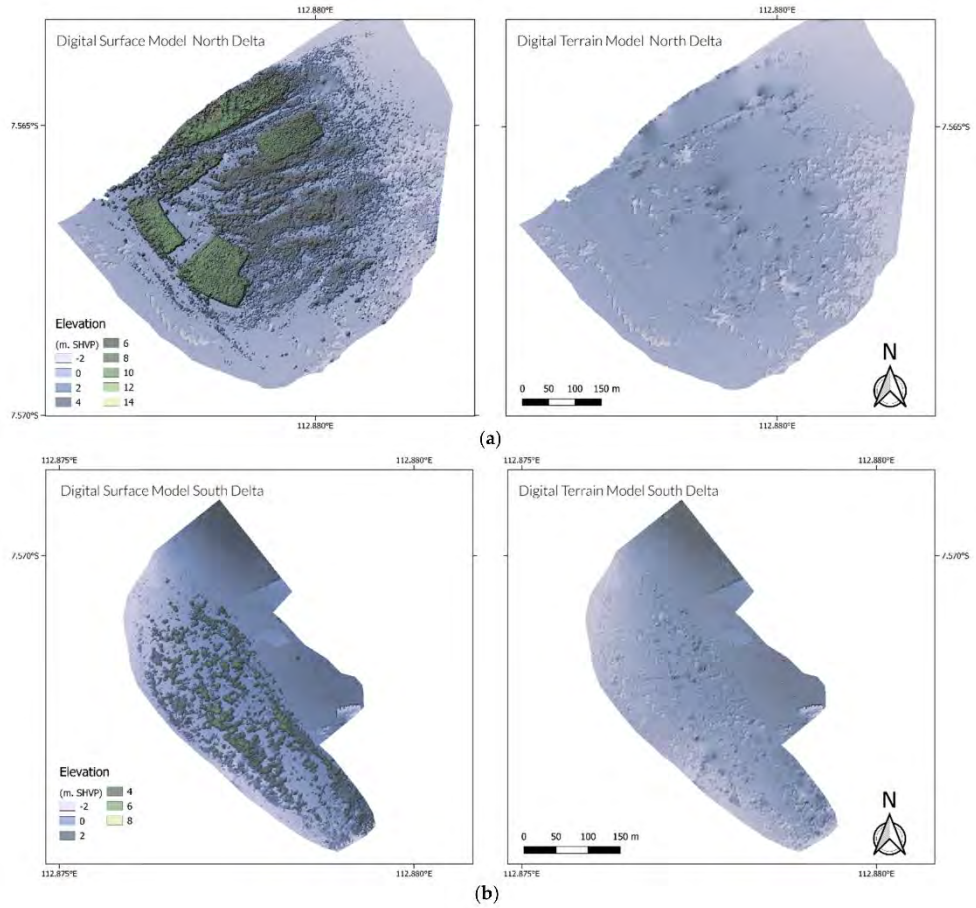

Figure 2.7. (a) Digital Surface Model (DSM) and Digital Terrain Model (DTM) of the northern delta and (b) DSM and DTM of the southern delta.

2.3.2. Canopy Height Model (CHM) and Tree Detection

The height normalised point clouds were rasterised to a CHM with a resolution of 0.1 m, and subjected to the individual tree detection. The 'tree_detection' function in the lidR package with the LMF algorithm was adjusted to detect mangrove trees above the breast height. The individual trees derived from the algorithm can be observed in Figure 2.8.

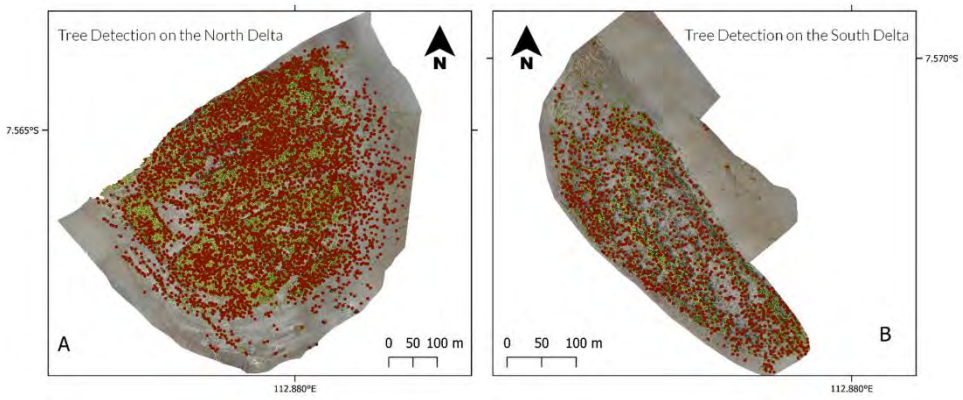

Figure 2.8. The detected individual tree as represented here as the red dots derived from UAV Structure from Motion (SfM) photogrammetry in (A) northern delta and (B) southern delta.

The root mean square error (RMSE) analysis of the individual tree detection based on fieldwork data and visual inspection is described in detail in Appendix 2-B, Table 2-A.2. The RMSE value for tree location was 0.23 m on average. All three validators provided similar RMSEr with values ranging 0.15, 0.28, and 0.25 m, while the maximum RMSEr was 0.48 m. As observed, the number of the detected trees for the dense mangrove forest was underestimated, whereas it was more accurate in the sparse mangrove forest.

The CHM-derived height demonstrated that the mangroves' median height is 3.5 m in the southern delta while the northern delta with its older mangroves had a median height of 4.2 m. As shown in Figure 2.9, the northern delta had bi-modal tree height distribution. The distribution is likely correlated to the mangrove planting activities in 2016. Corresponding rectangular shaped mangrove areas can be clearly seen in Figure 2.7a.

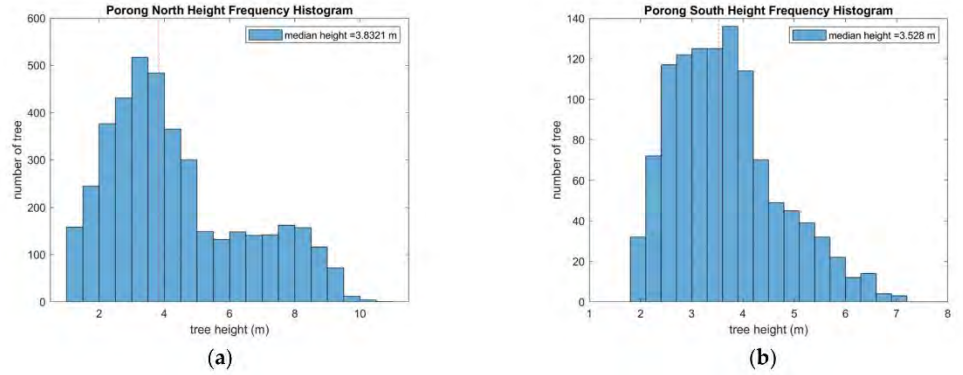

Figure 2.9. The detected mangrove trees height frequency histogram of (a) the north delta and (b) the south delta.

2.3.3. Mangrove Extent and Age Estimation

2.3.3.1. Mangrove Extent

Figure 2.10 and Figure 2.11 illustrate the development of the mangrove extent from 2009 to 2019. Figure 2.11 presents the result of the mangrove classification based on L7 (2009 Dry season–2012 Wet season), L8 (August 2013–August 2015), and the combination of S1–S2 (November 2015–November 2019). It can be observed that the mangrove belt expansion has strongly developed in the Porong River mouth. The mangroves on LUSI Island are clearly visible and have continuously expanded after the construction in 2011 (Figure 2.11). On the northern delta lobe, mangroves appeared in 2016 followed by the southern delta lobe in 2018. The land conversion to fish ponds in the hinterland is apparent as well in the figures.

Figure 2.10 provides an illustrative visualisation of the mangrove dynamics. Starting in 2006 the mangrove forests tended to expand seawards. The mangroves in northern and southern delta lobes contributed significantly to this. Considering the time series map, it is likely that the southern delta mangrove will be attached to the LUSI Island within the next few years.

The time series of the mangrove extent has been extracted for both on the Region of Interest (ROI) (Figure 2.12a) as well as for the LUSI Island-delta lobes (Figure 2.12b). Both areas exhibit a similar positive trend of development. Generally, it varies with season. The mangroves area recedes during the transition from dry to wet season and the mangroves regrow during the wet to dry season. However, the delta lobes' mangroves have a slightly different seasonal pattern. As in Figure 2.12b, the mangrove's seasonal variation is less pronounced. It is likely because it is more isolated and is affected less by human activities.

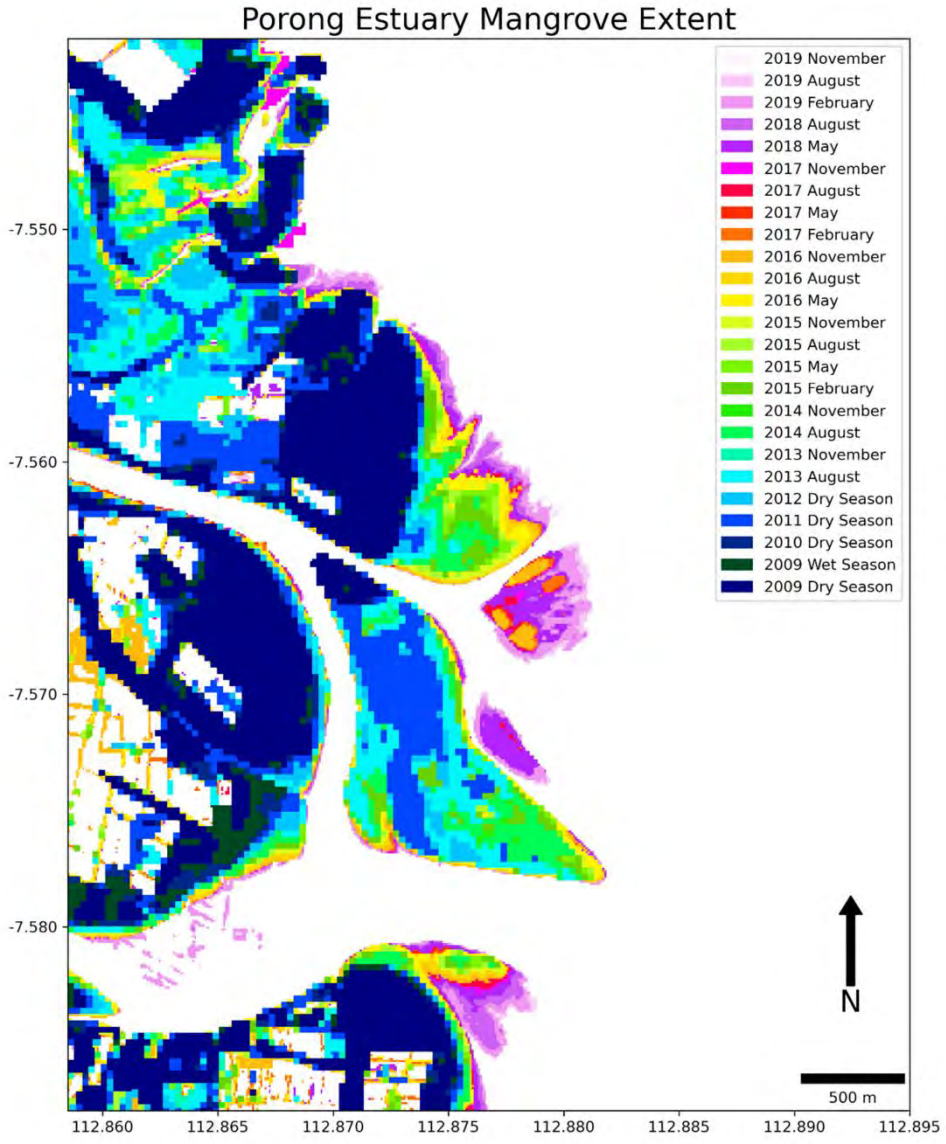

Figure 2.10. Time series of porong mangrove extent derived from Landsat 7, Landsat 8, and Sentinel 1–Sentinel 2 imagery

Figure 2.11. Details of the mangrove extent estimated by satellite imagery from the 2009 dry season to November 2019.

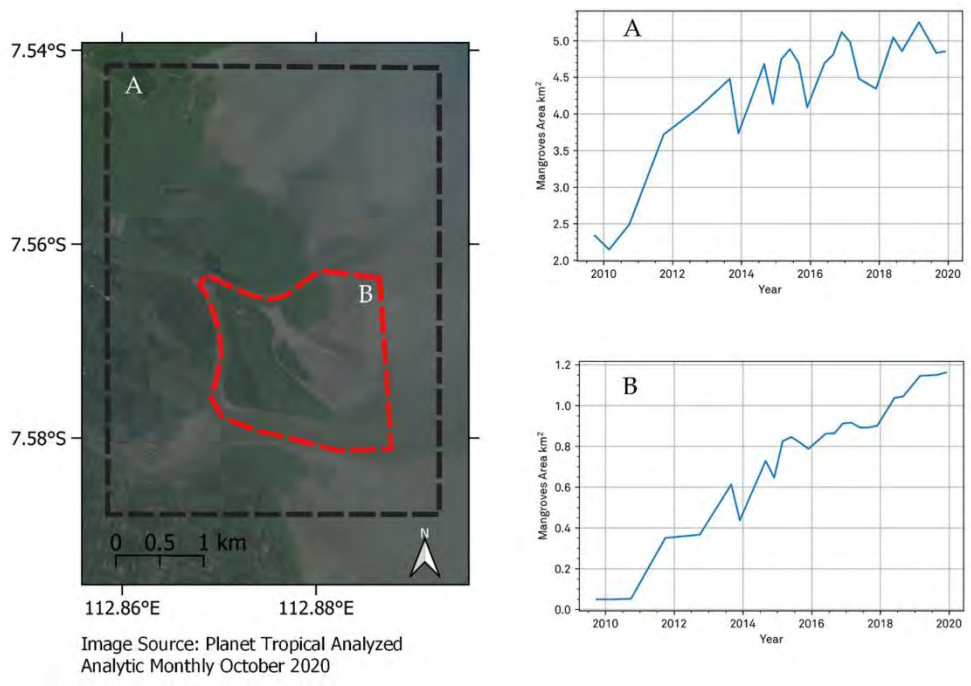

Figure 2.12. Time series of mangrove extent area development on (A) the region of interest (ROI) extends from 112.8585° S, −7.5418° E to 112.8927° S, −7.5879° E and focusing on (B) the Porong Estuary and the newly developed delta lobes which obviously exhibits an increasing trend of area development after 2011. The right figures show the time-series of mangrove area development for each region (A,B).

2.3.3.2. Accuracy Assessment of Porong's Mangrove Classification

Four confusion matrices of L7, L8, and S1/2 based classification show high accuracy when compared with the UAV ground reference data. The reference data was subdivided into 70% fraction of the total sample points (cf. Section 2.2.3.3) for training purposes, equal to 808 points for all classes. The rest (30% of the sample points) or 347 points in total were used for validation samples. The values of Overall Accuracy (OA), Kappa Coefficient, Producer Accuracy (PA), and Consumer Accuracy (CA) of all the classifications were all above 98%. L7 or L8 alone are already excellent sources for the classification of the one-month composite, but the combination of S1 and S2 is even superior to those. The trained OA, Kappa, PA, and CA of S1–S2 classification were all 100%. Due to the SLC error, the trained L7 classification generated from a six-month mean composite also resulted in 100% OA, Kappa, PA, and CA values. The L8-trained OA, Kappa, PA, and CA were 99.88%, 0.99, 99.65%, and 99.62%, respectively.

The validation accuracies also showed consistently excellent values similar to those of the training. The combination of S1–S2 has a value of 100% for all confusion matrices.

The L8-validated OA, Kappa, PA, and CA were 99.39%, 0.99, 97.92%, and 98.39%, respectively. The L7-validated OA, Kappa, PA, and CA were 99.54%, 0.99, 97.83%, and 98.18%, respectively.

2.3.3.3. Age Map

The age map (Figure 2.13) was estimated and referenced to November 2019 and derived backward to 2009. The age map indicates that the mangrove expansion of forests being attached to the mainland began in 2014. In comparison, the isolated forests (on the delta lobes) were found to have started expanding in 2016, most likely initiated by the mangrove planting in the northern delta, in contrast to the natural mangrove succession that took place in the southern delta.

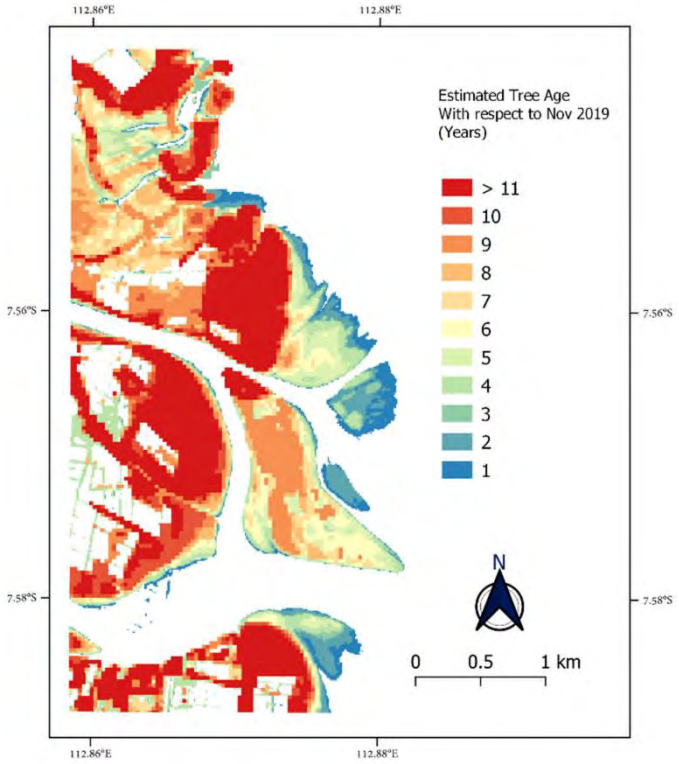

Figure 2.13. Map of mangroves age distribution in Porong Estuary as estimated with respect to the reference period of November 2019.

By taking advantage of the age map and the high-resolution CHM, a relationship of mangrove height dependent on stand age was setup for the two Porong delta lobes. A mean height distribution across the mangrove age map was calculated by clipping the mangroves' age polygon to a CHM raster. Figure 2.14 compares the age-height relationships from the delta lobes' mangroves. The northern delta mangroves were consistently taller than the southern ones at the same stand age. By only taking the

mangrove trees into account that were taller than 1.3 m, the average annual mangrove growth of the northern delta amounted to 2.26 m yr^{-1}. In contrast, the mangroves in the southern delta had an annual mangrove growth rate of 1.71 m yr^{-1}.

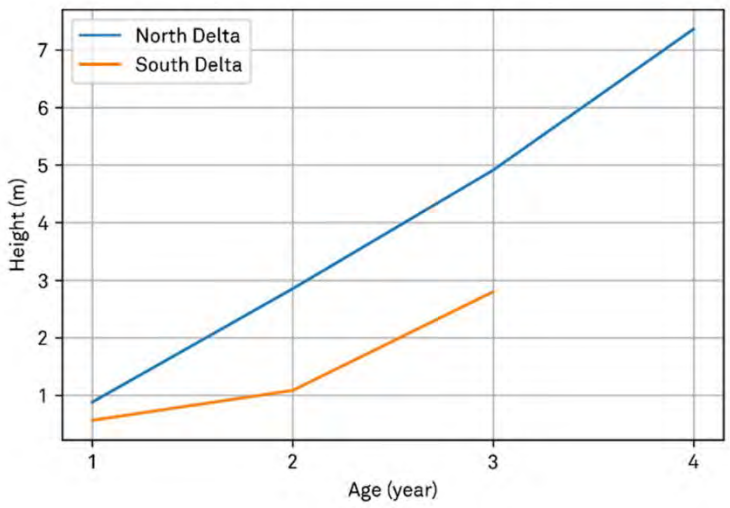

Figure 2.14. Relationship of the mangrove height dependent on stand age on Porong Delta Lobes.

2.4. Discussion

The study aimed to quantify the mangrove dynamics arising from the massive LUSI mudflow diversion operation that followed the extreme mud volcano eruption, in Sidoarjo, Indonesia. Our investigation started in January 2009 and continued until November 2019. This investigation of mangrove dynamics combined usage of UAV-based and satellite analyses with GEE cloud computing. This approach included the successful retrieval of mangrove biophysical properties in terms of canopy height and the individual position of mangrove trees (Figure 2.8) as well as a time series of mangrove belt development (Figure 2.10). This approach resulted to a new set of mangrove extent maps for our study location that is not covered by other existing products such as the WMA (Spalding et al., 2010) and GMFD v1 (Giri et al., 2011) that were released in 2000. The GCMFC-21 (Hamilton and Casey, 2016), GMW v2.0 (Bunting et al., 2018) and at the national-level provided by the Indonesian National Institute of Aeronautics and Space (LAPAN) (Pusat Pemanfaatan Penginderaan Jauh LAPAN, 2020), whose latest product at the time of writing dates from 2012, 2016, and 2019, respectively. The mangrove dataset provided by the GMW v2.0 from the period of 1996, 2007, 2008, 2009, 2010, 2015, and 2016, while LAPAN products were for the period of 2014, 2016, and 2019 —as this chapter was accepted for publication. Therefore, from those datasets the mangrove dynamics in Porong Estuary cannot be deduced. The spatial and temporal resolution of those dataset is not sufficient as Porong

has been experiencing extreme mud influx from LUSI and its transformation has been so rapid. This study resulted in a higher temporal resolution and detailed three monthly mangrove classification and their biophysical properties, especially in the highly dynamic delta lobes that expand seaward.

2.4.1. UAV-based Mangrove Forest Inventory

The derived tree locations were in close correspondence with field inventory data and expert analyses at an RMSEr in the order of 20 cm. However, since the low-cost UAV is equipped with an RGB camera system, the estimated tree location is limited to the description of the canopy top inherent in the CHM. It is different from the LiDAR system where the beam is able to penetrate the dense canopy cover. The UAV-based SfM photogrammetry method tended to underestimate the number of individual trees, even though it has a higher accuracy in the sparse mangrove forest. Based on the result, the low accuracy in the dense forest of the northern delta lobe is likely due to the mangrove plantation programme that has created a more homogenous canopy and an almost flat CHM. This prevented complete detection of all treetop positions. However, despite the underestimated tree location, considering that colonising mangrove species during primary succession is shade-intolerant, therefore, the loss in detection might be marginal, in particular when the canopy is still sparse. The estimated individual positions of the trees can give us more information regarding the height distribution of the mangrove's trees and density (Supplementary Materials S1[1]). As shown in Figure 2.9 we can observe the influence of mangrove planting on the north delta to the height variation indicated by the bimodal distribution (Figure 2.9a).

Despite its limitation, the UAV-based tree detection offers the advantages of lower technical requirements and lower costs when compared to a LiDAR system (Casella et al., 2020). With miniaturisation, increasing proliferation, and advancement in sensor technology, the possibility arises of adding multispectral sensors to accuracy of the UAV-based method while keeping it lightweight and low-cost. The image acquisition was conducted for five days or equal to 8.8 hectares/day since it was limited by the time frame of the optimum sunlight and battery capacity. The UAV survey in this study was conducted by two people. In comparison, traditional mangrove forest inventory with three experienced surveyors needs two complete days (seven hours/ day) to sample 0.05 hectare of the forest (Otero et al., 2018). Thus, UAV-based forest inventory is likely to increase the possibility for frequent and rapid mangrove monitoring. Moreover, this method can be further developed as citizen science monitoring. With an off-the-shelf drone, pre-planned flight, open tutorial, and validation procedure, the public can be involved in this

[1] Supplementary Materials S1 can be accessed from: https://www.mdpi.com/2072-4292/13/6/1084/s1

kind of mangrove monitoring programme. Depending on the needs, the UAV-based SfM photogrammetry is useful to estimate mangrove biophysical properties from the plot level up to the landscape-level. Moreover, another product generated in the workflow, for instance, the DTM is useful in studying the biogeomorphology to understand the feedback loop of vegetation and the environment forcing.

2.4.2. Mangrove Belt Expansion Identification in Google Earth Engine

The expansion of the mangrove belt has been substantiated with the supervised land cover classification. We have evidenced a total of 11 years of mangrove development (2009–2019) with high accuracy (more than 98%). Cloud computation with GEE to our advantage, we generated three monthly mangrove maps, with the exception of sixth-monthly maps during the period of 2009–2012. Most importantly, our map series has higher frequency than the above-mentioned global mangrove products.

2.4.3. Seasonal Pattern of Mangrove Dynamics

Based on the resulting maps, it is apparent that the year 2016 marked the start of the positive mangrove expansion, which seen in Figure 2.10 and the time-lapse animation in the Supplementary Animation S1[2]. There were two of the largest expansion areas in the Porong River mouth contributing 24% of the total mangrove area extracted inside the ROI as of November 2019 (Figure 2.12). It is highly likely that the mudflow diversion procedure has promoted mangrove belt expansion in Porong Estuary. Mud pumping disposal of LUSI discharged extra sediment supply thereby providing a suitable environment that enhanced mangrove expansion. Figure 2.11 provides detail of the significant increase of mangrove extent both on the ROI and focusing on the estuary. Dredging operation and the completion of LUSI Island construction in 2011 have contributed to the prominent increase of the mangrove area.

The mangrove expansion followed a seasonal pattern as Figure 2.12 clearly indicates. We observed recession of the mangrove extent during the transition of dry to wet season and regrowth during the wet to dry season. The wet season has the highest sedimentation rates related to the mudflow pumping operation in LUSI. The mud is disposed of in the wet season and stored in the reservoir during the dry season. The seasonal pattern in Porong was also indicated in the study by Sidik et al. (2016). In principle, net development trend of the mangrove area is positive. Investigated further, we can see amplitude of the high-low signal differs in the period of 2013–2017 from that in 2018–2019. In 2013–2017, we

[2] Supplementary Animation S1 can be accessed from: https://www.mdpi.com/2072-4292/13/6/1084/s1

can see low mangrove extent in the wet season followed by the high regrowth in the dry season. In contrast, from 2018 to 2019, we observe only a slight decrease in the wet season and a high roughly two-fold increase in the dry season. Focusing on the Porong river mouth, as shown in Figure 2.12b, the seasonal fluctuation is also recognised but is less pronounced as in Figure 2.12a. The graphs reveal continuous expansion until August 2013, irrespective of the region, thus no recession visible in both regions. From August to November 2013, there is a sudden recession, i.e., sharp decrease of area in region A and slightly less in region B. The recession took place in the middle of the dry season and the beginning of the wet season, thus at the end of the dry season. There is recovery occurring from November 2013 until August 2014, where recovery is more pronounced for region A (February and May clear satellite images are lacking in 2014). The recovery occurred during the wet to dry season. It seems that the recession occurred at the end of the dry season while recovering and return to expansion happens in the middle of the wet season and the first half of the dry season. This 2013 recession–recovery behaviour repeats in 2014–2017, where the fluctuation is noticeable in region A and less in region B. It is likely in the beginning mangroves start growing on the newly deposited, homogeneously distributed mud since its sediment attributes are rather suitable for their growth. Mangroves have access to water during wet season as well as during dry season. However, because of their existence, further sediment is deposited at the margin of the forest. This possibly transforms them into the basin mangrove type in certain areas, more so in the landward direction, less so on the delta lobes. When the trees start generative production, i.e., propagule production, at an age of three years seedling that are known to be more sensitive to salt and drought might die under the extreme conditions at the end of the dry season in the basins. This condition has developed from the interplay of vegetation and geomorphological processes—namely, the massive sediment load. Studies reported buried pneumatophore leads to mangrove mortality, for example in Mekong Delta (Nardin et al., 2021); high sedimentation concentration reduces the oxygen level in the mangrove's root (McKee and Mendelssohn, 1987; Sidik et al., 2016); and an enhanced of growth of Micronesia trees that is possibly due to associated decreases in root zone salinity (Krauss et al., 2007).

The delta lobes' mangroves response to high sedimentation rates is generally appear as lack of growth instead of a decrease. It is likely because the delta lobes are relatively isolated and therefore less affected by human activities, such as land conversion to fishponds that is obvious in the maps. Given the sharp decrease-increase pattern in Figure 2.12a (period 2014–2018) and slight decrease-increase as Figure 2.12a (period 2018–2019) Figure 2.12b it is likely that anthropogenic activities played an additional role. However, as a verification of that role is beyond the scope of this article, we suggest further investigation of this topic.

2.4.4. Mangroves' Age Class Estimation

The age map (Figure 2.13) was derived to understand the mangroves succession. When it is combined with the CHM, we can estimate the annual growth rate of the mangrove trees (Figure 2.14). The age map indicates a difference in the trend of mangrove expansion for those located in the river mouth and on the mainland. Expansion in the river mouth was altered by the LUSI Island's construction and the built-up of the delta lobes. It is likely that the mangrove planting programme affected the northern delta's spatial tree height variation. Apparently, it is also visible in the age-height relationship displayed in Figure 2.14. As the mangroves on the northern delta were planted, the mangroves tended to be in average two times taller in their first year than its southern counterparts. However, the data used to derive the age-height graph in this article is probably not long enough; for instance, the southern delta provides only three years of observation. Thus, two growth rates for the relationship, which is insufficient for performing statistical tests. Nevertheless, mangrove growth rates had a similar trend for both locations, despite a difference likely due to the mangrove planting. Moreover, the graph demonstrates the advantage of combining UAV-based VHR data and satellite imagery to characterise the mangrove structural attributes that need a large workforce if done traditionally.

2.4.5. Implications of the Study

To our knowledge, this study presents the first attempt to explore the mangrove dynamics in a prograding delta setting by integrating UAV and multiple sources of satellite imagery (L7, L8, S1, and S2) in GEE. Studies to classify mangrove forest have been conducted in the last two decades (Bunting et al., 2018; Giri et al., 2011). They were based not only on one source but also on the combination of multiple satellite sources (Chen et al., 2017; Lucas et al., 2020; Lymburner et al., 2020; Navarro et al., 2019) and became more popular with the advent of GEE. The resulting three-monthly classification maps are more frequent than the commonly produced annual mangrove maps. The frequent monitoring is deemed necessary in this environmental setting, since the sediment influx continues at an unprecedented rate, promoting rapid delta development and mangrove belt expansion. The results of the UAV and the entire methodology presented here shows the advantage of using an off-the-shelf drone. The CHM and individual tree locations present important structural attributes to characterise the mangrove forest. It is essential as there is likely a much closer linkage between diameter at breast height (D_{130}) and height rather than between crown radii and D_{130}. Accurate information of mangrove biophysical structure is critical for the ecologist, coastal manager, or policymaker.

2.5. CONCLUSION

The LUSI mud volcano eruption, arguably the largest mud eruption in the world, certainly affects the downstream landscape development. Particularly with the diversion operation that conveys a large amount of mudflow sediment into the river that eventually stimulates a rapid progradation of the delta compared to pre-LUSI conditions. This offers a unique opportunity to analyse mangrove dynamics on a rapidly prograding delta. We created time series of mangrove extent maps and mangrove biophysical structure with the following steps: (a) biophysical properties retrieval using UAV-based SfM photogrammetry; (b) three-monthly classification of mangrove areas using L7, L8, S1, and S2 in Google Earth Engine; and (c) derivation of mangrove age maps based on the satellite imagery. This improvement enables us to capture the highly dynamic setting in the study area. Moreover, the off-the-shelf UAV offers an efficient yet accurate technique to retrieve the important structural attributes, such as individual tree location and canopy height. When combined with satellite imagery analyses, the information can be used to characterise the mangrove forest and assess the effect of excessive mudflow discharge on the delta and mangrove development.

The proposed approaches allowed us to monitor the dynamics of mangrove extent and structural attributes in a rapidly prograding delta. The random forest supervised classification demonstrated a high accuracy (OA > 99.39%, kappa value 0.99, PA > 97.83%, and CA > 98.18%). The highest accuracy was obtained in the classification from the combined Sentinel 1 and 2, while the lowest resulted from the Landsat 7. The 11 years of mangrove extent mapping provided evidence of an overall positive trend in mangrove extent overlaid by seasonal variation. The receding mangrove area is detected during the transition from dry to wet season and regrow during the wet to dry season. The individual trees height and position derived from UAV showed the different distribution of the north and south delta lobes that is likely related to the mangrove planting.

The method enabled us to retrieve rapid and accurate information on mangrove biophysical properties with an off-the-shelf drone. Moreover, in combination with GEE based cloud computing, it is possible to derive a high spatiotemporal resolution mangrove extent map. The combination of UAV-derived spatial tree structure and the satellite-derived maps are needed to support fast and frequent mangrove monitoring that will be valuable for the ecologists, coastal managers, or policymakers.

2.6. APPENDICES

Appendix 2-A

Here we explain the settings of the pre-processing phase to generate 3D point clouds in the Agisoft Metashape Profesional. The settings in this appendix are for Agisoft Metashape Professional version 1.6.3 build 10723 (64 bit). The detailed description is depicted in Table 2-A.1 below.

Table 2-A.1. Settings of the Agisoft Metashape Professional.

Steps	Parameters	Value
Align Photos	Accuracy	'High'
	Generic Preselection	'Yes'
	Reference Preselection	'Source'
	Key Point Limit	50,000
	Tie Point Limit	4,000
	Guided Image Matching	'Yes'
	Adaptive Camera Model Fitting	"Yes"
	Camera Calibration	'Enable Rolling Shutter Compensation'
Dense Cloud Generation	Quality	'High'
	Depth Filtering	'Mild'
	Calculate Point Colours	activate
	Calculate Point Confidence	activate

Appendix 2-B

The calculation of positional accuracy of the detected trees is following the guidelines by the NSSDA Part 3: National Standard for Spatial Data Accuracy (Federal Geographic Data Committee, 1998). We assessed the horizontal accuracy of the detected trees against the visual observation by the three ob-server and fieldwork measurement. The RMSE values were assessed using the following equations:

$$RMSE_x = \frac{\sqrt{\sum_i \left(x_{data,i} - x_{check,i}\right)^2}}{n} \qquad (2\text{-}A.1)$$

$$RMSE_y = \frac{\sqrt{\sum_i \left(y_{data,i} - y_{check,i}\right)^2}}{n} \qquad (2\text{-}A.2)$$

$$RMSE_r = \sqrt{RMSE_x^2 + RMSE_y^2} \quad (2\text{-}A.3)$$

Where $x_{data,i}$, $y_{data,i}$ are the coordinates of the ith check point of the dataset and $x_{check,i}$, $y_{check,i}$ are the coordinates of the ith check points of the independent source of higher accuracy and n is the number of check point tested. The horizontal error at point i is defined as in the equation 2-A.4. The results of the positional accuracy are shown in the tables below.

Table 2-A.2. Detected trees positional accuracy.

Plots	RMSEx	RMSEy	RMSEr
Observer 1			
North 1	0.09	0.09	0.12
North 2	0.07	0.08	0.11
North 3	0.08	0.09	0.12
South 1	0.19	0.16	0.25
South 2	0.13	0.08	0.15
South 3	0.09	0.08	0.12
Average	-	-	0.15
Observer 2			
North 1	0.12	0.09	0.15
North 2	0.11	0.10	0.15
North 3	0.08	0.08	0.11
South 1	0.29	0.29	0.41
South 2	0.28	0.26	0.38
South 3	0.30	0.38	0.49
Average	-	-	0.28
Observer 3			
North 1	0.15	0.12	0.19
North 2	0.14	0.19	0.23
North 3	0.15	0.15	0.21
South 1	0.17	0.22	0.28
South 2	0.28	0.23	0.37
South 3	0.14	0.16	0.21
Average	-	-	0.25

3

SPATIALLY-EXPLICIT COUPLED INDIVIDUAL-BASED MANGROVE HYDRO-MORPHODYNAMIC MODEL

This chapter is based on the following publication:

Beselly, S.M., U. Grueters, M. Van Der Wegen, J. Reyns, J. Dijkstra, and D. Roelvink. 2023. Modelling Mangrove-Mudflat Dynamics with a Coupled Individual-Based-Hydro-Morphodynamic Model. Environmental Modelling & Software 169 (November 2023): 105814. https://doi.org/10.1016/j.envsoft.2023.105814.

Abstract: As climate-change-driven extremes potentially make coastal areas more vulnerable, mangroves can help sustainably protect the coasts. There is a substantial understanding of both mangrove dynamics and hydro-morphodynamic processes. However, the knowledge of complex eco-geomorphic interactions with physical-environmental stressors remains lacking. We introduce a novel coupled modelling approach consisting of an individual-based mangrove (mesoFON) and a process-based hydromorphodynamic model (Delft3D-FM). This coupled model is unique because it resolves spatiotemporal processes, including tidal, seasonal, and decadal environmental changes (water level, flow, sediment availability, and salinity) with full life-stages (propagule, seedling, sapling, mature) mangrove interaction. It allows us to mechanistically simulate forest expansion, retreat, and colonisation influenced by and with feedback on physical-environmental drivers. The model is applied in a schematized mixed fluvial-tidal deltaic mangrove forest in dominantly muddy sediment inspired by the prograding delta of Porong, Indonesia. Model results successfully reproduce observed mangrove extent development, age-height relationship, and morphodynamic delta features.

Keywords: Mangrove dynamics; Sediment dynamics; Mangrove-hydromorphodynamic model; Individual-based mangrove model; Delft3D-FM; Mangrove modelling; Eco-geomorphology

3.1. INTRODUCTION

Climate change-driven extremes are associated with unprecedented weather changes like a stronger wave climate, frequent storm surges, and coastal flooding (Cooley et al., 2022; Wong et al., 2014). Globally, this will increase the vulnerability of the coasts with their coastal ecosystems and more than 600 million people (Kirezci et al., 2020; Magnan et al., 2022; Merkens et al., 2016; Temmerman et al., 2023). Traditionally, coastal areas are protected by man-made infrastructure that needs continuous and costly maintenance (Cheong et al., 2013; Duarte et al., 2013; Temmerman et al., 2013). More recently, the potentially more sustainable and cost-effective Nature-based Solutions (NbS) approach has been proposed for climate change adaptation (Cooley et al., 2022; Hijuelos et al., 2019; Narayan et al., 2016). The NbS — including mangrove ecosystems — play a pivotal role in climate adaptation by enhancing coastal resilience through the utilisation of eco-geomorphological processes that naturally adapt to changing environmental forcing while being multifunctional and relatively cost-effective (Borsje et al., 2011; Chen et al., 2016; Temmerman et al., 2023). Mangroves can contribute to sustainable coastal protection in the face of climate change (Krauss et al., 2008), increasing coastal resilience regarding vertical (Norris et al., 2021) and lateral erosion (Pennings et al., 2021).

The knowledge of the contribution of mangroves to hydrodynamic processes has been relatively well appreciated and understood. Much research has been conducted to understand how the extensive rooting systems, trunks, and lower part of the canopy slow down the water flow, attenuate waves, and thereby in the calm period, facilitate the deposition of fine sediments (Alongi, 2008; Mazda et al., 1997; Norris et al., 2021). Some studies show the potential of mangroves as a buffer to large, infrequent disturbances such as tsunamis (Dahdouh-Guebas et al., 2005; Kathiresan and Rajendran, 2005), storms (Das and Vincent, 2009; Fairchild et al., 2021), and coastal flooding (in combination with levees) (van Wesenbeeck et al., 2017). Environmental conditions, in their turn, influence the mangrove dynamics. Elevated intertidal mudflats allow mangroves to develop, whereas sediment deficits may erode coasts and mangrove belts. Varying temperatures, salinity levels, and bed elevation can change the mangrove community composition or structure over time (Alongi, 2008; Duke et al., 1998; Lugo and Snedaker, 1974; Osland et al., 2017; Woodroffe, 1992).

In reality, mangrove systems will develop in complex, species-specific feedback processes with forcing conditions and environmental evolution. For example, mangroves will attenuate waves, which facilitates deposition and bed elevation impacting again on mangrove growth/starvation. However, uncertainty remains given the high-non-linearity (Barbier et al., 2008; Murray et al., 2019) and critical failure threshold (Spalding et al., 2014; van Hespen et al., 2022b) of the mangroves. These spatiotemporal variations make quantifying the functional capacity of mangroves a challenge (Temmerman et al., 2023).

Ideally, resolving the contribution and interactions of mangroves with the physical stressors requires a detailed, spatially explicit modelling approach that covers all mangrove characteristics and life-stages (Dahdouh-Guebas et al., 2022; van Hespen et al., 2022a), where it is currently lacking. The most widely used modelling tools in resolving mangrove-ecogemorphological interactions are spatial and statistical models, followed by process-based and conceptual models (Rivera-Monroy et al., 2022). Pretzsch (2009), van Maanen et al. (2015), and Xie et al. (2020) provide examples of dynamic models that cover the forest-scale characterized by a top-down hierarchy where the growth is prescribed based on specific physical-environmental stress for each 'numerical cell' at a specified time. Only a few numerical models include physical-ecological processes, e.g., interactions between mangroves and waves, tides, and sediment dynamics in mangrove forests (Buffington et al., 2021; Fanous et al., 2023; Rodríguez et al., 2017; van Maanen et al., 2015; Willemsen et al., 2016). These grid-based approaches apply grid-averaged dynamics that may not reflect the actual mangrove dynamics (Berger and Hildenbrandt, 2000).

In contrast, Individual-Based Models (IBM) use a tree-centred or bottom-up approach leading to the detailed capture of species ranges, forest structure, biomass, and system behaviour (Wang et al., 2014). Examples are MANGRO (Doyle et al., 1995), FORMAN (Chen and Twilley, 1998), and KiWi (Berger and Hildenbrandt, 2000). Further development of mangrove IBM models is MesoFON (Grueters et al., 2014), adding crown plasticity to include in tree competition, BETTINA (Peters et al., 2014), which includes mangrove feedback to salinity, and MANGA (Bathmann et al., 2020) with plant groundwater-salinity feedback. Forest expansion depends on the successful seedling establishment (Shih et al., 2022; van Hespen et al., 2022a). However, treatment of rejuvenation in IBMs is still insufficient to simulate the establishment of a mangrove ecosystem as it depends on the dispersal of propagules. Propagule dispersion is critical for colonising and regenerating mangrove forests (Zainol et al., 2022). The dispersal mechanism is mainly attributed to hydrodynamic processes (Duke et al., 1998; Shih et al., 2022), which is not covered by the models mentioned. Although the IBM models have the capability to simulate the feedback to specific physical-environmental drivers, most of them assume a constant physical-environmental driver in time with spatial limitation to a local scale or a few hectares.

This study aims to develop a model that explicitly solves the hydrodynamic and morphological processes and their spatially explicit interactions with an individual-based mangrove dynamics model. Developing such a mangrove-ecosystem model requires a multi-modelling approach (Dahdouh-Guebas et al., 2022; Rivera-Monroy et al., 2022). This integration of multiple models includes the coupling of hydrodynamic (flow-waves), sediment transport, nutrient transport, and vegetation dynamics models. The proposed modelling approach benefits from the detailed forest structure provided by IBM (MesoFON) to parameterize the physics of mangroves to the hydro-morphodynamic

model (Delft3D-FM), while IBM can use spatiotemporal physical-environmental changes simulated from the hydro-morphodynamic model. This approach can readily be expanded to the forest and ecosystem development at the landscape/ regional scale. It will provide a full life-stage interaction (propagule, seedling, sapling, mature tree) depending on variations in inundation depth, bed level, and salinity.

In a schematized way, the proposed modelling approach is validated against a real-life case study of the prograding delta in Porong, East Java, Indonesia, resulting from an upstream mud volcano outburst (Beselly et al., 2021). Porong Delta has been experiencing unprecedented sediment load due to the mud volcanic eruption with a factor of 3-4 compared to before the eruption (Jennerjahn et al., 2013). This extreme condition has promoted rapidly prograding delta along with mangrove belt development (Sidik et al., 2016). First, we assess our model performance by its ability to reproduce the development of the long-term pattern in the observed mangrove extent and age-height relationship. Second, evaluate the pattern of mangrove growth, seedling dispersal/ reproduction, and mangrove extent in response to varying sediment concentration, river discharge, and salinity distribution.

3.2. METHODS

3.2.1. Model Description

In a so-called hybrid modelling approach (Vincenot et al., 2016), we couple the landscape-scale process-based hydromorphodynamic Delft3D-Flexible Mesh (DFM) model (Deltares, 2021) and the individual-based MesoFON (MFON) mangrove model (Grueters et al., 2014). By coupling these two model paradigms, the coupled model DFMFON generally encompasses: 1) the establishment of an individual-based mangrove community by propagule import from simulated hydrodynamics, 2) the expansion of mangrove belt in mutual interaction with a hydro-morphodynamic model including bed level development, and 3) the persistence of mangrove forest by regeneration and rejuvenation of individual mangrove trees after environmental changes such as varying salinity levels and other hydrodynamic growth conditions.

3.2.1.1. Coupling procedure

As indicated in Figure 3.1, DFM calculates hydrodynamic processes (waves, tides, and river discharge), sediment transport, and resulting morphodynamic development with a maximum hydrodynamic time step of 200 seconds. At each time-step, DFM calculates the bulk drag coefficient induced by mangrove trees. At the coupling interval of 90 days, the coupling interface translates DFM grid-based variables (water levels, salinities, and bed levels) into MFON tile-based salinity and Window of Opportunity (WoO) (Balke et

al., 2011) maps. Additionally, the coupling interface generates propagule dispersal pathways from two-week DFM averaged tidal flow patterns. Based on these data, MFON updates the mangrove stands in a 90-day mangrove dynamics run. The coupling interface then translates the new MFON-generated mangrove stands into a DFM grid-based drag coefficient field for the following 90-day DFM run. In the outer coupling, belowground biomass bed level change is calculated. The 90-day coupling interval was chosen to allow for seasonal fluctuations of the local climate (wet and dry seasons) and to realistically incorporate the reproduction of mangroves, such as flowering, fruiting, and seedling production. As the real case study location is fully inundated within the tidal range, we assumed the (porewater) salinity effect on mangrove growth equals surface seawater salinity. We presume an optimum condition for the mangrove growth, not depending on nutrient availability or other water quality aspects like pH level and hydrogen sulphide concentration.

The coupling interface is developed in Python 3.9.7 and applies the Basic Model Interface (BMI) module (Hutton et al., 2020). BMI enables the efficient retrieval and update of DFM variables (i.e., water levels, velocities, salinities, drag coefficients, and bed levels). Through this, the model represents the full mangrove life stage and interactions with ecological and physical drivers at each stage.

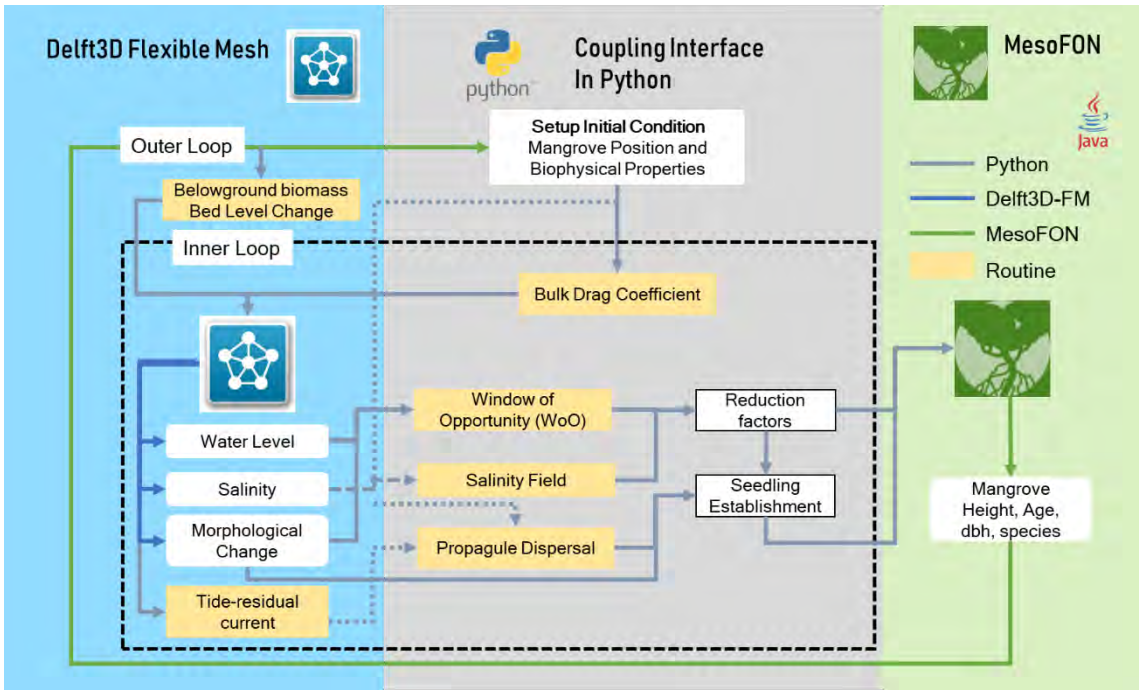

Figure 3.1. Overview of the coupled DFM-MFON model.

3.2.1.2. Entities and state variables

The model comprises single-species mangrove stands, and tiled landscape area maps as entities. The state variables of the trees in MFON were defined by the life stage (propagule, seedling, sapling, and mature tree), the species and biophysical properties: position, D_{130} (m), and height (m). The physical or hydro-morphodynamic drivers in DFM were defined as water level (m), salinity (ppt), spatial plant drag coefficient, water velocity (m/s), and bed level (m). The MFON tree environment was represented by 200x200m tiles from the DFM domain to prevent overloading each IBM with excessive numbers of individuals and to obtain the most optimum computational efficiency for individual-based simulation. The spatially varying salinity and WoO probability calculated in Python were converted to rasters and tiles (Figure 3.2).

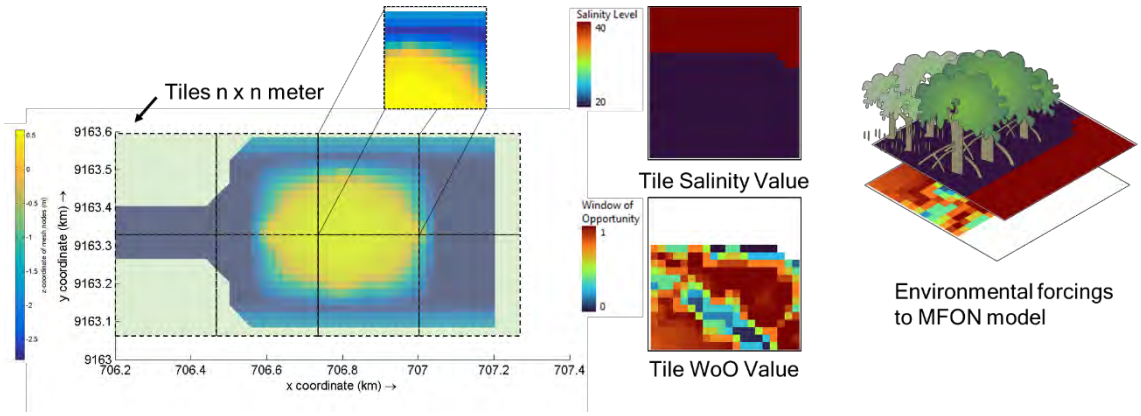

Figure 3.2. A schematic for retrieving and processing the variables of the DFM model. The (processed) values are converted into raster. The rasterised parameters were tiled and used as input for the MFON model.

3.2.1.3. Models

Delft3D-Flexible Mesh (DFM) hydro-morphodynamic model

We applied a state-of-the-art, process-based, open-source DFM in 2DH to solve the relevant hydro-morphodynamic processes and their spatiotemporal variations in the coastal, riverine, and estuarine areas (Deltares, 2021). DFM employs unstructured grids (triangles and quadrangles) to resolve shallow water equations under the Boussinesq assumption with a finite volume method. With the D-Flow module as its core for the hydrodynamic conditions (e.g., velocities, water elevations, and salinity), the DFM model is designed to interact with other DFM modules, e.g., D-Waves for wave modelling, D-Morphology for sediment transport and morphology. Additionally, DFM applies the BMI that enables initialising, running, retrieving, and altering parameters' values in standard interface calls (Figure 3.3).

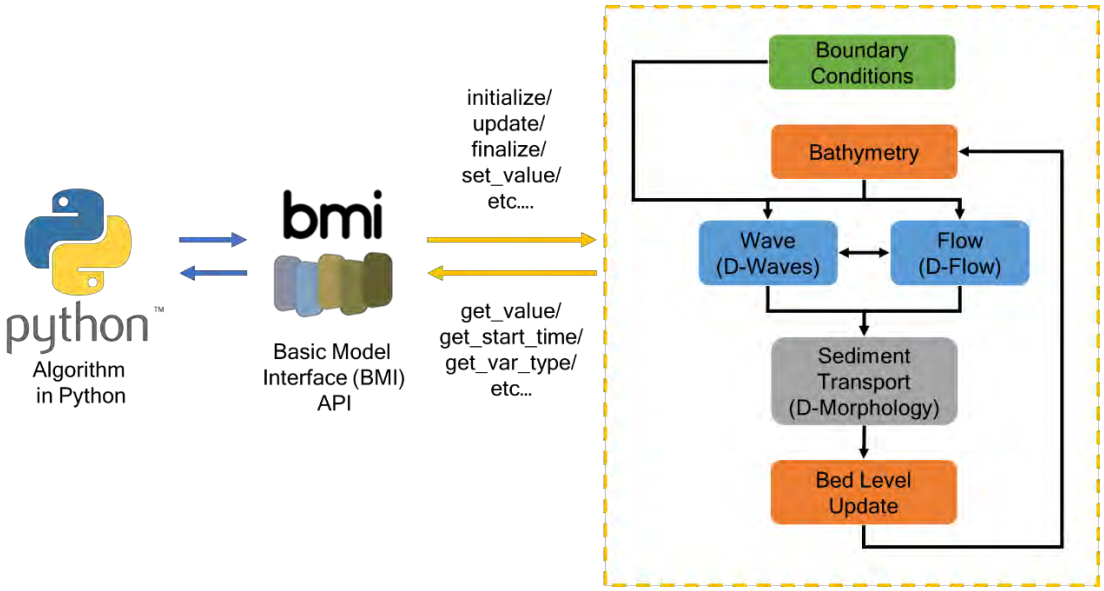

Figure 3.3. Overview of DFM full morphological loop model structure with the commonly used online coupled modules and BMI API function call in Python. The complete BMI functions for DFM can be explored at https://svn.oss.deltares.nl/. The BMI wrapper for the DFM model can be downloaded from the OpenEarth repository at https://github.com/openearth/bmi-python.

Mangrove systems are characterised by high turbulence, sometimes equivalent to the observed value in the surf zones (Norris et al., 2017), and well-mixed conditions that can be represented in the two-dimensional depth-averaged (2DH) model (Horstman et al., 2015). DFM separates the vegetation-induced resistance λ and bare bed roughness C ($m^{1/2}/s$) in the momentum equation (Deltares, 2021). The modified Baptist (Baptist et al., 2007) representative C and λ formula (Eq 3.1 and Eq 3.2) requires information on the height of vegetation h_v (m), density n (number of trees/ m^2), bulk drag coefficient (C_D), and bare bed roughness (C_b) for each grid cell. The calculated C_D will be used to estimate the mangrove-induced drag in the DFM model, whose implementation is provided in section 3.2.1.4.

$$C = C_b + \frac{\sqrt{g}}{\kappa}\ln\left(\frac{h}{h_v}\right)\sqrt{1+\frac{C_D n D h_v C_b^2}{2g}} \qquad (3.1)$$

$$\lambda = \frac{1}{2}C_D n D \frac{h_v}{h}\frac{C_b^2}{C^2} \qquad (3.2)$$

where h is water depth (m), κ is the dimensionless von Kármán constant, and D is stem diameter (m).

MesoFON (MFON) mangrove model

The overall purpose of the MFON model (Grueters et al., 2014) has been to simulate individual mangrove growth based on tree-to-tree competition and environmental conditions. The MFON model simulates up to ten mangrove species. The tree competition is based on the Field of Neighbourhood (FON) approach (Berger and Hildenbrandt, 2000). FON represents the radius of competition of each tree either above or below ground, where the strength of influence one tree exerts on another depends on the distance to the other tree (Figure 3.4) and the diameter of influence is related to the stem diameter. The recruitment and establishment in this study were updated and evaluated in the coupling interface to reflect the specific hydrodynamic conditions. MFON has the mangrove tree entity where crown plasticity is the most important process (deactivated in this study). MFON tree mortality processes depend on local disturbance events and in case of no growth in D_{130} averaged over five years. The most important design concept of MFON is how the mangrove tree senses and recognises the influence of neighbouring trees via its above- and below-ground FON.

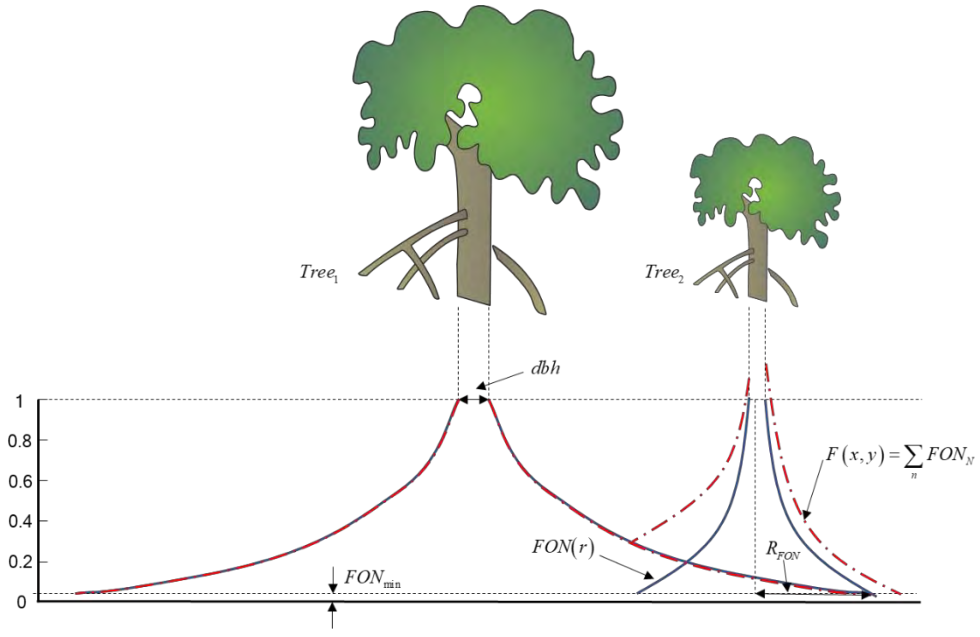

Figure 3.4. FON illustration as in MFON. It shows the intersecting FONs of two neighbouring trees (Tree1 and Tree2); the influence of Tree2 on Tree1 depends on the tree's size and how far the distance of each tree is.

3.2.1.4. Coupling interface

Mangroves interact with the environment and provide feedback dependent on the three factors that predominate physical processes, i.e., nutrients, salinity, and sea level/ hydroperiod (Grueters et al., 2014; Krauss et al., 2014; Wimmler et al., 2021). These factors are intertwined and affect the growth of mangrove trees, regulate species distribution and the zonation within the mangrove forest, and ultimately determine the productivity and extent of the mangrove ecosystem. The porewater salinity distribution (Lovelock et al., 2006; Piou et al., 2006) impact mangrove growth, and the spatial expansion depends on the tidal flooding and duration (Balke et al., 2015; Lovelock et al., 2015). These factors determine the mangroves' growth, dieback, and seaward expansion (through tree recruitment).

Drag Parameterisation

An accurate drag parameterisation is essential since the C_D value in mangrove forests depends on tree species and the root composition/ geometries (Mullarney et al., 2017), which varies over the water depth. However, considering the 2DH simulation, a bulk drag predictor was preferred. Therefore, we parameterised the presence of the mangroves as the bulk drag coefficient (C_D) using the formulations by van Maanen et al., 2015. This approach assumes that the drag force exerted on the mangroves depends on the vegetation length scale (L) in Eq. (3.4 as a function of the obstacles' projected area (A) and the obstacles volume (V_M) in a control volume (V). Eq. (3.3 was defined as the total of $C_{D,no}$ (drag coefficient of the bare surface) that was set to a value of 0.005. A dimensional constant e with a value of 5m is set to attain a realistic drag coefficient, as proposed by van Maanen et al. (2015).

$$C_D = C_{D,no} + \frac{e}{L} \tag{3.3}$$

$$L = \frac{V - V_M}{A} \tag{3.4}$$

The definition of obstacles volume (V_M) varies between species and hydroperiod. Therefore, we simplified the trunk as a truncated cone, with a diameter at the base d_0 and a diameter at each water depth d_{wd} derived from the species-specific diameter-height allometric relationship (Berger and Hildenbrandt, 2000) following the mangrove's age. Furthermore, mangroves have different rooting systems, i.e., pneumatophores of *Avicennia* spp., root knees of *Bruguiera* spp., and plank roots of *Kandelia* spp. Therefore,

we simplified the rooting systems (Figure 3.5) as cones (Eq. (3.5)), cylinders (Eq. (3.6)), and prisms (Eq. (3.7)), respectively (Du et al., 2021; Mazda et al., 2006, 1997).

$$V_{M,avicennia} = \sum_{i=1}^{n} \frac{\pi D_i^2 H_i}{12} \quad (3.5)$$

$$V_{M,brugueira} = \sum_{i=1}^{n} A_i H_i \quad (3.6)$$

$$V_{M,kandelia} = \sum_{i=1}^{n} A_i H_i \quad (3.7)$$

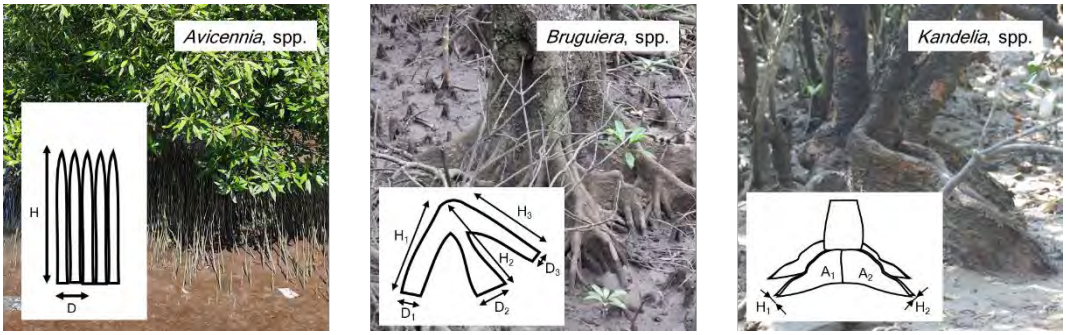

Figure 3.5. Simplification of the rooting systems and the parameterisation for bulk drag coefficient calculations.

The window of opportunity for propagule establishment

The effect of hydroperiod was taken into account by the concept of Window of Opportunity (WoO) (Balke et al., 2011). WoO describes the minimum disturbance-free period as a critical duration that allows seedling establishment. This disturbance-free period is defined by the time series of external forcing, e.g., tidal water level and waves. Balke et al. (2015) indicate that five inundation-free days are required for *Avicennia marina* to let the propagule's root securely anchor with a length of 1.6 cm. Before that, two days of root growth resulting in 0.5 cm length are essential to prevent seedling toppling due to inundation with no waves. We calculate the WoO probability by taking the daily maximum water level in each cell of Delft3D-FM to find the minimum three days inundation free period and calculate the probability.

Propagule production and tree recruitment

The reproduction phase of *Avicennia marina* trees is characterised by peak propagule production during the wet season (Almahasheer et al., 2016; Jiménez, 1992) with an obligate dispersal of one to two weeks (Booker et al., 1998; Clarke, 1993; Rabinowitz, 1978). Reports mentioned propagules could float up to several months and remain viable, for example, *R. apiculata* and *R. mucronata* in Micronesia, three months and five months, respectively (Drexler, 2001), and *B. sexangula* in Hawai'i (2 months) (Allen and Krauss, 2006). *Avicennia* spp. trees in the study area (Porong Estuary) are estimated to start producing propagules at the age of 3-4 years (Anwar and Gunawan, 2006; Sidik et al., 2013; Wirjoadmodjo and Hamzah, 1982). In the model, we parameterised the propagule production to occur in January (Anwar, 2006; Tala, 2020) for mangrove trees older than four years. The number of propagules produced by a tree per year (N) follows this equation:

$$N = f_{red,P} \times f_{red,sal} \times D \times A \qquad (3.8)$$

where $f_{red,P}$ and $f_{red,sal}$ are the reduction factors due to nutrient availability and salinity, respectively. D is the species-specific seedling density per crown surface area A, which is assumed to have a value of 0.06 (1/m^2). The $f_{red,P}$ is held constant with the value of 1 during the simulation (Grueters et al., 2019), assuming the nutrient availability is suitable for optimum growth, while the varying $f_{red,sal}$ is dependent on the seawater salinity map obtained from hydrodynamic simulation and is calculated as:

$$f_{red,sal} = \frac{1}{1+\exp\left(d\left(U_i - U\right)\right)} \qquad (3.9)$$

Where U is the salinity value in ppt, d is a constant that determines the decline of $f_{red,sal}$ with increasing salinity (-0.18 for *Avicennia* spp.). The constant U_i is the salinity at which $f_{red,sal}$ is 0.5 (72.0 ppt for *Avicennia* spp.) (Chen and Twilley, 1998). The salinity factor is considered important as high salinity values likely reduce propagule reproduction or dispersal (Lovelock et al., 2017). In the model, the salinity value is determined by taking the median value from the DFM model on each cell during the coupling period.

At first, the propagules are uniformly distributed (Srivastava and Khamis, 1978) along the area of the crown surface at $Pos\left(x,y\right)_n$. Next, as *A. marina* propagule is buoyant (Van der Stocken et al., 2019) and able to float irrespective of salinity (Clarke et al., 2001),

local propagule dispersal around the parental tree depends on the magnitude and direction of the current without the influence from the wind. The propagule dispersal is only calculated for the first two weeks after release, considering the minimum inundation-free period for *Avicennia* spp. to achieve the early anchorage of the propagules (Balke et al., 2015) obligate for seedling establishment. We calculated the average tidal current ($\vec{u}$) over the two weeks of simulation days to determine the transport pathway of propagules. Assuming the tidal current is the dominant process over the propagules buoyancy properties (Di Nitto et al., 2013), the final position ($Pos(x,y)_{final}$) can be formulated as:

$$Pos(x,y)_{final} = Pos(x,y)_{n} + \vec{u} \times dt \qquad (3.10)$$

The survival of the spatially distributed propagules is then evaluated by considering the tidal inundation period P_{WoO} and sediment disturbance $S_{disturb,sed}$ (burial due to sediment and uprooting due to erosion) following the WoO (Balke et al., 2015). Finally, the surviving seedlings are allowed to grow in their final position until sapling age (two years) and are subsequently transferred as saplings to the MesoFON module. We close the life cycle of the mangroves by introducing the propagules and seedlings. This is a novel contribution to the mangrove stand models since previous ones such as FORMAN (Chen and Twilley, 1998), KiWi (Berger and Hildenbrandt, 2000), and MesoFON (Grueters et al., 2014) simulated tree recruitment as saplings, except for MANGRO (Doyle et al., 1995) that simulated it as seedlings. Additionally, forest expansion is driven by the successful seedling establishment.

3.2.2. Experimental Design

3.2.2.1. Case study

The schematised model was set based on the physical characteristics of the prograding Porong Delta in Indonesia (Figure 3.6c). Porong Delta has been experiencing rapid progradation due to high sediment load from the diverted mud volcano outburst. We initiated the domain based on the northern delta lobe's geomorphological characteristics in 2016, as described by Beselly et al. (2021). In this period, the delta lobe was just emerged and was naturally colonized by the mangroves, even though mangrove planting activity was conducted in 2017. We collected a decade of daily river discharge, water level observation, and a series of campaigns of sediment sampling, bathymetry, sediment concentration, tidal, and waves. Mangrove observations were conducted in 2010, 2011 (Setiawan et al., 2019) and updated in 2019 (Beselly et al., 2021) and 2021.

3.2.2.2. Model parameterisation and schematisation

Figure 3.6d shows the schematised model consisting of a 1500m long funnel-shaped estuary with a river mouth converged from 140m at the landward head to 500m at the end of the basin. The river channel area was defined as a rectangular polygon with a length and width of 240m and 140m, respectively, followed by a delta area with the dimension of 500 m x 640 m, where the 120 m triangular-shaped polygons are in the transition. This domain's configuration comprised grid cells with a size of 20 m. The initial bathymetry was prescribed with the presence of the delta lobe in the middle of the estuary to quickly start the delta development and attain the dual channel (north-south) system as observed in the field. It has a depth of -2.8m in all domains, with 0.8m at the crest of the lobe. The erodible banks, river, and seabed have an initial sediment thickness of 30m. The sediment consists of mud. We used a uniform value of Chézy roughness 65 $m^{1/2} / s$ to represent the soft bed of cohesive sediment in the condition without vegetation.

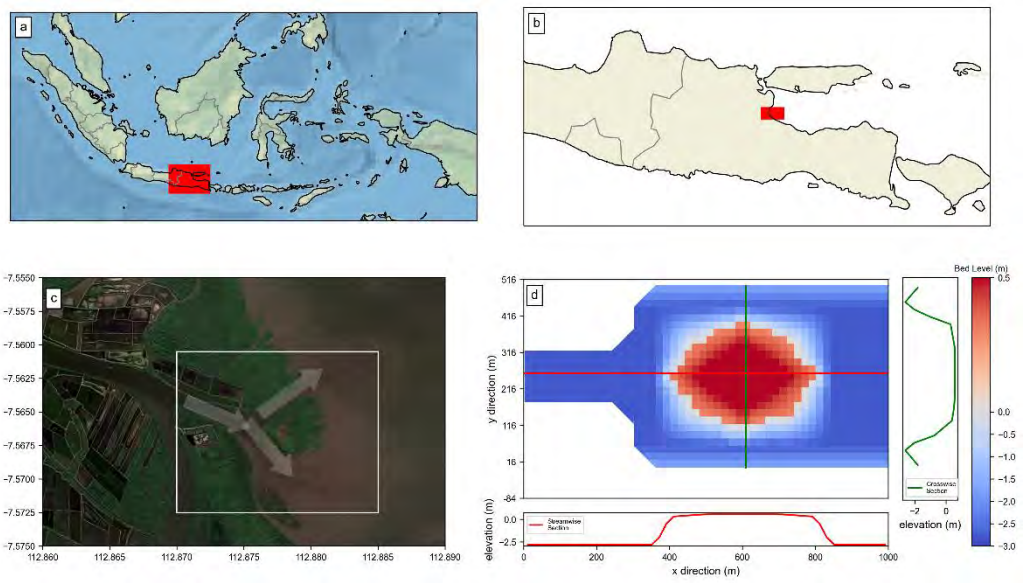

Figure 3.6. The real case study is located in Indonesia (a), East Java Province (b), focusing on the northern delta lobe in Porong Delta (c), where it is schematized into a funnel shape estuarine with a delta in the middle (d). In (d), the details of the model domain, grid arrangement, bathymetric, and cross sections are presented.

We forced the model with two open boundaries: (seasonal) fresh water river discharge at the landward end and tidal water level variation at the seaward boundary. Because of the low prevailing significant wave height, we did not include wind-generated waves in the schematised model. The river boundary was set as the only boundary to supply sediment and schematised to flow the discharge of 0 or 35 m^3/s during the dry season (June to November) and 150 m^3/s during the wet season (December to May) following the average seasonal discharge as observed. The seaward boundary has a semi-diurnal M2 signal with

an amplitude of 1.2m and an initial salinity of 25 ppt, as the tidal range in the study area. A suspended sediment concentration (SSC), varying between scenarios, was defined at the river boundary with a Thatcher-Harleman time lag of 90 minutes. Thatcher-Harleman time lag gradually releases the concentration during the prescribed period at the river boundary to prevent sudden variation of the suspended sediment concentration on tidal flow reversal (Deltares, 2021).

A morphological factor (MF) of 30 was used in this study. It means a single hydrodynamic tide results in morphological changes of 1 month, thus reducing the computational time. In the presence of waves, a maximum MF value of 50 may be applied, whereas values up to 400 may be used without waves (van der Wegen and Roelvink, 2008). With MF=30, three DFM simulation days equal three months or 90 days of morphological update. Thus, it will match the offline three-monthly coupling with MFON. Ultimately, two years of hydrodynamic simulation with MF can produce 60 years of morphodynamic evolution. This time scale was chosen to deal with the high computational demand of the MFON model while still having the representation of mangrove dynamics (at decadal time scale) and the (estuarine) landscape development. A detailed model setting is described in Appendix 3-A.

3.2.2.3. Initialisation

Initially, a forest plot area in the upstream part of the delta is distributed with randomly placed saplings. Next, the initial mangrove position (x and y) and uniform biophysical properties (species, diameter at breast height (D_{130}), and height) were prepared as a shapefile. An additional initialisation procedure was the definition of the seaward limit of the mangrove edge. Mangroves' seaward boundary is limited to the lowest low water level (LLWL) and 0.5 m additional elevation as the buffer. Next, we converted the bathymetry as a raster, clipped the raster following the seaward limit, and tiled the raster and mangrove shapefile as the MFON world. MFON parameter files were prepared for separate tiles, and the simulation can be started.

3.2.2.4. Scenarios

We defined eight different sensitivity scenarios as shown in Table 3.1. These scenarios reflect high-to-low salinity by varying river discharge quantity for each season and rich-to-poor sediment scenarios by varying the sediment concentration value. The settings are based on the actual conditions in Porong Estuary. Porong River, one of the major branches of the regulated Brantas Watershed, is equipped with a series of barrages and floodgates. These flood control structures make the river act more as a diversion channel, with almost no discharge during the dry season and high flow during the wet season. The suspended

sediment concentration (SSC) in Porong River depends on the hinterland's mud disposal operation.

3.2.2.5. Model results analysis

We assessed the simulation results with qualitative and quantitative analyses. Qualitatively, we look at the expansion pattern of the mangrove extent during the simulation period. We examine the shape of the mangrove extent and the stand structure. The simulated patterns are compared visually with the satellite observations presented by Beselly et al. (2021). Quantitatively, we divide the analysis to explain the mangrove and estuary feedback with the hydromorphodynamic phenomena as proxies. Vegetation responds to environmental forcing in the form of biophysical property changes. For instance, the most noticeable quantity (even from medium-resolution satellite products) is the mangrove area development. First, we sorted the geo-referenced simulated trees from the tallest to the smallest. Then, the canopy area is calculated as circular from the centre of each tree's stem. When the mangroves' canopies overlap, we intersect the area and calculate the union. With this approach, the smaller trees' area is not calculated, but the top of the canopy is. This approach is similar to the satellite-based mangrove extent observation. Another noticeable quantity is the mangrove height. We use the top of the canopy height to validate the simulation with the observation. The Porong mangrove forest shows seasonal variation dynamics. Here, we use the seasonal-trend decomposition (STL) using LOESS (locally estimated scatterplot smoothing) (Cleveland et al., 1990) to decompose the spatio-temporal variability of the mangroves into the trend and seasonal components. We performed STL analysis with the statsmodel v0.13.2 package in Python (Seabold and Perktold, 2010). The STL method has been commonly used to analyse the (seasonal) time series development, e.g., nutrient concentration trend in a coastal catchment (Wan et al., 2017), mangrove biomass (Furusawa et al., 2013), and mangrove forest cover phenology (Chamberlain et al., 2021). Regarding morphodynamic analyses, we compared the bed level with and without mangroves for each scenario. We also analysed the morphodynamic development and hydrodynamic responses in the vegetated domain.

Table 3.1. Sensitivity scenarios on seasonal variation in mangrove development

Scenario	Discharge (m^3/s)		Concentration (kg/m^3)		Condition
	Wet	Dry	Wet	Dry	
A	150	0	0.05	0	Hi Sal, Rich Sed (base scenario)

Scenario	Discharge (m^3/s)		Concentration (kg/m^3)		Condition
	Wet	Dry	Wet	Dry	
B1	150	0	0.03	0	Hi Sal, Med Sed
B2	150	0	0.01	0	Hi Sal, Poor Sed
C	150	35	0.05	0	Low Sal, Rich Sed
D1	150	35	0.03	0	Low Sal, Med Sed
D2	150	35	0.01	0	Low Sal, Poor Sed
E	150	35	0.05	0.01	Low Sal, Rich Sed (Wet and Dry)
F	150	35	0.03	0.01	Low Sal, Med Sed (Wet and Dry)

3.3. RESULTS

3.3.1. Mangrove-morphodynamics responses and feedback loop: general pattern

At the beginning of the simulation, we started all scenarios with a small patch of homogeneous *Avicennia marina* stands in the upstream part of the delta. To simulate the natural colonisation, we adopted a sparse saplings' density of 0.03/m^2, as observed in the case study location. These saplings have homogenous biophysical characteristics with 1.37 m height and 0.096 m D_{130} at the age of 1 year. The initial mangrove area covers around 8% of the delta area above the lowest low water level. The simulation results indicate approximately three major phases in the general development of the mangrove dynamics. These phases are discriminated from visual analysis of the DFM-MFON model results (Figure 3.7 and Appendix 3-B) and the mangrove area (Figure 3.8). Phase 1 represents the first 15 years of development (year 0 to year 15), Phase 2 represents years 15 to 30, and the final Phase 3 represents years 30 to 60. The developments' division is

clearly seen from slope changes and the spread of the scenario pathways, as in Figure 3.8. Please refer to Appendix 3-B for all scenario plots and Supplement 1[3] for the animations.

In the first phase of the simulation, mangroves tend to colonise the available space in the delta lobe, which is related to the available accommodation space. Mangroves expand and fill the space until they reach the physical limit (mean sea level). The gradual distribution of mangrove stands reflects older trees in the interior and younger trees at the fringe.

After about 15 years, the rate of mangrove area expansion has increased for every scenario compared to the initial years (Figure 3.8). The reason is that the mangrove population has matured and started producing more propagules. The available accommodation space in the platform begins to be filled with the propagules transported by the current. After that, in phase three, the propagules start to disperse outside the delta or into the allowable area along the northern and southern channels triggering mangrove establishment outside the delta (Figure 3.7).

[3] Supplementary materials can be accessed from: https://ars.els-cdn.com/content/image/1-s2.0-S1364815223002001-mmc1.zip

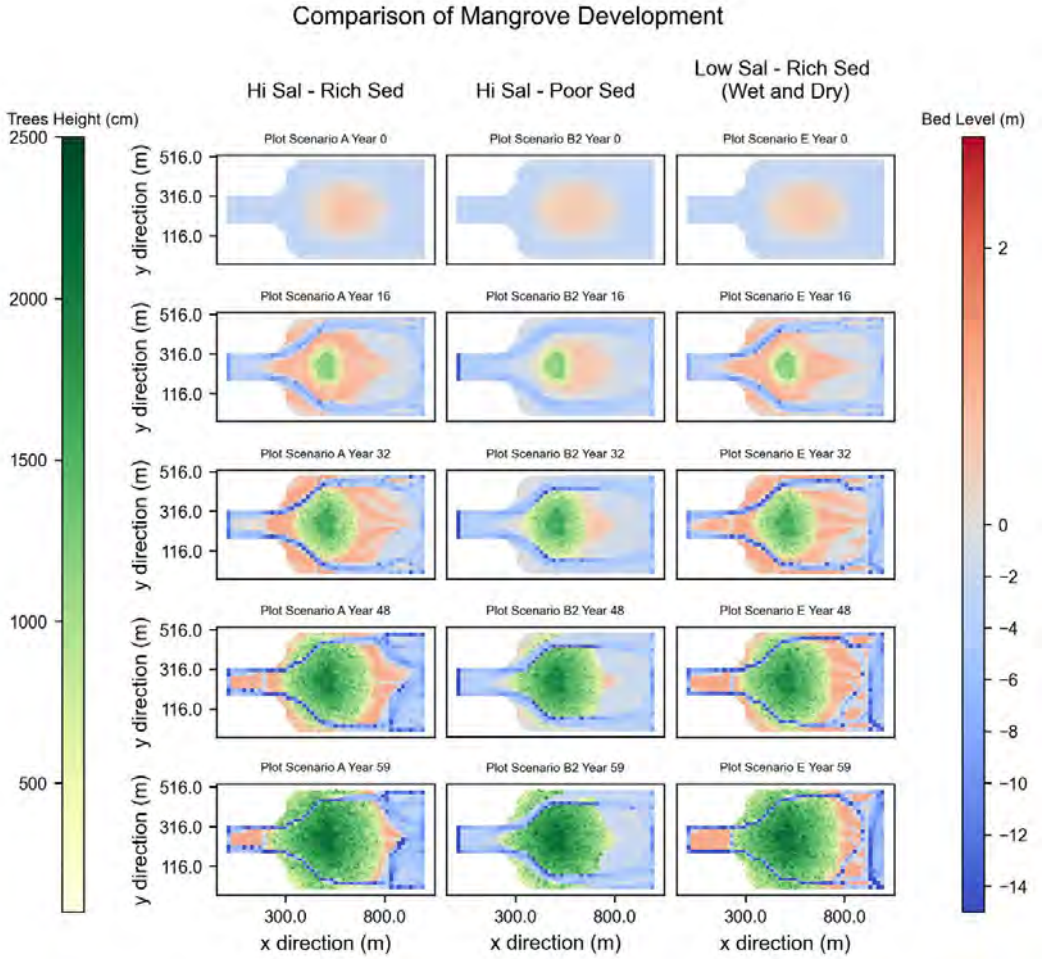

Figure 3.7. Snapshot of mangrove development from selected scenarios representing extreme environmental conditions (high-low salinity) and sediment availability (rich-poor sediment availability). In the scatter plot, the size of a tree is relative to its diameter; a larger circle implies a wider tree diameter. With this, we can examine the distribution and structure of the mangrove stand where the darker green scatter has older and taller trees.

Since the production of propagules correlates with the biophysical properties, the mangrove stands' height and age distribution affect the mangrove expansion pattern. Initially, more propagules are produced by the mature trees in the interior rather than by the younger population at the fringes. A mature tree is defined (Wilson, 2020) by the change from the non-flowering (juvenile) stage to the flowering (mature) stage. The number of propagules dispersed is more concentrated in the interior. Thus, the propagules drifting outside the delta remain few. As competition in the interior increases (Figure 3.9

and see Supplement 2[4] for all scenarios), successful recruitment in the interior becomes limited, but the mature mangroves at the fringes easily disperse the propagules around the delta. After 30 years, the newly established mangrove population adjacent to the northern and southern channels initiates the life cycle and even occupies the accommodation space inland.

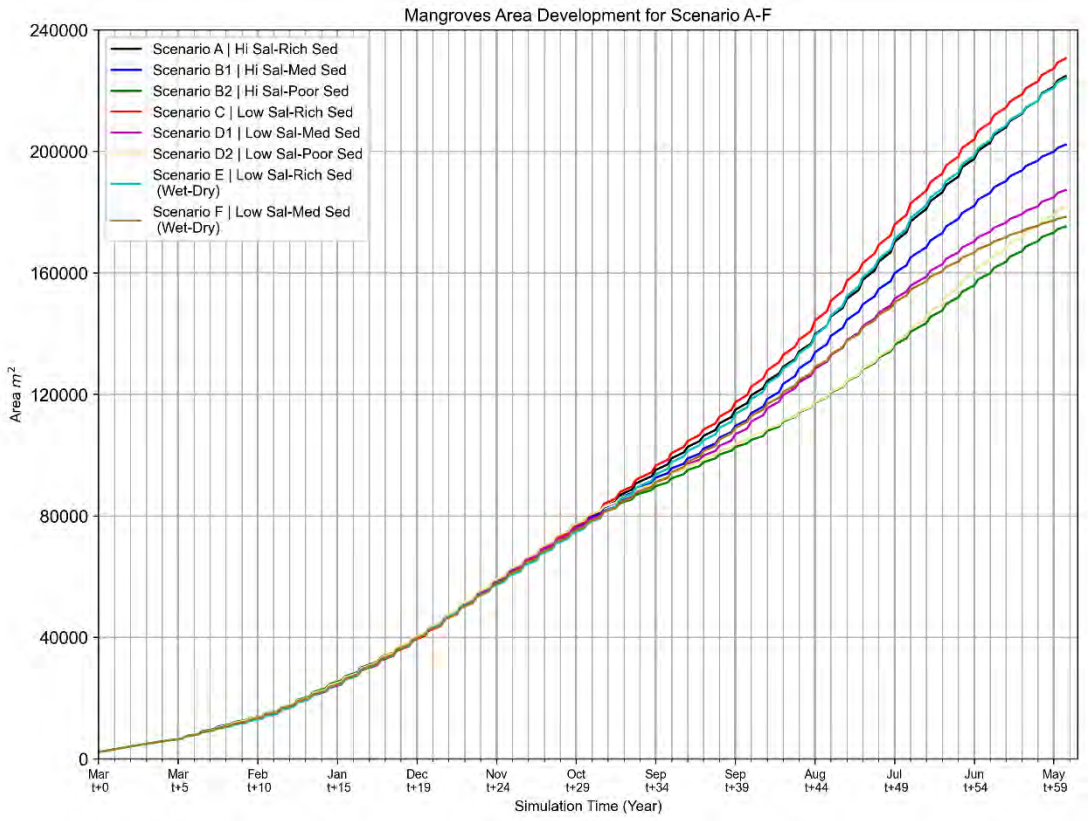

Figure 3.8. Simulated mangrove area development for 60 years of simulation.

Phase 2 and phase 3 show the contribution of sediment availability. In contrast to the slightly different pathway described in the mangrove's area development in phase 2, the top of the canopy parameter indicates a significant role in sediment availability. In contrast to poor sediment scenarios, rich sediment scenarios provide more accommodation space, less competition for space, and, therefore, an increase in the distribution of the higher mangrove stands. The higher sediment concentration scenarios create a wider and more elevated intertidal area. At the beginning of phase 3, a transition is observed with rich sediment scenarios having a higher mangrove population. It is noted

[4] Supplementary materials can be accessed from: https://ars.els-cdn.com/content/image/1-s2.0-S1364815223002001-mmc2.docx

that with the highly saturated mangrove population in the delta, the competition for space increases (Figure 3.9).

As the mangroves grow and reproduce, larger mangroves have wider FON related to stem diameter and tree height (Figure 3.4). Due to reproduction in the denser mangrove stands, the intersecting FONs raise the strength of influence one tree exerts on another. Hence, the intra-specific competition (competition within the same species in the same plot) value shown in Figure 3.9 increases over time. The mangrove population in the middle of the delta showed the most noticeable increasing pattern as the model was initialized in these tiles. The effect of high competition, a smaller WoO, and limited propagule dispersal have triggered dieback of the younger stands, as illustrated by the bend of northern channel and the centre of the southern channel. One can see the peak of the competition between year 40 and year 50 and the decline in the following years. In these tiles, the propagules were initially dispersed close to the fringing parental trees due to limited accommodation space. As a result of the higher competition, young trees are more likely to die off. In the next phase, mature trees located inland and those surviving grow with a lower competition resulting from the preceding dieback and the sedimentation facilitated by the reduced flow velocities in the forest. As reproduction restarts, the competition begins to increase.

The seasonal influence on the competition shows up as a cyclic pattern over the year. We observed the lowest competition at the beginning of the wet season and the peak of competition at the middle and the end of the dry season. The low competition value in the wet season is likely related to the dieback of some mangroves due to the strong competition in the dry season of the previous year and relatively favourable conditions during the wet season. With the optimal growth of the mangroves during the wet season and simultaneous increase in density due to propagule production, the trees experience the highest competition value during the dry season.

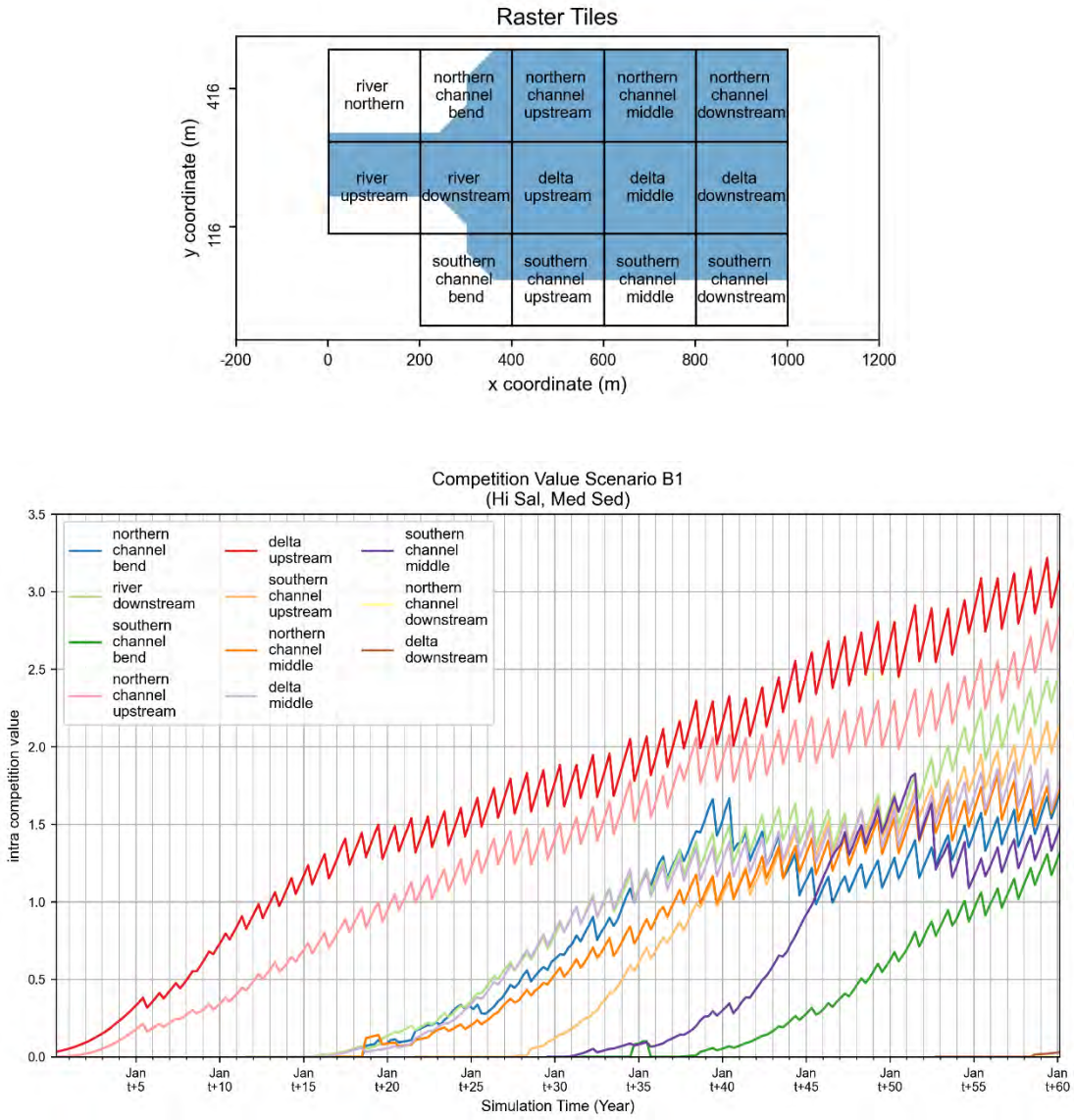

Figure 3.9. The tiles of the MFON model (top panel) Intra-specific competition value (bottom panel) for each tile in Scenario A. Intra-specific competition value is averaged over each tile. The competition plot for all scenarios is provided in Supplement 2.

The schematized model can qualitatively reproduce the observed expansion pattern in the Porong Delta, as shown in Figure 3.10. The simulated mangrove extent in Figure 3.10b resembles the extent in the observed pattern in Figure 3.10a obtained from integrating satellite and drone analysis from Beselly et al. (2021). The simulated mangrove extent tends to follow a similar shape as in Porong. However, the schematized model cannot reproduce a similar expansion rate as in the case study. The reasons can be explained as follows. First, we assume only single species in the model (*Avicennia* spp). Second, the northern delta lobe has multiple sources of propagules, i.e., from the northern mainland

and the LUSI Island which can increase the number of individuals in the northern delta lobe. Third, in the absence of data for Porong, we assume that the reproduction rate is similar to that of *Avicennia germinans* (Grueters et al., 2014), even though reproduction is known to be species-specific. Forth, January-February is the peak of the rainy season. In this condition, the contribution of river discharge and local precipitation can contribute to longer-distance propagule transport from the multiple mangrove forests in the vicinity.

The canopy height trend of mangrove stands from the model shows a good agreement with the observation with an R^2 value of 0.982 and mean absolute error of 1.105m (Figure 3.10c). This value is compared to age-height relationship of the canopy height model from 2016 to 2021. Considering the simplified environmental forcing in the model and the variation of the environmental conditions in the case study, we expected a difference for each scenario but a similar trend.

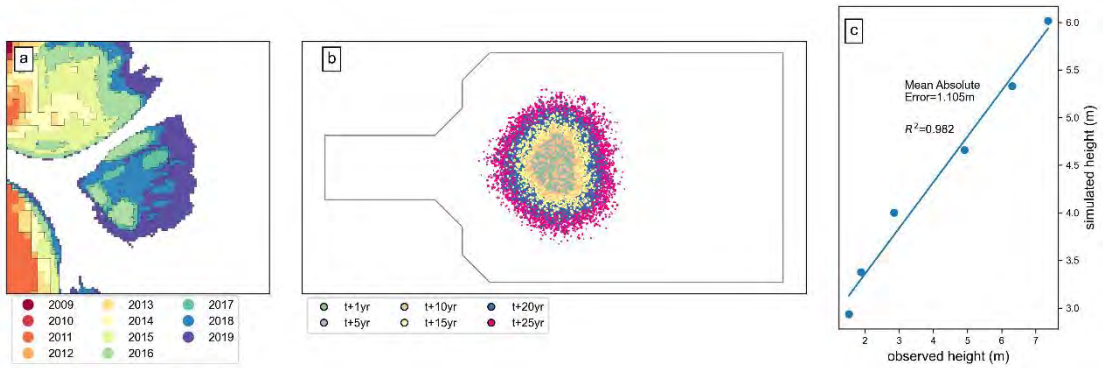

Figure 3.10. Qualitative comparison of the DFMFON model with the Porong Delta (Indonesia) case study (Beselly et al., 2021). Beselly et al. produced an annual mangrove extent map (a) that reasonably matched the modelled development of mangrove extent in a schematized model domain (b) as well as the reasonable agreement of the observed and modelled height development (c).

3.3.2. Mangrove responses under seasonally changing environmental conditions

3.3.2.1. Response to salinity

We found no direct effect of salinity on tree development in the low range chosen for the scenarios (0 to 25ppt). No apparent difference exists between low and high salinity conditions in all scenarios, either in the canopy area or propagule production. This is due to the fact that *Avicennia* spp. are among the most salt-tolerant mangroves (Jayatissa et al., 2008) and will not be significantly affected until a salinity value of over 60 ppt is exceeded (Chen and Twilley, 1998).

We visually compare different salinity treatments (Hi Sal-Low Sal) within the same sediment load scenario (Table 3.1), i.e., the comparison of Hi Sal and Low Sal treatment for Rich Sed scenarios (A-C), Med Sed (B1-D1), and Poor Sed (B2-D2). We compare the effect of salinity on the canopy area (Figure 3.8), on mangrove forest development for all sediment load scenarios (in Appendix 3-C), and propagule production (Figure 3.11). Appendix 3-D provides boxplots of monthly salinity values for each scenario. The effect of contrasting salinity conditions on the mangrove expansion pattern and the propagule production is relatively minor. The slightly larger mangrove extent in a lower salinity environment, as shown in Figure 3.8, relates to how we parameterize low salinity by adding freshwater discharge during the dry season. Additional discharge from the river boundary during the dry season transported sediment, created more accommodation space, and thus increased the probability of seedlings being established. In addition, to clarify the argumentation, we devised all saline conditions of all Low Sal scenarios. These additional simulations would not represent real-world scenarios but rather allow us to test the pure effect of Low Saline compared to Full Saline conditions as opposed to the combined effect of salinity and high fresh-water discharged examined above. Results in Supplement 3[5] show that low salinity of 25ppt makes a minor contribution to mangrove development, while sediment availability and the resulting accommodation space contribute more.

[5] Supplementary materials can be accessed from: https://ars.els-cdn.com/content/image/1-s2.0-S1364815223002001-mmc3.docx

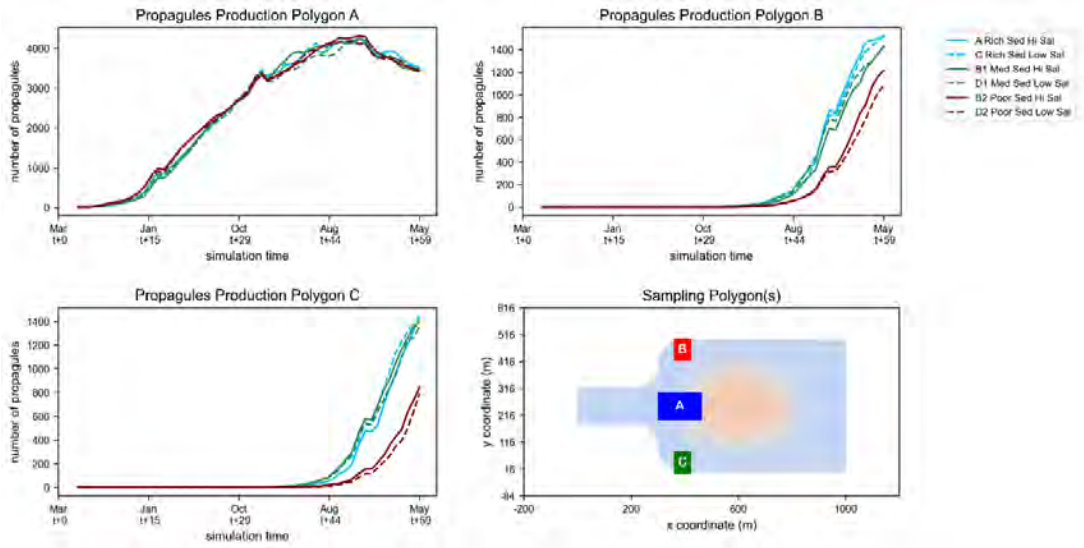

Figure 3.11. Propagule production comparison plot for variation in salinity conditions. The figure compares the effect of salinity variation on propagule productions in similar sediment concentration environments. The surveyed polygons were carefully selected to ensure the minimal effect of changes in morphology by selecting the area with the lowest difference in cumulative erosion-sedimentation value. With this, we are confident the sampling polygons can represent different salinity treatments in the domain's main delta and northern-southern limit.

3.3.2.2. Response to sediment availability

Among the simulated physical drivers, sediment availability plays an important role in mangrove forest expansion (Rogers, 2021, Woodroffe et al., 2016, Xie et al., 2022). More sediment supply increases the accommodation space under accretive conditions. More accommodation space, in turn, increases the probability for the dispersed propagules to find space to settle and, in case the inundation period is low, to anchor the rooting system and develop. We compared the contrasting sediment conditions of the same saline environment, i.e., (Rich-Med-Poor Sed) with (Hi Sal): A-B1-B2, (Rich-Med-Poor Sed) with (Low Sal): C-D1-D2, and (Rich-Med Sed) with (Low Sal) and with (extra sediment in the dry season): E-F.

In Figure 3.7 and Figure 3.12, we observe rich sediment scenarios promoting the generation of a wider mudflat and, thus, more mangrove colonization in a larger accommodation space, primarily visible in the streamwise or east-west cross-section (blue line). Looking at the panels, it is clear that the extent of the initial bed level (black line) is wide enough for the mangroves to expand. Sediment supply and fluvial discharge stimulated propagules in the delta to establish downstream. The flat and sufficiently high

bed level increases the WoO and the establishment probability. Throughout the simulation period, the level of the riverbed changes slightly downstream. However, an upstream prograding pattern can be observed, where mudflat builds up, and mangroves establish. The outermost fringe of the mangrove is located at the edge of the mudflat on the line of the lowest low water level (LLWL).

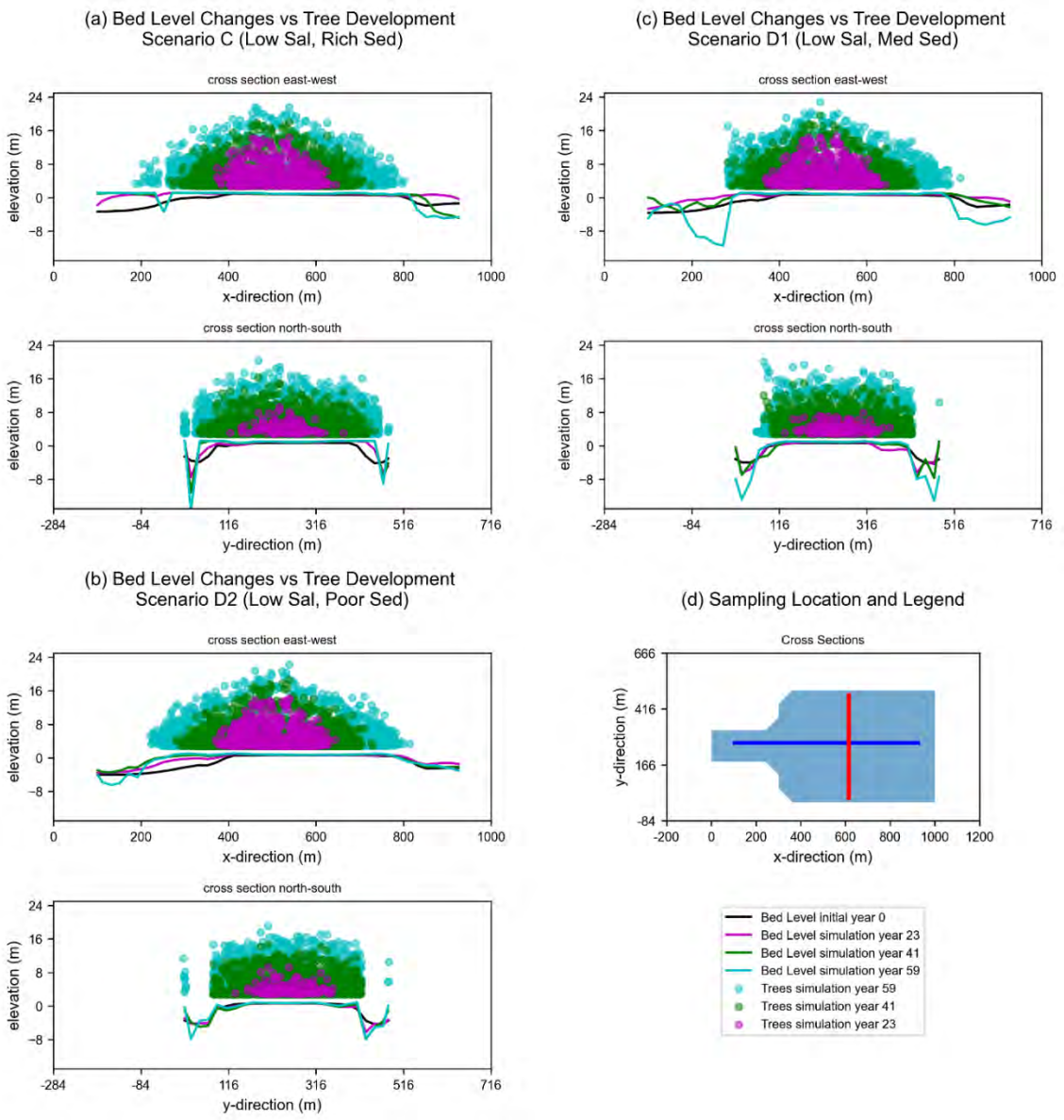

Figure 3.12. The plot of mangrove forest development for scenario C (panel a), scenario D1 (panel b), scenario D2 (panel c), and the cross-section(s) on panel d. The plot shows the time series development of bed level and trees 23, 41, and 59 years after initialisation.

Looking at the north-south cross-section, the dependence of mangrove establishment on bed level is more visible. In scenarios C and D1, a creek-like depression was created on the northward side of the mangrove forest after 23 years. However, since the depression was shallow enough, it was colonised by the mangroves. As an effect, this increased the bed level and widened the platform to the north and south. Therefore, more accommodation space was available, and thus, mangroves occupied the space until the LLWL line. We can also see the establishment due to propagule dispersal in the northern and southern limits of the domain, where accommodation space was available. It is more visible in scenario D2; until year 23, the bed level was lower, and no mangroves could establish. However, beginning with the year 41, the bed level was higher, and therefore, it could be occupied by the propagules and established seedlings. The contribution of belowground biomass is visible in all the plots, especially in the interior, even though minimal, in the order of millimetres annually.

3.3.2.3. Seasonality

To isolate the seasonality effect from the long-term trend, we decomposed mangrove area development at quarterly intervals (90 days) using LOESS analysis. Figure 3.13 illustrates the decomposition into the mangrove area trend and seasonal components of Scenario A. Other scenarios show a similar component pattern in Supplement 4[6].

The seasonal component demonstrates that the development of the mangrove area follows an oscillating pattern mirroring the seasonal boundary conditions. A similar seasonality pattern of mangrove expansion (wet-dry season) was observed in the Porong Delta (Beselly et al., 2021). Spatially, the extent of the variation is similar across the scenarios, ranging from +500m^2 to -500m^2. Temporally, within one year of simulation, one can observe growth during the wet season and decline during the dry season with an overall positive net rate.

In the seasonal variation panel of Figure 3.13, we observe a wet-dry season cycle of mangrove dynamics. Mangroves expand in January, concurrent with the beginning of the propagules production. The mangroves are growing optimally during the wet season, given the river's freshwater discharge and high sediment supply. At the end of the wet season, the young mangroves maintain growth, profiting from low competition for the space provided by the sediment deposition and the relatively lower salinity associated with the wet season. This favourable environment prevails until September, which is in the middle of the dry season. The peak of mangrove expansion is in September, given the

[6] Supplementary materials can be accessed from: https://ars.els-cdn.com/content/image/1-s2.0-S1364815223002001-mmc4.docx

optimal conditions inherited from the wet season. After this peak, competition stress increases (Figure 3.9) as the environment becomes less favourable due to low sediment availability and reduced bed level. The smaller (younger) trees die first while neighbouring trees develop less. The decrease in the mangrove area indicates that this process continues until January, when the cycle starts again with propagule production.

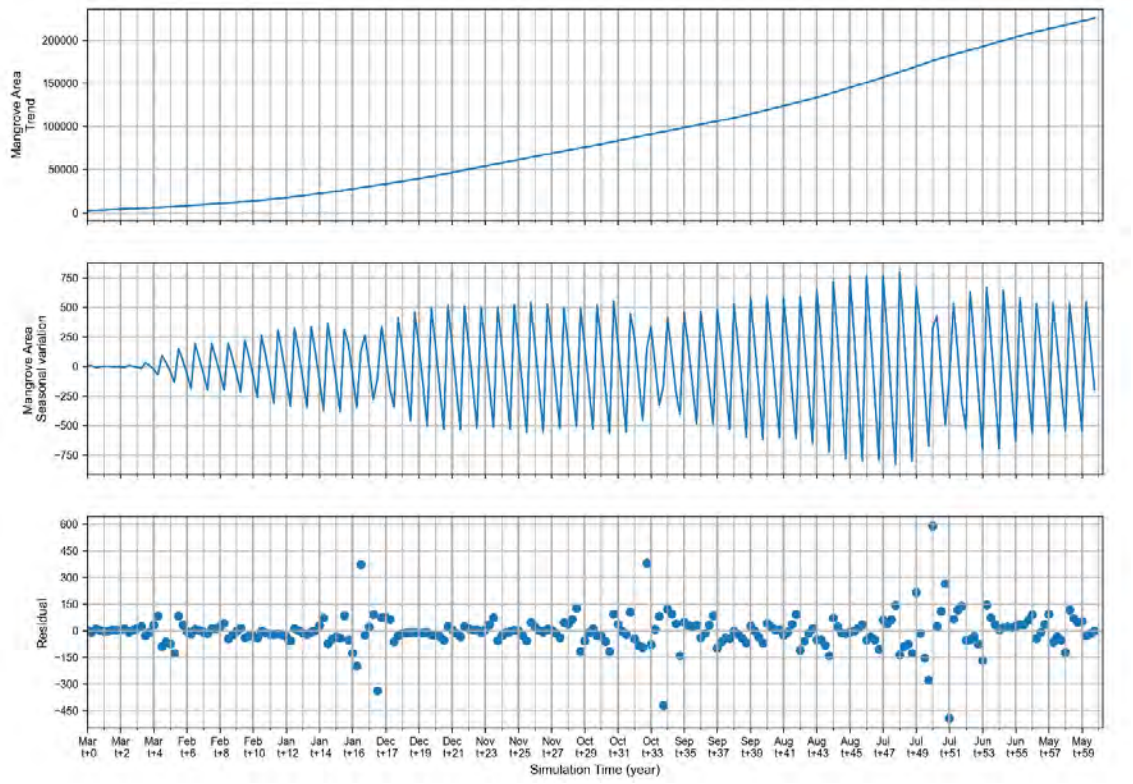

Figure 3.13. Temporal decomposition with LOESS for scenario A. Here in the plot, we decompose the seasonal variation of the mangrove area (m^2) to the trend (above panel), seasonal variation (middle panel), and residual component (lowest panel).

Residual or remainder represents noise in the data, where a residual of 0 means that seasonal and trend components well represent the time series. Four relatively high residuals are present in the lower panel of Figure 3.13. We associated those with the breakpoints that separated the three phases of mangrove area development as described in section 3.3.1. The first breakpoint occurred after five years of development; it marks the beginning of the phase when the initial population has matured, and the first generation of seedlings is recruited. The second breakpoint occurred after about 15 years and is associated with the onset of phase 2 when mature populations occupied the middle delta and produced more propagules. As the mudflat was wide enough and the WoO probability was high, the transported propagules occupied the space and were established. The third breakpoint occurred 30 years after initialization; it is associated with the beginning of phase 3, in which the northern and the southern channel were occupied by

propagules originating from parental trees of the middle delta. As the northern and southern channel populations grew, they started their reproduction phase at breakpoint 4.

3.3.2.4. Mangrove stand structure

Figure 3.14b shows histograms of tree number-height distributions as indicators of the stand structure sampled on various rectangular plots (Figure 3.14a) over time. The pattern of all scenarios is almost identical. Therefore, we have chosen Scenario A as a representative to describe the stand structure. We sampled the tree structure in four polygons. Polygon A represents the delta forest with the centre point taken from the initial trees with a size of 100x100m and Polygon B with a size of 300x300m. Polygon C is sized 100x100m and is located upstream with the same latitude as Polygon A and B. The decision to put Polygon C upstream is to explore whether the younger population in C, in comparison to the population in A and B, exhibits a different pattern. Polygon D has a size of 100x300m, located at the fringe of the main delta and channel. We provide comparative stand structure plots at 5-year intervals to represent the three major phases as in section 3.3.1. Hence, 12 plots are made available for each polygon. The complete plots for all sampling polygons and other scenarios are provided in Supplement 5[7].

The histograms show a slight or almost flat decline with increasing height (in cm) in the first 20 years of the simulations. Year 0 shows the height class distribution of the initial trees. After five years, we see two bars with the initial trees that matured on the right bar and the distribution of young trees on the left bar. Year 10 and year 15 represent the stand structure of young mangrove populations where the number of parental trees limits the sapling population. Given the space availability, most of the younger trees in year 10 survive to year 15. From the age of 20 years, mangrove stands become older with a higher density. This corresponds to the increasing propagule production. Despite the larger number of new saplings, with competition, younger trees died first since their FONs overlapped with the larger FONs of older trees due to their higher density. It is clearly seen by the constant distribution of older trees that they survived to the next observation period.

Comparing polygons A and B, both have a similar pattern. However, since Polygon B includes the fringe area, the fraction of younger trees in the population is higher. Polygon A contains fewer saplings since it has an older population, larger height, larger diameter at breast height at 130cm above the ground (D_{130}), and thus lower density. Polygons C and D are located in the fringing area. Therefore, they both have lower sapling density

[7] Supplementary materials can be accessed from: https://ars.els-cdn.com /content/image/1-s2.0-S1364815223002001-mmc5.docx

than A and B. A prevalence of the younger individuals and a high expansion capacity are typical characteristics of fringing mangroves.

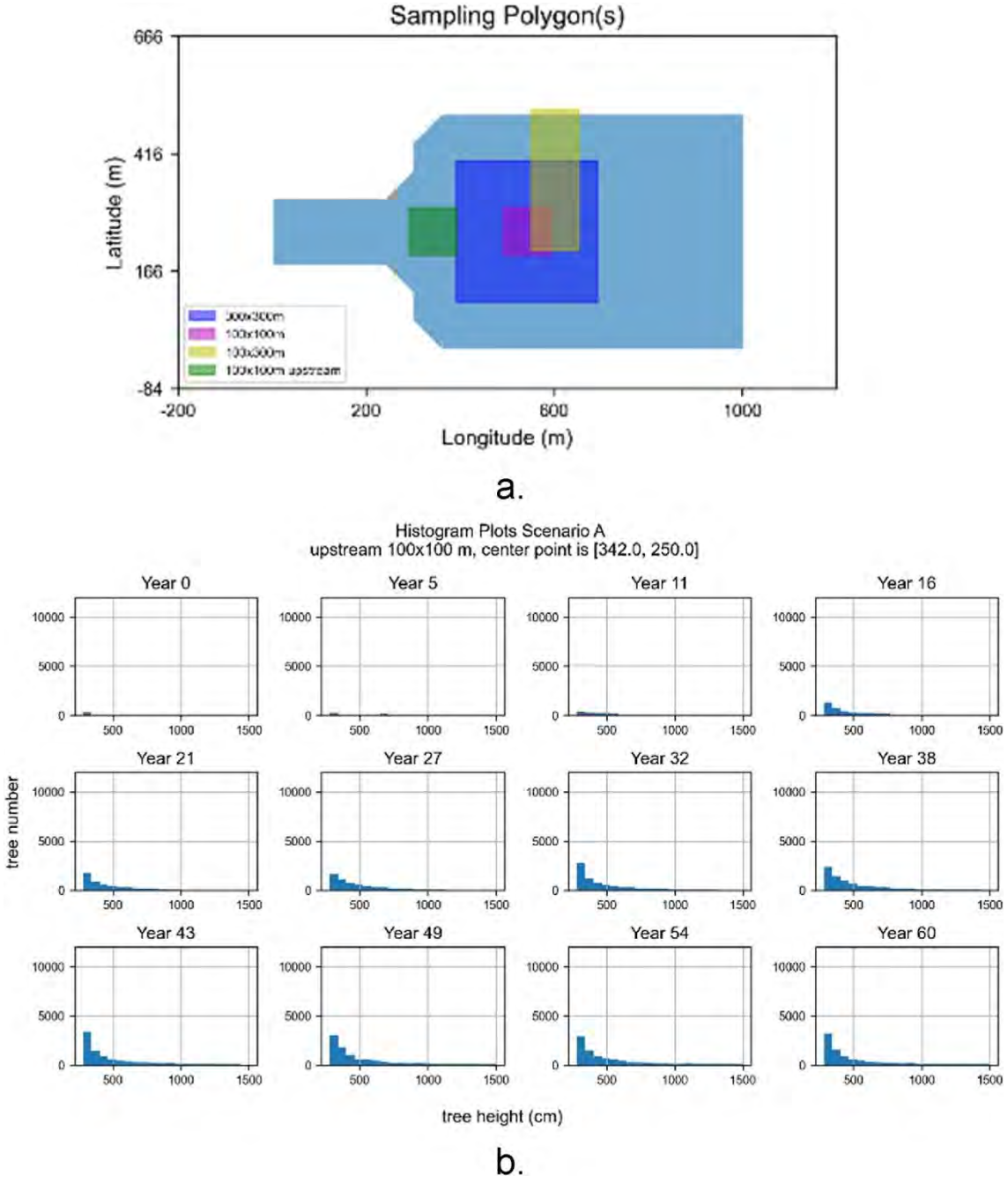

Figure 3.14. Tree number-height histograms on the selected polygons for Scenario A. Surveyed polygons (a), histogram of polygon 100x100m (b), histogram of polygon 100x100m in the upstream (c), histogram 100x300m (d), and histogram of polygon 300x300m (e). The histograms for other scenarios are provided in Supplement 5.

3.3.3. Hydro-morphodynamic evolution of the deltaic mangrove

In this section, we explore the impacts of mangroves on morphological evolution and hydrodynamics.

3.3.3.1. Influence of mangroves on hydrodynamics

The differences in hydrodynamics between simulations, including and excluding mangroves, are mainly due to the role of mangrove-induced drag and turbulence, which alters the magnitude and direction of the flow. Figure 3.15 illustrates how the presence of mangroves alters hydrodynamics. We capture the strength and direction of currents as patches-and-vector plots for Scenario E. The ebb tide exhibits the largest flow velocities because of the combined effect of tide and river flow. The simulation is year 56, meaning that the mangrove population in the delta is in a dense, mature state, and the population has colonised the northern and southern parts. When the vegetated area becomes inundated, an additional drag by the mangroves reduces the strength of the current to almost 0m/s. In comparison, excluding mangroves in the same area with the same bathymetry yields a larger value between 0.05 and 0.1m/s. A difference in magnitude is detailed in Figure 3.15c. The extra resistance provided by the mangroves in the delta lobe and the northern-southern part resulted in a concentration of flow in the channels. Therefore, we observed a higher flow rate in both channels regardless of whether the simulation included or excluded mangroves.

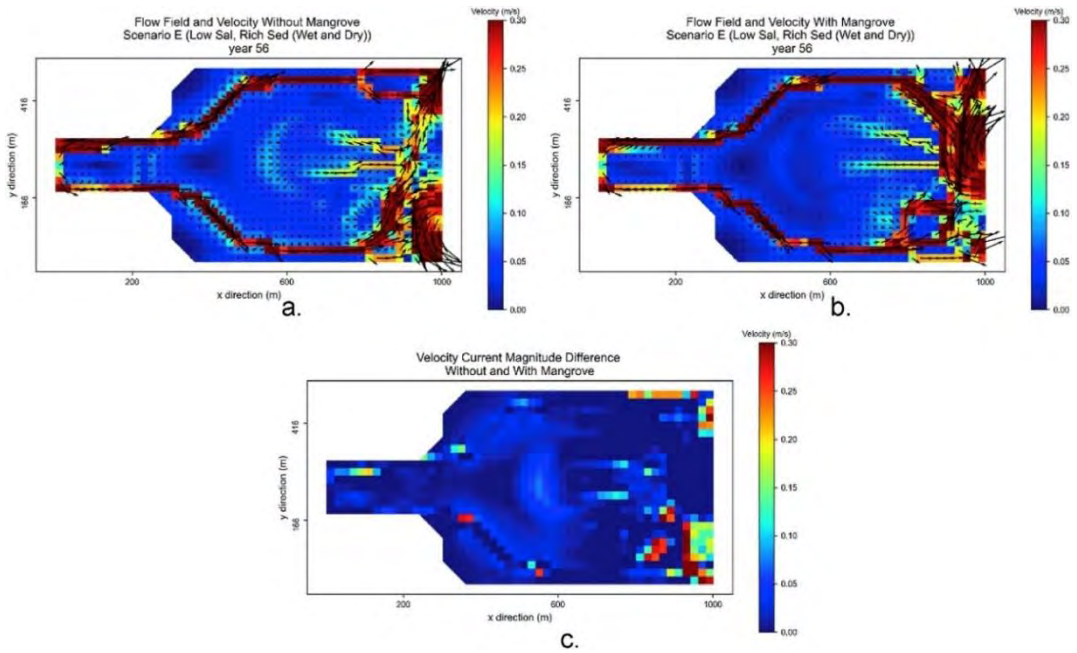

Figure 3.15. Snapshot plot of the flow field and velocity for simulations (a) with- and (b) no- mangroves for Scenario E. The difference in current magnitude between excluding and including the mangrove scenario is presented in (c).

3.3.3.2. Morphological evolution, with and without mangroves

The hydro-morphological model was first used to simulate the prograding delta development resulting from fluvial sediment supply including-excluding mangroves and to examine the effect of mangroves. As shown in Figure 3.12 and section 3.3.2.2, sediment availability is an important physical driver limiting mangrove forests' lateral expansion. Low sediment concentrations of the Poor Sed scenarios do not gain as much surface level as the Rich Sed scenarios. Since mangroves require suitable habitat (accommodation space), the Poor Sed scenarios tended to contain smaller mangrove areas in comparison to Rich Sed conditions.

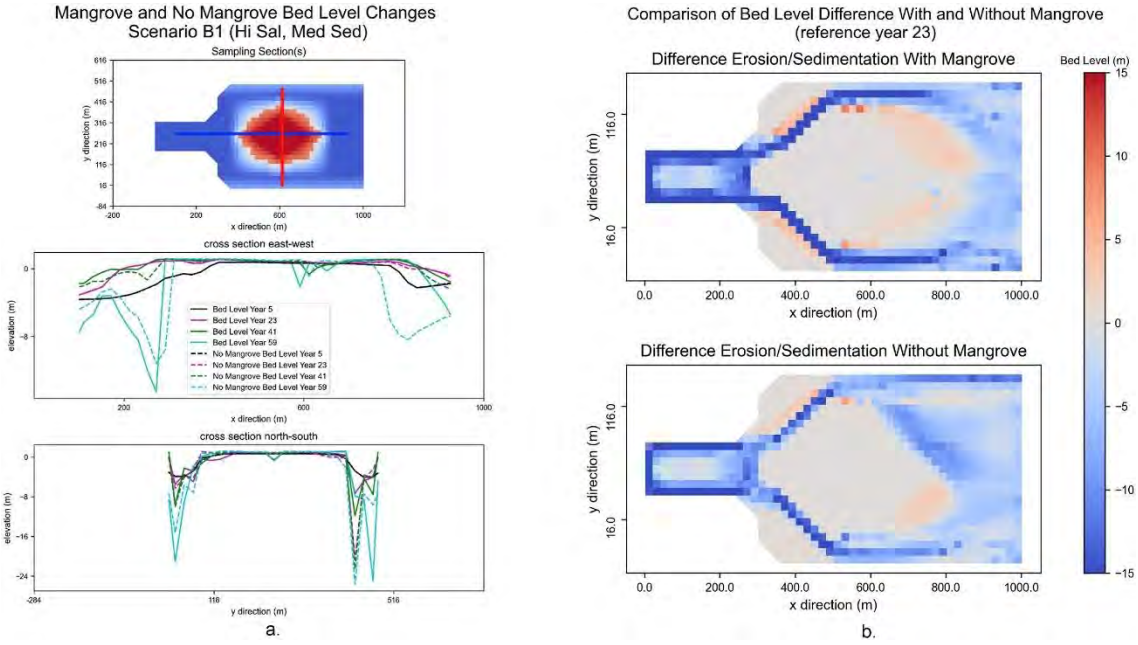

Figure 3.16. (a) Bed level evolution in simulations with mangrove (full line curves) and without mangrove (dashed curves) for Scenario B1. The streamwise or east-west section is depicted as a blue line, whereas the crosswise or north-south section is depicted as a red line. (b) Bed level difference of no- and with-mangroves simulation at coupling 243 (year 60) with reference year 23 for Scenario B1. The complete set of bed-level difference plots for all scenarios is provided in Appendix 5.

Figure 3.16 compares bed level evolution for mangroves and no-mangroves simulations at four moments in time. The timestamps reflect the early dynamics (year 5), phase 1 (year 23), phase 2 (year 41), and approaching the end of the simulation (year 59). The effect of mangroves is clearly seen in the years 41 and 59. As the mangroves individually grow larger and population-wise wider, they alter the hydrodynamics by increasing the bulk drag coefficient. Their presence promotes the deposition of freshly supplied sediment on the updrift and lee side of the delta. The streamwise plot shows it is more significant on the seaward side. The no-mangroves simulation faced considerable erosion.

Large bed level changes occurred (Figure 3.16a) within the first five years due to deposition in the upstream part of the delta, the build-up of a new tidal flat downstream, and the deepening of the northern and southern channels. River discharge in the upstream boundary causes an accelerating current in the northern-southern channels and incises the bathymetry. The presence of a delta island at the bifurcation locally reduces the velocity-enhancing deposition. The downstream of the delta also experiences deposition because of decelerating flow due to the presence of dense forest. The tidal currents promote the formation of additional tidal flats with an elliptic-like shape at the lee side. In the first 15-20 years, the impact of mangroves on morphological development remains limited. It is because mangroves are still small and sparse and thus have limited effects on hydrodynamics. After this time, the impact of mangroves becomes larger, with some differences between scenarios.

Since sediment supply initially dominates the morphodynamics, we used the year 23-bed level as the reference for the following analysis (Figure 3.16b). Overall, simulations with-mangroves show more deposition in mangrove-colonised areas than simulations without mangroves, particularly in the northeastern part of the delta. Under no-mangroves conditions, the delta is incised by a northwest-southeast channel. In contrast, the with-mangroves condition leads to wider accommodation space in the delta and higher bed levels in the northern and southern parts of the channel. In a condition where the mangrove stand structure is wide and dense and located in a sediment-rich environment, it is likely that mangroves could act as ecosystem engineers. In this sense, the forest has the capacity to build its own environment by slowing down the current and building up the mudflat on the lee side. When the inundation regime favours mangrove establishment, mangroves opportunistically occupy the new mudflat. Where the accommodation space is abundant and the population is relatively small, for instance, in sediment-rich conditions and with more accommodation space, the mangroves are likely to be opportunistic. In this study, the mangrove dynamics of the first 15-20 years were characterized by the opportunistic-colonizer behaviour of the mangroves, filling the accommodation space.

3.4. DISCUSSION

3.4.1. Interplay of the physical, environment, and mangrove dynamics

The DFMFON model has been developed to address the challenge of understanding how mangroves respond to changes in the physical environment and how the dynamic response of mangroves feeds back to the physical environment. Our study advances the currently segregated knowledge by coupling an individual-based mangrove model with a mechanistic hydro-morphodynamic model. To the best of our knowledge, this is the first

modelling study that explicitly solves the question of how a mangrove population responds in terms of stand structure and tree sizes to the hydro-morphodynamic drivers and salinity variability. This is considered an important advance, for instance, to meet an increasing necessity in predicting the mangrove forest structure trajectory in detailed physical-environmental scenarios (Dahdouh-Guebas et al., 2022; Twilley and Rivera-Monroy, 2005).

Our coupled DFMFON model satisfactorily elucidates the intertwined role of physical drivers (hydromorphodynamics), environmental drivers (salinity), and mangroves on a seasonal basis. Based on the physical characteristics of the Porong Delta, the schematized 2DH model simulations can reproduce the realistic spatiotemporal variation of mangrove dynamics on a sediment-rich system. Our study shows how the feedback effect of mangroves on the physical-environmental drivers leads to alternating expansion and contraction of mangrove extent instead of linear growth (Alongi, 2008; Krauss et al., 2014; McKee, 2011; Rogers, 2021).

Our numerical experiments unravel the dependency of the mangrove ecosystem on the available accommodation space. Evidence of this is the influence of the prograding mudflat platform on seaward mangrove expansion (Rogers, 2021; Woodroffe et al., 2016) and the influence of flow velocity on propagule dispersal. The presence of mangrove stands provides positive morphological feedback by the additional flow resistance. It promotes the mudflat build-up downstream (as also reported by Furukawa and Wolanski, 1996), provided that the stands are mature, dense enough and are situated in the direction of the dominant current. The interactions vary through space and time; hydrodynamic patterns are primarily influenced by the local topography through the first 15 years or phase 1 and mangrove-induced in phases 2 and 3 when the population reaches its maturity (Figure 3.7, Figure 3.8, and Figure 3.13). The hydrodynamic conditions are temporally varying when subjected to the spatiotemporal changes in forest structure since the hydrodynamic is dependent on mangrove biophysical properties (Maza et al., 2021b). Therefore, we observed the difference in mangrove response (with mangrove canopy area as a proxy) to the stressors at several breakpoints in time. Mangroves play a limited role in morphological changes during the first 20 years as their low and less dense structure has a limited impact on hydrodynamics (Figure 3.16), shown by the little difference in bed level between scenarios with and without mangroves. When the mangrove forest has grown mature enough and achieved sufficient structure, its presence is relevant in adding hydrodynamic resistance and, thus, helps to promote the build-up of the mudflat platform. It can be argued that the transition from mangroves acting as colonizers to mangroves functioning as ecosystem engineers occur when mangroves are mature, tall, and structurally dense enough. Thus, in this state, environmental variation has little effect on growth. When accommodation space is available, the mangroves shift to colonisers by dispersing their propagules. At the same time, the ecosystem engineer function maintains the resilience of the recently recruited seedlings through their innate tree-to-tree

competition. These processes will eventually result in the optimal number of established trees after the stand has reached the self-thinning line depending on the habitat conditions.

Mangroves' vertical growth and lateral expansion depend on physical drivers and competition. Simulation results provide little correlation between the variability of mangrove dynamics and the seasonal variation of environmental stressors (Figure 3.9 and Figure 3.13). Even though bed level accretion due to sediment availability is the dominant factor, hydrodynamic condition plays a role in dispersing the propagules during the propagule production season, contributing to the resilience of the forest (Dahdouh-Guebas et al., 2022; Shih et al., 2022). The contribution of salinity is rather minor considering low salinity variation and *A. marina* as among the most salt-tolerant mangrove species. The net development of the mangrove forest is a product of seasonal variation, being lowest after the more stressful conditions in the dry season. The abundant fresh water and fluvial sediment fluxes at the beginning of the wet season help mangroves rejuvenate and distribute the propagules in their vicinity. The positive trend continues until the middle of the dry season. The stressful environment then adds to competition, hinders growth, and increases mortality, particularly among juveniles. The capability to model seasonality, as in our work, is important for understanding the phenological response of mangroves to stressors, which determines the dynamics and productivity (Sharma et al., 2014; K. Zhang et al., 2016). Several studies demonstrate the mangroves' response to substantial seasonal fluctuation, e.g., of temperature (Duke, 1990), light (Suwa and Hagihara, 2008), precipitation (Duke et al., 1984), nutrient (Lagomasino et al., 2014), freshwater and hydroperiod (Kamruzzaman et al., 2013; Slim et al., 1996; Wafar et al., 1997).

3.4.2. Model limitations, potential uses, and future research needs

The development of this DFMFON-coupled model is intended as a design tool to quantify the functionality and persistence of the mangrove ecosystem as coastal protection that is currently lacking (Dahdouh-Guebas et al., 2022; Ellison et al., 2020; Schoonees et al., 2019). Therefore, parameterisation of physical-environmental drivers has been chosen to describe the main relationships between mangroves and changes in physical processes and vice versa. We decided to consider only salinity as the main environmental driver that controls mangrove growth (Sudhir et al., 2022), without feedback from mangroves on salinity distribution due to freshwater uptake (Bathmann et al., 2020). Besides salinity, we assume favourable environmental conditions that cause no biotic damage to mangroves, as presented in Figure 3.17. The main underlying assumption in terms of tree growth, competition, and salinity tolerance is that *A. marina* behaves like *A. germinans, except for* propagule production, which resembles that of *A. marina* in Porong Forest, and WoO parameterization based on those measured by Balke et al., (2015) in the Firth of

Thames, New Zealand. Mangrove growth and mortality are indeed a complex processes. The environmental drivers provide the resources and regulators for tree diameter and height growth, while physical drivers limit the lateral expansion of the mangrove stand. With DFMFON, we explicitly determine the productivity of the mangrove based on the complete feedback loop of the physical drivers (water level, flow, and bed level) and the influence of environmental drivers (salinity).

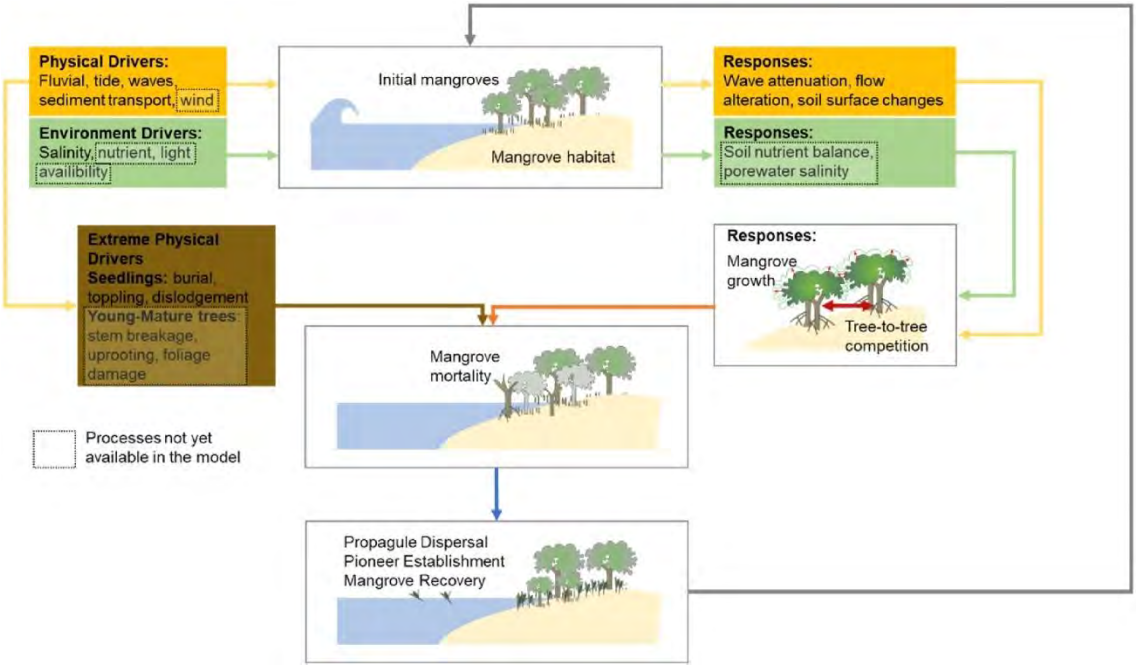

Figure 3.17. Simplified overview of mangroves' relevant processes and interactions and the physical-environmental drivers in the DFMFON model.

Mangrove establishment and propagule dispersal are the critical elements in assessing the persistence of mangrove forests (Van der Stocken et al., 2019). Estimating how a forest recovers after a large, infrequent disturbance such as a tropical storm is still a challenge. Current approaches use long remote sensing observations from other locations in the vicinity of the impacted forest (Krauss and Osland, 2019; Vizcaya-Martínez et al., 2022) to estimate the recovery time. The propagule distribution depends on the hydrodynamic condition, and the probability of the establishment is based on the WoO value. This contribution will be beneficial to fill the gap in simulated mangrove dynamics by incorporating the complete life cycle of mangroves and by considering physical processes in the model. Currently, our model only considers seedling-based regeneration and cannot model the re-sprouting mechanism (Krauss and Osland, 2019). We assume that the dispersal and settling of propagules only occur for a short period of time, i.e., two weeks after release (Section 3.2.1.4), taking into account the propagules' availability, travel time, and the obligate dispersal.

Competition and environment, in combination, are the main factors determining the mortality of saplings and mature trees alike. The WoO approach is used in the model to simulate the mortality during the propagule and seedling stage. The model does not include mechanical tree damage. For instance, exposure to extreme wind and waves during storm surges can break stems or uproot trees. Including mangroves' resistance to such exposure in the model should be relevant when considering the function of coastal protection (Morris et al., 2019; World Bank, 2017). Several mechanistic models can estimate tree breakage, e.g., HWIND and GALES (Gardiner et al., 2008) and individual branches mechanical tests (van Hespen et al., 2021). However, HWIND and GALES models have been applied for even-aged forest plantations, while the mechanical test focused more on individual trees. Additionally, the mortality threshold for mangroves for such breakage mechanisms is not yet known.

The model has shown that it can reliably replicate mangrove forest expansion. It has deepened the mechanistic understanding of large-scale and long-term mangrove forest expansion behaviour in different detailed environment scenarios. Development of this model may lead towards improved prediction of changes in mangrove forest structure and species composition (Aslan et al., 2016; Ellison et al., 2022) due to climate change and anthropogenic activities. An increase in economic activities is sometimes identified as the main driver of mangrove forest conversion to shrimp farms, rice agriculture, oil palm plantations, or construction projects (Jayanthi et al., 2022; Richards and Friess, 2016). These kinds of activities could result in habitat segregation, where the interconnectedness with ecosystems in the vicinity is important for, e.g., nutrient exchange and, in the end, could lead to the collapse of the mangrove ecosystem (Curnick et al., 2019). Since little is known about mangrove fragmentation and disconnectivity (Dahdouh-Guebas et al., 2022), we can apply the model to investigate the sensitivity of mangrove forest persistence capacity to the loss rate of mangrove patches, their shape, size, and distance. Apart from local topography and prevailing storm intensities, structural characteristics of mangrove forests, such as species composition, tree height, and density, are important parameters for assessing their capability to provide nature-based coastal protection. We could extend the DFMFON model with a wave model to investigate the sensitivity of mangrove wave attenuation to spatiotemporal changes in forest structure and composition (Maza et al., 2021b).

3.5. CONCLUSIONS

In our study, a mechanistic simulation model that captures the interrelationships of individual tree responses and the changing environment was created by coupling the DFM and MFON models. To our knowledge, our novel eco-morphodynamic model is the first that offers to examine the sensitivity of mangrove forest structure to changes in hydrodynamics (water level and current), morphology (bed level), and salinity in a

feedback loop. The model demonstrates the seasonal variation in mangrove dynamics and is the first to account for the interactions between mangroves and stressors at all life stages from propagule to seedling (≤ 1.37m and ≥ 1.37m), sapling, and mature stages, including short/ long distance propagule dispersal. This gives an advantage to mechanistically model forest expansion, retreat, and colonisation influenced by physical-environmental drivers. The simulations were initialized in a schematized delta setting with a small patch of saplings and seasonal fluvial forcing. When the stand is young and sparse, the mangrove forest has a modest effect on morphology, and the bed-level development with vegetation is quite similar to the scenario without vegetation. As long as accommodation space is available, the mangrove population tends to occupy the space within its physical drivers limit. In contrast, mature and dense mangrove populations are likely capable of altering their habitat by promoting the deposition in the direction of the dominant current. Overall, the model exercise presented here highlights the benefit of integrating an individual-based mangrove and a hydromorphodynamic model in providing a mechanistic understanding regarding the feedback loop of physical-environmental drivers and changes in mangrove forest structure over space and time.

3.6. APPENDICES

Appendix 3-A

Table 3-A.1. DFM Model Parameters

Parameter	Value	Unit	Remark
Domain	2500 x 500	[m]	Porong Delta
Cell Size	20 x 20	[m]	
Model Time Span	60	[years]	
Hydrodynamic Time Step	200	[s]	DtUser
Morphological Factor	30	-	MorFac
Sediment Type	Mud	-	SedTyp
Reference Density for hindered settling	1600	[kg/m3]	Cref
Specific Density	2650	[kg/m3]	RhoSol

Parameter	Value	Unit	Remark
Dry Bed Density	500	[kg/m3]	CDryB
Fresh Settling Velocity	0.005	[m/s]	WS0
Saline Settling Velocity	0.005	[m/s]	WSM
Critical Bed Shear Stress, Sedimentation	1000	[N/m2]	TcrSed
Critical Bed Shear Stress, Erosion	0.3	[N/m2]	TcrEro
Erosion Parameter	5.0x105	[kg/m2/s]	EroPar
Initial Sediment Layer Thickness at Bed	30	[m]	IniSedThick
Spin-up Interval	540	[s]	

Appendix 3-B

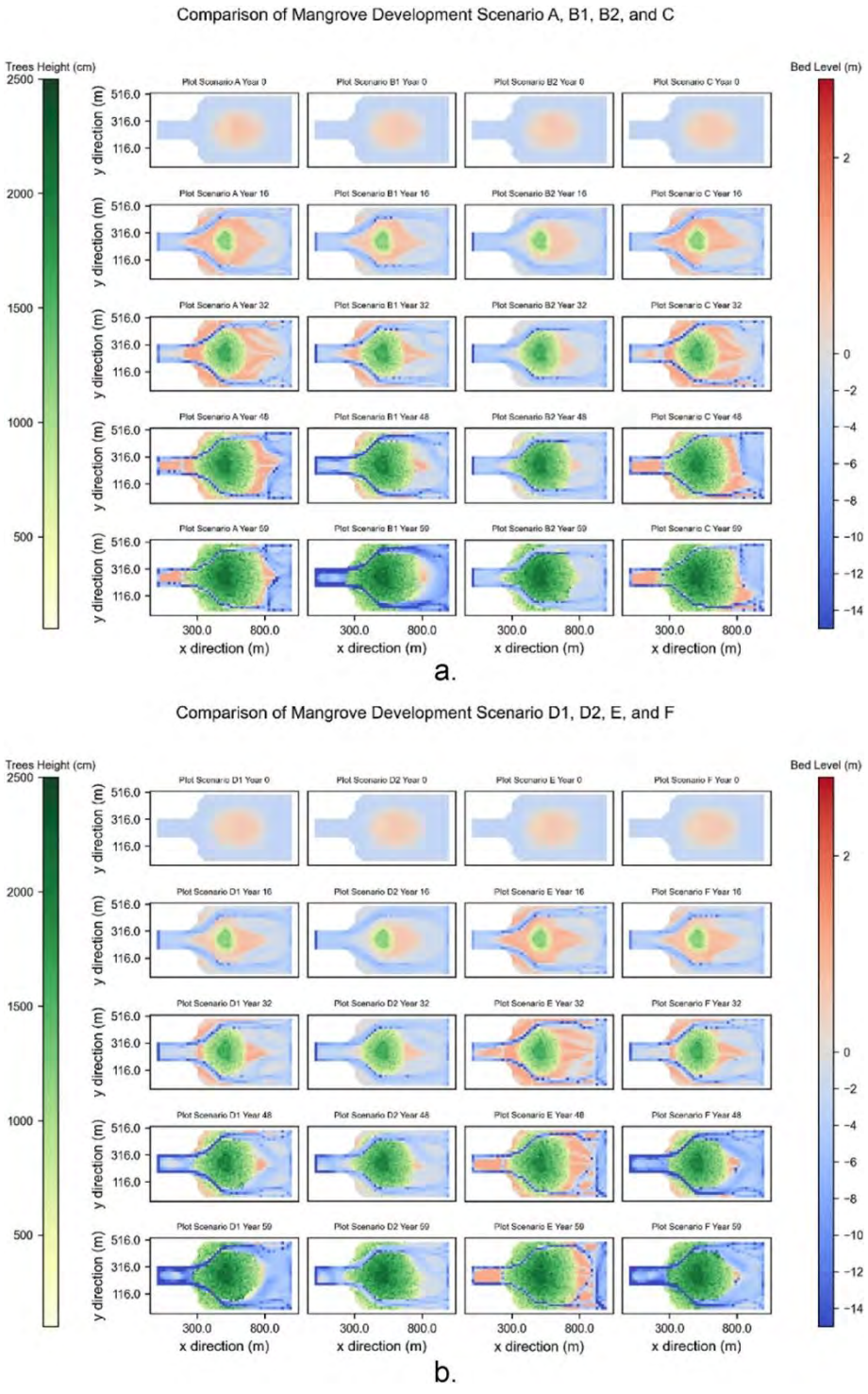

Figure 3.A.1. Plot of the mangrove development for all scenarios. Scenario A (Hi Sal, Rich Sed), B1 (Hi Sal, Med Sed), B2 (Hi Sal, Poor Sed), and C (Low Sal, Rich Sed) in panel a and scenario D1 (Low Sal, Med Sed), D2 (Low Sal, Poor Sed), E (Low Sal, Rich Sed [Wet and Dry]), and F (Low Sal, Med Sed [Wet and Dry]) in panel b.

Appendix 3-C

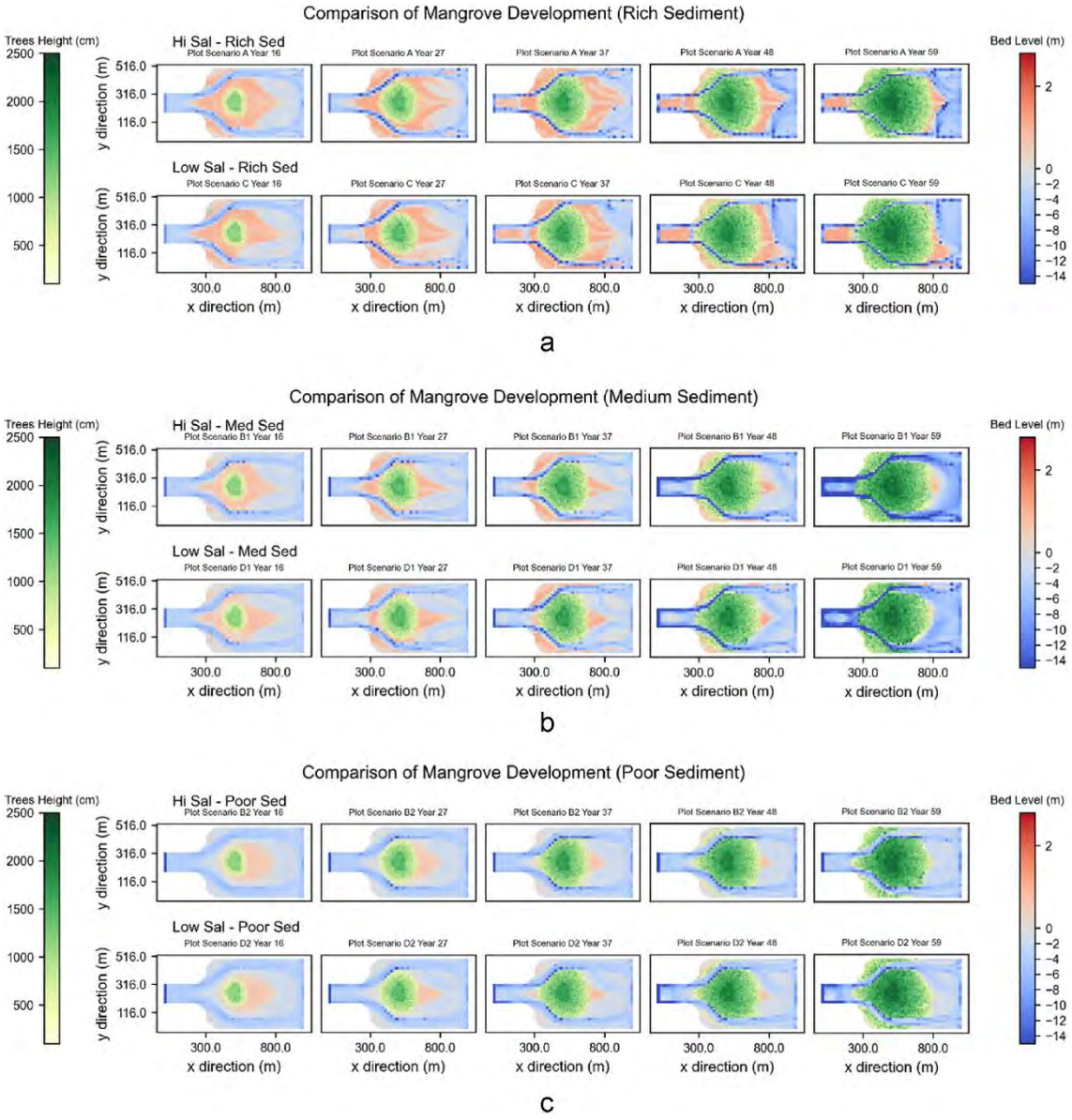

Figure 3.A.2. Comparison of the effect of salinity to mangrove dynamics. The three panels show contrasting simulation results of the contrasting salinity environment on the same availability condition.

Appendix 3-D

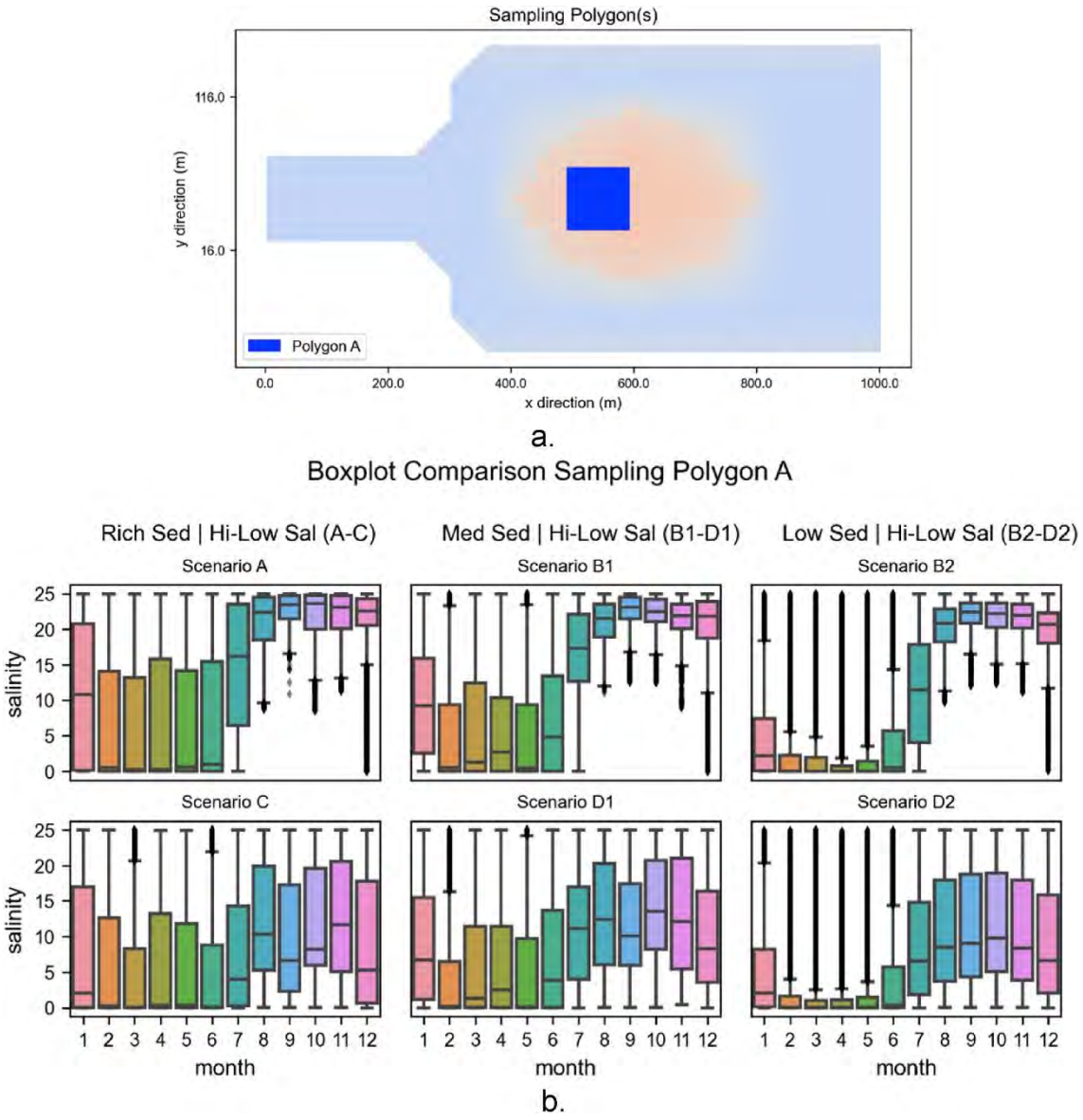

Figure 3.A.3. Boxplot of simulated salinity sampled on Polygon A. Monthly variation of salinity value on Polygon A for different salinity conditions. the boxplot is arranged vertically, where similar sediment concentration is in the same column, with high salinity condition above the low salinity plot.

Appendix 3-E

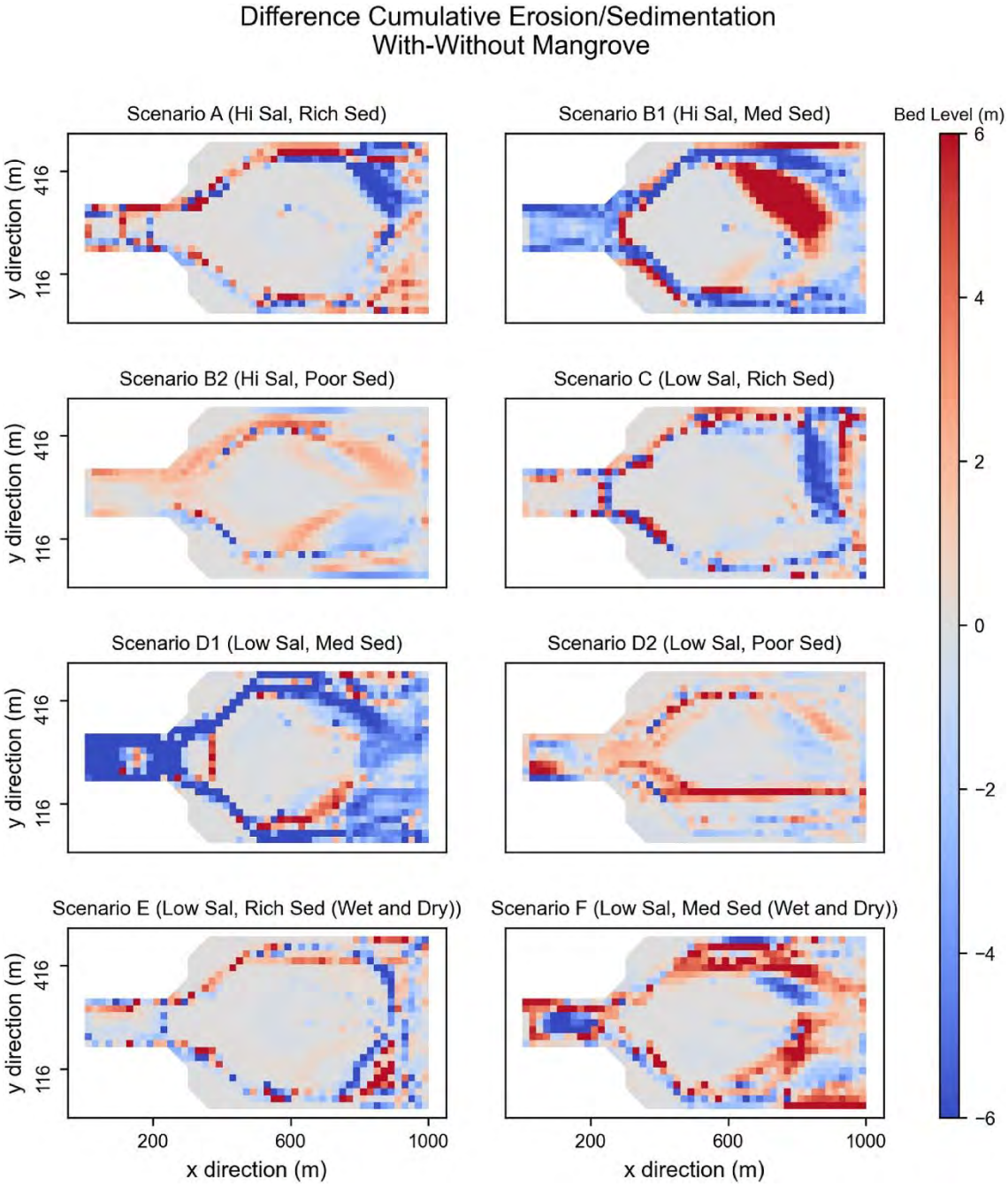

Figure 3.A.4. Delta difference cumulative of bed level from with and without mangrove with cumulative erosion/sediment is calculated with the reference of year 23 as in section 3.3.3.2.

4

MODELLING MANGROVE RESTORATION TO OPTIMIZE CARBON SEQUESTRATION

This chapter is based on the following publication:

Beselly, S.M., M. Van Der Wegen, J. Reyns, U. Grueters, J. Dijkstra, and D. Roelvink. Strategic mangrove restoration increases carbon sequestration capacity (in preparation for a submission)

Abstract: Mangrove forests' restoration has gained traction as a sustainable solution to mitigate the effects of greenhouse gas emissions and to provide other ecosystem services, such as coastal protection against flooding. Restoration projects are often informed by expert judgement rather than a quantitative understanding and have a high failure rate. Monitoring mangrove restoration performance may take decades and has a strong case study dependency. To optimise restoration strategies, we developed an advanced individual-based mangrove and process-based hydro-morphodynamic model to simulate multi-species mangrove forest trajectories and account for the feedback from the physical environment. We find a large impact of planting zonation on the mudflat behaviour, with seaward erosion and in-forest-landward deposition. Planting mangroves close to mean sea level decreases carbon storage potential due to increased mudflat erosion. Configuring planting in multiple patches proves beneficial to mangrove biomass development, expansion, and sediment accumulation. Combined with sound monitoring, the developed tool can potentially optimize planned mangrove restoration strategies.

Keywords: Carbon sequestration; Mangrove wetlands; Mangrove restoration; Eco-hydromorphodynamics; Mangrove modelling; Delft3D-FM; Ecological modelling

4.1. INTRODUCTION

Global carbon mitigation goals aim to reach net zero emissions by 2050 (Saintilan et al., 2023) and to cut current carbon emissions to half by 2030 to limit global warming to 1.5°C (United Nations Environment Programme, 2015). Coastal ecosystems, known as blue carbon, contribute to more than half of carbon sequestration in the ocean, albeit occupying just 0.5% of the total sea floor (Macreadie et al., 2021). Long-term carbon sequestration per unit vegetated area in coastal forest ecosystems is estimated to be three to five times that of terrestrial forests (Mcleod et al., 2011).

Mangrove forests can play a crucial role in achieving global targets on climate change mitigation and adaptation (Duarte et al., 2013; Howard et al., 2017; Temmerman et al., 2023) due to their comparatively large carbon burial rate (Mcleod et al., 2011) compared to other blue carbon pools. A key factor in mangroves' efficiency in sequestering carbon is their complex aerial root structure trapping fine sediment (Krauss et al., 2014). Due to waterlogged and anaerobic conditions, up to 90% of the organic carbon originating from either local mangroves or external sources is preserved in the sediment and fine root system (Krauss et al., 2014; Sharma et al., 2022), acting as a long-term carbon sink (Howard et al., 2017). In addition, mangroves comprise unique ecosystems and provide valuable ecosystem services (van Wesenbeeck et al., 2017) and other carbon-related benefits (Macreadie et al., 2019). One of these services is attenuating storm surges and dissipating wind waves (Temmerman et al., 2023), thereby reducing coastal flood risk (Temmerman et al., 2023; van Zelst et al., 2021). Wave attenuation potential depends on both biophysical mangrove properties (Marois and Mitsch, 2015; Montgomery et al., 2018) and geomorphic settings (hydrodynamic conditions, sediment properties, local topography, and the coastal landscape) (Gijsman et al., 2021; Temmerman et al., 2023).

Being historically perceived as of low monetary value, mangrove forest eradication by land use conversion has globally decreased mangrove coverage (Hamilton and Casey, 2016). This has led to mangrove belts being amongst the most threatened forests (Almahasheer et al., 2016; *The State of the World's Mangroves 2022*, 2022) and to increased flood risk for 15 million people that were currently protected by the presence of mangrove forests annually (Menéndez et al., 2020). When deforested and reclaimed, the soil is no longer waterlogged, exposed to O_2, and changes to aerobic conditions (Mcleod et al., 2011). Moreover, the loss of mangroves may lead to the degradation of coastal wetlands, thus increasing the release of the long-buried carbon (Howard et al., 2017). Consequently, mangrove loss can shift the role of mangrove forests from carbon sink to carbon source, potentially contributing up to 10% of total emissions from deforestation (Donato et al., 2011).

Recognising their value for climate change mitigation and adaptation, mangrove ecosystem conservation and restoration have high strategic potential as a sustainable

climate solution. A multitude of countries and international organisations advocate proactive green belt policies (UNFCCC. Secretariat, 2021). Mangrove restoration and conservation is targeted (Sasmito et al., 2023) by the UN Decade of Ecosystem Restoration 2021-2030 (UN General Assembly, 2019), Sustainable Development Goals (United Nations, 2018), and Aichi Biodiversity Targets (United Nations, 1992). The global conservation community has committed to increasing mangrove cover by 20% in 2030 (Global Mangrove Alliance, 2021; Sasmito et al., 2023). Prompt actions are critical given the close deadline of both targets in carbon emission reduction and mangrove conservation. Restoration efforts can be complex and require a set of systematic and structured stages consisting of planning, implementation, and evaluation (Lewis and Brown, 2014; Teutli-Hernández et al., 2020) including socio-cultural conditions (Dahdouh-Guebas et al., 2021), land ownership (Sasmito et al., 2023), along with cost-benefit analyses (Ellison et al., 2020; World Bank, 2022), apart from a thorough understanding of the bio-physical dynamics of mangrove systems themselves.

Mangrove restoration strategies are site-specific and species-specific (Zimmer et al., 2022), and their success often depends on the suitability of the site, species, and support from local communities (Tom Wilms et al., 2021; Winterwerp et al., 2020). Despite the increase in interest in nature-based coastal defences and the clear multiple benefits of restoring mangrove forest (Morris et al., 2018; Temmerman et al., 2013), 80-90% of reported restoration projects experience failure(Lewis and Brown, 2014) where reasons for failure often remain unclear (Ellison et al., 2020; López-Portillo et al., 2017). The leading bio-physical causes relate to a mismatch of mangrove species and poor understanding of the hydro-morphological system and other ecological elements (Ellison et al., 2020; Lewis and Brown, 2014; Primavera and Esteban, 2008). Limited understanding is partly due to a non-existent baseline dataset on interventions and missing consistent observation over decades (Macreadie et al., 2019; Sharma et al., 2022; Zimmer et al., 2022). Nevertheless, mangrove planting remains a popular conservation practice (van Bijsterveldt et al., 2022), considering the increasing need for fast creation of mangrove belts and planting as mandated by law in several countries.

This study investigates optimal restoration strategies concerning spatial mangrove planting configurations, taking into account feedback from their tidal flat environment to optimize carbon sequestration potential. The potential sequestration function is represented as carbon sinks in the above-belowground biomass and soil carbon pools. Mangrove forests' carbon and nutrient exchange is determined by factors in different scales, i.e., local scale dominated by mangrove species composition, regional scale influenced by geomorphological setting and hydrodynamics, and global scale governed by its climate and latitude (Adame and Lovelock, 2011). Of these factors, processes on local and regional scales are the primary determinant factors in influencing the import and export of the materials (Adame et al., 2010), e.g., vegetation effect on barrier coasts under sea level rise (Boechat Albernaz et al., 2023).

In an effort to manage mangrove wetlands for targeted ecosystem services, mechanistic understanding of mangrove-mudflat biophysical feedback is crucial (Cahoon et al., 2021). It requires an approach that allows us to investigate the spatial sediment distribution (Adame et al., 2010) and material exchange (Adame and Lovelock, 2011) in a mangrove-mudflat system on the local-regional scale. Predicting mangrove forest trajectories requires the inclusion of detailed physical-environmental scenarios (Dahdouh-Guebas et al., 2022) with interactions of mangrove establishment-dieback and propagule dispersal (Van der Stocken et al., 2019). We apply the mechanistic and spatially explicit mangrove-eco-morphodynamic model DFMFON (Beselly et al., 2023). The DFMFON model couples two modelling paradigms, i.e., the process-based hydro-morphodynamic model Delft3D-Flexible Mesh (Deltares, 2021) and the individual-based mangrove model MesoFON (Grueters et al., 2014). DFMFON describes mangrove-mudflat dynamics, including the life stage progression (mangrove establishment, growth, and mortality) along with the systems' morphodynamic evolution conditioned by wave and tidal forcing, sediment dynamics, bed level change, and salinity. The model has been applied to reproduce mangrove extent development and its canopy height along with the prograding delta features in Porong Delta, Indonesia (Beselly et al., 2023).

We apply the DFMFON model to an open, near-equilibrium accreting muddy coast setting (Winterwerp et al., 2013), characterized by a typical mudflat slope of 1:1000 below mean sea level (MSL) and convex upward profile in the upper elevation (Friedrichs and Aubrey, 1996). A spring-neap tidal water level cycle, constant wave forcing, and constant sediment concentration at the seaward boundary force the open coast profile. These forcing conditions generate a near-equilibrium, landward sloping profile where high suspended sediment concentrations prevail at the intertidal flat, but tide-residual sediment transports remain negligible (Wegen et al., 2019). This cross-sectional profile is a characteristic of mudflat. Seedlings, consisting of *Avicennia marina* and *Rhizophora apiculata,* two pioneering species commonly planted in restoration activities in Indonesia (Beselly et al., 2021; Sasmito et al., 2023; Sidik et al., 2018) are planted at 3m distance intervals (Asian Development Bank, 2018; Hideki Miyakawa et al., 2014) with a similar diameter at breast height positioned 130cm above the bed level (D_{130}), resembling reforestation or afforestation approach (Song et al., 2023). As the existing guidelines (Beeston et al., 2023; Lewis and Brown, 2014; Teutli-Hernández et al., 2020) do not feature a specific configuration of mangrove planting, we apply various configurations of mangrove placements (Table 4.1 and Figure 4.1), including single (200m) and multiple (100m with 160m gap) patches to observe the results on ecological and morphological development. In each configuration, we place mangroves at a particular vertical level related to the tide (mean sea level, mean high water spring, and mean high water neap). Scenarios run for 20 morphological years during which mangroves grow and generate propagules that are dispersed, settle and develop into new mangroves, in a feedback process with associated hydrodynamic and morphodynamic developments. We

investigate hydrodynamic characteristics, morphological development, mangrove extent and biomass development to quantify the carbon sequestration potential. Detailed model configurations and process descriptions are available in the method section.

Table 4.1. Summary of the scenarios undertaken in this study

Scenario	Mangrove placement	Mangrove Configuration
A	Single patch: Above mean sea level	200m × 200m
B	Single patch: Below mean high water spring	200m × 200m
C	Single patch: Above mean high water neap	200m × 200m
D	Single patch: Below mean high water neap	200m × 200m
E	Two patches: below mean high water spring and above mean high water neap	200m × 100m, with a 160m gap
F	Two patches: above mean high water neap and below mean high water neap	200m × 100m, with a 160m gap

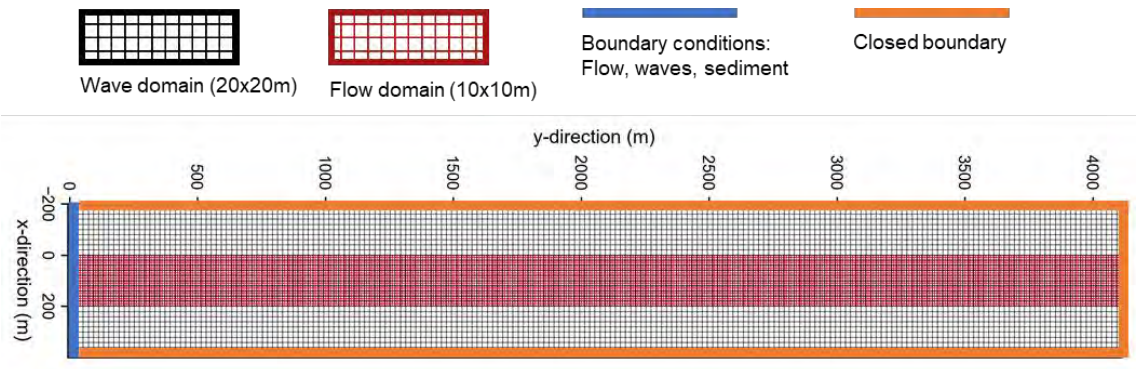

Figure 4.1. Model setup in DFM model and mangrove placement scenarios. DFM model domain consists of flow and wave models in an online coupling. The illustration of the scenarios is not to scale. Details of the simulations are available in supplement[8].

[8] Supplementary materials can be accessed from: https://edu.nl/37a3r

4.2. RESULTS AND DISCUSSIONS

4.2.1. Hydrodynamic characteristics and morphodynamic evolution

In the absence of mangroves, the mud profile continues to develop and accretes sediment with clear spring-neap tidal depositional signals near the boundary (Figure 4.2), albeit at a very low rate. The introduction of mangroves has a clear impact on coastal morphology. The presence of mangroves promotes sediment deposition in the patch interior and erosion at the seaward fringe, to a greater extent in scenarios B, C F, and to a lesser extent in scenarios D and G. Scenario B even traps some sediment landward from the mangrove patch. Interestingly, the mangrove forests in the upper intertidal (above MHWN) promote a relatively high depositional rate in the interior. As shown in Figure 4.3b, the presence of mangroves facilitates vertical accretion rate in the forest interior by up to two times compared to the no-vegetation scenario. The modelled mean accumulation rate in the mangrove interior is found to nearly correspond to the global average for undisturbed conserved mangroves (Pérez et al., 2018), about 3.6±0.4 mm yr^{-1} (Figure 4.3b). It displays, despite the schematization the model provides a realistic rate. Drag induced by mangroves can have an extended influence on reaching the seaward boundary close to the lowest tidal water level. The scenario with mangroves near MSL shows profound erosion at the seaward fringe and deposition in the mangrove interior towards its landward surroundings. Higher, more landward mangrove planting decreases erosion near the fringe and tends to deposit sediment within the interior. Under those circumstances, mangroves drive the redistribution of sediment over the profile, causing the bed level to be near the boundary seaward (Figure 4.3b). For that reason, it indicates the extent of mangrove influences on morphology in this system. The morphodynamic patterns from scenarios with multiple vegetation patches resemble the single-patch scenarios matching the lower patch (Figure 4.2). In most cases, the deposited volume in the mangrove patch located in the lower intertidal is even less than the eroded volume at the seaward portion of the fringe, suggesting the possibility of a negative impact on bare mudflat sediment stock by the introduction of mangroves.

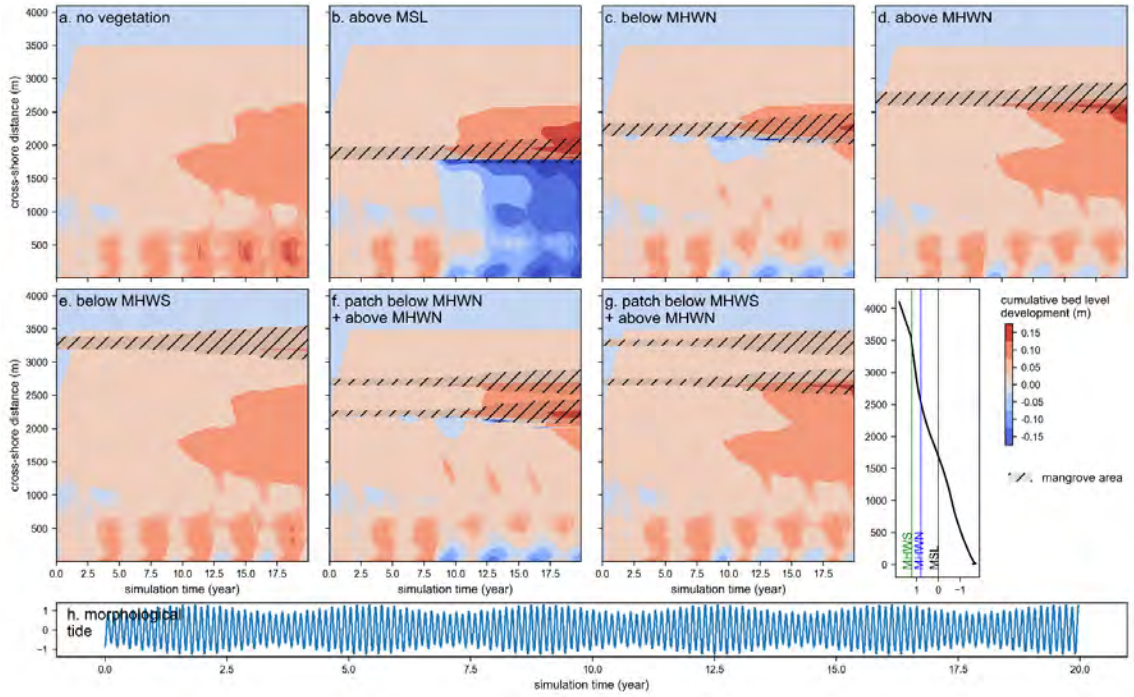

Figure 4.2. Simulated alongshore averaged bed-level development. Panels a-g show the spatiotemporal cumulative bed level development in each scenario. The mangrove extent is shown as black hatches overlaying the bed level. Panel h shows the ocean boundary with morphological spring-neap tide forcing.

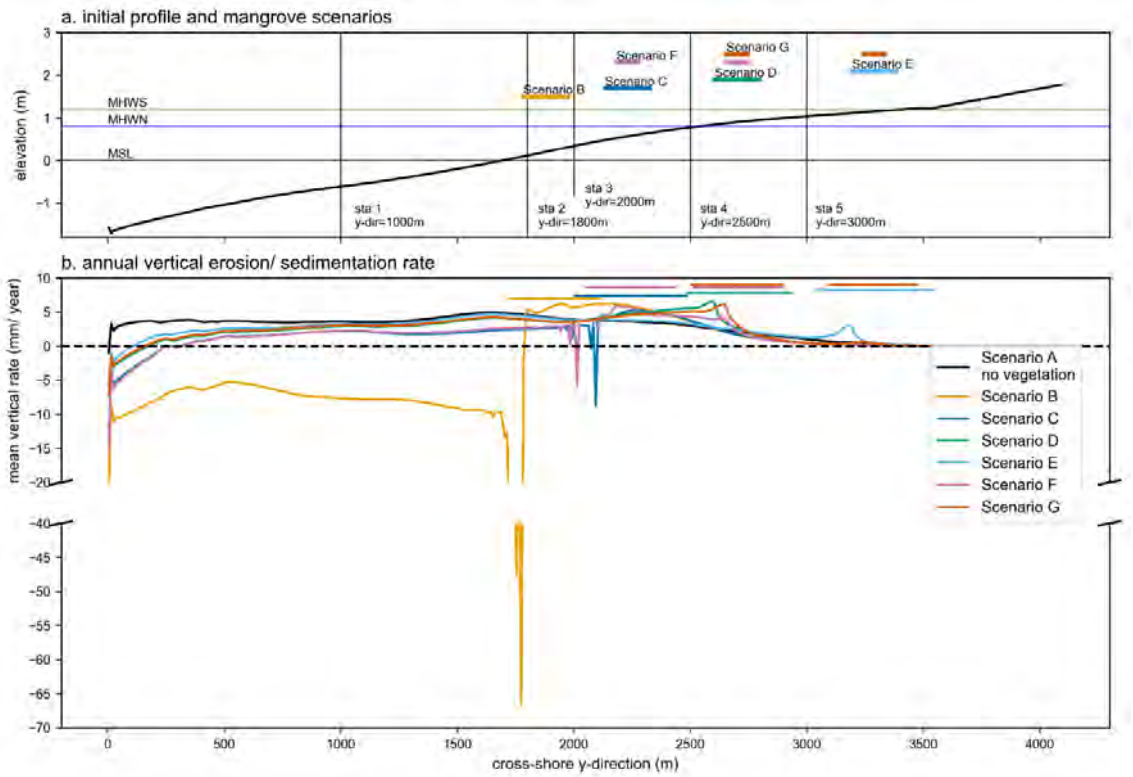

Figure 4.3. Initial profile, mangrove planting scenarios, and annual vertical erosion/ sedimentation rate. Panel a describes the initial profile, tidal levels, and scenario placement. The observation stations represent the seaward, fringe, and mangrove patch interior. The observation stations are arranged as follows: sta 1 at y-dir=1000m represents the offshore; sta 2 at y-dir=1800m represents the fringe for above MSL (scenario B); sta 3 at y-dir=2000m represents the forest interior of scenario B and fringe for below MHWN scenario C and F; sta 4 at y-dir=2500m represents forest interior for (scenario C and F) and fringe for above MHWN (scenario D and G); and sta 5 at y-dir=3000m represents the fringe for below MHWS (scenario E). We do not consider the forest interior of scenario E because it is close to MHWS and less frequently inundated. Panel b shows the annual alongshore average erosion/sedimentation rate (y-direction), mm/yr. The alongshore annual average rate is calculated over the entire 20-year simulation period. Coloured lines above the graphs represent the extent of the mangrove forest after 20 years. Scenario line colours are consistent throughout the article.

The drag-inducing effect of the growing mangrove community is apparent and, therefore, influences the tidal asymmetry and the associated transport capacity. Together with fine sediment erosion and deposition lag effects, tidal asymmetry of water levels and velocities influences tide-residual sediment transport, where a slight asymmetry can result in a large net influx of sediment into the forest over a tidal cycle (Friedrichs, 2011; Hunt et al.,

2015). To explore these effects, Figure 4.4 shows tidal stage versus velocity plots for the entire 20-year simulation period. The observation stations are selected to represent the tidal stages at the mudflat, the fringe, and the mangrove patch interior of each scenario.

We observe near-equilibrium conditions in the bare mudflat scenario A (Figure 4.4a), where the velocities are similar along the entire profile during the tidal cycle, with a slightly larger flood velocity, indicating an accretive system. Figure 4.4b-g clearly exhibits the reinforcing effect of drag induced by growing mangroves on the tidal asymmetry. The systems become flood-dominated (larger flood velocity) in the mangrove forest interior and ebb-dominated (larger ebb velocity) at and seaward of the fringes. Water levels and velocities are lower in and landward of the mangrove patches. These effects become stronger when mangroves grow in size and colonize more areas. On average, mangroves start to substantially affect the hydrodynamics once they have passed an age of 10 years.

Mangroves induced drag that limits flow and attenuates waves favouring sediment deposition in the forest interior (Horstman et al., 2018; Temmerman et al., 2023). Larger pressure gradients drive larger sediment fluxes during the flood. During ebb, a pressure gradient develops when water levels at the mudflat drop faster than in and landward of the mangrove patches. High friction delays the flow when ebb water drains, maintaining relatively high water levels in the patch interior. Turbulence from breaking waves enhances sediment resuspension, particularly during the low water near the fringe in the seaward direction. At the fringes, the increased bed slope and pressure gradient lead to larger ebb velocities, favouring further offshore sediment transport. This pattern is consistent with previous observations and modelling studies, e.g., Gijsman et al., (2023), van Maanen et al., (2015), and Bryan et al., (2017). Denser and larger-diameter mangrove populations enhance this effect. The effect of mangrove-induced drag on tidal asymmetry is valid in all scenarios regardless of the relative position of mangrove forests to MSL. In the case of multiple patches, the most seaward-located patch governs the mechanism. Under similar conditions, mangroves situated at higher elevations have less pronounced effects. Particularly for patches above MHWN, the transition from peak flood in the interior to lower ebb in the seaward or the other way around during flood is relatively short. Thus, the findings in our simulations support previous studies, which show that the sediment accumulation rate was greater near the fringe than in the interior.

The model results show a strong correlation between the position of mangroves relative to MSL and sediment deposition. Mangroves located between the mean high-water spring (MHWS) and the mean high-water neap tidal elevation (MHWN) tend to favour deposition. In contrast, mangroves between MHWN and mean sea level (MSL) tend to induce scarp erosion at the seaward fringe edge. In contrast, scenarios featuring patches closer to MSL have a more pronounced scarping effect. This is attributed (a) to a larger, landward-located water volume that needs to be drained, (b) to faster-lowering water

levels during ebb at elevations closer to MSL, and (c) to associated larger pressure gradients within the mangrove interior. The pronounced modelled fringe edge erosion was also observed in field studies of mangrove environments (De Dominicis et al., 2023; Pelckmans et al., 2023). The supplement presents additional numerical experiments on morphostatic profiles, that explain this effect in more detail.

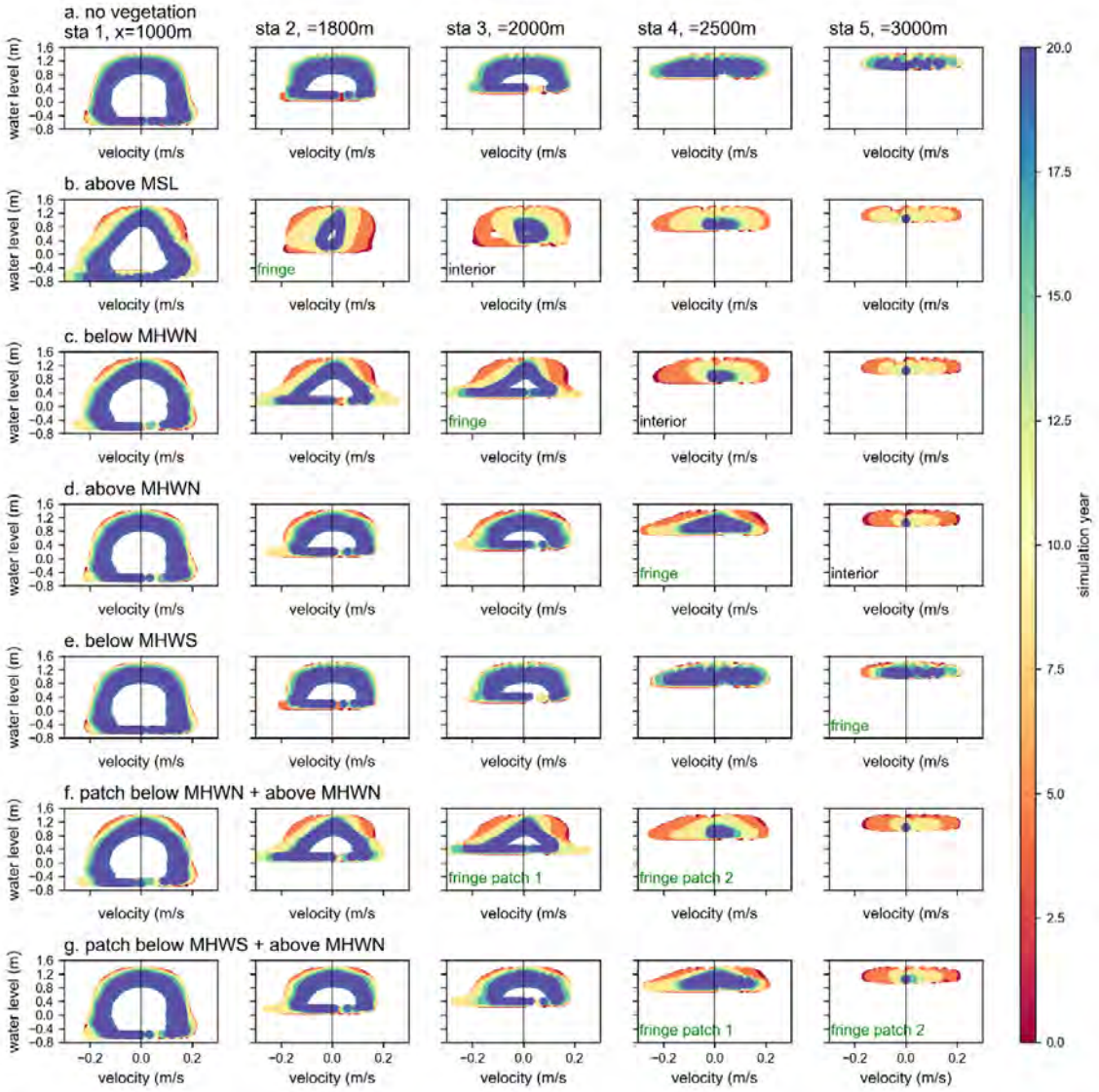

Figure 4.4. Tidal stage plots extracted from numerical modelling results. Panels a-g show the evolution of the cross-shore averaged tidal stage over simulation time, where water velocity (m/s) is plotted against water level (m) at 5 different observation stations of each scenario during spring tide. Observation stations are described in Figure 4.3. Velocities are positive in the landward (flood) direction.

4.2.2. Mangrove biomass development

Planting scenarios in two patches with gap and higher than high water neap result in the highest biomass and widest extent. We observed a pronounced sensitivity of the canopy cover area (Figure 4.5) and number of trees (Figure 4.6) to mangrove placement. The final cover area can vary by a factor of two between mangroves located at the low water level and those placed at the high water spring level. This striking difference is attributed solely to the initial mangrove patch position relative to MSL. The maximum cover area is achieved in scenario G (patches below MHWS+above MHWN) followed by scenario F (patches below MHWN+above MHWN) (Figure 4.5). The canopy area evolution can be divided into three distinct phases: During the first period, until year 5, patched scenarios cover slightly larger areas than the single block scenarios. Next, between year 5 and 10, trajectories diverge, depending on bed elevation within each of the two types of planting scenarios (single vs. multiple patches). As the community grows older, the higher bed level provides a shorter hydroperiod and less energetic wave conditions, enhancing the probability of seedling establishment. Since the competition remains low, mangroves grow optimally, resulting in a larger extent compared to those located lower on the profile, featuring less favourable conditions for establishment and growth. After 12.5 years of growth, leveraging the advantage of being in a higher topographical position, the canopy area in scenario C, located below MHWN, surpasses that in scenario B, where the patch is located above MSL. The slightly better window of opportunity due to lower inundation frequency in scenario C provides a relative advantage, which becomes more apparent when the species initiate propagule production. The improved window of opportunity increases the probability of stranded propagules to survive and grow into saplings. Therefore, scenario C contains a higher number of trees (Figure 4.6) and a wider canopy cover than scenario B. Overall, mangrove placement at particular levels on the topographic profile exerts a strong influence on the number of trees in the community after 20 years. Mangroves located below MHWS have the largest communities, and community sizes tend to decline in the order: scenario above MHWN, below MHWN, and above MSL. Patchiness offers a clear advantage as tree numbers in those planting scenarios surpass those in single block scenarios after year 12.5-15.

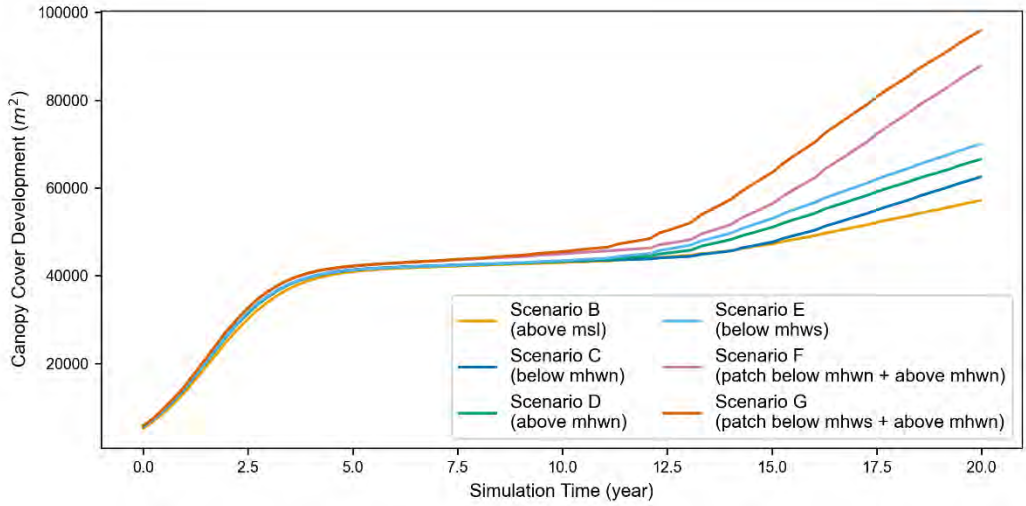

Figure 4.5. Canopy cover area development. Development of canopy cover area over 20 years in different planting scenarios .

Canopy cover area development represents the top of the canopy and, therefore, corresponds to the tallest stands (Beselly et al., 2023). The species-specific number of tree development, as shown in Figure 4.6a provides additional insight into whether the mangrove community is declining, expanding, or heading towards (dynamic) equilibrium by including all life stages in the community.

Until generative reproduction commences within the first 5 years, the number of trees remains constant across all scenarios (Figure 4.6a). Although *Avicennia marina* grows more slowly in biomass production than *Rhizophora apiculata* (Berger and Hildenbrandt, 2000), it has a higher seedling production rate (Grueters et al., 2019). Additionally, *Rhizophora apiculata* propagules require a longer inundation-free period than *Avicennia marina* to settle. This causes the *Avicennia marina* population to dominate the forest in terms of the number of trees.

As illustrated in Figure 4.6a and b, after 15 years, the mangrove community in all single-patch scenarios stabilizes gradually. An exception is the scenario above MSL (scenario B), which shows a decline after year 12 in the *Avicennia marina* population and a transition to a steady number of *Rhizophora apiculata* trees. In contrast, the number of trees in the two-patches scenarios continues to rise. The increase in the number of trees in Figure 4.6a reflects an expanding mangrove forest or a less competitive environment with more younger mangrove trees established. Conversely, a decrease in tree numbers indicates a more competitive mangrove forest, with high juvenile mortality and more growth of the mature trees or a stronger signature of the self-thinning mechanism. Despite the slower growth rate of the *Rhizophora apiculata* population, the increasing trend for all species is quite similar. Seedling mortality in the mangrove community is mainly

controlled by the inundation period, where the hydro-morphodynamic feedback by the expanding and denser forest lowers the WoO. In the first 10 years, the biophysical properties (surface area, density, and D_{130}) of the mangrove forest have only a minor effect on hydrodynamics leading to a negligible influence on morphodynamic development (Figure 4.2 and Figure 4.4). Under these conditions, the WoO is lower at the seaward fringe and higher towards the interior and landward fringe. After 10 years, the increased mangrove density and D_{130} cause higher friction leading to tidal asymmetry and pressure gradient. This tidal asymmetry delays the interior water level, extending the inundation period and preventing propagule establishment. The increased velocity induced by the pressure gradient moves propagules from the seaward fringe offshore, reducing seedling establishment. As a result, the number of trees remains static with no colonization occurring at neither the seaward fringe or the interior. In contrast, scenarios with multiple patches continue to produce viable saplings in both colonization areas: the seaward fringe at the upper patch and the landward fringe at the lower patch. Plots of WoO and propagule production on observation plots are provided in the supplement.

Although *Rhizophora apiculata* has a smaller population size, the mean diameter of mature trees at the upper end of the diameter distribution is substantially larger for *Rhizophora apiculata* than that for *Avicennia marina* (Figure 4.6b). We observe a dominance of the large *Rhizophora apiculata* population after year 10. However, given that *Avicennia marina* produces more propagules, we find an equivalent number of juveniles across all scenarios. In years 15 and 20, the dominant distribution of $D_{130} < 5$cm trees in *Avicennia marina* demonstrates its dominance in seedling production. During this period, the surviving population from year 15 shifts into the $D_{130} >$30cm category in year 20. This histogram illustrates that two-patches scenarios consistently have a wider distribution of tree diameters. All single-block scenarios experienced a decreasing number of juveniles, with scenario B having the lowest compared to the patched scenarios. This indicates that the community will be dominated by mature trees with high competition.

Rhizophora apiculata (dashed lines) has developed a considerably larger biomass from year 2 onwards (Figure 4.6c), similar to the observation by Berger and Hildenbrandt, (2000). However, this is less pronounced for *Avicennia marina*, as juveniles dominate the diameter distribution (Figure 4.6b). Once again, scenarios with multiple patches and gap produce more biomass due to their wider extent (Figure 4.2) and higher number of trees (Figure 4.6a). Beyond 20 years, the higher WoO in multiple patches scenarios leads to lateral expansion due to colonisation, higher survivability of juveniles progressing into mature trees, and ultimately higher biomass capacity.

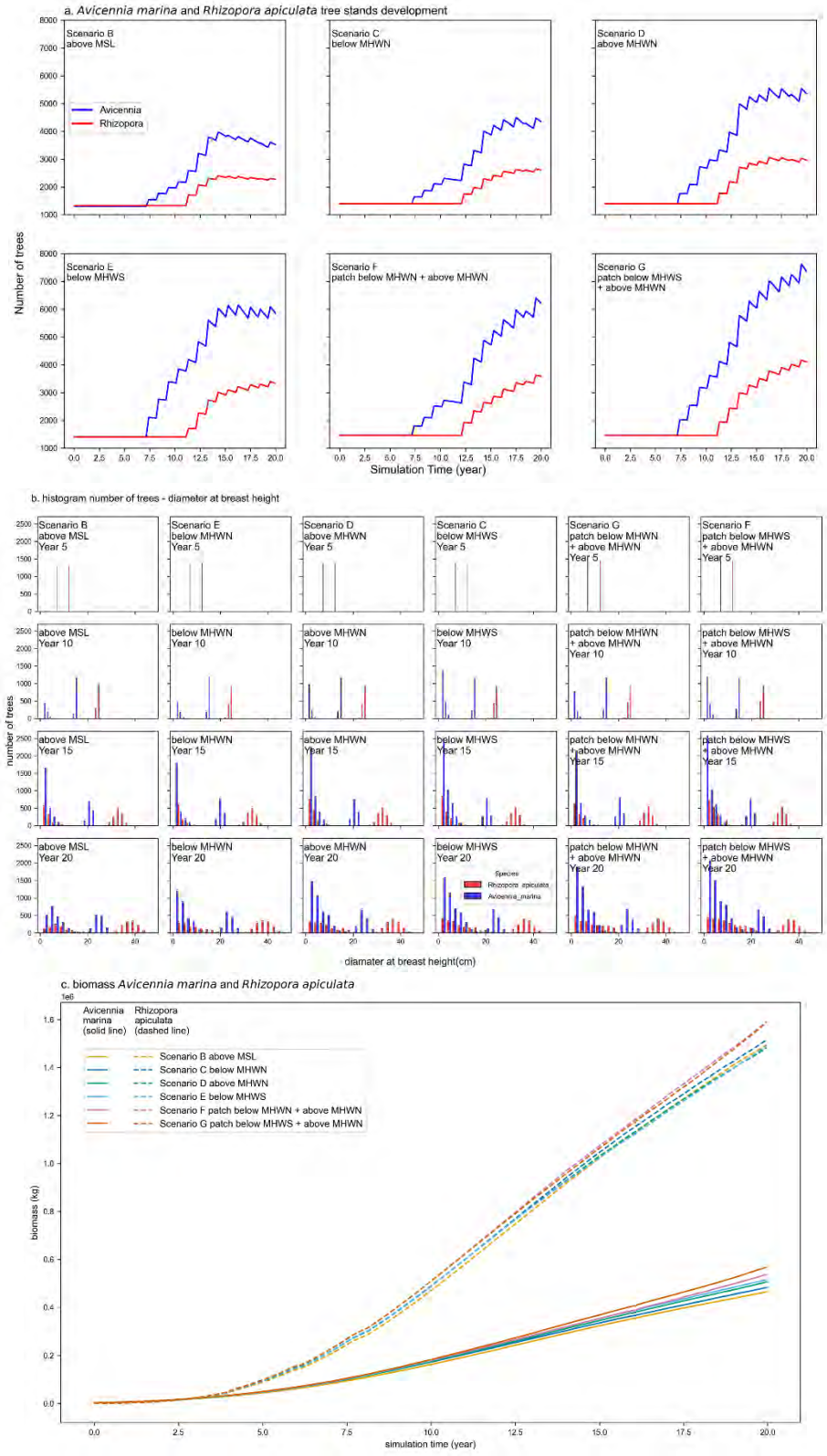

Figure 4.6. Mangrove populations' development (a) Mangrove populations' (number of trees) development in space-available case. This plot captures aggregated mangrove

tree population for each species over the simulation period. (b) distribution of mangrove diameter at breast height (D_{130}) in cm at every 5 years for Rhizophora apiculata (red bars) and Avicennia marina (blue bars). Propagules are produced when the tree has reached the flowering stage, with species-specific propagule density per crown surface area. (c) Overall biomass over the 20 years simulation period for the two-competing species Avicennia marina (solid line) and Rhizophora apiculata (dashed line). Biomass (kg) was calculated following the approximation by Comley and McGuinness, (2005) for Avicennia marina, Kauffman and Cole, (2010) and Ong et al., (2004) for Rhizophora apiculata as in Murdiyarso et al., (2015). Biomass content in the plot is the sum of all mangrove species individuals on each time stamp.

4.2.3. Carbon mitigation capability and potential

We estimate potential mangrove carbon (C) stock in three carbon pools: a) aboveground biomass carbon (AGC) represents all living parts of vegetation above the soil, including stem, branches, and foliage, b) belowground biomass carbon (BGC) represents biomass of belowground roots below the soil surface (Adame et al., 2017), and c) soil organic carbon (SOC) which is the change in carbon accumulation due to the modelled cumulative erosion/sedimentation. We assume that sediment imported from the seaward boundary contains organic matter with 10% carbon content, in accordance with values reported for observation projects in Indonesia (Kusumaningtyas et al., 2022; Murdiyarso et al., 2015). The schematized domain corresponds to an accreting coastal system that feeds on mud of riverine origin transported alongshore; where the allochthonous sediment dominates in-situ carbon burial. The methods section explains the estimation of AGC, BGC, and SOC.

Figure 4.7 shows that, in line with findings in the previous section, all scenarios below the level of MHWN show a reduced soil organic carbon accumulation compared to the no vegetation case (scenario A). Scenarios with all combinations situated above MHWN (scenarios D, E, G) accumulate more sediment than scenario A. Scenario D (below MHWS) surpasses scenario A after year 10. At the end of the simulation, the two-patches scenario with a combination above MHWN and below MHWS (scenario G) has the highest SOC. Interestingly, although all two-patches scenarios have the largest canopy area, scenarios with a combination situated below MHWN (scenario F) feature less SOC than scenario A. Scenario B (above MSL) has the smallest amount of net SOC accumulation, almost vanishing near the end of the simulation. The SOC accumulation rate is quite similar in all scenarios. However, all scenarios below MHWN reverse their response pattern in year 10 and regain sediment afterward (Figure 4.7), whereas only SOC in scenario B keeps decreasing.

We calculate carbon stock changes for the carbon pools modelled above. All scenarios show an increase in carbon stock over time. However, scenario B has reached its limit within 20 years for the SOC. In comparison, scenarios below MHWN are shown to have

reached optimum density for ecology (AGB-BGB contribution) after 20 years. Interestingly, two patches scenarios are still in an expanding trend, where they have a chance to sequester more carbon until the forest reaches maximum mangrove community density, depending on the forest composition (Berger and Hildenbrandt, 2000). It shows the benefit of strategically providing a less competitive environment and gap (space) to allow for higher successful landward seedling establishment.

Our simulations suggest that SOC is the highest contributor among the carbon pools for all scenarios. Recent studies (Macreadie et al., 2021; Murdiyarso et al., 2021; Sasmito et al., 2020; Song et al., 2023) mention SOC is the highest contributor to the total ecosystem carbon stock. However, it is essential to note that the SOC's source in those studies is majorly of autochthonous origin, where we assume the availability is still limited within our domain. Additionally, our modelling exercise resembles mangrove afforestation within 20 years after planting, in which allochthonous carbon prevails (Chen et al., 2023; Song et al., 2023). Scenario B represents an exception due to its deep scarp erosion pattern and the reversal of the rising SOC trend after year 10.

Consistent with Figure 4.6c, there is no substantial difference in the biomass carbon pools among scenarios as shown in Figure 4.7. The finding in biomass carbon seems inconsistent with the findings of the previous section, i.e., a twofold increase in canopy cover (Figure 4.5) and a clear rise in tree number (Figure 4.6a). This phenomenon can be explained by the number of trees-diameter histograms in Figure 4.6b. The community of the forest is dominated by the younger trees with D_{130} < 5cm. This is particularly evident when the community exceeds the age of 10 years. Although the younger trees are dominant in number, the total biomass is dominated by the contribution of surviving first-generation trees. On the other hand, the accumulated SOC exhibits a significant difference, benefiting from sediment trapping efficiency.

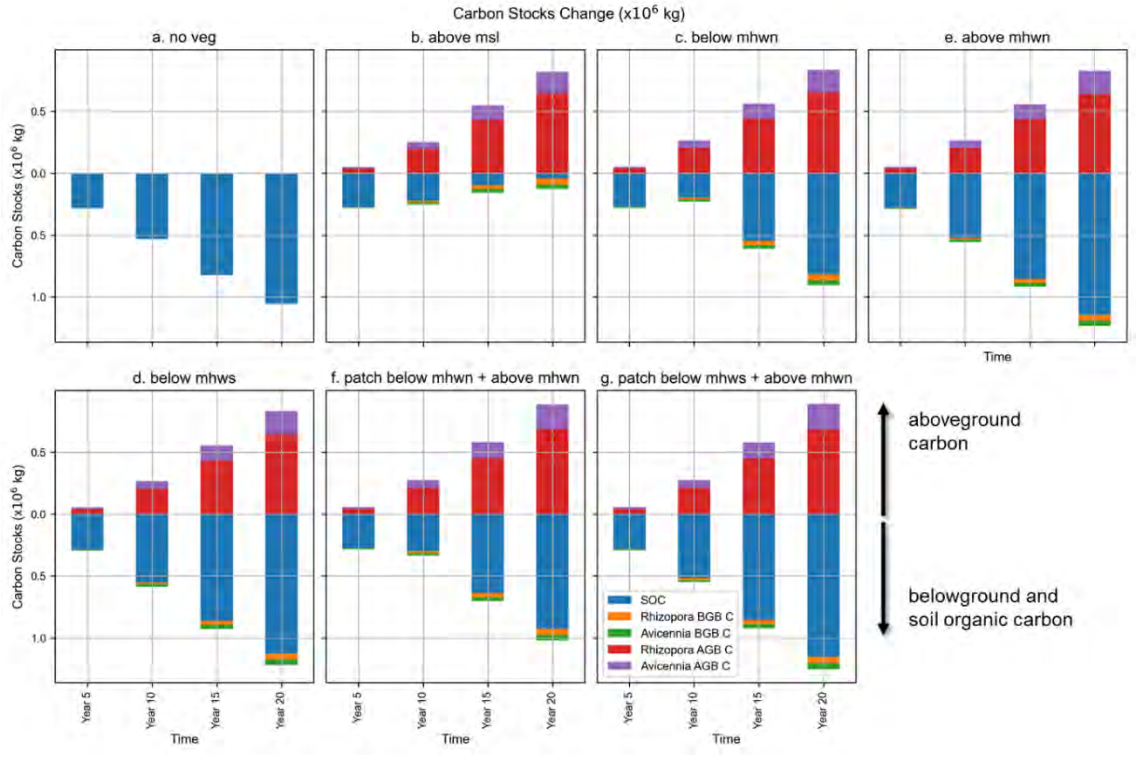

Figure 4.7. Carbon stock changes. Simulated carbon stock changes from three carbon pools (living vegetation above- belowground and soil organic carbon). The y-axis shows the value of carbon stocks changes (in 10^6 kg) with positive values in both directions, where a value above zero represents aboveground carbon and below zero represents belowground and soil organic carbon. Above and belowground biomass carbon are estimated based on the mangrove species properties. Soil organic carbon is estimated from cumulative sediment volume changes from the whole model domain.

4.2.4. Implications for mangrove restoration management

Most studies link tree species to carbon sequestration potential (Aye et al., 2023; Sahu and Kathiresan, 2019) or focus on optimisation of restoration strategies in terms of ecology (Lewis and Brown, 2014; SER (Society for Ecological Restoration Science and Policy Working Group), 2002), intervention approach (Primavera et al., 2011), species type(s) (Bai et al., 2021), geomorphic settings (Hatje et al., 2023), or planting density (Guo et al., 2018). These studies typically cover a large spatiotemporal scale, i.e., minimum at the forest scale, where gradual and slow changes occur. However, the restoration success and potential carbon sequestration are also related to the successful establishment (Shih et al., 2022; Van der Stocken et al., 2019), tied to a short spatiotemporal scale (Balke and Friess, 2016). This implies that smaller-scale processes need to be included to understand the system's behaviour on a larger scale (Pretzsch, 2009). Our modelling results show that a fractional modification, such as strategic

placement on a specific elevation with respect to tidal levels, provides a disparate outcome. The knowledge gained in this modelling exercise can offer guidelines to restoration attempts.

The simulations reveal that assessing restoration success may not only be evaluated in terms of large mangrove extent or the potential biomass, particularly if the monitoring period after restoration is limited in time. In this case, we assume the monitoring period is similar to a typical engineering time scale (20 years). As such, morphological development, referred to as SOC accumulation, is the sensitive yet potentially influential parameter demonstrated in this work. For instance, scenario B (above MSL) indeed has the lowest extent (Figure 4.5) and the smallest number of trees (Figure 4.6a). Nevertheless, the simulated biomass carbon does not significantly differ from other scenarios (Figure 4.6c). Our study suggests successful mangrove restoration may not be seen exclusively from biomass carbon accumulation. However, the total carbon stock can be even lower than the no vegetation scenario (Figure 4.7) due to soil loss and the associated soil organic carbon stock. The results indicate the importance of efficient mangrove placement in restoration works to avoid counterintuitive results.

It is notable that mangrove restoration is now becoming a global movement, followed by the slowing down of forest loss (Global Mangrove Alliance, 2021; López-Portillo et al., 2017). Mangrove restoration can be a potential solution in climate change mitigation when the restoration failures are minimized. In this study, we demonstrate the possibility of conducting predictive behaviour of mangrove forests following their placement and the changes in carbon stocks. From the perspective of mangrove restoration projects, it can potentially reduce the cost by strategically planting the seedlings and excessive trial-and-error, making it predictable and affordable.

The findings suggest practically focusing on mangrove restoration in the high water neap elevation in the initial project. We observed stable tree-number distribution and a consistent pattern of biomass production after year 15. Although a mangrove's lifetime can take more than a century, we suggest monitoring in an undisturbed restoration project that can be conducted within 20 years. Make it reasonably practical and easy to implement, following the current standard in engineering projects.

4.3. METHODS

4.3.1. Coupled mangrove-hydro-morphodynamic model

Mangroves thrive in a dynamic coastal environment at the wedge of high and low water. In response, mangroves need to interact and provide feedback with multiple physical-environmental drivers, i.e., nutrient availability, salinity, and sea level / hydroperiod (Grueters et al., 2014; Krauss et al., 2014). The interactions with these drivers will affect

their growth, dieback, and species distribution, determining the productivity and the extent of the mangrove ecosystem. The interactions occur at different spatiotemporal (habitat, ecological, and geomorphological scales) and life stages (propagule, seedling, sapling, and mature). Any disturbances at each hierarchy would alter the higher hierarchy and cascade into the ecosystem level (Twilley et al., 1999). In turn, it affects the interactions and traits of the abiotic-biotic factors at the lower level. For instance, the rise of ecosystem-scale sea levels affects the hydroperiod and the related morphological development. The changes in bed level variation will alter seedlings' establishment and thus affect the mangrove stands competition, changing the mangrove community structure (Rivera-Monroy et al., 2017). Therefore, we apply a hierarchical approach (Twilley et al., 1999) to describe mangrove dynamics and the feedback loop based on their ecological (local) and geomorphological factors.

The spatially explicit interactions between hydro-morphological processes and mangrove dynamics are simulated with DFMFON (Beselly et al., 2023), a coupled individual-based mangrove MesoFON (Grueters et al., 2014) (MFON) and landscape-scale hydro-morphodynamic Delft3D-Flexible Mesh (Deltares, 2021) (DFM) model, resolving local-scale to landscape-scale, respectively. The coupled model resolves the feedback loop between the short-term changes in local abiotic factors (i.e., flow, sediment availability, waves, and salinity) and the long-term bio-geomorphic mangrove forest dynamics. These interactions occur and are modelled within each life-stage of the mangrove tree (propagule, seedling, sapling, and mature), including short-/long distance propagule dispersal. DFM translates mangrove biophysical characteristics as the bulk drag coefficient at each time step, affecting the hydro-morphodynamics. The simulated DFM variables (water level, salinity, and bed level) are defined as mangrove stressors to update mangrove stands in MFON every 90 morphological days. The 90-day interval was chosen to realistically incorporate mangrove reproduction (e.g., flowering, fruiting, and seedling production) while keeping the wet and dry seasonal climate forcings.

Mangrove individual-based model

The individual-based mangrove model MFON aims to simulate individual mangrove development based on the tree-to-tree competition and variation of environmental conditions, i.e., salinity and nutrient availability. The competition routine is based on the Field of Neighbourhood (FON) approach (Berger and Hildenbrandt, 2000), which defines the strength of influence of one tree upon another as dependent on the radius of competition, either above or below ground, related to the tree's stem diameter. Mangrove growth is governed by the level of competition for resources and is limited by salinity. Mortality will occur in case of no growth in D_{130} for 5 years and local disturbance events.

Tree recruitment and establishment are processed by the DFMFON routines, which take into account the physical stresses from hydrodynamics simulated in DFM. During the seedlings' production period, the two-week averaged flow pattern is captured and used to

estimate propagule dispersal. The selected period is in line with the generally observed obligatory two-week dispersal period (Beselly et al., 2023). The successful establishment of the dispersed propagules is evaluated following the local inundation frequency, applying the conceptual model termed Window of Opportunity (WoO) (Balke et al., 2011), while also taking into account seedlings' burial and toppling due to hydrodynamics (van Hespen et al., 2022b). WoO is parameterised from species-specific inundation-free days as the critical period to let the root securely anchor in the soil. The WoO threshold for *Avicennia sp.* is defined as 3 inundation-free days, based on an experiment conducted by Balke et al., (2015). For *Rhizophora sp.*, we used Watson's hydrological classification (Watson, 1928) that was derived for Malaysian mangroves and has been improved for varied tidal regimes based on studies in South East Asian Mangroves (Indonesia and Vietnam) in the study by Van Loon et al., (2016). *Rhizophora sp.* is classified as hydrological class 3 with 100-200 minutes per inundation, while *Avicennia sp.* is in successional class 2* with 200-450 minutes per inundation for successful anchoring of a seedling. Therefore, *Rhizophora sp.* requires an inundation-free duration of up to 2 times longer than *Avicennia sp.* Hence, we assume the WoO value for *Rhizophora sp.* is 5 days.

Hydro-morphodynamic model

An open-source hydro-morphodynamic DFM model is used in the study to simulate flow, sediment dynamics, and morphological processes. This model is set to solve two-dimensionally (depth-averaged) shallow water equations on an unstructured grid and is widely used in coastal and estuarine environment (Best et al., 2018; Bryan et al., 2017; Wegen et al., 2019). Wind-wave propagation is simulated using D-Waves module in DFM (Deltares, 2021). D-Waves is based on the SWAN spectral wave model, capable of simulating the evolution of short-crested, random wind-waves in coastal areas. D-Morphology (Deltares, 2021) module in DFM is activated to solve the suspended sediment transport in the muddy coast by solving the advection-diffusion equation, applying the Partheniades-Krone formulation to estimate erosion and deposition.

The mangrove resistance on hydrodynamics is represented in DFM using modified Baptist predictor (Baptist et al., 2007) by separating vegetation-induced resistance λ and bare bed roughness C in momentum equation (Deltares, 2021) (Eq. 4.1 and Eq. 4.2). The Baptist equation is implemented considering the relations of vegetation height h_v (m), density n (number of trees/m^2), bulk drag coefficient C_D and unvegetated bed roughness C_b to water depth h. With κ is the dimensionless von Kármán constant and D is stem diameter (m).

$$C = C_b + \frac{\sqrt{g}}{\kappa}\ln\left(\frac{h}{h_v}\right)\sqrt{1+\frac{C_D n D h_v C_b^2}{2g}} \quad (4.1)$$

$$\lambda = \frac{1}{2}C_D n D \frac{h_v}{h}\frac{C_b^2}{C^2} \quad (4.2)$$

The C_D coefficient is assumed to be equal to the drag force exerted on mangroves, which is a function of the projected area (A) and the submerged mangrove biomass (V_M) in a control volume (V). The C_D predictor, following the formulation by van Maanen et al., (2015) is defined in Eq. 4.4. C_D is calculated as the sum of the total drag coefficient on the bare surface $C_{D,no}$, with a value of 0.005 and the ratio between the dimensional constant e set as 5m and the vegetation length (L). These coefficients were defined to attain a realistic bulk drag coefficient. Vegetation length depends on species-specific mangrove root geometries varying over the water depth.

$$L = \frac{V - V_M}{A} \quad (4.3)$$

$$C_D = C_{D,no} + \frac{e}{L} \quad (4.4)$$

The obstacle volume depends on species-specific geometry and water depth. For instance, even at the same water depth and with the same D_{130}, V_M of *Avicennia sp.* is different from that of *Rhizophora* sp. Primarily, the distinct root system of *Avicennia* sp. and *Rhizophora* sp., characterized by pneumatophore and stilt roots, respectively, account for this difference. Therefore, we partition V_M contribution of the stem and roots. The stem is simplified as a truncated cone, with diameter at the bed level D_0 and diameter at each water depth D_w, following species-specific diameter-height allometric relationship. The contribution of mangrove rooting systems for *Avicennia* sp. for single pneumatophore is simplified as cones (Du et al., 2021) and multiplied by the maximum number of pneumatophopore n, derived from the tree's D_{130}. *Rhizophora* sp. stilt roots morphology is characterised following the Ohira stilt root model (Ohira et al., 2013), considering the tree shape factors, i.e., D_{130}, root height (H_R), number of roots (N_R), root diameter (Φ_R),

angle between the root and the level line at shoot point (θ), and root-spread distance from the trunk to the root edge (x_2). The details on V_M calculation can be found in supplement.

4.3.2. Model Configurations

The muddy open coast setting is employed as a basis of the bio-geomorphic topology. In restoration efforts, this open coast topology is considered to have medium opportunity and less land-ownership conflict (Sasmito et al., 2023). The scenario represents an active restoration approach (Teutli-Hernández et al., 2020). It is assumed no abundant propagules are available in the surroundings, and a proactive attempt (Zimmer et al., 2022) has been made to establish mangroves in previously unvegetated areas. The scenarios also take into account the use of mangroves as nature-based solutions for climate adaptation along with hybrid engineering applications. We schematised the domain as a seawall or levee in located at the landward end at an elevation higher than the MHWS, demarcating a clear landward limit of accommodation space and a mangrove greenbelt seaward of it.

The overarching goal of the study is to investigate the optimum configurations of mangroves to achieve the maximum carbon stock accumulation. To this end, the simulation should ideally be carried out over the life span of the mangroves, which can be centuries (Berger and Hildenbrandt, 2000). However, the simulation period is set to be 20 years in order to consider any time-related organizational limits in the observation and monitoring of the restoration success and to enable a fair comparison with the application of hard structures.

Intertidal mudflat

Here, the model is employed in a schematized way as the process-based model DFM retains the explicit causal mechanism in representing reality. We recognise that a schematised model may not ideally capture all processes and may simplify the system. However, the important and predominant variables included in the model reflect and reproduce the important features in the real system, as described in van der Wegen and Roelvink, (2008). The idealised model (Figure 4.1) is constructed on a homogenous 10×10m grid to capture the variation in a mangrove stand changes to match the plot dimension commonly used for mangrove surveys (Beselly et al., 2021; Best et al., 2022). This grid is arranged in a rectangular flow- and morphology-related domain with a width of 200m in the x-direction and a length of 4000m in the y-direction. The wave-related rectangular domain consists of a 20mx20m grid and is dimensioned at 600mx4100m (x- and y-direction). It is built coarser and wider to prevent boundary effects in the flow direction.

The bare intertidal flat in a degraded environment needs a long time to be recolonised naturally (Ren et al., 2008). Human assistance in an attempt to improve hydrological conditions in mangrove wetlands by restoring the sediment fluxes is being applied for instance in restoration projects in South East Asia (Winterwerp et al., 2013). Therefore, in the model, we parameterised it as an open coast with a typical mangrove mudflat (Winterwerp et al., 2013), on a 2D depth-averaged domain with a mudflat slope of 1:1000 below mean sea level, forced by spring-neap tides and single wave climate. The spring-neap tides are constructed with the morfacTide toolbox (Schrijvershof et al., 2023) and are represented through fortnightly modulation of the semidiurnal tide of typical tidal forcing (Winterwerp et al., 2013) with MHWN of 0.8m and MHWS of 1.2m. A consistent narrow band of wind waves directed perpendicular to the shoreline is forced with a wave module in DFM, attaining a significant wave height of 0.2m and wave period of 6s. A sediment concentration of 0.03kg/m^3 is constantly supplied during the simulation period. The wave parameters and sediment concentration are typical of the muddy coast in the north of Java, Indonesia. The morphological update is accelerated with the morphological factor (MorFac) in DFM, which ranges from 30 to 100 in mangrove-salt marsh wetlands (Beselly et al., 2023; Best et al., 2018; van Maanen et al., 2015). We run the initial linear intertidal profile for 120 years until it reaches the quasi-equilibrium profile, meaning the erosion-deposition rate is almost identical along the course of the simulation period. Following the series of sensitivity analyses, we applied a MorFac of 90 with a settling velocity of 0.0009m/s, erosion parameter of 0.00007 kg/m²s, and critical shear stress for erosion (τ_{ce}) 0.24 N/m². Detailed grid configuration and the complete set of model variables are presented in supplement.

Mangrove restoration scenarios

In order to replicate assisted rehabilitation/ planting attempts, we assume that only the initial seedlings survive the first planting phase and develop into saplings with homogenous D_{130} . The initially planted mangroves have a tree height of 1.418 m (*Avicennia marina)* and 1.447 m (*Rhizophora apiculata)*, in allometry to their biophysical characteristics (D_{130}). Once a propagule has been successfully established, the seedling always survives and develops into a sapling, with the tree height approaching breast height by the end of their first 2 years. This is in accordance with the mangrove growth function that is based on the D_{130} and the associated parameters. The restoration is defined on 200mx200m and 200mx100m grids, for single and multiple patches, respectively (Table 4.1). A widely applied technique in restoration by planting is to combine pioneering species, that are reported to have higher survivability (van Bijsterveldt et al., 2022) and help increase diversity (Sidik et al., 2013). Therefore, the MFON model was calibrated for *Avicennia marina* and *Rhizophora apiculata,* two

common pioneering species for planting distributed in Porong Delta, Indonesia and South East Asia, respectively (Sidik et al., 2013; Song et al., 2023). The seedlings are planted on top of the barren intertidal flat soil, assuming to have a consistent optimum nutrient content. This is the limitation of the model, as the plantation age progresses, the organic matter, clay proportion, and salinity content in the unvegetated intertidal flats are likely to increasingly improve (Ren et al., 2008).

4.3.3. Carbon stocks estimation

The C stocks presented here reflect the carbon accumulation or carbon stock changes from the initial state. Mangrove litter and deadwood are also important carbon pools in this ecosystem. However, we did not count these components in the estimation because their contribution is relatively small (Murdiyarso et al., 2021) due to the limited availability in our system, and no empirical relationship to determine the magnitude in a dynamic way was found. Therefore, we assume a consistent organic carbon (OC) content across space and time. We employed an allometric relationship of species-specific aboveground biomass (AGB) and belowground biomass (BGB) for Southeast-Asian mangroves following Murdiyarso et al., (2015) and estimated carbon (C) with a multiplier of 0.47 and 0.39 for AGB and BGB, respectively (Murdiyarso et al., 2015). We estimated SOC as a product of dry bulk density (kg m^{-3}), cumulative change in soil volume (m^3), and OC content. Although the bulk density and OC content vary with depth (Donato et al., 2011), for practical estimation, we assume they do not vary across depth and horizontal space. We used dry bulk density consistent with the hydro-morphodynamic model parameter (500 kg m^{-3}), whereas we applied a median OC content of 10%. Both values are within the range reported in Murdiyarso et al., (2015) and Donato et al., (2011). With the assumption of the reduced carbon density in the seaward direction, the SOC is calculated from the point of mean sea level to the landward limit of the model domain. Additionally, the substantial sediment loss in Scenario B resulted in negative carbon stocks, not allowing comparative analysis.

5

CONCLUSIONS AND RECOMMENDATIONS

This chapter provides the outcomes of the dissertation by discussing the answers to the research questions and their implications. The chapter concludes with recommendations for future research.

This study aims to assess the importance of complex eco-geomorphic interactions and feedback processes of physical-environmental drivers in coastal mangrove environments to the benefit of developing trustworthy tools for predicting mangrove forest dynamics, to be used, for example, in the design of mangrove restoration strategies.

The outcomes of the research are formulated as the answer to the research questions, providing the main conclusions and their implications. This chapter ends by giving reflections and recommendations for future research.

5.1. RESEARCH OUTPUTS

Below, we answer the research questions formulated in chapter 1 based on research results described in chapters 2 to 4.

Question 1: What are the various timescales of mangrove dynamics on a prograding delta?

The high fluvial influx of mud to the Porong Estuary, Indonesia, significantly contributes to the accelerated development of the delta in the river mouth. The resulting annual and decadal landscape scale development clearly shows that mangrove forests expand following continuous delta development. However, isolating the mangrove extent detection to a finer seasonal time scale, we found a clear spatiotemporal variation of mangrove extent in correlation with seasonal (6-monthly) forcings and their dependency on the development of intertidal morphology. We observed a recession of the mangrove extent during the transition of the dry-to-wet season and regrowth during the wet-to-dry season, particularly the regrowth marked by the flowering period. The main driver for the Porong Delta expansion is the excessive mud supply from the mud volcanic eruption in the hinterland, stimulating the rapid growth of the delta lobes compared to before the eruption. Observation showed evidence, replicated in the model, of dependency of spatiotemporal mangrove regrowth-dieback on the wet-dry seasonal fluvial discharge and variation of sediment fluxes. The high freshwater river discharge during the wet season promoted mangroves to rejuvenate and disperse the propagules, while the deposited sediment fluxes increased the bed level, assisting the propagules to establish. On the contrary, in the dry season, the dry and saline environment increased competition, hindered growth, and enhanced mortality, particularly among juveniles.

We detected the spatiotemporal changes in mangrove extent by integrating multiple sources of satellite imagery and Unoccupied Aerial Vehicles (UAVs). A high-frequency mangrove extent map was created from a combination of multiple sources of satellite imagery (Landsat 7, Landsat 8, Sentinel 1, and Sentinel 2) in Google Earth Engine. The combination of multiple sources of satellite imagery allowed the development of 3-monthly mangrove extent maps that emphasize the sensitivity of mangrove extent to

seasonal forcings. The spatial distribution of mangrove height and population density coupled with the age map derived from the Unoccupied Aerial Vehicle (UAV) confirms multiple timescales of mangrove development.

Mangrove forests in Porong adapt to physical forces (river discharge and sediment supply) and, more importantly, benefit from the available accommodation space as a result of morphological development. This emphasizes the need to consider multiple time scales (ecology/ mangrove and morphology) to have a system understanding of the mangrove ecosystem. The frequent monitoring of mangrove forests is deemed necessary not only for the high sediment influx system as in the Porong Delta but also, for instance, in mangrove restoration activities. Integration of earth observation systems such as very high-resolution UAV and medium resolution from satellite observation can be a solution to achieve a cheap, fast, robust, and accurate understanding of mangrove ecosystems.

Question 2: What is the skill of a mangrove-morphodynamic model that explicitly represents biocomplex interactions of individual mangroves and physical-environmental stressors?

We modelled complex eco-geomorphic interactions with a bottom-up hierarchical approach. Within this approach, we parameterized the multi-spatiotemporal variations of mangrove ecological and hydro-morphological processes, solved at every life-stage scale, cascading from low (local level) to higher (landscape level) hierarchy. To address this, we explicitly complete the feedback loop of the physical-environmental drivers (water level, flow, waves, bed level, and salinity) and full mangrove tree life stages (propagule, seedling, sapling, and mature). Finally, we coupled a process-based hydro-morphological model (DFM) that accepts the presence of mangroves to influence friction, while the spatiotemporal outputs of DFM (water level, flow, bed level, and salinity) affect propagule dispersal, seedlings establishment, and tree competition in MFON.

The model qualitatively reflects the deltaic development and mangrove belt expansion for a case study in the Porong Delta, Indonesia. The model can simulate delta progradation, mangrove forests' seasonal dieback, regrowth, and intertidal flat colonization as observed in the study area. The model agrees well with the modeled mangrove stand height development and can reproduce the mangrove extent pattern, albeit that performance with respect to the expansion rate was less. The difference in expansion rate is expected, considering that the mangrove species are represented by one dominant species and neglects other sources of propagules from the vicinity.

Simulation results indicate the spatiotemporal shift in the role of mangroves acting as colonizers to functioning as ecosystem engineers. In a young and sparse forest, hydro-morphodynamic is controlled by local topography, with mangroves playing a limited role. During this time, mangrove growth depends on the availability of accommodation space. The population is sensitive to physical-environmental changes, where limited propagule

dispersal and high inundation frequency trigger the dieback of the younger stands. By the time the population becomes denser and more mature, reduced flow velocities in the forest stimulate sedimentation and a lower inundation frequency, resulting in a higher probability of seedling establishment of more abundant propagules, thus stimulating the mangrove's ecosystem engineer function. This process ultimately results in an optimal number of established trees stands enforced by self-thinning.

Further development of this model may lead to the improved prediction of mangrove forest structure and species development, albeit with the uncertainty of physical-environmental drivers and anthropogenic pressure. The mechanistic relationship provided in the model may be useful to investigate small and large-scale and long-term mangrove forest expansion/dieback in different detailed scenarios. For instance, we can apply the model to investigate habitat segregation leading to the collapse of the mangrove ecosystem; due to anthropogenic activities such as mangrove forest conversion to fish ponds or road construction. Another application would be assessing the persistence and protection level for the application for coastal protection under changes in storm intensities, with spatiotemporal variation of species composition, tree height, density, and man-made construction.

Question 3: Can we optimize the design of mangrove restoration strategies in support of carbon sequestration optimization?

The currently available approaches to estimating carbon sequestration potential typically cover large spatiotemporal scales (minimum at forest scale), which indicate gradual and slow changes. Research literature indicates that restoration success and correlated potential carbon sequestration are tightly coupled with successful mangrove establishment. However, the bottom-up traditional approaches that segregate ecology and hydro-geomorphology overlook the processes that control mangrove succession.

Our modelling results indicate that optimizing plantation zonation may promote favorable outcomes on morphology, ecology, and thus carbon stock accumulation. Our model outcomes further explain erosional trends resulting from ill-defined mangrove plantation schemes also observed in several case studies. Mangroves planted between mean high water neap and mean high water spring deposit more sediment and have a significant mangrove extent. In addition to having the highest deposition, scenarios with multiple patches plantation stimulate mangrove area expansion.

An important finding is that the restoration success from the perspective of carbon sequestration function may not only be evaluated from the resulting mangrove extent or potential biomass. We showed that soil organic carbon, having the largest contribution to carbon pools, is also sensitive to a simple planting placement. However, given the restoration projects with a 20 years time horizon, our study suggests successful mangrove restoration may not be seen exclusively from biomass carbon accumulation. Inefficient

planting strategies may lead to low total carbon stock accumulation even lower than the scenario without planting, due to soil loss and the associated soil organic carbon.

5.2. RECOMMENDATIONS AND FURTHER RESEARCH

Our modeling attempts have contributed to an ongoing exploration on the important parameters of mudflat-mangrove system dynamics. Currently, our knowledge of important trait-based parameters is limited to a few species; extending it to other species and different regions is deemed necessary. An example is the window of opportunity approach to describe seedling establishment that is valid for *Avicennia alba* in Singaporean Mangroves (Balke et al., 2011) and *Avicennia marina* in Firth of Thames, New Zealand (Balke et al., 2015). Interest in investigating this parameter has increased, for instance, as shown in the study of hydro-morphodynamics factors in seedling establishment for 8 mangrove species in China (van Hespen et al., 2022b). Replicating such a study for an extended database of mangroves and regions is possible. Current growth functions such as the one in (Berger and Hildenbrandt, 2000) initiates the growth parameter when the mangroves have reached the sapling stage, equal to breast height (137cm). It is worth investigating the mangrove's growth after a successful seedling establishment into the sapling stage.

Mangrove presence has important impacts on hydrodynamics, e.g., attenuating waves and altering the flow. This is a relevant reseach topic, considering mangroves function as sustainable solution in disaster risk reduction. However, mangrove capacity in attenuating waves, for example, varies between locations. It depends on the mangroves' biophysical characteristics (frontal area, density, and composition) and wave conditions (wave height and wave period). To approximate wave propagation, formulations require a function of mangrove projected area and volume on different water depth. Idealized vegetation configurations are commonly applied, such as for *Avicennia* sp. (van Maanen et al., 2015) and *Rhizophora* sp. (Ohira et al., 2013), all of these assume water depth will inundate the whole mangrove structure below the canopy. The hydrodynamic estimation will benefit most if such a database describing the function of (prop, pencil, cone, butrress) root, stem, and canopy exists. The corelations would be better to be built based on the commonly used key parameters such as trunk diameter at breast height.

While the current study focuses more on the primary production and surface contributions, the contribution of below ground biomass to bed level is noticed, especially in the capability of mangrove areas to adjust to sea level rise (Krauss et al., 2014). Similar to that, the role of e.g., mangrove litter and detritus to sediment accumulation in the forest interior is considerable (Ding and Fu, 2021). However, the challenge remains how to estimate their contribution and the relationship to determine the magnitude in a dynamic way in the model.

Mortality in the model is controlled by the competition between sapling-mature trees and during seedling establishment stage. Limited literature is available investigating mechanical tree damage, for instance due to the exposure to extreme wind and waves. This will be relevant, especially to understand the role of mangrove as coastal protection (Morris et al., 2019; World Bank, 2017). Such a mechanistic limit on the extreme conditions leading to tree mortality, once it is known will be useful to investigate mangroves' persistence.

The process-based mangrove-hydro-morphodynamic model presented in this research is validated, focusing on Porong Delta, Indonesia. As of any other models, for site- or species-specific use, this coupled model requires to be validated with field datasets, with the emphasis on mangrove attributes trajectories, particularly, the growth parameter and seedlings production. More efforts are needed to gather local to forest scale dataset in mangrove wetland, as these available datasets will be useful to further validate the model. There are increasing remotely-sensed monitoring efforts in mangrove ecosystems, such as Global Mangrove Watch (Bunting et al., 2022), and several field-based observations, e.g., in Guyana (Best et al., 2022) and New Zealand (Gijsman et al., 2023). While remotely-sensed observation can provide a larger extent in understanding the dynamics of mangrove forests in their area development or vegetation phenology, a field-based dataset is limited to its temporal period and location. Additionally, as mentioned previously, the field dataset collected in the study area requires state-of-the-art equipment that needs trained experts to operate and can be costly — considering the remoteness of the mangrove forests. Off-the-shelf tools such as UAV, demonstrated in Chapter 2, can be a promising solution to provide very high-resolution imagery to complement satellite-based tools with lower resolution (10-30m). Remotely sensed datasets in this way can only detect changes above the canopy and, hence, estimate the dynamics with canopy height or leaf index as a proxy; observing processes occurring under the canopy remains a challenge to investigate. Innovative low cost and autonomous monitoring tools are being developed, such as LSED (Laser based Surface Elevation Dynamics) sensor (Z. Hu et al., 2020) to monitor daily bed level changes and Mini Buoy (Balke et al., 2021) to observe water level and current velocity in the wetland. Such low-cost observation equipment can potentially provide an extended period and a larger extent of the study.

There are roughly two types of process-based, eco-hydro-morphodynamic models (see Chapter 1). Each type of model serves the specific needs of simulations. The question remains, how much complexity should we include in the models? Such as to what extent does including the effect of light availability, precipitation, or including interactions with subsurface hydrodynamics in the model affect the accuracy. Applying these tools requires more considerations than just adding physical and ecological processes. While more datasets will provide opportunities to improve and include more processes in the model, the type of model applied depends also on the study objectives and research questions. In future research, a systematic comparison between individual-based and population

dynamic vegetation models coupled with hydro-morphodynamics can be conducted, considering, e.g., geomorphic and sedimentary settings, single or multiple species, or based on short- or long-term physical-environmental changes.

REFERENCES

Adame, M.F., Cherian, S., Reef, R., Stewart-Koster, B., 2017. Mangrove root biomass and the uncertainty of belowground carbon estimations. For. Ecol. Manag. 403, 52–60. https://doi.org/10.1016/j.foreco.2017.08.016

Adame, M.F., Lovelock, C.E., 2011. Carbon and nutrient exchange of mangrove forests with the coastal ocean. Hydrobiologia 663, 23–50. https://doi.org/10.1007/s10750-010-0554-7

Adame, M.F., Neil, D., Wright, S.F., Lovelock, C.E., 2010. Sedimentation within and among mangrove forests along a gradient of geomorphological settings. Estuar. Coast. Shelf Sci. 86, 21–30. https://doi.org/10.1016/j.ecss.2009.10.013

Aldrian, E., Chen, C.-T.A., Adi, S., Prihartanto, Sudiana, N., Nugroho, S.P., 2008. Spatial and seasonal dynamics of riverine carbon fluxes of the Brantas catchment in East Java. J. Geophys. Res. 113, G03029. https://doi.org/10.1029/2007JG000626

Allen, J.A., Krauss, K.W., 2006. Influence of Propagule Flotation Longevity and Light Availability on Establishment of Introduced Mangrove Species in Hawai'i. Pac. Sci. 60, 367–376. https://doi.org/10.1353/psc.2006.0015

Almahasheer, H., Duarte, C.M., Irigoien, X., 2016. Phenology and Growth dynamics of Avicennia marina in the Central Red Sea. Sci. Rep. 6, 37785. https://doi.org/10.1038/srep37785

Alongi, D.M., 2022. Impacts of Climate Change on Blue Carbon Stocks and Fluxes in Mangrove Forests. Forests 13, 149. https://doi.org/10.3390/f13020149

Alongi, D.M., 2008. Mangrove forests: Resilience, protection from tsunamis, and responses to global climate change. Estuar. Coast. Shelf Sci. 76, 1–13. https://doi.org/10.1016/j.ecss.2007.08.024

Alongi, D.M., 2002. Present state and future of the world's mangrove forests. Environ. Conserv. 29, 331–349. https://doi.org/10.1017/S0376892902000231

Amani, M., Ghorbanian, A., Ahmadi, S.A., Kakooei, M., Moghimi, A., Mirmazloumi, S.M., Moghaddam, S.H.A., Mahdavi, S., Ghahremanloo, M., Parsian, S., Wu, Q., Brisco, B., 2020. Google Earth Engine Cloud Computing Platform for Remote Sensing Big Data Applications: A Comprehensive Review. IEEE J. Sel. Top. Appl. Earth Obs. Remote Sens. 13, 5326–5350. https://doi.org/10.1109/JSTARS.2020.3021052

Amani, M., Salehi, B., Mahdavi, S., Granger, J.E., Brisco, B., Hanson, A., 2017. Wetland Classification Using Multi-Source and Multi-Temporal Optical Remote Sensing Data in Newfoundland and Labrador, Canada. Can. J. Remote Sens. 43, 360–373. https://doi.org/10.1080/07038992.2017.1346468

Anchang, J.Y., Prihodko, L., Ji, W., Kumar, S.S., Ross, C.W., Yu, Q., Lind, B., Sarr, M.A., Diouf, A.A., Hanan, N.P., 2020. Toward Operational Mapping of Woody Canopy Cover in Tropical Savannas Using Google Earth Engine. Front. Environ. Sci. 8, 4. https://doi.org/10.3389/fenvs.2020.00004

Anwar, C., 2006. Prediksi Musim Buah Empat Jenis Mangrove Berdasar Hasil Fenologinya. J. Penelit. Hutan Dan Konserv. Alam 3, 237–247. https://doi.org/10.20886/jphka.2006.3.3.237-247

Anwar, C., Gunawan, H., 2006. Peranan Ekologis dan Sosial Ekonomis Hutan Mangrove dalam Mendukung Pembangunan Wilayah Pesisir, in: Prosiding Ekspose Hasil-Hasil Penelitian. Presented at the Konservasi dan Rehabilitasi Sumberdaya Hutan, Departemen Kehutanan Badan Penelitian dan Pengembangan Kehutanan Pusat Penelitian dan Pengembangan Hutan dan Konservasi Alam, Padang, p. 316.

Asian Development Bank, 2018. A Community-Based Mangrove Planting Handbook for Papua New Guinea. Asian Development Bank, Manila, Philippines. https://doi.org/10.22617/TIM189796-2

Aslan, A., Rahman, A.F., Warren, M.W., Robeson, S.M., 2016. Mapping spatial distribution and biomass of coastal wetland vegetation in Indonesian Papua by combining active and passive remotely sensed data. Remote Sens. Environ. 183, 65–81. https://doi.org/10.1016/j.rse.2016.04.026

Aye, W.N., Tong, X., Li, J., Tun, A.W., 2023. Assessing the Carbon Storage Potential of a Young Mangrove Plantation in Myanmar. Forests 14. https://doi.org/10.3390/f14040824

Ayrey, E., Fraver, S., Kershaw, J.A., Kenefic, L.S., Hayes, D., Weiskittel, A.R., Roth, B.E., 2017. Layer Stacking: A Novel Algorithm for Individual Forest Tree Segmentation from LiDAR Point Clouds. Can. J. Remote Sens. 43, 16–27. https://doi.org/10.1080/07038992.2017.1252907

Badan Meteorologi dan Geofisika, 2020. Prakiraan Musim Hujan 2020/2021 di Indonesia, 1st ed. Badan Meteorologi dan Geofisika Republik Indonesia, Jakarta.

Bai, J., Meng, Y., Gou, R., Lyu, J., Dai, Z., Diao, X., Zhang, H., Luo, Y., Zhu, X., Lin, G., 2021. Mangrove diversity enhances plant biomass production and carbon storage in Hainan island, China. Funct. Ecol. 35, 774–786. https://doi.org/10.1111/1365-2435.13753

Balke, T., Bouma, T., Horstman, E., Webb, E., Erftemeijer, P., Herman, P., 2011. Windows of opportunity: thresholds to mangrove seedling establishment on tidal flats. Mar. Ecol. Prog. Ser. 440, 1–9. https://doi.org/10.3354/meps09364

Balke, T., Friess, D.A., 2016. Geomorphic knowledge for mangrove restoration: a pan-tropical categorization: Geomorphic Knowledge for Mangrove Restoration. Earth Surf. Process. Landf. 41, 231–239. https://doi.org/10.1002/esp.3841

Balke, T., Herman, P.M.J., Bouma, T.J., 2014. Critical transitions in disturbance-driven ecosystems: identifying Windows of Opportunity for recovery. J. Ecol. 102, 700–708. https://doi.org/10.1111/1365-2745.12241

Balke, T., Swales, A., Lovelock, C.E., Herman, P.M.J., Bouma, T.J., 2015. Limits to seaward expansion of mangroves: Translating physical disturbance mechanisms into seedling survival gradients. J. Exp. Mar. Biol. Ecol. 467, 16–25. https://doi.org/10.1016/j.jembe.2015.02.015

Balke, T., Vovides, A., Schwarz, C., Chmura, G.L., Ladd, C., Basyuni, M., 2021. Monitoring tidal hydrology in coastal wetlands with the "Mini Buoy": applications for mangrove restoration. Hydrol. Earth Syst. Sci. 25, 1229–1244. https://doi.org/10.5194/hess-25-1229-2021

Balke, T., Webb, E.L., van den Elzen, E., Galli, D., Herman, P.M.J., Bouma, T.J., 2013. Seedling establishment in a dynamic sedimentary environment: a conceptual framework using mangroves. J. Appl. Ecol. 50, 740–747. https://doi.org/10.1111/1365-2664.12067

Ball, M., Sobrado, M., 1999. Ecophysiology of mangroves: challenges in linking physiological processes with patterns in forest structure. Physiol. Plant Ecol. Br. Ecol. Soc. Blackwell Sci. Lond. 331–346.

Ball, M.C., 2002. Interactive effects of salinity and irradiance on growth: implications for mangrove forest structure along salinity gradients. Trees 16, 126–139. https://doi.org/10.1007/s00468-002-0169-3

Baptist, M.J., Babovic, V., Rodríguez Uthurburu, J., Keijzer, M., Uittenbogaard, R.E., Mynett, A., Verwey, A., 2007. On inducing equations for vegetation resistance. J. Hydraul. Res. 45, 435–450. https://doi.org/10.1080/00221686.2007.9521778

Barbier, E.B., Hacker, S.D., Kennedy, C., Koch, E.W., Stier, A.C., Silliman, B.R., 2011. The value of estuarine and coastal ecosystem services. Ecol. Monogr. 81, 169–193. https://doi.org/10.1890/10-1510.1

Barbier, E.B., Koch, E.W., Silliman, B.R., Hacker, S.D., Wolanski, E., Primavera, J., Granek, E.F., Polasky, S., Aswani, S., Cramer, L.A., Stoms, D.M., Kennedy, C.J., Bael, D., Kappel, C.V., Perillo, G.M.E., Reed, D.J., 2008. Coastal Ecosystem-Based Management with Nonlinear Ecological Functions and Values. Science 319, 321–323. https://doi.org/10.1126/science.1150349

Bathmann, J., Peters, R., Naumov, D., Fischer, T., Berger, U., Walther, M., 2020. The MANgrove–GroundwAter feedback model (MANGA) – Describing belowground competition based on first principles. Ecol. Model. 420, 108973. https://doi.org/10.1016/j.ecolmodel.2020.108973

Beeston, M., Cameron, C., Hagger, V., Howard, J., Lovelock, C., Sippo, J., Tonneijk, F., van Bijsterveldt, C., van Eijk, P. (Eds.), 2023. Best practice guidelines for mangrove restoration. Global Mangrove Alliance.

Belgiu, M., Drăguţ, L., 2016. Random forest in remote sensing: A review of applications and future directions. ISPRS J. Photogramm. Remote Sens. 114, 24–31. https://doi.org/10.1016/j.isprsjprs.2016.01.011

Berger, U., Hildenbrandt, H., 2000. A new approach to spatially explicit modelling of forest dynamics: spacing, ageing and neighbourhood competition of mangrove trees. Ecol. Model. 132, 287–302. https://doi.org/10.1016/S0304-3800(00)00298-2

Berger, U., Rivera-Monroy, V.H., Doyle, T.W., Dahdouh-Guebas, F., Duke, N.C., Fontalvo-Herazo, M.L., Hildenbrandt, H., Koedam, N., Mehlig, U., Piou, C., Twilley, R.R., 2008. Advances and limitations of individual-based models to

analyze and predict dynamics of mangrove forests: A review. Aquat. Bot. 89, 260–274. https://doi.org/10.1016/j.aquabot.2007.12.015

Beselly, S.M., Grueters, U., van Der Wegen, M., Reyns, J., Dijkstra, J., Roelvink, D., 2023. Modelling mangrove-mudflat dynamics with a coupled individual-based-hydro-morphodynamic model. Environ. Model. Softw. 105814. https://doi.org/10.1016/j.envsoft.2023.105814

Beselly, S.M., van der Wegen, M., Grueters, U., Reyns, J., Dijkstra, J., Roelvink, D., 2021. Eleven Years of Mangrove–Mudflat Dynamics on the Mud Volcano-Induced Prograding Delta in East Java, Indonesia: Integrating UAV and Satellite Imagery. Remote Sens. 13, 1084. https://doi.org/10.3390/rs13061084

Best, ü. S.N., Van der Wegen, M., Dijkstra, J., Willemsen, P.W.J.M., Borsje, B.W., Roelvink, D.J.A., 2018. Do salt marshes survive sea level rise? Modelling wave action, morphodynamics and vegetation dynamics. Environ. Model. Softw. 109, 152–166. https://doi.org/10.1016/j.envsoft.2018.08.004

Best, Ü.S.N., van der Wegen, M., Dijkstra, J., Reyns, J., van Prooijen, B.C., Roelvink, D., 2022. Wave attenuation potential, sediment properties and mangrove growth dynamics data over Guyana's intertidal mudflats: assessing the potential of mangrove restoration works. Earth Syst. Sci. Data 14, 2445–2462. https://doi.org/10.5194/essd-14-2445-2022

Bispo, P.D.C., Pardini, M., Papathanassiou, K.P., Kugler, F., Balzter, H., Rains, D., dos Santos, J.R., Rizaev, I.G., Tansey, K., dos Santos, M.N., Spinelli Araujo, L., 2019. Mapping forest successional stages in the Brazilian Amazon using forest heights derived from TanDEM-X SAR interferometry. Remote Sens. Environ. 232, 111194. https://doi.org/10.1016/j.rse.2019.05.013

Board, O.S., National Academies of Sciences, E., and Medicine, 2019. Negative emissions technologies and reliable sequestration: a research agenda.

Boechat Albernaz, M., Brückner, M.Z.M., Van Maanen, B., Van Der Spek, A.J.F., Kleinhans, M.G., 2023. Vegetation Reconfigures Barrier Coasts and Affects Tidal Basin Infilling Under Sea Level Rise. J. Geophys. Res. Earth Surf. 128, e2022JF006703. https://doi.org/10.1029/2022JF006703

Booker, J., Keogh, B., Chu, D., Conner, J., Hooper, I., 1998. Reproduction Strategies of Mangroves [WWW Document]. Reprod. Strateg. Mangroves. URL https://www.nhmi.org/mangroves/rep.htm (accessed 3.2.22).

Borsje, B.W., van Wesenbeeck, B.K., Dekker, F., Paalvast, P., Bouma, T.J., van Katwijk, M.M., de Vries, M.B., 2011. How ecological engineering can serve in coastal protection. Ecol. Eng. 37, 113–122. https://doi.org/10.1016/j.ecoleng.2010.11.027

Breiman, L., 2001. Random Forests. Mach. Learn. 45, 5–32. https://doi.org/10.1023/A:1010933404324

Bridges, T., Bourne, E.M., King, J., Kuzmitski, H., Moynihan, E., Suedel, B., 2018. Engineering With Nature : An Atlas. Environmental Laboratory (U.S.). https://doi.org/10.21079/11681/27929

Bridges, T., King, J., Simm, J., Beck, M., Collins, G., Lodder, Q., Mohan, R., 2021. International Guidelines on Natural and Nature-Based Features for Flood Risk Management. Engineer Research and Development Center (U.S.). https://doi.org/10.21079/11681/41946

Brückner, M.Z.M., Braat, L., Schwarz, C., Kleinhans, M.G., 2020. What Came First, Mud or Biostabilizers? Elucidating Interacting Effects in a Coupled Model of Mud, Saltmarsh, Microphytobenthos, and Estuarine Morphology. Water Resour. Res. 56. https://doi.org/10.1029/2019WR026945

Brückner, M.Z.M., Schwarz, C., Dijk, W.M., Oorschot, M., Douma, H., Kleinhans, M.G., 2019. Salt Marsh Establishment and Eco-Engineering Effects in Dynamic Estuaries Determined by Species Growth and Mortality. J. Geophys. Res. Earth Surf. 124, 2962–2986. https://doi.org/10.1029/2019JF005092

Bryan, K.R., Nardin, W., Mullarney, J.C., Fagherazzi, S., 2017. The role of cross-shore tidal dynamics in controlling intertidal sediment exchange in mangroves in Cù Lao Dung, Vietnam. Cont. Shelf Res. 147, 128–143. https://doi.org/10.1016/j.csr.2017.06.014

Buffington, K.J., MacKenzie, R.A., Carr, J.A., Apwong, M., Krauss, K.W., Thorne, K.M., 2021. Mangrove species' response to sea-level rise across Pohnpei, Federated States of Micronesia (Report No. 2021–1002), Open-File Report. Reston, VA. https://doi.org/10.3133/ofr20211002

Bunting, P., Rosenqvist, A., Hilarides, L., Lucas, R.M., Thomas, N., 2022. Global Mangrove Watch: Updated 2010 Mangrove Forest Extent (v2.5). Remote Sens. 14, 1034. https://doi.org/10.3390/rs14041034

Bunting, P., Rosenqvist, A., Lucas, R., Rebelo, L.-M., Hilarides, L., Thomas, N., Hardy, A., Itoh, T., Shimada, M., Finlayson, C., 2018. The Global Mangrove Watch—A New 2010 Global Baseline of Mangrove Extent. Remote Sens. 10, 1669. https://doi.org/10.3390/rs10101669

Cahoon, D.R., Hensel, P., Rybczyk, J., McKee, K.L., Proffitt, C.E., Perez, B.C., 2003. Mass tree mortality leads to mangrove peat collapse at Bay Islands, Honduras after Hurricane Mitch. J. Ecol. 91, 1093–1105. https://doi.org/10.1046/j.1365-2745.2003.00841.x

Cahoon, D.R., McKee, K.L., Morris, J.T., 2021. How Plants Influence Resilience of Salt Marsh and Mangrove Wetlands to Sea-Level Rise. Estuaries Coasts 44, 883–898. https://doi.org/10.1007/s12237-020-00834-w

Cappuccino, N., 1995. Chapter 1 - Novel Approaches to the Study of Population Dynamics, in: Cappuccino, N., Price, P.W. (Eds.), Population Dynamics. Academic Press, San Diego, pp. 3–16. https://doi.org/10.1016/B978-012159270-7/50002-6

Carrasco, L., O'Neil, A., Morton, R., Rowland, C., 2019. Evaluating Combinations of Temporally Aggregated Sentinel-1, Sentinel-2 and Landsat 8 for Land Cover Mapping with Google Earth Engine. Remote Sens. 11, 288. https://doi.org/10.3390/rs11030288

Carugati, L., Gatto, B., Rastelli, E., Lo Martire, M., Coral, C., Greco, S., Danovaro, R., 2018. Impact of mangrove forests degradation on biodiversity and ecosystem functioning. Sci. Rep. 8, 13298. https://doi.org/10.1038/s41598-018-31683-0

Casella, E., Drechsel, J., Winter, C., Benninghoff, M., Rovere, A., 2020. Accuracy of sand beach topography surveying by drones and photogrammetry. Geo-Mar. Lett. 40, 255–268. https://doi.org/10.1007/s00367-020-00638-8

Chamberlain, D.A., Phinn, S.R., Possingham, H.P., 2021. Mangrove Forest Cover and Phenology with Landsat Dense Time Series in Central Queensland, Australia. Remote Sens. 13, 3032. https://doi.org/10.3390/rs13153032

Chen, B., Xiao, X., Li, X., Pan, L., Doughty, R., Ma, J., Dong, J., Qin, Y., Zhao, B., Wu, Z., Sun, R., Lan, G., Xie, G., Clinton, N., Giri, C., 2017. A mangrove forest map of China in 2015: Analysis of time series Landsat 7/8 and Sentinel-1A imagery in Google Earth Engine cloud computing platform. ISPRS J. Photogramm. Remote Sens. 131, 104–120. https://doi.org/10.1016/j.isprsjprs.2017.07.011

Chen, G., Zhang, M., Yao, X., Zhu, Y., Hu, Y., Hui, D., Li, J., Chen, J., Deng, Q., 2023. Soil Organic Carbon Sequestration after 20-Year Afforestation of Mangrove Plantations on Qi'ao Island, Southern China. Agronomy 13, 2389. https://doi.org/10.3390/agronomy13092389

Chen, R., Twilley, R.R., 1998. A gap dynamic model of mangrove forest development along gradients of soil salinity and nutrient resources. J. Ecol. 86, 37–51. https://doi.org/10.1046/j.1365-2745.1998.00233.x

Chen, Y., Li, Yan, Cai, T., Thompson, C., Li, Yi, 2016. A comparison of biohydrodynamic interaction within mangrove and saltmarsh boundaries: Bio-Hydrodynamics within Mangrove and Saltmarsh Boundaries. Earth Surf. Process. Landf. 41, 1967–1979. https://doi.org/10.1002/esp.3964

Cheong, S.-M., Silliman, B., Wong, P.P., van Wesenbeeck, B., Kim, C.-K., Guannel, G., 2013. Coastal adaptation with ecological engineering. Nat. Clim. Change 3, 787–791. https://doi.org/10.1038/nclimate1854

Christensen, B., 1978. Biomass and primary production of Rhizophora apiculata Bl. in a mangrove in southern Thailand. Aquat. Bot. 4, 43–52. https://doi.org/10.1016/0304-3770(78)90005-0

Christensen, B., Wium-Andersen, S., 1977. Seasonal growth of mangrove trees in Southern Thailand. I. The phenology of Rhizophora apiculata Bl. Aquat. Bot. 3, 281–286. https://doi.org/10.1016/0304-3770(77)90030-4

Clarke, P.J., 1993. Dispersal of grey mangrove (Avicennia marina) propagules in southeastern Australia. Aquat. Bot. 45, 195–204. https://doi.org/10.1016/0304-3770(93)90021-N

Clarke, P.J., Kerrigan, R.A., Westphal, C.J., 2001. Dispersal potential and early growth in 14 tropical mangroves: do early life history traits correlate with patterns of adult distribution?: *EARLY LIFE HISTORY OF TROPICAL MANGROVES*. J. Ecol. 89, 648–659. https://doi.org/10.1046/j.0022-0477.2001.00584.x

Cleveland, R.B., Cleveland, W.S., Terpenning, I., 1990. STL: A Seasonal-Trend Decomposition Procedure Based on Loess. J. Off. Stat. 6, 3.

Coastal engineering manual: the Official United States Army Corps of engineers manual, 2002. , Coastal hydraulics laboratory publicaction.

Cochran, W.G., 1977. Sampling techniques, 3d ed. ed, Wiley series in probability and mathematical statistics. Wiley, New York.

Comley, B.W.T., McGuinness, K.A., 2005. Above- and below-ground biomass, and allometry, of four common northern Australian mangroves. Aust. J. Bot. 53, 431. https://doi.org/10.1071/BT04162

Congalton, R.G., Green, K., 2008. Assessing the Accuracy of Remotely Sensed Data Principles and Practices, Second Edition, 2nd edition. ed. CRC Press, Boca Raton.

Conlin, M., Cohn, N., Ruggiero, P., 2018. A Quantitative Comparison of Low-Cost Structure from Motion (SfM) Data Collection Platforms on Beaches and Dunes. J. Coast. Res. 34, 1341. https://doi.org/10.2112/JCOASTRES-D-17-00160.1

Cooley, S.R., Schoeman, D.S., Bopp, L., Boyd, P., Donner, S., Ito, S.-I., Wolfgang, K., Martinetto, P., Ojea, E., Racault, M.-F., Rost, B., Skern-Mauritzen, M. (Eds.), 2022. Oceans and Coastal Ecosystems and Their Services, in: Climate Change 2022: Impacts, Adaptation and Vulnerability. Contribution of Working Group II to the Sixth Assessment Report of the Intergovernmental Panel on Climate Change. Cambridge University Press, Cambridge, United Kingdom ; New York, NY, pp. 379–550. https://doi.org/10.1017/9781009325844.005

Cortés, I.M., 2019. Exploring the Role of Evaporation and Precipitation Rates on Mangrove Island Morphology. Montclair State University, New Jersey, USA.

Cox, G.M., Gibbons, J.M., Wood, A.T.A., Craigon, J., Ramsden, S.J., Crout, N.M.J., 2006. Towards the systematic simplification of mechanistic models. Ecol. Model. 198, 240–246. https://doi.org/10.1016/j.ecolmodel.2006.04.016

Cuddington, K., Fortin, M.-J., Gerber, L.R., Hastings, A., Liebhold, A., O'Connor, M., Ray, C., 2013. Process-based models are required to manage ecological systems in a changing world. Ecosphere 4, art20. https://doi.org/10.1890/ES12-00178.1

Curnick, D.J., Pettorelli, N., Amir, A.A., Balke, T., Barbier, E.B., Crooks, S., Dahdouh-Guebas, F., Duncan, C., Endsor, C., Friess, D.A., Quarto, A., Zimmer, M., Lee, S.Y., 2019. The value of small mangrove patches. Science 363, 239–239. https://doi.org/10.1126/science.aaw0809

Dahdouh-Guebas, F., Ajonina, G.N., Amir, A.A., Andradi-Brown, D.A., Aziz, I., Balke, T., Barbier, E.B., Cannicci, S., Cragg, S.M., Cunha-Lignon, M., Curnick, D.J., Duarte, C.M., Duke, N.C., Endsor, C., Fratini, S., Feller, I.C., Fromard, F., Hugé, J., Huxham, M., Kairo, J.G., Kajita, T., Kathiresan, K., Koedam, N., Lee, S.Y., Lin, H.-J., Mackenzie, J.R., Mangora, M.M., Marchand, C., Meziane, T., Minchinton, T.E., Pettorelli, N., Polanía, J., Polgar, G., Poti, M., Primavera, J., Quarto, A., Rog, S.M., Satyanarayana, B., Schaeffer-Novelli, Y., Spalding, M., Van Der Stocken, T., Wodehouse, D., Yong, J.W.H., Zimmer, M., Friess, D.A.,

2020. Public Perceptions of Mangrove Forests Matter for Their Conservation. Front. Mar. Sci. 7, 603651. https://doi.org/10.3389/fmars.2020.603651

Dahdouh-Guebas, F., Friess, D.A., Lovelock, C.E., Connolly, R.M., Feller, I.C., Rogers, K., Cannicci, S., 2022. Cross-cutting research themes for future mangrove forest research. Nat. Plants 8, 1131–1135. https://doi.org/10.1038/s41477-022-01245-4

Dahdouh-Guebas, F., Hugé, J., Abuchahla, G.M.O., Cannicci, S., Jayatissa, L.P., Kairo, J.G., Kodikara Arachchilage, S., Koedam, N., Mafaziya Nijamdeen, T.W.G.F., Mukherjee, N., Poti, M., Prabakaran, N., Ratsimbazafy, H.A., Satyanarayana, B., Thavanayagam, M., Vande Velde, K., Wodehouse, D., 2021. Reconciling nature, people and policy in the mangrove social-ecological system through the adaptive cycle heuristic. Estuar. Coast. Shelf Sci., Mangroves and People: Impacts and Interactions 248, 106942. https://doi.org/10.1016/j.ecss.2020.106942

Dahdouh-Guebas, F., Jayatissa, L.P., Di Nitto, D., Bosire, J.O., Lo Seen, D., Koedam, N., 2005. How effective were mangroves as a defence against the recent tsunami? Curr. Biol. 15, R443–R447. https://doi.org/10.1016/j.cub.2005.06.008

Dalrymple, R.A., Kirby, J.T., Hwang, P.A., 1984. Wave Diffraction Due to Areas of Energy Dissipation. J. Waterw. Port Coast. Ocean Eng. 110, 67–79. https://doi.org/10.1061/(ASCE)0733-950X(1984)110:1(67)

Damastuti, E., De Groot, R., Debrot, A.O., Silvius, M.J., 2022. Effectiveness of community-based mangrove management for biodiversity conservation: A case study from Central Java, Indonesia. Trees For. People 7, 100202. https://doi.org/10.1016/j.tfp.2022.100202

Das, S., Vincent, J.R., 2009. Mangroves protected villages and reduced death toll during Indian super cyclone. Proc. Natl. Acad. Sci. 106, 7357–7360. https://doi.org/10.1073/pnas.0810440106

Das, S.C., Das, S., Tah, J., 2022. Mangrove Ecosystems and Their Services, in: Das, S.C., Pullaiah, Ashton, E.C. (Eds.), Mangroves: Biodiversity, Livelihoods and Conservation. Springer Nature Singapore, Singapore, pp. 139–152. https://doi.org/10.1007/978-981-19-0519-3_6

Davis, S.M., Childers, D.L., Lorenz, J.J., Wanless, H.R., Hopkins, T.E., 2005. A conceptual model of ecological interactions in the mangrove estuaries of the Florida Everglades. Wetlands 25, 832–842. https://doi.org/10.1672/0277-5212(2005)025[0832:ACMOEI]2.0.CO;2

Day, J.W., Christian, R.R., Boesch, D.M., Yáñez-Arancibia, A., Morris, J., Twilley, R.R., Naylor, L., Schaffner, L., Stevenson, C., 2008. Consequences of Climate Change on the Ecogeomorphology of Coastal Wetlands. Estuaries Coasts 31, 477–491. https://doi.org/10.1007/s12237-008-9047-6

De Dominicis, M., Wolf, J., van Hespen, R., Zheng, P., Hu, Z., 2023. Mangrove forests can be an effective coastal defence in the Pearl River Delta, China. Commun. Earth Environ. 4, 13. https://doi.org/10.1038/s43247-022-00672-7

DeAngelis, D.L., Grimm, V., 2014. Individual-based models in ecology after four decades. F1000Prime Rep. 6. https://doi.org/10.12703/P6-39

Deltares, 2021. Delft3D Flexible Mesh Suite: D-Flow Flexible Mesh, 0.9.1. ed. Deltares, Delft.

Di Nitto, D., Erftemeijer, P.L.A., van Beek, J.K.L., Dahdouh-Guebas, F., Higazi, L., Quisthoudt, K., Jayatissa, L.P., Koedam, N., 2013. Modelling drivers of mangrove propagule dispersal and restoration of abandoned shrimp farms. Biogeosciences 10, 5095–5113. https://doi.org/10.5194/bg-10-5095-2013

Ding, L., Fu, S., 2021. Effects of different types of undecomposed surface litter on the sediment transport capacity. Geoderma 385, 114842. https://doi.org/10.1016/j.geoderma.2020.114842

DJI Mavic Pro & Mavic Pro Platinum – Every Creative Moment – DJI [WWW Document], n.d. . DJI Off. URL https://www.dji.com/nl/mavic (accessed 11.16.20).

Donato, D.C., Kauffman, J.B., Murdiyarso, D., Kurnianto, S., Stidham, M., Kanninen, M., 2011. Mangroves among the most carbon-rich forests in the tropics. Nat. Geosci. 4, 293–297. https://doi.org/10.1038/ngeo1123

Donchyts, G., Baart, F., Winsemius, H., Gorelick, N., Kwadijk, J., van de Giesen, N., 2016. Earth's surface water change over the past 30 years. Nat. Clim. Change 6, 810–813. https://doi.org/10.1038/nclimate3111

Doyle, T.W., Smith III, T.J., Robblee, M.B., 1995. Wind damage effects of Hurricane Andrew on mangrove communities along the southwest coast of Florida, USA. J. Coast. Res. 159–168.

Drexler, J.Z., 2001. Maximum Longevities of Rhizophora apiculata and R. mucronata Propagules. Pac. Sci. 55, 17–22. https://doi.org/10.1353/psc.2001.0004

DroneDeploy Documentation [WWW Document], n.d. . DroneDeploy Doc. URL https://support.dronedeploy.com/docs (accessed 2.18.21).

Du, P., Samat, A., Waske, B., Liu, S., Li, Z., 2015. Random Forest and Rotation Forest for fully polarized SAR image classification using polarimetric and spatial features. ISPRS J. Photogramm. Remote Sens. 105, 38–53. https://doi.org/10.1016/j.isprsjprs.2015.03.002

Du, Q., Qin, Z., Ming, S., Zhang, C., 2021. Differences in the vertical accretion of sediment among mangrove species with different aerial root types. Estuar. Coast. Shelf Sci. 256, 107375. https://doi.org/10.1016/j.ecss.2021.107375

Du, S., Zhang, Y., Qin, R., Yang, Z., Zou, Z., Tang, Y., Fan, C., 2016. Building Change Detection Using Old Aerial Images and New LiDAR Data. Remote Sens. 8, 1030. https://doi.org/10.3390/rs8121030

Duarte, C.M., Losada, I.J., Hendriks, I.E., Mazarrasa, I., Marbà, N., 2013. The role of coastal plant communities for climate change mitigation and adaptation. Nat. Clim. Change 3, 961–968. https://doi.org/10.1038/nclimate1970

Duke, N., Bunt, J., Williams, W., 1984. Observations on the Floral and Vegetative Phenologies of North-Eastern Australian Mangroves. Aust. J. Bot. 32, 87–99.

Duke, N.C., 1990. Phenological Trends with Latitude in the Mangrove Tree Avicennia Marina. J. Ecol. 78, 113–133. https://doi.org/10.2307/2261040

Duke, N.C., Ball, M.C., Ellison, J.C., 1998. Factors influencing biodiversity and distributional gradients in mangroves. Glob. Ecol. Biogeogr. Lett. 7, 27–47.

Duke, N.C., Meynecke, J.-O., Dittmann, S., Ellison, A.M., Anger, K., Berger, U., Cannicci, S., Diele, K., Ewel, K.C., Field, C.D., Koedam, N., Lee, S.Y., Marchand, C., Nordhaus, I., Dahdouh-Guebas, F., 2007. A World Without Mangroves? Science 317, 41–42. https://doi.org/10.1126/science.317.5834.41b

Ellison, A.M., Felson, A.J., Friess, D.A., 2020. Mangrove Rehabilitation and Restoration as Experimental Adaptive Management. Front. Mar. Sci. 7, 327. https://doi.org/10.3389/fmars.2020.00327

Ellison, J.C., Buffington, K.J., Thorne, K.M., Gesch, D., Irwin, J., Danielson, J., 2022. Elevations of mangrove forests of Pohnpei, Micronesia. Estuar. Coast. Shelf Sci. 268, 107780. https://doi.org/10.1016/j.ecss.2022.107780

European Space Agency, 2015. SENTINEL-2 User Handbook, Issue 1 Rev 2. ed, ESA Standard Document. European Space Agency, Paris.

European Space Agency, 2012. Sentinel-1: ESA's Radar Observatory Mission for GMES Operational Services. ESA Communications, Noordwijk, the Netherlands.

Fairchild, T.P., Bennett, W.G., Smith, G., Day, B., Skov, M.W., Möller, I., Beaumont, N., Karunarathna, H., Griffin, J.N., 2021. Coastal wetlands mitigate storm flooding and associated costs in estuaries. Environ. Res. Lett. 16, 074034. https://doi.org/10.1088/1748-9326/ac0c45

Fanous, M., Daneshkhah, A., Eden, J.M., Remesan, R., Palade, V., 2023. Hydro-morphodynamic modelling of mangroves imposed by tidal waves using finite element discontinuous Galerkin method. Coast. Eng. 182, 104303. https://doi.org/10.1016/j.coastaleng.2023.104303

Fassnacht, F.E., Schiller, C., Kattenborn, T., Zhao, X., Qu, J., 2019. A Landsat-based vegetation trend product of the Tibetan Plateau for the time-period 1990–2018. Sci. Data 6, 78. https://doi.org/10.1038/s41597-019-0075-9

Federal Geographic Data Committee, 1998. National Standard for Spatial Data Accuracy, Geospatial Positioning Accuracy Standards. Federal Geographic Data Committee, Virginia.

Feldpausch, T.R., Lloyd, J., Lewis, S.L., Brienen, R.J.W., Gloor, M., Monteagudo Mendoza, A., Lopez-Gonzalez, G., Banin, L., Abu Salim, K., Affum-Baffoe, K., Alexiades, M., Almeida, S., Amaral, I., Andrade, A., Aragão, L.E.O.C., Araujo Murakami, A., Arets, E.J.M.M., Arroyo, L., Aymard C., G.A., Baker, T.R., Bánki, O.S., Berry, N.J., Cardozo, N., Chave, J., Comiskey, J.A., Alvarez, E., de Oliveira, A., Di Fiore, A., Djagbletey, G., Domingues, T.F., Erwin, T.L., Fearnside, P.M., França, M.B., Freitas, M.A., Higuchi, N., E. Honorio C., Iida, Y., Jiménez, E., Kassim, A.R., Killeen, T.J., Laurance, W.F., Lovett, J.C., Malhi, Y., Marimon, B.S., Marimon-Junior, B.H., Lenza, E., Marshall, A.R., Mendoza, C., Metcalfe, D.J., Mitchard, E.T.A., Neill, D.A., Nelson, B.W., Nilus, R., Nogueira, E.M.,

Parada, A., Peh, K.S.-H., Pena Cruz, A., Peñuela, M.C., Pitman, N.C.A., Prieto, A., Quesada, C.A., Ramírez, F., Ramírez-Angulo, H., Reitsma, J.M., Rudas, A., Saiz, G., Salomão, R.P., Schwarz, M., Silva, N., Silva-Espejo, J.E., Silveira, M., Sonké, B., Stropp, J., Taedoumg, H.E., Tan, S., ter Steege, H., Terborgh, J., Torello-Raventos, M., van der Heijden, G.M.F., Vásquez, R., Vilanova, E., Vos, V.A., White, L., Willcock, S., Woell, H., Phillips, O.L., 2012. Tree height integrated into pantropical forest biomass estimates. Biogeosciences 9, 3381–3403. https://doi.org/10.5194/bg-9-3381-2012

Friedrichs, C.T., 2011. Tidal flat morphodynamics: A synthesis.

Friedrichs, C.T., Aubrey, D.G., 1996. Uniform bottom shear stress and equilibrium hyposometry of intertidal flats, in: Pattiaratchi, C. (Ed.), Coastal and Estuarine Studies. American Geophysical Union, Washington, D. C., pp. 405–429. https://doi.org/10.1029/CE050p0405

Friess, D.A., Krauss, K.W., Horstman, E.M., Balke, T., Bouma, T.J., Galli, D., Webb, E.L., 2012. Are all intertidal wetlands naturally created equal? Bottlenecks, thresholds and knowledge gaps to mangrove and saltmarsh ecosystems. Biol. Rev. 87, 346–366. https://doi.org/10.1111/j.1469-185X.2011.00198.x

Friess, D.A., Yando, E.S., Abuchahla, G.M.O., Adams, J.B., Cannicci, S., Canty, S.W.J., Cavanaugh, K.C., Connolly, R.M., Cormier, N., Dahdouh-Guebas, F., Diele, K., Feller, I.C., Fratini, S., Jennerjahn, T.C., Lee, S.Y., Ogurcak, D.E., Ouyang, X., Rogers, K., Rowntree, J.K., Sharma, S., Sloey, T.M., Wee, A.K.S., 2020. Mangroves give cause for conservation optimism, for now. Curr. Biol. 30, R153–R154. https://doi.org/10.1016/j.cub.2019.12.054

Fu, X.-M., Tang, H.-Y., Liu, Y., Zhang, M.-Q., Jiang, S.-S., Yang, F., Li, X.-Y., Wang, C.-Y., 2021. Resource status and protection strategies of mangroves in China. J. Coast. Conserv. 25, 42. https://doi.org/10.1007/s11852-021-00800-z

Furukawa, K., Wolanski, E., 1996. Sedimentation in Mangrove Forests. Mangroves Salt Marshes 1, 3–10. https://doi.org/10.1023/A:1025973426404

Furusawa, T., Fuchigami, Y., Kobayashi, S., Yokota, M., 2013. Evaluation of Mangrove Biomass Changes due to Different Human Activities in Batam Island, Indonesia, Determined Using MODIS EVI and ASTER Data. People Cult. Ocean. 29, 35–50.

Gardiner, B., Byrne, K., Hale, S., Kamimura, K., Mitchell, S.J., Peltola, H., Ruel, J.-C., 2008. A review of mechanistic modelling of wind damage risk to forests. Forestry 81, 447–463. https://doi.org/10.1093/forestry/cpn022

Ghorbanian, A., Kakooei, M., Amani, M., Mahdavi, S., Mohammadzadeh, A., Hasanlou, M., 2020. Improved land cover map of Iran using Sentinel imagery within Google Earth Engine and a novel automatic workflow for land cover classification using migrated training samples. ISPRS J. Photogramm. Remote Sens. 167, 276–288. https://doi.org/10.1016/j.isprsjprs.2020.07.013

Gijsman, R., Horstman, E.M., Swales, A., MacDonald, I.T., Bouma, T.J., Van Der Wal, D., Wijnberg, K.M., 2023. Mangrove forest drag and bed stabilisation effects on

intertidal flat morphology. Earth Surf. Process. Landf. esp.5758. https://doi.org/10.1002/esp.5758

Gijsman, R., Horstman, E.M., van der Wal, D., Friess, D.A., Swales, A., Wijnberg, K.M., 2021. Nature-Based Engineering: A Review on Reducing Coastal Flood Risk With Mangroves. Front. Mar. Sci. 8, 702412. https://doi.org/10.3389/fmars.2021.702412

Gillis, L., Bouma, T., Jones, C., van Katwijk, M., Nagelkerken, I., Jeuken, C., Herman, P., Ziegler, A., 2014. Potential for landscape-scale positive interactions among tropical marine ecosystems. Mar. Ecol. Prog. Ser. 503, 289–303. https://doi.org/10.3354/meps10716

Gilman, E., Ellison, J., Coleman, R., 2007. Assessment of mangrove response to projected relative sea-level rise and recent historical reconstruction of shoreline position. Environ. Monit. Assess. 124, 105–130.

Giri, C., Ochieng, E., Tieszen, L.L., Zhu, Z., Singh, A., Loveland, T., Masek, J., Duke, N., 2011. Status and distribution of mangrove forests of the world using earth observation satellite data: Status and distributions of global mangroves. Glob. Ecol. Biogeogr. 20, 154–159. https://doi.org/10.1111/j.1466-8238.2010.00584.x

Global Mangrove Alliance (Ed.), 2021. Global Mangrove Alliance Roadmap 2021.

Glover, H.E., Stokes, D.J., Ogston, A.S., Bryan, K.R., Pilditch, C.A., 2022. Decadal-scale impacts of changing mangrove extent on hydrodynamics and sediment transport in a quiescent, mesotidal estuary. Earth Surf. Process. Landf. n/a. https://doi.org/10.1002/esp.5317

Goldberg, L., Lagomasino, D., Thomas, N., Fatoyinbo, T., 2020. Global declines in human-driven mangrove loss. Glob. Change Biol. 26, 5844–5855. https://doi.org/10.1111/gcb.15275

Gorelick, N., Hancher, M., Dixon, M., Ilyushchenko, S., Thau, D., Moore, R., 2017. Google Earth Engine: Planetary-scale geospatial analysis for everyone. Remote Sens. Environ. 202, 18–27. https://doi.org/10.1016/j.rse.2017.06.031

Grueters, U., Ibrahim, M.R., Satyanarayana, B., Dahdouh-Guebas, F., 2019. Individual-based modeling of mangrove forest growth: MesoFON – Recent calibration and future direction. Estuar. Coast. Shelf Sci. 106302. https://doi.org/10.1016/j.ecss.2019.106302

Grueters, U., Seltmann, T., Schmidt, H., Horn, H., Pranchai, A., Vovides, A.G., Peters, R., Vogt, J., Dahdouh-Guebas, F., Berger, U., 2014. The mangrove forest dynamics model mesoFON. Ecol. Model. 291, 28–41. https://doi.org/10.1016/j.ecolmodel.2014.07.014

Guan, H., Li, J., Chapman, M., Deng, F., Ji, Z., Yang, X., 2013. Integration of orthoimagery and lidar data for object-based urban thematic mapping using random forests. Int. J. Remote Sens. 34, 5166–5186. https://doi.org/10.1080/01431161.2013.788261

Guo, P., Sun, Y., Su, H., Wang, M., Zhang, Y., 2018. Spatial and temporal trends in total organic carbon (TOC), black carbon (BC), and total nitrogen (TN) and their

relationships under different planting patterns in a restored coastal mangrove wetland: case study in Fujian, China. Chem. Speciat. Bioavailab. 30, 47–56. https://doi.org/10.1080/09542299.2018.1484673

Hagger, V., Worthington, T.A., Lovelock, C.E., Adame, M.F., Amano, T., Brown, B.M., Friess, D.A., Landis, E., Mumby, P.J., Morrison, T.H., O'Brien, K.R., Wilson, K.A., Zganjar, C., Saunders, M.I., 2022. Drivers of global mangrove loss and gain in social-ecological systems. Nat. Commun. 13, 6373. https://doi.org/10.1038/s41467-022-33962-x

Hamilton, S.E., Casey, D., 2016. Creation of a high spatio-temporal resolution global database of continuous mangrove forest cover for the 21st century (CGMFC-21): CGMFC-21. Glob. Ecol. Biogeogr. 25, 729–738. https://doi.org/10.1111/geb.12449

Hamzah, F., Widakti, N., Sidik, F., 2015. The Growth of Mangroves in Created Wetland in the Porong River, East Java, Indonesia. J. Trop. Crop Sci. 2.

Hansen, M.C., Potapov, P.V., Moore, R., Hancher, M., Turubanova, S.A., Tyukavina, A., Thau, D., Stehman, S.V., Goetz, S.J., Loveland, T.R., Kommareddy, A., Egorov, A., Chini, L., Justice, C.O., Townshend, J.R.G., 2013. High-Resolution Global Maps of 21st-Century Forest Cover Change. Science 342, 850. https://doi.org/10.1126/science.1244693

Hatje, V., Copertino, M., Patire, V.F., Ovando, X., Ogbuka, J., Johnson, B.J., Kennedy, H., Masque, P., Creed, J.C., 2023. Vegetated coastal ecosystems in the Southwestern Atlantic Ocean are an unexploited opportunity for climate change mitigation. Commun. Earth Environ. 4, 160. https://doi.org/10.1038/s43247-023-00828-z

Hideki Miyakawa, Rujito Agus S., Sarno, 2014. Panduan Teknis Restorasi di Kawasan Konservasi -Ekosistem Mangrove Lahan Bekas Tambak-, Project on Capacity Building for Restoration of Ecosystems in Conservation Areas. ed. JICA-RECA, Jakarta.

Hijuelos, A.C., Dijkstra, J.T., Carruthers, T.J.B., Heynert, K., Reed, D.J., van Wesenbeeck, B.K., 2019. Linking management planning for coastal wetlands to potential future wave attenuation under a range of relative sea-level rise scenarios. PLOS ONE 14, e0216695. https://doi.org/10.1371/journal.pone.0216695

Hill, J.W., Bourke, L.A., Horton, C.M., Staples, T.L., Lovelock, C.E., 2020. Limited relationships between mangrove forest structure and hydro-edaphic conditions in subtropical Queensland, Australia. Estuar. Coast. Shelf Sci. 106930. https://doi.org/10.1016/j.ecss.2020.106930

Hoekstra, P., 1989a. The development of two major Indonesian river deltas: morphology and sedimentary aspects of the Solo and Porong delta, East Java, in: van der Linden, W.J.M., Cloetingh, S.A.P.L., Kaasschieter, J.P.K., van de Graaff, W.J.E., Vandenberghe, J., van der Gun, J.A.M. (Eds.), Coastal Lowlands. Springer Netherlands, Dordrecht, pp. 143–159. https://doi.org/10.1007/978-94-017-1064-0_9

Hoekstra, P., 1989b. Hydrodynamics and depositional processes of the Solo and Porong Deltas, East Java, Indonesia, in: van der Linden, W.J.M., Cloetingh, S.A.P.L., Kaasschieter, J.P.K., van de Graaff, W.J.E., Vandenberghe, J., van der Gun, J.A.M. (Eds.), Coastal Lowlands. Springer Netherlands, Dordrecht, pp. 161–173. https://doi.org/10.1007/978-94-017-1064-0_10

Horstman, E.M., Bryan, K.R., Mullarney, J.C., 2021. Drag variations, tidal asymmetry and tidal range changes in a mangrove creek system. Earth Surf. Process. Landf. esp.5124. https://doi.org/10.1002/esp.5124

Horstman, E.M., Bryan, K.R., Mullarney, J.C., Pilditch, C.A., Eager, C.A., 2018. Are flow-vegetation interactions well represented by mimics? A case study of mangrove pneumatophores. Adv. Water Resour. 111, 360–371. https://doi.org/10.1016/j.advwatres.2017.11.018

Horstman, E.M., Dohmen-Janssen, C.M., Bouma, T.J., Hulscher, S.J.M.H., 2015. Tidal-scale flow routing and sedimentation in mangrove forests: Combining field data and numerical modelling. Geomorphology 228, 244–262. https://doi.org/10.1016/j.geomorph.2014.08.011

Howard, J., Sutton-Grier, A., Herr, D., Kleypas, J., Landis, E., Mcleod, E., Pidgeon, E., Simpson, S., 2017. Clarifying the role of coastal and marine systems in climate mitigation. Front. Ecol. Environ. 15, 42–50. https://doi.org/10.1002/fee.1451

Hu, T., Zhang, Y., Su, Y., Zheng, Y., Lin, G., Guo, Q., 2020. Mapping the Global Mangrove Forest Aboveground Biomass Using Multisource Remote Sensing Data. Remote Sens. 12, 1690. https://doi.org/10.3390/rs12101690

Hu, Z., Zhou, J., Wang, C., Wang, H., He, Z., Peng, Y., Zheng, P., Cozzoli, F., Bouma, T.J., 2020. A Novel Instrument for Bed Dynamics Observation Supports Machine Learning Applications in Mangrove Biogeomorphic Processes. Water Resour. Res. 56. https://doi.org/10.1029/2020WR027257

Huete, A., Didan, K., Miura, T., Rodriguez, E.P., Gao, X., Ferreira, L.G., 2002. Overview of the radiometric and biophysical performance of the MODIS vegetation indices. Remote Sens. Environ. 83, 195–213. https://doi.org/10.1016/S0034-4257(02)00096-2

Huete, A.R., 1988. A soil-adjusted vegetation index (SAVI). Remote Sens. Environ. 25, 295–309. https://doi.org/10.1016/0034-4257(88)90106-X

Hunt, S., Bryan, K.R., Mullarney, J.C., 2015. The influence of wind and waves on the existence of stable intertidal morphology in meso-tidal estuaries. Geomorphology 228, 158–174. https://doi.org/10.1016/j.geomorph.2014.09.001

Hutchison, J., Manica, A., Swetnam, R., Balmford, A., Spalding, M., 2014. Predicting Global Patterns in Mangrove Forest Biomass. Conserv. Lett. 7, 233–240. https://doi.org/10.1111/conl.12060

Hutton, E., Piper, M., Tucker, G., 2020. The Basic Model Interface 2.0: A standard interface for coupling numerical models in the geosciences. J. Open Source Softw. 5, 2317. https://doi.org/10.21105/joss.02317

IPCC, 2022. Climate Change 2022 – Impacts, Adaptation and Vulnerability: Working Group II Contribution to the Sixth Assessment Report of the Intergovernmental Panel on Climate Change, 1st ed, Summary for Policymakers. Cambridge University Press, Cambridge, UK and New York, USA. https://doi.org/10.1017/9781009325844

Jayanthi, M., Samynathan, M., Thirumurthy, S., Duraismay, M., Kabiraj, S., Vijayakumar, S., Panigrahi, A., Kumaran, M., Muralidhar, M., 2022. Is aquaculture development responsible for mangrove conversion in India? - A geospatial study to assess the influence of natural and anthropogenic factors on mangroves in the last three decades. Aquaculture 561, 738696. https://doi.org/10.1016/j.aquaculture.2022.738696

Jayatissa, L.P., Wickramasinghe, W.A.A.D.L., Dahdouh-Guebas, F., Huxham, M., 2008. Interspecific Variations in Responses of Mangrove Seedlings to Two Contrasting Salinities. Int. Rev. Hydrobiol. 93, 700–710. https://doi.org/10.1002/iroh.200711017

Jennerjahn, T.C., Gilman, E., Krauss, K.W., Lacerda, L.D., Nordhaus, I., Wolanski, E., 2017. Mangrove Ecosystems under Climate Change, in: Rivera-Monroy, V.H., Lee, S.Y., Kristensen, E., Twilley, R.R. (Eds.), Mangrove Ecosystems: A Global Biogeographic Perspective: Structure, Function, and Services. Springer International Publishing, Cham, pp. 211–244. https://doi.org/10.1007/978-3-319-62206-4_7

Jennerjahn, T.C., Ittekkot, V., Klöpper, S., Adi, S., Purwo Nugroho, S., Sudiana, N., Yusmal, A., Prihartanto, Gaye-Haake, B., 2004. Biogeochemistry of a tropical river affected by human activities in its catchment: Brantas River estuary and coastal waters of Madura Strait, Java, Indonesia. Estuar. Coast. Shelf Sci. 60, 503–514. https://doi.org/10.1016/j.ecss.2004.02.008

Jennerjahn, T.C., Jänen, I., Propp, C., Adi, S., Nugroho, S.P., 2013. Environmental impact of mud volcano inputs on the anthropogenically altered Porong River and Madura Strait coastal waters, Java, Indonesia. Estuar. Coast. Shelf Sci. 130, 152–160. https://doi.org/10.1016/j.ecss.2013.04.007

Jiménez, J.A., 1992. 16 - Mangrove Forests of the Pacific Coast of Central America, in: Seeliger, U. (Ed.), Coastal Plant Communities of Latin America. Academic Press, San Diego, pp. 259–267. https://doi.org/10.1016/B978-0-08-092567-7.50022-2

Jin, H., Stehman, S.V., Mountrakis, G., 2014. Assessing the impact of training sample selection on accuracy of an urban classification: a case study in Denver, Colorado. Int. J. Remote Sens. 35, 2067–2081. https://doi.org/10.1080/01431161.2014.885152

Jørgensen, S.E., Fath, B.D., 2011. 9 - Individual-Based Models, in: Jørgensen, S.E., Fath, B.D. (Eds.), Developments in Environmental Modelling. Elsevier, pp. 291–308. https://doi.org/10.1016/B978-0-444-53567-2.00009-0

Joyce, K.E., Duce, S., Leahy, S.M., Leon, J., Maier, S.W., 2019. Principles and practice of acquiring drone-based image data in marine environments. Mar. Freshw. Res. 70, 952–963.

Kamruzzaman, Md., Sharma, S., Hagihara, A., 2013. Vegetative and reproductive phenology of the mangrove *Kandelia obovata*: PHENOLOGY OF *KANDELIA OBOVATA*. Plant Species Biol. 28, 118–129. https://doi.org/10.1111/j.1442-1984.2012.00367.x

Karyadi, Soegiarto, Aris Harnanto, 2012. Pengaliran Lumpur Sidoarjo ke Laut Melalui Kali Porong. Bayumedia Publishing, Malang. Indonesia.

Kathiresan, K., Rajendran, N., 2005. Coastal mangrove forests mitigated tsunami. Estuar. Coast. Shelf Sci. 65, 601–606. https://doi.org/10.1016/j.ecss.2005.06.022

Kauffman, J.B., Cole, T.G., 2010. Micronesian Mangrove Forest Structure and Tree Responses to a Severe Typhoon. Wetlands 30, 1077–1084. https://doi.org/10.1007/s13157-010-0114-y

Kelleway, J., Serrano, O., Baldock, J., Cannard, T., Lavery, P., Lovelock, C., Macreadie, P., Masqué, P., Saintilan, N., Steven, A., 2017. Technical review of opportunities for including blue carbon in the Australian Government's Emissions Reduction Fund. Canberra ACT CSIRO.

Kirezci, E., Young, I.R., Ranasinghe, R., Muis, S., Nicholls, R.J., Lincke, D., Hinkel, J., 2020. Projections of global-scale extreme sea levels and resulting episodic coastal flooding over the 21st Century. Sci. Rep. 10, 11629. https://doi.org/10.1038/s41598-020-67736-6

Kleinhans, M., Douma, H., Addink, E.A., 2019. Fate of pioneering vegetation patches in a dynamic meandering river. Earth Surf. Process. Landf. 44, 1618–1632. https://doi.org/10.1002/esp.4596

Kodikara, K.A.S., Mukherjee, N., Jayatissa, L.P., Dahdouh-Guebas, F., Koedam, N., 2017. Have mangrove restoration projects worked? An in-depth study in Sri Lanka: Evaluation of mangrove restoration in Sri Lanka. Restor. Ecol. 25, 705–716. https://doi.org/10.1111/rec.12492

Krauss, K.W., Keeland, B.D., Allen, J.A., Ewel, K.C., Johnson, D.J., 2007. Effects of Season, Rainfall, and Hydrogeomorphic Setting on Mangrove Tree Growth in Micronesia. Biotropica 39, 161–170. https://doi.org/10.1111/j.1744-7429.2006.00259.x

Krauss, K.W., Lovelock, C.E., McKee, K.L., López-Hoffman, L., Ewe, S.M.L., Sousa, W.P., 2008. Environmental drivers in mangrove establishment and early development: A review. Aquat. Bot. 89, 105–127. https://doi.org/10.1016/j.aquabot.2007.12.014

Krauss, K.W., McKee, K.L., Lovelock, C.E., Cahoon, D.R., Saintilan, N., Reef, R., Chen, L., 2014. How mangrove forests adjust to rising sea level. New Phytol. 202, 19–34. https://doi.org/10.1111/nph.12605

Krauss, K.W., Osland, M.J., 2019. Tropical cyclones and the organization of mangrove forests: a review. Ann. Bot. mcz161. https://doi.org/10.1093/aob/mcz161

Kure, S., Winarta, B., Takeda, Y., Udo, K., Umeda, M., Mano, A., Tanaka, H., 2014. Effects of mud flows from the LUSI mud volcano on the Porong River estuary, Indonesia. J. Coast. Res. 70, 568–573. https://doi.org/10.2112/SI70-096.1

Kusumaningtyas, M.A., Kepel, T.L., Solihuddin, T., Lubis, A.A., Putra, A.D.P., Sugiharto, U., Ati, R.N.A., Salim, H.L., Mustikasari, E., Heriati, A., Daulat, A., Sudirman, N., Suryono, D.D., Rustam, A., 2022. Carbon sequestration potential in the rehabilitated mangroves in Indonesia. Ecol. Res. 37, 80–91. https://doi.org/10.1111/1440-1703.12279

Lagomasino, D., Fatoyinbo, T., Lee, S., Feliciano, E., Trettin, C., Simard, M., 2016. A Comparison of Mangrove Canopy Height Using Multiple Independent Measurements from Land, Air, and Space. Remote Sens. 8, 327. https://doi.org/10.3390/rs8040327

Lagomasino, D., Price, R.M., Whitman, D., Campbell, P.K.E., Melesse, A., 2014. Estimating major ion and nutrient concentrations in mangrove estuaries in Everglades National Park using leaf and satellite reflectance. Remote Sens. Environ. 154, 202–218. https://doi.org/10.1016/j.rse.2014.08.022

Lavigne, F., 2004. Rate of sediment yield following small-scale volcanic eruptions: a quantitative assessment at the Merapi and Semeru stratovolcanoes, Java, Indonesia. Earth Surf. Process. Landf. 29, 1045–1058. https://doi.org/10.1002/esp.1092

Lee, J.S., Jurkevich, L., Dewaele, P., Wambacq, P., Oosterlinck, A., 1994. Speckle filtering of synthetic aperture radar images: A review. Remote Sens. Rev. 8, 313–340. https://doi.org/10.1080/02757259409532206

Lee, S.Y., Hamilton, S., Barbier, E.B., Primavera, J., Lewis, R.R., 2019. Better restoration policies are needed to conserve mangrove ecosystems. Nat. Ecol. Evol. 3, 870–872. https://doi.org/10.1038/s41559-019-0861-y

Lewis, R.R., 2005. Ecological engineering for successful management and restoration of mangrove forests. Ecol. Eng. 24, 403–418. https://doi.org/10.1016/j.ecoleng.2004.10.003

Lewis, R.R., Brown, B., 2014. Ecological Mangrove Rehabilitation A Field Manual for Practitioner.

López-Portillo, J., Lewis, R.R., Saenger, P., Rovai, A., Koedam, N., Dahdouh-Guebas, F., Agraz-Hernández, C., Rivera-Monroy, V.H., 2017. Mangrove Forest Restoration and Rehabilitation, in: Rivera-Monroy, V.H., Lee, S.Y., Kristensen, E., Twilley, R.R. (Eds.), Mangrove Ecosystems: A Global Biogeographic Perspective: Structure, Function, and Services. Springer International Publishing, Cham, pp. 301–345. https://doi.org/10.1007/978-3-319-62206-4_10

Lovelock, C.E., Ball, M.C., Feller, I.C., Engelbrecht, B.M.J., Ling Ewe, M., 2006. Variation in hydraulic conductivity of mangroves: influence of species, salinity, and nitrogen and phosphorus availability. Physiol. Plant. 127, 457–464. https://doi.org/10.1111/j.1399-3054.2006.00723.x

Lovelock, C.E., Cahoon, D.R., Friess, D.A., Guntenspergen, G.R., Krauss, K.W., Reef, R., Rogers, K., Saunders, M.L., Sidik, F., Swales, A., Saintilan, N., Thuyen, L.X., Triet, T., 2015. The vulnerability of Indo-Pacific mangrove forests to sea-level rise. Nature 526, 559–563. https://doi.org/10.1038/nature15538

Lovelock, C.E., Ellison, J., 2007. Vulnerability of mangroves and tidal wetlands of the Great Barrier Reef to climate change.

Lovelock, C.E., Feller, I.C., Reef, R., Hickey, S., Ball, M.C., 2017. Mangrove dieback during fluctuating sea levels. Sci. Rep. 7, 1680. https://doi.org/10.1038/s41598-017-01927-6

Lucas, R., Van De Kerchove, R., Otero, V., Lagomasino, D., Fatoyinbo, L., Omar, H., Satyanarayana, B., Dahdouh-Guebas, F., 2020. Structural characterisation of mangrove forests achieved through combining multiple sources of remote sensing data. Remote Sens. Environ. 237, 111543. https://doi.org/10.1016/j.rse.2019.111543

Lugo, A.E., Snedaker, S.C., 1974. The Ecology of Mangroves. Annu. Rev. Ecol. Syst. 5, 39–64. https://doi.org/10.1146/annurev.es.05.110174.000351

Luijendijk, A., Hagenaars, G., Ranasinghe, R., Baart, F., Donchyts, G., Aarninkhof, S., 2018. Author Correction: The State of the World's Beaches. Sci. Rep. 8. https://doi.org/10.1038/s41598-018-28915-8

Lymburner, L., Bunting, P., Lucas, R., Scarth, P., Alam, I., Phillips, C., Ticehurst, C., Held, A., 2020. Mapping the multi-decadal mangrove dynamics of the Australian coastline. Remote Sens. Environ. 238, 111185. https://doi.org/10.1016/j.rse.2019.05.004

Macreadie, P.I., Anton, A., Raven, J.A., Beaumont, N., Connolly, R.M., Friess, D.A., Kelleway, J.J., Kennedy, H., Kuwae, T., Lavery, P.S., Lovelock, C.E., Smale, D.A., Apostolaki, E.T., Atwood, T.B., Baldock, J., Bianchi, T.S., Chmura, G.L., Eyre, B.D., Fourqurean, J.W., Hall-Spencer, J.M., Huxham, M., Hendriks, I.E., Krause-Jensen, D., Laffoley, D., Luisetti, T., Marbà, N., Masque, P., McGlathery, K.J., Megonigal, J.P., Murdiyarso, D., Russell, B.D., Santos, R., Serrano, O., Silliman, B.R., Watanabe, K., Duarte, C.M., 2019. The future of Blue Carbon science. Nat. Commun. 10, 3998. https://doi.org/10.1038/s41467-019-11693-w

Macreadie, P.I., Costa, M.D.P., Atwood, T.B., Friess, D.A., Kelleway, J.J., Kennedy, H., Lovelock, C.E., Serrano, O., Duarte, C.M., 2021. Blue carbon as a natural climate solution. Nat. Rev. Earth Environ. 2, 826–839. https://doi.org/10.1038/s43017-021-00224-1

Magnan, A.K., Oppenheimer, M., Garschagen, M., Buchanan, M.K., Duvat, V.K.E., Forbes, D.L., Ford, J.D., Lambert, E., Petzold, J., Renaud, F.G., Sebesvari, Z., van de Wal, R.S.W., Hinkel, J., Pörtner, H.-O., 2022. Sea level rise risks and societal adaptation benefits in low-lying coastal areas. Sci. Rep. 12, 10677. https://doi.org/10.1038/s41598-022-14303-w

Mahdianpari, M., Salehi, B., Mohammadimanesh, F., Homayouni, S., Gill, E., 2019. The First Wetland Inventory Map of Newfoundland at a Spatial Resolution of 10 m Using Sentinel-1 and Sentinel-2 Data on the Google Earth Engine Cloud Computing Platform. Remote Sens. 11, 43. https://doi.org/10.3390/rs11010043

Marois, D.E., Mitsch, W.J., 2015. Coastal protection from tsunamis and cyclones provided by mangrove wetlands – a review. Int. J. Biodivers. Sci. Ecosyst. Serv. Manag. 11, 71–83. https://doi.org/10.1080/21513732.2014.997292

Martin Isenburg, n.d. LAStools [WWW Document]. URL http://lastools.org/ (accessed 11.23.20).

Masek, J.G., Vermote, E.F., Saleous, N.E., Wolfe, R., Hall, F.G., Huemmrich, K.F., Gao, F., Kutler, J., Lim, T.-K., 2006. A Landsat Surface Reflectance Dataset for North America, 1990–2000. IEEE Geosci. Remote Sens. Lett. 3, 68–72. https://doi.org/10.1109/LGRS.2005.857030

Maza, M., Lara, J.L., Losada, I.J., 2021a. Predicting the evolution of coastal protection service with mangrove forest age. Coast. Eng. 103922. https://doi.org/10.1016/j.coastaleng.2021.103922

Maza, M., Lara, J.L., Losada, I.J., 2021b. Predicting the evolution of coastal protection service with mangrove forest age. Coast. Eng. 168, 103922. https://doi.org/10.1016/j.coastaleng.2021.103922

Maza, M., Lara, J.L., Losada, I.J., 2019. Experimental analysis of wave attenuation and drag forces in a realistic fringe Rhizophora mangrove forest. Adv. Water Resour. 131, 103376. https://doi.org/10.1016/j.advwatres.2019.07.006

Mazda, Y., Magi, M., Ikeda, Y., Kurokawa, T., Asano, T., 2006. Wave reduction in a mangrove forest dominated by Sonneratia sp. Wetl. Ecol. Manag. 14, 365–378. https://doi.org/10.1007/s11273-005-5388-0

Mazda, Y., Wolanski, E., King, B., Sase, A., Ohtsuka, D., Magi, M., 1997. Drag force due to vegetation in mangrove swamps. Mangroves Salt Marshes 1, 193–199.

Mazzini, A., 2018. 10 years of Lusi eruption: Lessons learned from multidisciplinary studies (LUSI LAB). Mar. Pet. Geol. 90, 1–9. https://doi.org/10.1016/j.marpetgeo.2017.12.025

Mazzini, A., Svensen, H., Akhmanov, G.G., Aloisi, G., Planke, S., Malthe-Sørenssen, A., Istadi, B., 2007. Triggering and dynamic evolution of the LUSI mud volcano, Indonesia. Earth Planet. Sci. Lett. 261, 375–388. https://doi.org/10.1016/j.epsl.2007.07.001

Mazzoleni, M., Paron, P., Reali, A., Juizo, D., Manane, J., Brandimarte, L., 2020. Testing UAV-derived topography for hydraulic modelling in a tropical environment. Nat. Hazards 103, 139–163. https://doi.org/10.1007/s11069-020-03963-4

McIvor, A., Möller, I., Spencer, T., Spalding, M., 2012. Reduction of Wind and Swell Waves by Mangroves (Natural Coastal Protection Series: Report 1), Cambridge Coastal Research Unit Working Paper 40. The Nature Conservancy and Wetlands International, Cambridge, UK.

McIvor, A., Spencer, T., Möller, I., Spalding, M., 2013. The response of mangrove soil surface elevation to sea level rise (Natural Coastal Protection Series: Report 3), Cambridge Coastal Research Unit Working Paper 42. The Nature Conservancy and Wetlands International, Cambridge, UK.

McKee, K.L., 2011. Biophysical controls on accretion and elevation change in Caribbean mangrove ecosystems. Estuar. Coast. Shelf Sci. 91, 475–483. https://doi.org/10.1016/j.ecss.2010.05.001

McKee, K.L., Mendelssohn, I.A., 1987. Root metabolism in the black mangrove (Avicennia germinans (L.) L): Response to hypoxia. Environ. Exp. Bot. 27, 147–156. https://doi.org/10.1016/0098-8472(87)90065-7

Mcleod, E., Chmura, G.L., Bouillon, S., Salm, R., Björk, M., Duarte, C.M., Lovelock, C.E., Schlesinger, W.H., Silliman, B.R., 2011. A blueprint for blue carbon: toward an improved understanding of the role of vegetated coastal habitats in sequestering CO 2. Front. Ecol. Environ. 9, 552–560. https://doi.org/10.1890/110004

Mehvar, S., Filatova, T., Dastgheib, A., De Ruyter van Steveninck, E., Ranasinghe, R., 2018. Quantifying Economic Value of Coastal Ecosystem Services: A Review. J. Mar. Sci. Eng. 6, 5. https://doi.org/10.3390/jmse6010005

Mendez, F.J., Losada, I.J., 2004. An empirical model to estimate the propagation of random breaking and nonbreaking waves over vegetation fields. Coast. Eng. 51, 103–118. https://doi.org/10.1016/j.coastaleng.2003.11.003

Menéndez, P., Losada, I.J., Torres-Ortega, S., Narayan, S., Beck, M.W., 2020. The Global Flood Protection Benefits of Mangroves. Sci. Rep. 10, 4404. https://doi.org/10.1038/s41598-020-61136-6

Mercier, A., Betbeder, J., Rumiano, F., Baudry, J., Gond, V., Blanc, L., Bourgoin, C., Cornu, G., Ciudad, C., Marchamalo, M., Poccard-Chapuis, R., Hubert-Moy, L., 2019. Evaluation of Sentinel-1 and 2 Time Series for Land Cover Classification of Forest–Agriculture Mosaics in Temperate and Tropical Landscapes. Remote Sens. 11, 979. https://doi.org/10.3390/rs11080979

Merkens, J.-L., Reimann, L., Hinkel, J., Vafeidis, A.T., 2016. Gridded population projections for the coastal zone under the Shared Socioeconomic Pathways. Glob. Planet. Change 145, 57–66. https://doi.org/10.1016/j.gloplacha.2016.08.009

Milliman, J.D., Syvitski, J.P.M., 1992. Geomorphic/Tectonic Control of Sediment Discharge to the Ocean: The Importance of Small Mountainous Rivers. J. Geol. 100, 525–544. https://doi.org/10.1086/629606

Ministry of Marine Affairs and Fisheries, 2010. Kajian Pemanfaatan dan Pengembangan Muara Kali Porong Tahun 2010. Ministry of Marine Affairs and Fisheries, Jakarta.

Ministry of Marine Affairs and Fisheries, 2009. Kajian Sebaran Lumpur dan Perubahan Dasar Perairan Akibat Semburan Lumpur Sidoarjo Menggunakan Model Numerik. Ministry of Marine Affairs and Fisheries, Jakarta.

Moloney, J.G., Hilton, M.J., Sirguey, P., Simons-Smith, T., 2018. Coastal Dune Surveying Using a Low-Cost Remotely Piloted Aerial System (RPAS). J. Coast. Res. 345, 1244–1255. https://doi.org/10.2112/JCOASTRES-D-17-00076.1

Montgomery, J., Bryan, K., Horstman, E., Mullarney, J., 2018. Attenuation of Tides and Surges by Mangroves: Contrasting Case Studies from New Zealand. Water 10, 1119. https://doi.org/10.3390/w10091119

Mori, N., Chang, C.-W., Inoue, T., Akaji, Y., Hinokidani, K., Baba, S., Takagi, M., Mori, S., Koike, H., Miyauchi, M., Suganuma, R., Sabunas, A., Miyashita, T., Shimura,

T., 2022. Parameterization of Mangrove Root Structure of Rhizophora stylosa in Coastal Hydrodynamic Model. Front. Built Environ. 7, 782219. https://doi.org/10.3389/fbuil.2021.782219

Morris, RebeccaL., Strain, E.M.A., Konlechner, T.M., Fest, B.J., Kennedy, D.M., Arndt, S.K., Swearer, S.E., 2019. Developing a nature-based coastal defence strategy for Australia. Aust. J. Civ. Eng. 17, 167–176. https://doi.org/10.1080/14488353.2019.1661062

Morris, R.L., Bishop, M.J., Boon, P., Browne, N.K., Carley, J.T., Fest, B.J., Fraser, M.W., Ghisalberti, M., Lovelock, C.E., Lowe, R.J., Rogers, A.A., Simpson, V., Strain, E.M.A., van Rooijen, A.A., Waters, E., Swearer, S.E., 2021. The Australian guide to nature-based methods for reducing risk from coastal hazards, Earth Systems and Climate Change Hub Report No 26. NESP Earth Systems and Climate Change Hub, Australia.

Morris, R.L., Konlechner, T.M., Ghisalberti, M., Swearer, S.E., 2018. From grey to green: Efficacy of eco-engineering solutions for nature-based coastal defence. Glob. Change Biol. 24, 1827–1842. https://doi.org/10.1111/gcb.14063

Mukherjee, N., Sutherland, W.J., Khan, M.N.I., Berger, U., Schmitz, N., Dahdouh-Guebas, F., Koedam, N., 2014. Using expert knowledge and modeling to define mangrove composition, functioning, and threats and estimate time frame for recovery. Ecol. Evol. 4, 2247–2262. https://doi.org/10.1002/ece3.1085

Mullarney, J.C., Henderson, S.M., Reyns, J.A.H., Norris, B.K., Bryan, K.R., 2017. Spatially varying drag within a wave-exposed mangrove forest and on the adjacent tidal flat. Cont. Shelf Res. 147, 102–113. https://doi.org/10.1016/j.csr.2017.06.019

Murdiyarso, D., Purbopuspito, J., Kauffman, J.B., Warren, M.W., Sasmito, S.D., Donato, D.C., Manuri, S., Krisnawati, H., Taberima, S., Kurnianto, S., 2015. The potential of Indonesian mangrove forests for global climate change mitigation. Nat. Clim. Change 5, 1089–1092. https://doi.org/10.1038/nclimate2734

Murdiyarso, D., Sasmito, S.D., Sillanpää, M., MacKenzie, R., Gaveau, D., 2021. Mangrove selective logging sustains biomass carbon recovery, soil carbon, and sediment. Sci. Rep. 11, 12325. https://doi.org/10.1038/s41598-021-91502-x

Murray, N.J., Phinn, S.R., DeWitt, M., Ferrari, R., Johnston, R., Lyons, M.B., Clinton, N., Thau, D., Fuller, R.A., 2019. The global distribution and trajectory of tidal flats. Nature 565, 222–225. https://doi.org/10.1038/s41586-018-0805-8

Narayan, S., Beck, M.W., Reguero, B.G., Losada, I.J., van Wesenbeeck, B., Pontee, N., Sanchirico, J.N., Ingram, J.C., Lange, G.-M., Burks-Copes, K.A., 2016. The Effectiveness, Costs and Coastal Protection Benefits of Natural and Nature-Based Defences. PLOS ONE 11, e0154735. https://doi.org/10.1371/journal.pone.0154735

Nardin, W., Edmonds, D.A., Fagherazzi, S., 2016. Influence of vegetation on spatial patterns of sediment deposition in deltaic islands during flood. Adv. Water Resour. 93, 236–248. https://doi.org/10.1016/j.advwatres.2016.01.001

Nardin, W., Vona, I., Fagherazzi, S., 2021. Sediment deposition affects mangrove forests in the Mekong delta, Vietnam. Cont. Shelf Res. 213, 104319. https://doi.org/10.1016/j.csr.2020.104319

Narine, L.L., Popescu, S.C., Malambo, L., 2020. Using ICESat-2 to Estimate and Map Forest Aboveground Biomass: A First Example. Remote Sens. 12, 1824. https://doi.org/10.3390/rs12111824

Nature-Based Solutions Resource Guide, 2022. . White House Council on Environmental Quality, White House Office of Science and Technology Policy, White House Office of Domestic Climate Policy, Washington D.C.

Navarro, A., Young, M., Allan, B., Carnell, P., Macreadie, P., Ierodiaconou, D., 2020. The application of Unmanned Aerial Vehicles (UAVs) to estimate above-ground biomass of mangrove ecosystems. Remote Sens. Environ. 242, 111747. https://doi.org/10.1016/j.rse.2020.111747

Navarro, J.A., Algeet, N., Fernández-Landa, A., Esteban, J., Rodríguez-Noriega, P., Guillén-Climent, M.L., 2019. Integration of UAV, Sentinel-1, and Sentinel-2 Data for Mangrove Plantation Aboveground Biomass Monitoring in Senegal. Remote Sens. 11, 77. https://doi.org/10.3390/rs11010077

Norris, B.K., Mullarney, J.C., Bryan, K.R., Henderson, S.M., 2021. Relating millimeter-scale turbulence to meter-scale subtidal erosion and accretion across the fringe of a coastal mangrove forest. Earth Surf. Process. Landf. esp.5047. https://doi.org/10.1002/esp.5047

Norris, B.K., Mullarney, J.C., Bryan, K.R., Henderson, S.M., 2017. The effect of pneumatophore density on turbulence: A field study in a Sonneratia -dominated mangrove forest, Vietnam. Cont. Shelf Res. 147, 114–127. https://doi.org/10.1016/j.csr.2017.06.002

Ohira, W., Honda, K., Nagai, M., Ratanasuwan, A., 2013. Mangrove stilt root morphology modeling for estimating hydraulic drag in tsunami inundation simulation. Trees 27, 141–148. https://doi.org/10.1007/s00468-012-0782-8

Ong, J.E., Gong, W.K., Wong, C.H., 2004. Allometry and partitioning of the mangrove, Rhizophora apiculata. For. Ecol. Manag. 188, 395–408. https://doi.org/10.1016/j.foreco.2003.08.002

Onuf, C.P., Teal, J.M., Valiela, I., 1977. Interactions of Nutrients, Plant Growth and Herbivory in a Mangrove Ecosystem. Ecology 58, 514–526. https://doi.org/10.2307/1939001

Oorschot, M. van, Kleinhans, M., Geerling, G., Middelkoop, H., 2016. Distinct patterns of interaction between vegetation and morphodynamics: Distinct Patterns of Interaction Between Vegetation and Morphodynamics. Earth Surf. Process. Landf. 41, 791–808. https://doi.org/10.1002/esp.3864

Osland, M.J., Feher, L.C., Griffith, K.T., Cavanaugh, K.C., Enwright, N.M., Day, R.H., Stagg, C.L., Krauss, K.W., Howard, R.J., Grace, J.B., Rogers, K., 2017. Climatic controls on the global distribution, abundance, and species richness of mangrove forests. Ecol. Monogr. 87, 341–359. https://doi.org/10.1002/ecm.1248

Otero, V., Van De Kerchove, R., Satyanarayana, B., Martínez-Espinosa, C., Fisol, M.A.B., Ibrahim, M.R.B., Sulong, I., Mohd-Lokman, H., Lucas, R., Dahdouh-Guebas, F., 2018. Managing mangrove forests from the sky: Forest inventory using field data and Unmanned Aerial Vehicle (UAV) imagery in the Matang Mangrove Forest Reserve, peninsular Malaysia. For. Ecol. Manag. 411, 35–45. https://doi.org/10.1016/j.foreco.2017.12.049

Otero, V., Van De Kerchove, R., Satyanarayana, B., Mohd-Lokman, H., Lucas, R., Dahdouh-Guebas, F., 2019. An Analysis of the Early Regeneration of Mangrove Forests using Landsat Time Series in the Matang Mangrove Forest Reserve, Peninsular Malaysia. Remote Sens. 11, 774. https://doi.org/10.3390/rs11070774

Patel, N., Kaushal, B., 2010. Improvement of user's accuracy through classification of principal component images and stacked temporal images. Geo-Spat. Inf. Sci. 13, 243–248. https://doi.org/10.1007/s11806-010-0380-0

Pekel, J.-F., Cottam, A., Gorelick, N., Belward, A.S., 2016. High-resolution mapping of global surface water and its long-term changes. Nature 540, 418–422. https://doi.org/10.1038/nature20584

Pelckmans, I., Belliard, J.-P., Dominguez-Granda, L.E., Slobbe, C., Temmerman, S., Gourgue, O., 2023. Mangrove ecosystem properties regulate high water levels in a river delta. Nat. Hazards Earth Syst. Sci. 23, 3169–3183. https://doi.org/10.5194/nhess-23-3169-2023

Pendleton, L., Donato, D.C., Murray, B.C., Crooks, S., Jenkins, W.A., Sifleet, S., Craft, C., Fourqurean, J.W., Kauffman, J.B., Marbà, N., Megonigal, P., Pidgeon, E., Herr, D., Gordon, D., Baldera, A., 2012. Estimating Global "Blue Carbon" Emissions from Conversion and Degradation of Vegetated Coastal Ecosystems. PLoS ONE 7, e43542. https://doi.org/10.1371/journal.pone.0043542

Pérez, A., Libardoni, B.G., Sanders, C.J., 2018. Factors influencing organic carbon accumulation in mangrove ecosystems. Biol. Lett. 14, 20180237. https://doi.org/10.1098/rsbl.2018.0237

Peters, R., Vovides, A.G., Luna, S., Grüters, U., Berger, U., 2014. Changes in allometric relations of mangrove trees due to resource availability – A new mechanistic modelling approach. Ecol. Model. 283, 53–61. https://doi.org/10.1016/j.ecolmodel.2014.04.001

Piercy, C.D., Charbonneau, B.R., Russ, E.R., Swannack, T.M., 2023. Examining the commonalities and knowledge gaps in coastal zone vegetation simulation models. Earth Surf. Process. Landf. n/a. https://doi.org/10.1002/esp.5565

Piou, C., Feller, I.C., Berger, U., Chi, F., 2006. Zonation Patterns of Belizean Offshore Mangrove Forests 41 Years After a Catastrophic Hurricane1. Biotropica 38, 365–374. https://doi.org/10.1111/j.1744-7429.2006.00156.x

Popescu, S.C., Wynne, R.H., Nelson, R.F., 2002. Estimating plot-level tree heights with lidar: local filtering with a canopy-height based variable window size. Comput. Electron. Agric. 37, 71–95. https://doi.org/10.1016/S0168-1699(02)00121-7

Pretzsch, H., 2009. Forest Dynamics, Growth and Yield: From Measurement to Model. Springer Berlin Heidelberg, Berlin, Heidelberg. https://doi.org/10.1007/978-3-540-88307-4

Primavera, J., Rollon, R., Samson, M., 2011. The pressing challenges of mangrove rehabilitation: Pond reversion and coastal protection. In ecohydrology and restoration, in treatise on estuarine and coastal science.

Primavera, J.H., Esteban, J.M.A., 2008. A review of mangrove rehabilitation in the Philippines: successes, failures and future prospects. Wetl. Ecol. Manag. 16, 345–358. https://doi.org/10.1007/s11273-008-9101-y

Pulighe, G., Baiocchi, V., Lupia, F., 2016. Horizontal accuracy assessment of very high resolution Google Earth images in the city of Rome, Italy. Int. J. Digit. Earth 9, 342–362. https://doi.org/10.1080/17538947.2015.1031716

Pusat Pemanfaatan Penginderaan Jauh LAPAN, 2020. Peta Sebaran Hutan Mangrove di Indonesia [WWW Document]. Peta Sebaran Hutan Mangrove Indones. URL http://103.31.159.29/maps/624 (accessed 1.11.21).

Rabinowitz, D., 1978. Dispersal Properties of Mangrove Propagules. Biotropica 10, 47. https://doi.org/10.2307/2388105

Reef, R., Feller, I.C., Lovelock, C.E., 2010. Nutrition of mangroves. Tree Physiol. 30, 1148–1160. https://doi.org/10.1093/treephys/tpq048

Ren, H., Jian, S., Lu, H., Zhang, Q., Shen, W., Han, W., Yin, Z., Guo, Q., 2008. Restoration of mangrove plantations and colonisation by native species in Leizhou bay, South China. Ecol. Res. 23, 401–407. https://doi.org/10.1007/s11284-007-0393-9

Rentschler, J., Salhab, M., Jafino, B.A., 2022. Flood exposure and poverty in 188 countries. Nat. Commun. 13, 3527. https://doi.org/10.1038/s41467-022-30727-4

Richards, D.R., Friess, D.A., 2016. Rates and drivers of mangrove deforestation in Southeast Asia, 2000–2012. Proc. Natl. Acad. Sci. 113, 344–349. https://doi.org/10.1073/pnas.1510272113

Rivera-Monroy, V.H., Lee, S.Y., Kristensen, E., Twilley, R.R. (Eds.), 2017. Mangrove Ecosystems: A Global Biogeographic Perspective: Structure, Function, and Services. Springer International Publishing, Cham. https://doi.org/10.1007/978-3-319-62206-4

Rivera-Monroy, V.H., Twilley, R.R., Bone, D., Childers, D.L., Coronado-Molina, C., Feller, I.C., Herrera-Silveira, J., Jaffe, R., Mancera, E., Rejmankova, E., 2004. A conceptual framework to develop long-term ecological research and management objectives in the wider Caribbean region. BioScience 54, 843–856.

Rivera-Monroy, V.H., Zhao, X., Wang, H., Xue, Z.G., 2022. Are Existing Modeling Tools Useful to Evaluate Outcomes in Mangrove Restoration and Rehabilitation Projects? A Minireview. Forests 13, 1638. https://doi.org/10.3390/f13101638

Rodríguez, J.F., Saco, P.M., Sandi, S., Saintilan, N., Riccardi, G., 2017. Potential increase in coastal wetland vulnerability to sea-level rise suggested by considering

hydrodynamic attenuation effects. Nat. Commun. 8, 16094. https://doi.org/10.1038/ncomms16094

Rodriguez-Galiano, V.F., Ghimire, B., Rogan, J., Chica-Olmo, M., Rigol-Sanchez, J.P., 2012. An assessment of the effectiveness of a random forest classifier for land-cover classification. ISPRS J. Photogramm. Remote Sens. 67, 93–104. https://doi.org/10.1016/j.isprsjprs.2011.11.002

Roelvink, D., Huisman, B., Elghandour, A., Ghonim, M., Reyns, J., 2020. Efficient Modeling of Complex Sandy Coastal Evolution at Monthly to Century Time Scales. Front. Mar. Sci. 7, 535. https://doi.org/10.3389/fmars.2020.00535

Roelvink, J.A., Reniers, A., 2012. A guide to modeling coastal morphology, Advances in coastal and ocean engineering. World Scientific, Singapore ; Hackensack, NJ.

Rogers, K., 2021. Accommodation space as a framework for assessing the response of mangroves to relative sea-level rise. Singap. J. Trop. Geogr. 42, 163–183. https://doi.org/10.1111/sjtg.12357

Roskoden, R.R., Bryan, K.R., Schreiber, I., Kopf, A., 2020. Rapid transition of sediment consolidation across an expanding mangrove fringe in the Firth of Thames New Zealand. Geo-Mar. Lett. 40, 295–308. https://doi.org/10.1007/s00367-019-00589-9

Roussel, J.-R., Auty, D., Coops, N.C., Tompalski, P., Goodbody, T.R.H., Meador, A.S., Bourdon, J.-F., de Boissieu, F., Achim, A., 2020. lidR: An R package for analysis of Airborne Laser Scanning (ALS) data. Remote Sens. Environ. 251, 112061. https://doi.org/10.1016/j.rse.2020.112061

Sahu, S.K., Kathiresan, K., 2019. The age and species composition of mangrove forest directly influence the net primary productivity and carbon sequestration potential. Biocatal. Agric. Biotechnol. 20, 101235. https://doi.org/10.1016/j.bcab.2019.101235

Saintilan, N., Horton, B., Törnqvist, T.E., Ashe, E.L., Khan, N.S., Schuerch, M., Perry, C., Kopp, R.E., Garner, G.G., Murray, N., Rogers, K., Albert, S., Kelleway, J., Shaw, T.A., Woodroffe, C.D., Lovelock, C.E., Goddard, M.M., Hutley, L.B., Kovalenko, K., Feher, L., Guntenspergen, G., 2023. Widespread retreat of coastal habitat is likely at warming levels above 1.5 °C. Nature. https://doi.org/10.1038/s41586-023-06448-z

Sasmito, S.D., Basyuni, M., Kridalaksana, A., Saragi-Sasmito, M.F., Lovelock, C.E., Murdiyarso, D., 2023. Challenges and opportunities for achieving Sustainable Development Goals through restoration of Indonesia's mangroves. Nat. Ecol. Evol. https://doi.org/10.1038/s41559-022-01926-5

Sasmito, S.D., Kuzyakov, Y., Lubis, A.A., Murdiyarso, D., Hutley, L.B., Bachri, S., Friess, D.A., Martius, C., Borchard, N., 2020. Organic carbon burial and sources in soils of coastal mudflat and mangrove ecosystems. CATENA 187, 104414. https://doi.org/10.1016/j.catena.2019.104414

Schoonees, T., Gijón Mancheño, A., Scheres, B., Bouma, T.J., Silva, R., Schlurmann, T., Schüttrumpf, H., 2019. Hard Structures for Coastal Protection, Towards Greener

Designs. Estuaries Coasts 42, 1709–1729. https://doi.org/10.1007/s12237-019-00551-z

Schrijvershof, R.A., van Maren, D.S., Torfs, P.J.J.F., Hoitink, A.J.F., 2023. A Synthetic Spring-Neap Tidal Cycle for Long-Term Morphodynamic Models. J. Geophys. Res. Earth Surf. 128. https://doi.org/10.1029/2022JF006799

Seabold, S., Perktold, J., 2010. Statsmodels: Econometric and Statistical Modeling with Python. Presented at the Python in Science Conference, Austin, Texas, pp. 92–96. https://doi.org/10.25080/Majora-92bf1922-011

Sentinel-1 SAR GRD: C-band Synthetic Aperture Radar Ground Range Detected, log scaling [WWW Document], n.d. URL https://developers.google.com/earth-engine/datasets/catalog/COPERNICUS_S1_GRD (accessed 11.26.20).

SER (Society for Ecological Restoration Science and Policy Working Group), 2002. The SER primer on ecological restoration. Sci. Policy Work. Group 9.

Setiawan, A., Realino, B., Triyulianti, I., Hamzah, F., Murdimanto, A., Putri, M.R., Nugroho, D., 2019. Using WorldView-2 Imagery to Estimate Mangroves Density in the Porong Estuary, in: Barale, V., Gade, M. (Eds.), Remote Sensing of the Asian Seas. Springer International Publishing, Cham, pp. 377–393. https://doi.org/10.1007/978-3-319-94067-0_21

Sharma, S., Hoque, A.T.M.R., Analuddin, K., Hagihara, A., 2014. A model of seasonal foliage dynamics of the subtropical mangrove species Rhizophora stylosa Griff. growing at the northern limit of its distribution. For. Ecosyst. 1, 15. https://doi.org/10.1186/s40663-014-0015-2

Sharma, S., Suwa, R., Ray, R., Rozaimi, M., MacKenzie, R.A., Nakaoka, M., 2022. Preface: Blue carbon studies in ASIA-PACIFIC regions: Current status, gaps, and future perspectives. Ecol. Res. 37, 5–8. https://doi.org/10.1111/1440-1703.12290

Shih, S.-S., Huang, Z.-Z., Hsu, Y.-W., 2022. Nature-based solutions on floodplain restoration with coupled propagule dispersal simulation and stepping-stone approach to predict mangrove encroachment in an estuary. Sci. Total Environ. 851, 158097. https://doi.org/10.1016/j.scitotenv.2022.158097

Shore Protection Manual, 1973. . U.S. Army Coastal Engineering Research Center ; For sale by the Supt. of Docs., U.S. Govt. Print. Off., [Fort Belvoir, Va.], Washington.

Sidik, F., Hidayatullah, T., Kadarisman, H.P., Lovelock, C.E., 2013. Evaluation of Mangrove Development in a Created Mangrove Wetland in Porong, East Java, in: Regional Symposium on Mangrove Ecosystem Management In Southeast Asia. Presented at the Mainstreaming Mangroves, Ministry of Forestry Indonesia, Surabaya, Indonesia.

Sidik, F., Lawrence, A., Wagey, T., Zamzani, F., Lovelock, C.E., 2023. Blue carbon: A new paradigm of mangrove conservation and management in Indonesia. Mar. Policy 147, 105388. https://doi.org/10.1016/j.marpol.2022.105388

Sidik, F., Neil, D., Lovelock, C.E., 2016. Effect of high sedimentation rates on surface sediment dynamics and mangrove growth in the Porong River, Indonesia. Mar. Pollut. Bull. 107, 355–363. https://doi.org/10.1016/j.marpolbul.2016.02.048

Sidik, F., Supriyanto, B., Krisnawati, H., Muttaqin, M.Z., 2018. Mangrove conservation for climate change mitigation in Indonesia. Wiley Interdiscip. Rev. Clim. Change 9, e529. https://doi.org/10.1002/wcc.529

Slim, F., Gwada, P., Kodjo, M., Hemminga, M., 1996. Biomass and litterfall of Ceriops tagal and Rhizophora mucronata in the mangrove forest of Gazi Bay, Kenya. Mar. Freshw. Res. 47, 999–1007.

Song, S., Ding, Y., Li, W., Meng, Y., Zhou, J., Gou, R., Zhang, C., Ye, S., Saintilan, N., Krauss, K.W., Crooks, S., Lv, S., Lin, G., 2023. Mangrove reforestation provides greater blue carbon benefit than afforestation for mitigating global climate change. Nat. Commun. 14, 756. https://doi.org/10.1038/s41467-023-36477-1

Spalding, M., Kainuma, M., Collins, L., 2010. World Atlas of Mangroves. Taylor & Francis Group, London.

Spalding, M.D., McIvor, A.L., Beck, M.W., Koch, E.W., Möller, I., Reed, D.J., Rubinoff, P., Spencer, T., Tolhurst, T.J., Wamsley, T.V., Wesenbeeck, B.K., Wolanski, E., Woodroffe, C.D., 2014. Coastal Ecosystems: A Critical Element of Risk Reduction. Conserv. Lett. 7, 293–301. https://doi.org/10.1111/conl.12074

Srivastava, P.B.L., Khamis, D., 1978. Progress of natural regeneration after final felling under the current silvicultural practices in matang mangrove reserve. Pertanika1 2, 126–135.

Su, J., Friess, D.A., Gasparatos, A., 2021. A meta-analysis of the ecological and economic outcomes of mangrove restoration. Nat. Commun. 12, 5050. https://doi.org/10.1038/s41467-021-25349-1

Sudhir, S., Arunprasath, A., Sankara Vel, V., 2022. A critical review on adaptations, and biological activities of the mangroves. J. Nat. Pestic. Res. 1, 100006. https://doi.org/10.1016/j.napere.2022.100006

Suwa, R., Hagihara, A., 2008. Seasonal changes in canopy photosynthesis and foliage respiration in a Rhizophora stylosa stand at the northern limit of its natural distribution. Wetl. Ecol. Manag. 16, 313–321. https://doi.org/10.1007/s11273-007-9066-2

Tala, WD.S., 2020. The Study of Mangrove Reproductive Phenology in The Rhizophoraceae Family (Bruguiera gymnorrhiza (L.) Lamk., Ceriops tagal (Perr.) C.B. Rob., Rhizophora apiculata Blume. and Rhizophora mucronata Lamk.). J. Biol. Trop. 20, 406–415. https://doi.org/10.29303/jbt.v20i3.2091

Tamiminia, H., Salehi, B., Mahdianpari, M., Quackenbush, L., Adeli, S., Brisco, B., 2020. Google Earth Engine for geo-big data applications: A meta-analysis and systematic review. ISPRS J. Photogramm. Remote Sens. 164, 152–170. https://doi.org/10.1016/j.isprsjprs.2020.04.001

Temmerman, S., Horstman, E.M., Krauss, K.W., Mullarney, J.C., Pelckmans, I., Schoutens, K., 2023. Marshes and Mangroves as Nature-Based Coastal Storm Buffers. Annu. Rev. Mar. Sci. 15, annurev-marine-040422-092951. https://doi.org/10.1146/annurev-marine-040422-092951

Temmerman, S., Meire, P., Bouma, T.J., Herman, P.M.J., Ysebaert, T., De Vriend, H.J., 2013. Ecosystem-based coastal defence in the face of global change. Nature 504, 79–83. https://doi.org/10.1038/nature12859

Teutli-Hernández, C., Herrera-Silveira, J.A., Cisneros-de la Cruz, D.J., Roman-Cuesta, R., 2020. Mangrove ecological restoration guide: Lessons learned, Mainstreaming Wetlands into the Climate Agenda: A multilevel approach (SWAMP). CIFOR/CINVESTAV-IPN/UNAM-Sisal/PMC, Bogor, Indonesia.

Thanh, V.Q., Reyns, J., Wackerman, C., Eidam, E.F., Roelvink, D., 2017. Modelling suspended sediment dynamics on the subaqueous delta of the Mekong River. Cont. Shelf Res. 147, 213–230. https://doi.org/10.1016/j.csr.2017.07.013

The Jakarta Post, 2009. Mangrove forest to be developed at Porong River mouth [WWW Document]. Jkt. Post. URL https://www.thejakartapost.com/news/2009/04/29/mangrove-forest-be-developed-porong-river-mouth.html (accessed 11.19.20).

The State of the World's Mangroves 2022, 2022nd ed, 2022. . Global Mangrove Alliance.

Thi Ha, H., Duarte, C.M., Tri, N.H., Terrados, J., Borum, J., 2003. Growth and population dynamics during early stages of the mangrove Kandelia candel in Halong Bay, North Viet Nam. Estuar. Coast. Shelf Sci. 58, 435–444. https://doi.org/10.1016/S0272-7714(03)00109-4

Tiggeloven, T., De Moel, H., Van Zelst, V.T.M., Van Wesenbeeck, B.K., Winsemius, H.C., Eilander, D., Ward, P.J., 2022. The benefits of coastal adaptation through conservation of foreshore vegetation. J. Flood Risk Manag. 15, e12790. https://doi.org/10.1111/jfr3.12790

Tom Wilms, Fokko van der Goot, Femke Tonneijck, Fegi Nurhabni, Leo Sembiring, 2021. Building with Nature Approach. Building with Nature to restore eroding tropical muddy coasts., Ecoshape technical report. Ecoshape International, Dordrecht, The Netherlands.

Topouzelis, K., Psyllos, A., 2012. Oil spill feature selection and classification using decision tree forest on SAR image data. ISPRS J. Photogramm. Remote Sens. 68, 135–143. https://doi.org/10.1016/j.isprsjprs.2012.01.005

Tucker, C.J., 1979. Red and photographic infrared linear combinations for monitoring vegetation. Remote Sens. Environ. 8, 127–150. https://doi.org/10.1016/0034-4257(79)90013-0

Twilley, R.R., Castañeda-Moya, E., Rivera-Monroy, V.H., Rovai, A., 2017. Productivity and Carbon Dynamics in Mangrove Wetlands, in: Rivera-Monroy, V.H., Lee, S.Y., Kristensen, E., Twilley, R.R. (Eds.), Mangrove Ecosystems: A Global Biogeographic Perspective: Structure, Function, and Services. Springer International Publishing, Cham, pp. 113–162. https://doi.org/10.1007/978-3-319-62206-4_5

Twilley, R.R., Rivera-Monroy, V.H., 2005. Developing Performance Measures of Mangrove Wetlands Using Simulation Models of Hydrology, Nutrient Biogeochemistry, and Community Dynamics. J. Coast. Res. 79–93.

Twilley, R.R., Rivera-Monroy, V.H., Chen, R., Botero, L., 1999. Adapting an Ecological Mangrove Model to Simulate Trajectories in Restoration Ecology. Mar. Pollut. Bull. 37, 404–419. https://doi.org/10.1016/S0025-326X(99)00137-X

UN General Assembly, 2019. United Nations Decade on Ecosystem Restoration (2021–2030), A/RES/73/284.

UNFCCC. Secretariat, 2021. Nationally determined contributions under the Paris Agreement. Synthesis report by the secretariat (Synthesis reports No. FCCC/PA/CMA/2021/8), Glasgow Climate Change Conference - October/November 2021. Glasgow.

United Nations, 2018. The 2030 Agenda and the Sustainable Development Goals: An opportunity for Latin America and the Caribbean, LC/G.2681-P/Rev.3. ed. United Nations, Santiago.

United Nations, 1992. Convention on Biological Diversity.

United Nations Environment Programme, 2023. Decades of Mangrove Forest Change: What Does it Mean for Nature, People and the Climate?, Technical Report. UNEP, Nairobi, Kenya.

United Nations Environment Programme, 2015. Paris Agreement.

User Guides - Sentinel-1 SAR - Overview - Sentinel Online [WWW Document], n.d. URL https://sentinel.esa.int/web/sentinel/user-guides/sentinel-1-sar/overview (accessed 11.26.20).

User Guides - Sentinel-2 MSI - Overview - Sentinel Online [WWW Document], n.d. URL https://sentinel.esa.int/web/sentinel/user-guides/sentinel-2-msi/overview (accessed 11.26.20).

USGS, 2013. Landsat — A Global Land-Imaging Mission. (U.S. Geological Survey Fact Sheet), Fact Sheet.

USGS Landsat 7 Surface Reflectance Tier 1 | Earth Engine Data Catalog [WWW Document], n.d. URL https://developers.google.com/earth-engine/datasets/catalog/LANDSAT_LE07_C01_T1_SR (accessed 11.27.20).

USGS Landsat 8 Surface Reflectance Tier 1 | Earth Engine Data Catalog [WWW Document], n.d. URL https://developers.google.com/earth-engine/datasets/catalog/LANDSAT_LC08_C01_T1_SR (accessed 11.27.20).

van Bijsterveldt, C.E.J., Debrot, A.O., Bouma, T.J., Maulana, M.B., Pribadi, R., Schop, J., Tonneijck, F.H., van Wesenbeeck, B.K., 2022. To Plant or Not to Plant: When can Planting Facilitate Mangrove Restoration? Front. Environ. Sci. 9, 690011. https://doi.org/10.3389/fenvs.2021.690011

Van Bochove, J.-W., Sullivan, E., Nakamura, T. (Eds.), 2014. The importance of mangroves to people: a call to action. UNEP, Cambridge.

Van der Stocken, T., Wee, A.K.S., De Ryck, D.J.R., Vanschoenwinkel, B., Friess, D.A., Dahdouh-Guebas, F., Simard, M., Koedam, N., Webb, E.L., 2019. A general framework for propagule dispersal in mangroves: A general framework for

propagule dispersal in mangroves. Biol. Rev. 94, 1547–1575. https://doi.org/10.1111/brv.12514

van der Wegen, M., Jaffe, B.E., Roelvink, J.A., 2011. Process-based, morphodynamic hindcast of decadal deposition patterns in San Pablo Bay, California, 1856-1887: MORPHODYNAMIC HINDCAST IN SAN PABLO BAY. J. Geophys. Res. Earth Surf. 116. https://doi.org/10.1029/2009JF001614

van der Wegen, M., Roelvink, J.A., 2008. Long-term morphodynamic evolution of a tidal embayment using a two-dimensional, process-based model. J. Geophys. Res. 113. https://doi.org/10.1029/2006JC003983

van Hespen, R., Hu, Z., Borsje, B., De Dominicis, M., Friess, D.A., Jevrejeva, S., Kleinhans, M., Maza, M., van Bijsterveldt, C.E.J., Van der Stocken, T., van Wesenbeeck, B., Xie, D., Bouma, T.J., 2022a. Mangrove forests as a nature-based solution for coastal flood protection: Biophysical and ecological considerations. Water Sci. Eng. https://doi.org/10.1016/j.wse.2022.10.004

van Hespen, R., Hu, Z., Peng, Y., Borsje, B.W., Kleinhans, M., Ysebaert, T., Bouma, T.J., 2021. Analysis of coastal storm damage resistance in successional mangrove species. Limnol. Oceanogr. 66, 3221–3236. https://doi.org/10.1002/lno.11875

van Hespen, R., Hu, Z., Peng, Y., Zhu, Z., Ysebaert, T., Bouma, T.J., 2022b. Identifying trait-based tolerance to sediment dynamics during seedling establishment across eight mangrove species. Limnol. Oceanogr. lno.12202. https://doi.org/10.1002/lno.12202

Van Loon, A.F., Te Brake, B., Van Huijgevoort, M.H.J., Dijksma, R., 2016. Hydrological Classification, a Practical Tool for Mangrove Restoration. PLOS ONE 11, e0150302. https://doi.org/10.1371/journal.pone.0150302

van Maanen, B., Coco, G., Bryan, K.R., 2015. On the ecogeomorphological feedbacks that control tidal channel network evolution in a sandy mangrove setting. Proc. R. Soc. Math. Phys. Eng. Sci. 471, 20150115. https://doi.org/10.1098/rspa.2015.0115

Van Wesenbeeck, B., van Rees, F., Tonneijck, F., Katherine Cronin, Han Winterwerp, 2021. System Understanding; Building with Nature to restore eroding tropical muddy coasts. Ecoshape technical report, Ecoshape technical report. Ecoshape International, Dordrecht, The Netherlands.

van Wesenbeeck, B.K., de Boer, W., Narayan, S., van der Star, W.R.L., de Vries, M.B., 2017. Coastal and riverine ecosystems as adaptive flood defenses under a changing climate. Mitig. Adapt. Strateg. Glob. Change 22, 1087–1094. https://doi.org/10.1007/s11027-016-9714-z

van Zelst, V.T.M., Dijkstra, J.T., van Wesenbeeck, B.K., Eilander, D., Morris, E.P., Winsemius, H.C., Ward, P.J., de Vries, M.B., 2021. Cutting the costs of coastal protection by integrating vegetation in flood defences. Nat. Commun. 12, 6533. https://doi.org/10.1038/s41467-021-26887-4

Vermote, E., Justice, C., Claverie, M., Franch, B., 2016. Preliminary analysis of the performance of the Landsat 8/OLI land surface reflectance product. Remote Sens. Environ. 185, 46–56. https://doi.org/10.1016/j.rse.2016.04.008

Vincenot, C.E., Mazzoleni, S., Parrott, L., 2016. Editorial: Hybrid Solutions for the Modeling of Complex Environmental Systems. Front. Environ. Sci. 4. https://doi.org/10.3389/fenvs.2016.00053

Vizcaya-Martínez, D.A., Flores-de-Santiago, F., Valderrama-Landeros, L., Serrano, D., Rodríguez-Sobreyra, R., Álvarez-Sánchez, L.F., Flores-Verdugo, F., 2022. Monitoring detailed mangrove hurricane damage and early recovery using multisource remote sensing data. J. Environ. Manage. 320, 115830. https://doi.org/10.1016/j.jenvman.2022.115830

Wafar, S., Untawale, A.G., Wafar, M., 1997. Litter Fall and Energy Flux in a Mangrove Ecosystem. Estuar. Coast. Shelf Sci. 44, 111–124. https://doi.org/10.1006/ecss.1996.0152

Walters, B.B., Rönnbäck, P., Kovacs, J.M., Crona, B., Hussain, S.A., Badola, R., Primavera, J.H., Barbier, E., Dahdouh-Guebas, F., 2008. Ethnobiology, socio-economics and management of mangrove forests: A review. Aquat. Bot. 89, 220–236. https://doi.org/10.1016/j.aquabot.2008.02.009

Wan, Y., Wan, L., Li, Y., Doering, P., 2017. Decadal and seasonal trends of nutrient concentration and export from highly managed coastal catchments. Water Res. 115, 180–194. https://doi.org/10.1016/j.watres.2017.02.068

Wang, W.J., He, H.S., Fraser, J.S., Thompson, F.R., Shifley, S.R., Spetich, M.A., 2014. LANDIS PRO: a landscape model that predicts forest composition and structure changes at regional scales. Ecography 37, 225–229. https://doi.org/10.1111/j.1600-0587.2013.00495.x

Ward, R.D., Friess, D.A., Day, R.H., Mackenzie, R.A., 2016. Impacts of climate change on mangrove ecosystems: a region by region overview. Ecosyst. Health Sustain. 2, e01211. https://doi.org/10.1002/ehs2.1211

Watson, J.G., 1928. Mangrove forests of the Malay Peninsula, Malayan forest records ; no. 6.

Wegen, M., Roelvink, J.A., Jaffe, B.E., 2019. Morphodynamic Resilience of Intertidal Mudflats on a Seasonal Time Scale. J. Geophys. Res. Oceans 124, 8290–8308. https://doi.org/10.1029/2019JC015492

Widyaningrum, E., Gorte, B.G.H., 2017. Comprehensive Comparison of Two Image-based Point Clouds from Aerial Photos with Airborne LiDAR for Large-Scale Mapping, in: ISPRS - International Archives of the Photogrammetry, Remote Sensing and Spatial Information Sciences. pp. 557–565. https://doi.org/10.5194/isprs-archives-XLII-2-W7-557-2017

Willemsen, P.W.J.M., Horstman, E.M., Borsje, B.W., Friess, D.A., Dohmen-Janssen, C.M., 2016. Sensitivity of the sediment trapping capacity of an estuarine mangrove forest. Geomorphology 273, 189–201. https://doi.org/10.1016/j.geomorph.2016.07.038

Wilson, P., 2020. A-Z of tree terms: A companion to British arboriculture (third edition), Third. ed. Ethelburga House.

Wimmler, M.-C., Bathmann, J., Peters, R., Jiang, J., Walther, M., Lovelock, C.E., Berger, U., 2021. Plant–soil feedbacks in mangrove ecosystems: establishing links between empirical and modelling studies. Trees 35, 1423–1438. https://doi.org/10.1007/s00468-021-02182-z

Winterwerp, H., Wilms, T., Siri, H., Vries, J., Noor, Y., Van Wesenbeeck, B., Cronin, K., Van Eijk, P., Tonneijck, F., 2016. Building with nature: sustainable protection of mangrove coasts. Terra Aqua 1, 5–15.

Winterwerp, J.C., Albers, T., Anthony, E.J., Friess, D.A., Mancheño, A.G., Moseley, K., Muhari, A., Naipal, S., Noordermeer, J., Oost, A., Saengsupavanich, C., Tas, S.A.J., Tonneijck, F.H., Wilms, T., Van Bijsterveldt, C., Van Eijk, P., Van Lavieren, E., Van Wesenbeeck, B.K., 2020. Managing erosion of mangrove-mud coasts with permeable dams – lessons learned. Ecol. Eng. 158, 106078. https://doi.org/10.1016/j.ecoleng.2020.106078

Winterwerp, J.C., Erftemeijer, P.L.A., Suryadiputra, N., van Eijk, P., Zhang, L., 2013. Defining Eco-Morphodynamic Requirements for Rehabilitating Eroding Mangrove-Mud Coasts. Wetlands 33, 515–526. https://doi.org/10.1007/s13157-013-0409-x

Wirjoadmodjo, H., Hamzah, Z., 1982. Beberapa pengalaman Perum Perhutani dalam Pengelolaan Hutan Mangrove, in: Prosiding Seminar Ekosistem Mangrove. Presented at the Ekosistem Mangrove, Balai Penelitian Hutan, Perum Perhutani, Biotrop, Dit. Bina Program Kehutanan, Jakarta.

Wong, P.P., Losada, I.J., Gattuso, J.-P., Hinkel, J., Khattabi, A., McInnes, K.L., Saito, Y., Sallenger, A. (Eds.), 2014. Coastal Systems and Low-Lying Areas, in: Climate Change 2014: Impacts, Adaptation, and Vulnerability. Part A: Global and Sectoral Aspects. Contribution of Working Group II to the Fifth Assessment Report of the Intergovernmental Panle on Climate Change. Cambridge University Press, Cambridge, United Kingdom ; New York, NY, pp. 361–409.

Woodroffe, C., 1992. Mangrove sediments and geomorphology, in: Robertson, A.I., Alongi, D.M. (Eds.), Tropical Mangrove Ecosystems, Coastal and Estuarine Studies. American Geophysical Union, Washington, D. C., pp. 7–41. https://doi.org/10.1029/CE041p0007

Woodroffe, C.D., Rogers, K., McKee, K.L., Lovelock, C.E., Mendelssohn, I.A., Saintilan, N., 2016. Mangrove Sedimentation and Response to Relative Sea-Level Rise. Annu. Rev. Mar. Sci. 8, 243–266. https://doi.org/10.1146/annurev-marine-122414-034025

World Bank, 2022. The Economics of Large-scale Mangrove Conservation and Restoration in Indonesia: Technical Report, Technical Report. ed, Technical Report. World Bank, Washington, D.C. https://doi.org/10.1596/37605

World Bank, 2017. Implementing Nature Based Flood Protection : Principles and Implementation Guidance (Working Paper). World Bank, Washington DC, USA.

World Bank, 2016. Managing Coasts with Natural Solutions: Guidelines for Measuring and Valuing the Coastal Protection Services of mangroves and Coral Reefs.

World Bank Group, 2018. Building with nature (English) (Brief No. 126688), West Africa Coastal Areas Management Program,case study no. 4. World Bank Group, Washington, D.C.

Wu, Q., 2020. geemap: A Python package for interactive mapping with Google Earth Engine. J. Open Source Softw. 5, 2305. https://doi.org/10.21105/joss.02305

Wulder, M.A., White, J.C., Nelson, R.F., Næsset, E., Ørka, H.O., Coops, N.C., Hilker, T., Bater, C.W., Gobakken, T., 2012. Lidar sampling for large-area forest characterization: A review. Remote Sens. Environ. 121, 196–209. https://doi.org/10.1016/j.rse.2012.02.001

Xie, D., Schwarz, C., Brückner, M.Z.M., Kleinhans, M.G., Urrego, D.H., Zhou, Z., van Maanen, B., 2020. Mangrove diversity loss under sea-level rise triggered by bio-morphodynamic feedbacks and anthropogenic pressures. Environ. Res. Lett. 15, 114033. https://doi.org/10.1088/1748-9326/abc122

Xie, D., Schwarz, C., Kleinhans, M.G., Zhou, Z., van Maanen, B., 2022. Implications of Coastal Conditions and Sea-Level Rise on Mangrove Vulnerability: a Bio-morphodynamic Modelling Study. J. Geophys. Res. Earth Surf. 127, e2021JF006301. https://doi.org/10.1029/2021JF006301

Xiong, J., Thenkabail, P.S., Gumma, M.K., Teluguntla, P., Poehnelt, J., Congalton, R.G., Yadav, K., Thau, D., 2017. Automated cropland mapping of continental Africa using Google Earth Engine cloud computing. ISPRS J. Photogramm. Remote Sens. 126, 225–244. https://doi.org/10.1016/j.isprsjprs.2017.01.019

Yeo, D., Srivathsan, A., Puniamoorthy, J., Maosheng, F., Grootaert, P., Chan, L., Guénard, B., Damken, C., Wahab, R.A., Yuchen, A., Meier, R., 2021. Mangroves are an overlooked hotspot of insect diversity despite low plant diversity. BMC Biol. 19, 202. https://doi.org/10.1186/s12915-021-01088-z

Yoshikai, M., Nakamura, T., Herrera, E.C., Suwa, R., Rollon, R., Ray, R., Furukawa, K., Nadaoka, K., 2023. Representing the impact of *Rhizophora* mangroves on flow in a hydrodynamic model (COAWST_rh v1.0): the importance of three-dimensional root system structures. Geosci. Model Dev. 16, 5847–5863. https://doi.org/10.5194/gmd-16-5847-2023

Yuan, L., Zhu, G., Xu, C., 2020. Combining synthetic aperture radar and multispectral images for land cover classification: a case study of Beijing, China. J. Appl. Remote Sens. 14, 1. https://doi.org/10.1117/1.JRS.14.026510

Zainol, Z., Peris, A.D., Akhir, M.F., Rahim, N.H.A., Satyanarayana, B., Dahdouh-Guebas, F., 2022. Mangrove Propagule Dispersal in a Shallow and Narrow Coastal Lagoon: A Simulation-Based Assessment of the Setiu Wetlands, Malaysia. Forests 13, 1525. https://doi.org/10.3390/f13091525

Zhang, K., Liu, H., Li, Y., Xu, H., Shen, J., Rhome, J., Smith, T.J., 2012. The role of mangroves in attenuating storm surges. Estuar. Coast. Shelf Sci. 102–103, 11–23. https://doi.org/10.1016/j.ecss.2012.02.021

Zhang, K., Thapa, B., Ross, M., Gann, D., 2016. Remote sensing of seasonal changes and disturbances in mangrove forest: a case study from South Florida. Ecosphere 7. https://doi.org/10.1002/ecs2.1366

Zhang, W., Qi, J., Wan, P., Wang, H., Xie, D., Wang, X., Yan, G., 2016. An Easy-to-Use Airborne LiDAR Data Filtering Method Based on Cloth Simulation. Remote Sens. 8, 501. https://doi.org/10.3390/rs8060501

Zhu, X., Hou, Y., Weng, Q., Chen, L., 2019. Integrating UAV optical imagery and LiDAR data for assessing the spatial relationship between mangrove and inundation across a subtropical estuarine wetland. ISPRS J. Photogramm. Remote Sens. 149, 146–156. https://doi.org/10.1016/j.isprsjprs.2019.01.021

Zhu, Z., Huang, M., Zhou, Z., Chen, G., Zhu, X., 2022. Stronger conservation promotes mangrove biomass accumulation: Insights from spatially explicit assessments using UAV and Landsat data. Remote Sens. Ecol. Conserv. 8, 656–669. https://doi.org/10.1002/rse2.268

Zimmer, M., Ajonina, G.N., Amir, A.A., Cragg, S.M., Crooks, S., Dahdouh-Guebas, F., Duke, N.C., Fratini, S., Friess, D.A., Helfer, V., Huxham, M., Kathiresan, K., Kodikara, K.A.S., Koedam, N., Lee, S.Y., Mangora, M.M., Primavera, J., Satyanarayana, B., Yong, J.W.H., Wodehouse, D., 2022. When nature needs a helping hand: Different levels of human intervention for mangrove (re-)establishment. Front. For. Glob. Change 5, 784322. https://doi.org/10.3389/ffgc.2022.784322

LIST OF ACRONYMS

AGB	Above Ground Biomass
AGC	Above Ground Biomass Carbon
BA	Basal Area
BMI	Basic Model Interface
BGB	Below Ground Biomass
BGC	Below Ground Biomass Carbon
BCE	Blue Carbon Ecosystems
CHM	Canopy Height Model
CART	Classification and Regression Tree
CA	Consumer Accuracy
GCMFC-21	Continuous Global Mangrove Forest Cover for the 21st Century
DFM	Delft3D-Flexible Mesh
D_{130}	Diameter at breast height at 130cm above the ground
DGPS	Differential Global Positioning System
DEM	Digital Elevation Model
DSM	Digital Surface Model
DTM	Digital Terrain Model
EVI	Enhanced Vegetation Index
ESA	European Space Agency

FON	Field of Neighbourhood
FON	Field of Neighbourhood
GMFD	Global Mangrove Forest Distribution
GMW	Global Mangrove Watch
GPS	Global Positioning System
GEE	Google Earth Engine
GCP	Ground Control Point
GRD	Ground Range Detected
IBM	Individual-based Model
KNN	K-Nearest Neighbour
LU/LC	Land Use/Land Cover Classification
L7	Landsat 7
L8	Landsat 8
LMF	Local Maximum Filter
LOESS	Locally Estimated Scatterplot Smoothing
LLWL	Lowest Low Water Level
LUSI	Lumpur Sidoarjo
ML	Maximum Likelihood
MHWN	Mean High Water Neap
MHWS	Mean High Water Spring
MSL	Mean Sea Level
MFON	MesoFON

MMAF	Ministry of Marine Affairs and Fisheries
MF	Morphological Factor
NSSDA	National Standard for Spatial Data Accuracy
NbS	Nature-based Solutions
NDMI	Normalised Difference Moisture Index
NDVI	Normalised Difference Vegetation Index
OA	Overall Accuracy
PA	Producer Accuracy
RF	Random Forest
ROI	Region of Interests
RMSE	Root Mean Square Error
SLR	Sea Level Rise
STL	Seasonal-trend decomposition
S1	Sentinel 1
S2	Sentinel 2
SRTM	Shuttle Radar Topography Mission
SER	Society for Ecological Restoration Science
SOC	Soil Organic Carbon
SAVI	Soil-Adjusted Vegetation Index
SfM	Structure from Motion
SVM	Support Vector Machine
SAR	Synthetic Aperture Radar

2DH	Two-Dimensional depth-averaged
UN	United Nations
UNEP	United Nations Environment Programme
UAV	Unoccupied Aerial Vehicle
VHR	Very High Resolution
WoO	Window of Opportunity
WAM	World Atlas of Mangrove

LIST OF TABLES

LIST OF FIGURES

ABOUT THE AUTHOR

Sebrian Beselly was born on 24 September 1989, in Malang, East Java, precisely in a scenic *then* small town Batu, standing at the foot of Mount Arjuna. In the ancient Javanese wayang story, in which the stories depicted the Hindu epics, Arjuna is the third of the royal Pandawa's brothers and a central character in the wayang story with his skill in archery, not to mention his gorgeous good-looking. This is not without reason this *now* Batu City bears the same beauty, boasting the natural sceneries as a characteristic of a mountainous region. He grew up with a love of mountains, trees, and water, occasionally hiking with his pramuka (boy scout) group, with an imagination of adventures. In the neighbouring city, downtown Malang, he followed his love of the water through water resources engineering at the Universitas Brawijaya, which eventually led him to discover the beauty of waves and coasts. After 4 years he graduated with a cumlaude and shared his thoughts as a valedictorian in the graduation ceremony. Upon graduation, he received a scholarship to study for his Master's in Civil and Environmental Engineering via a double degree programme between Universitas Brawijaya and the University of Miyazaki, Japan. In Miyazaki and Malang, he completed his Master of Engineering thesis in modelling hydro-morphological development of Lamong Bay in East Java following the construction of the port reclamation. At this point, he realised his love for doing research and passion in academia. He found an opportunity to be part of the water resources engineering department as a junior lecturer. During this time, he was granted a PhD scholarship and pursued his ambition to delve deeper into the interdisciplinary approach to the intersection of coastal engineering and ecology at IHE Delft. There, he learned and developed a new hybrid model of landscape-based hydromorphodynamic and individual-based mangrove models. Sebrian is thrilled to contribute to capacity development and research in coastal and urban hazards and risks at IHE Delft and Indonesia. When not busy with his research he can be found enjoying good action movies, curling with a good book, or cycling around the city.

Journal publications

Beselly, Sebrian Mirdeklis, Mick van der Wegen, Uwe Grueters, Johan Reyns, Jasper Dijkstra, and Dano Roelvink. "Eleven Years of Mangrove–Mudflat Dynamics on the Mud Volcano-Induced Prograding Delta in East Java, Indonesia: Integrating UAV and Satellite Imagery." Remote Sensing 13, no. 6 (March 12, 2021): 1084. https://doi.org/10.3390/rs13061084.

Beselly, Sebrian Mirdeklis, Uwe Grueters, Mick Van Der Wegen, Johan Reyns, Jasper Dijkstra, and Dano Roelvink. "Modelling Mangrove-Mudflat Dynamics with a Coupled Individual-Based-Hydro-Morphodynamic Model." Environmental Modelling & Software 169 (November 2023): 105814. https://doi.org/10.1016/j.envsoft.2023.105814.

Alkadri, Miktha Farid, Syaiful Alam, Herry Santosa, Adipandang Yudono, and **Sebrian Mirdeklis Beselly**. "Investigating Surface Fractures and Materials Behavior of Cultural Heritage Buildings Based on the Attribute Information of Point Clouds Stored in the TLS Dataset." Remote Sensing 14, no. 2 (January 17, 2022): 410. https://doi.org/10.3390/rs14020410.

Beselly, Sebrian Mirdeklis, Mick van der Wegen, Johan Reyns, Uwe Grueters, Jasper Dijkstra, and Dano Roelvink. "Strategic mangrove restoration increases carbon sequestration capacity." (in preparation)

Conference abstracts

Beselly, S M, Dano Roelvink, Mick van der Wegen, Johan Reyns, and Jasper Dijkstra. Modelling of Coastal Ecogeomorphological Change in a Vegetated Estuary. Delft: IHE Delft PhD Symposium, 2018.

Beselly, S M, Mick van der Wegen, Dano Roelvink, Uwe Grueters, Johan Reyns, and Jasper Dijkstra. Drone-based 'Structure-from-Motion' (SfM) Photogrammetry Analysis of Mangrove Dynamics in the Prograding Delta in Porong, Indonesia.Texel: Nederland Centrum voor Kustonderzoek (NCK), 2020 (cancelled due to COVID-19).

Beselly, S M, Mick van der Wegen, Dano Roelvink, Uwe Grueters, Johan Reyns, and Jasper Dijkstra. Retrieving Mangrove Biophysical Properties using Drone-Based Structure-from-Motion (SfM) Photogrammetry. Online: Mangrove Day 2nd Annual Meeting, 2020.

Beselly, S M, Mick van der Wegen, Dano Roelvink, Uwe Grueters, Johan Reyns, and Jasper Dijkstra. Dynamics of Mangroves in Porong Delta based on UAV SfM Photogrammetry, Sentinel-1, Sentinel-2, and Landsat in Google Earth Engine. Delft: IHE Delft PhD Symposium, 2020.

Beselly, S M, Mick van der Wegen, Dano Roelvink, Uwe Grueters, Jasper Dijkstra, and Johan Reyns. Retrieving Mangrove Biophysical Properties Using Drone-Based Structure-from-Motion (SfM) Photogrammetry. Online: American Geophysical Union (AGU), 2020.

Beselly, S M, Mick van der Wegen, Uwe Grueters, Johan Reyns, Jasper Dijkstra, and Dano Roelvink. Integrating UAV and Satellite Imagery: Mangrove-Mudflat Evolution on a Prograding Delta. Delft: Coastal Dynamics, 2021.

Beselly, S M, Mick van der Wegen, Uwe Grueters, Johan Reyns, Jasper Dijkstra, and Dano Roelvink. Mud Volcano Induced Seasonal Mangrove-Mudflat Dynamics. Online: Nederland Centrum voor Kustonderzoek (NCK), 2021.

Beselly, S M, Mick Van der Wegen, Uwe Grueters, Johan Reyns, Jasper Dijkstra, and Dano Roelvink. Unravelling Mangrove Biophysical Feedback on Rapidly Prograding Delta by Integration of UAV and Satellite Imagery. New Orleans, LA and Online: American Geophysical Union (AGU), 2021

Beselly, S M, Uwe Grueters, Mick van der Wegen, Johan Reyns, Dano Roelvink, and Jasper Dijkstra. Simulation of the Mangrove-Mudflat Dynamics with A New Coupled Individual-Based Mangrove-Morphodynamic Model. Enschede: Nederland Centrum voor Kustonderzoek (NCK), 2022.

Beselly, S M, Uwe Grueters, Mick van der Wegen, Johan Reyns, Dano Roelvink, and Jasper Dijkstra. Simulation of the interplay of mangroves ecosystems, environments and morphological development. San Sebastian: Estuarine and Coastal Sciences Association (ECSA), 2022.

Conference proceedings

Beselly, S M, Mick van der Wegen, Dano Roelvink, Uwe Grueters, Jasper Dijkstra, and Johan Reyns. “Retrieving Mangrove Biophysical Properties Using Drone-Based Structure-from-Motion (SfM) Photogrammetry.” American Geophysical Union (AGU), 2020. https://doi.org/10.1002/essoar.10506488.1.

Beselly, S M, Mick Van der Wegen, Uwe Grueters, Jasper Dijkstra, Johan Reyns, and Dano Roelvink. “Unravelling Mangrove Biophysical Feedback on Rapidly Prograding Delta by Integration of UAV and Satellite Imagery.” New Orleans, LA and Online: American Geophysical Union (AGU), 2021. https://doi.org/10.1002/essoar.10510177.1.

Beselly, S M, and M A Sajali. “Citizen-Science with off-the-Shelf UAV for Coastal Monitoring.” IOP Conference Series: Earth and Environmental Science 930, no. 1 (December 1, 2021): 012001. https://doi.org/10.1088/1755-1315/930/1/012001.

Beselly, S M, R D Lufira, and U Andawayanti. “Seasonal Spatio-Temporal Land Cover Dynamics in the Upper Brantas Watershed.” IOP Conference Series: Earth and Environmental Science 930, no. 1 (December 1, 2021): 012021. https://doi.org/10.1088/1755-1315/930/1/012021.

Awards

American Geophysical Union (AGU) Fall Meeting 2020 Student Travel Grant

Best paper in the International Conference of Water Resources Development and Environmental Protection (ICWRDEP) 2021, Malang, Indonesia. Paper title: Citizen-Science with off-the-Shelf UAV for Coastal Monitoring

2024 Syvitski Student Modeler award by Community Surface Dynamics Modeling System (CSDMS), CSDMS Annual Meeting 2024, Montclair State University, Montclair, New Jersey, USA

Outreach

(IHE Delft) Young Professional representation. Young Professionals in World Water Week 2018. Stockholm: Stockholm International Water Institute (SIWI), 2018.

Guest Lecture. Introduction on Deltas and Rivers in Indonesia; Outside of the Dutch Coasts Context. Online: De Haagse Hogeschool, 2020.

Speaker. The Green World of Brawijaya for Better Future. World Cleanup Day Brawijaya. Online: Brawijaya Student Association, 2020.

Video Interview. International Day for the Conservation of the Mangrove Ecosystem. IHE Delft Series. Online and News: IHE Delft, 2020.

Speaker. Tackling Water Crisis as a Water Profesional. Study in Holland. Online: Nuffic Neso, 2021.

Contributor. Tools for The Design and Assessment of Resilient Mangrove Coasts -and other Nature-Based Solutions: Nature-based Solutions and Integraed Perspectives. Asia Water Forum 2022. Online: Asia Development Bank, 2022.

Moderator. Groundbreaking: Wujudkan Pengelolaan SDA Berkelanjutan. Young Water Sustainability Leaders Bootcamp. Online: Indonesia Ministry of Public Works and Housing and ECADIN, 2022.

Speaker. Study in the Netherlands. Online: Nuffic Neso, 2022.

Speaker. From ClimateScan to BrantaSae; a Water Quality Database with its Activities. Week of Indonesia-Netherlands Education and Research (WINNER). Online: ALMI, BRIN, KNAW, Nuffic Neso, and NWO, 2022.

Speaker. Maju Mundur Studi dan Riset Sumber Daya Air. Young Water Sustainability Leaders Sharing Session. Delft and Online: Indonesia Ministry of Public Works and Housing and ECADIN, 2022.

Netherlands Research School for the
Socio-Economic and Natural Sciences of the Environment

D I P L O M A

for specialised PhD training

The Netherlands research school for the
Socio-Economic and Natural Sciences of the Environment
(SENSE) declares that

Sebrian Mirdeklis Beselly Putra

born on 24th September 1989 in Malang, Indonesia

has successfully fulfilled all requirements of the
educational PhD programme of SENSE.

Delft, 12 July 2024

Chair of the SENSE board

Prof. dr. Martin Wassen

The SENSE Director

Prof. Philipp Pattberg

The SENSE Research School has been accredited by the Royal Netherlands Academy of Arts and Sciences (KNAW)

KONINKLIJKE NEDERLANDSE
AKADEMIE VAN WETENSCHAPPEN

The SENSE Research School declares that **Sebrian Mirdeklis Beselly Putra** has successfully fulfilled all requirements of the educational PhD programme of SENSE with a work load of 53.2 EC, including the following activities:

SENSE PhD Courses

- Environmental research in context (2018)
- Research in context activity: 'Organising the IHE Delft PhD Symposium 2019'

Selection of Other PhD and Advanced MSc Courses

- Research Design, TU Delft (2018)
- Summer Course Visual Methods for Water Communication, IHE-Delft (2018)
- Analytic Storytelling, TU Delft (2019)
- Netherlands Centre for Coastal Research Summer School (2019)
- Software Carpentry Workshop, 4TU.Centre for Research Data (2019)
- Workshop on programming JS using libraries D3JS and Three, JS, IHE Delft (2019)
- Process-based Coastal Modelling, IHE-Delft (2019)
- Coastal Systems, IHE-Delft (2019)
- Data Visualisation as a tool for Scientific Research, TU Delft (2020)
- Introduction to Delft3D Modelling, IHE-Delft (2021)

Management and Didactic Skills Training

- Member of PhD Association Board, IHE-Delft (2020-2022)
- Organising BrantaScan Project Workshop,Universitas Brawijaya and TU Delft (2021)
- Organising Tailor-Made Training 'Managing Coastal and Pluvial Flood Risk in the Cities', Nuffic Neso Indonesia

Selection of Oral Presentations

- *Retrieving Mangrove Biophysical Properties using Drone-Based Structure-from-Motion (SfM) Photogrammetry*. Mangrove Days 2020, 13 May 2020, Delft, The Netherlands
- *Integrating UAV and Satellite Imagery: Mangrove-Mudflat Evolution on a Prograding Delta*. Coastal Dynamics, 28 June-02 July 2021, Delft, The Netherlands
- *Simulation of the Mangrove-Mudflat Dynamics with A New Coupled Individual-Based Mangrove-Morphodynamic Model*. The Netherlands Centre for Coastal Research, 16-18 March 2022, Enschede, The Netherlands
- *Simulation of the Interplay of Mangroves Ecosystems, Environments and Morphological Development*. Estuarine and Coastal Sciences Association, 5-8 September 2022, San Sebastian, Spain

SENSE coordinator PhD education

Dr. ir. Peter Vermeulen

IHE DELFT
Institute for Water Education
under the auspices of UNESCO

TU Delft Delft University of Technology

Mangroves are acknowledged for their wide range of ecosystem services. As such, mangrove conservation has been considered one of the top priorities within coastal communities worldwide. Despite global commitments and support from countries and international organisations, the majority of mangrove restoration projects have been reported to fail. This study aims to develop a better understanding of complex eco-geomorphic interactions and feedback processes in the evolution of coastal mangrove environments. A newly developed model (DFMFON) resolves the feedback processes between hydro-morphodynamic forcing (waves, tides, river flow, sediment supply, salinity, and morphodynamics) and mangrove life stages ranging from (dispersal of) propagules to the development of seedlings and sapling into mature trees. The model successfully reproduces observed spatiotemporal (seasonal-decadal) mangrove development, like the age-height relationship, as well as morphodynamic delta evolution in Porong Estuary, Indonesia. The model is then used to optimize mangrove restoration strategies and carbon sequestration capacity in coastal systems. The case study observations and tool presented in this thesis open up possibilities for optimising mangrove restoration management schemes for climate mitigation and adaptation in sustainable coastal systems.

This book is printed on paper from sustainably managed forests and controlled sources

9 789073 445635